MICROSCOPIC AND MACROSCOPIC VISUALIZATION OF DISPLACEMENT OF OIL FROM POROUS MEDIA

by

JACOB CHERIAN, B.E.

A THESIS

IN

PETROLEUM ENGINEERING

Submitted to the Graduate Faculty
of Texas Tech University in
Partial Fulfillment of
the Requirements for
the Degree of

MASTER OF SCIENCE

IN

PETROLEUM ENGINEERING

Approved

_____

Chairperson of the Committee

_____

Accepted

_____

Dean of the Graduate School

August, 2002

ACKNOWLEDGEMENTS

Mere words are not enough to thank the people who have helped me make this thesis in its present form. The most important person to whom I am, thankful is, Dr. Scott M. Frailey, Texas Tech University. His constant support, and encouragement is priceless and he has provided me thoughtful reviews and numerous intelligent suggestions. Credit goes to him for making a researcher out of me.

Dr. Akanni S. Lawal with his aggressive motivational power and availability even at the wee hours was instrumental in providing incalculable encouragement towards the completion of this thesis.

My gratitude also goes to Dr. James Lea, who had provided financial assistance at the most wanted times.

Scott Austin gave me the introduction to Visual Basic while at Henwood Energy, Sacramento, CA. The Visual Basic knowledge required to go into this thesis was primarily acquired through him.

My wife Benoy and my son Chris have missed me numerous days and long nights. On several occasions they have missed me all night. This never-ending thesis would have never been complete without their patience and support. I dedicate this thesis to the most understanding person in the world – Benoy, who stood by my side from the day she applied to this university. She needs special mention for helping me in the critical and final stages of this work.

I would like to thank for the valuable computer time provided by my colleagues, Parameswaran Nampoothiri and David Murray who used to let me use our single office computer. I thank Nampoothiri for buying a computer for himself and David for going and using the facility at the Chemical Engineering computer lab thereby was allowing me to carry on my work.

Few other people need special mention. Sriram Sundararajan of the Computer Science Department provided me with accommodation and made travel arrangements during the final stages of thesis work. Manish Ved spent an entire day with me wrapping up the complete package on time. Barbi Dickensheet of Texas Tech University spent long hours correcting my final version.

As always, my gratitude goes to my parents who encouraged me to pursue higher studies at the graduate level.

For the wisdom I gained from completing this thesis. I thank my Lord.

TABLE OF CONTENTS

ABSTRACT

Waterflooding has gained a prominent role among the various recovery mechanisms used to recover oil, due to its simplicity and economic advantage. It is therefore imperative that people have a thorough understanding about the waterflooding concepts and possess scientific and engineering imagination to optimize oil production from oil reservoirs. Microscopic visualization at the pore level and macroscopic visualization at the reservoir level could fuel one's imagination thus strengthening the knowledge base and creativity by better understanding the displacement of oil with water.

The present work discusses the waterflood concepts using an interactive computer program to visualize the movement of oil through porous media at the microscopic and macroscopic level. An approach using visualization technique has been adopted to better understand the displacement performance of a linear waterflood using Buckley-Leverett Theory. The visualization technique enhances the visual effects by delivering concise and clear images of oil displacement during a waterflood process. Input parameters such as porosity, saturation and mobility ratio can be varied to visualize the variations in both microscopic and macroscopic oil displacement processes.

LIST OF TABLES

LIST OF FIGURES

LIST OF ABBREVIATIONS

v	kinematic viscosity of the fluid
ρ	density of the fluid, grams per cubic centimeter, ratio of pore body to the
λ_D	mobility of displacing fluid
λ_d	mobility of the displaced fluid
σ_{ow}	interfacial tension between oil and water
p_c	capillary pressure
p_o	pressure in the oil phase
p_w	pressure in the water phase
$\overline{S}_w$	average water saturation in linear system
μ	absolute viscosity of the fluid
$\Delta\rho$	water-oil density difference
α_d	angle of the formation dip to the horizontal
μ_g	gas viscosity
ρ	density
ρ_g	density of gas
μ_o	oil viscosity
ρ_o	density of oil
μ_w	water viscosity

ρ_w	density of water
E_D	microscopic displacement efficiency
E_V	macroscopic (volumetric) displacement efficiency
f_o	fractional flow of oil
F_{O2}	fractional flow of oil at outlet of linear system
f_{iw}	fractional flow of water corresponding to saturation S_{iw}
f_{bt}	fractional flow of water at breakthrough
f_w	fractional flow of water
f_{w2}	fractional flow of water corresponding to saturation S_{w2}
f'_{w2}	derivative of water fractional-flow curve at saturation S_{w2}
F_{WO}	water : oil ratio
g	acceleration due to gravity
$\bar{k}$	median permeability
k_σ	permeability at 84.1 percent of the cumulative sample
k	formation permeability
k_g	effective permeability to gas
k_o	effective permeability to oil
k_{rg}	relative permeability to gas
k_{ro}	relative permeability to oil
k_{rw}	relative permeability to water
k_w	effective permeability to water

L	distance along direction of movement
M	mobility ratio
$M_{\bar{s}}$	mobility ratio based on average saturation
N_{ca}	capillary number
N_p	oil displaced by a flood
Q_l	cumulative pore volume's injected
q	volumetric flow rate
r	radius
S_{bt}	saturation of water at breakthrough
S_w	water saturation
$\bar{S}_w$	average water saturation
S_{iw}	initial water saturation
S_{or}	residual oil saturation
S_{w2}	water saturation at end of linear system
S_{wD}	dimensionless water saturation
t_D	dimensionless time or pore volume injected
t_{D2}	dimensionless time when water saturation S_{w2} arrives at the end of linear system
u	darcy velocity
U_T	total fluid velocity
V	permeability variation
V_g	volume of gas
V_o	volume of oil

V_w	volume of water
x	distance along the axis of tore
x_f	identified in figure 41
x_j	identified in figure 41
x_D	dimensionless distance from the origin
t_D	dimensionless time
W_i	initial volume of water.
Π	$P_c r_1/\sigma$, dimensionless
Π_c	value of Π between $x = 0$ and $x = x_j$
Π_f	value of Π at $x = x_j$
Π_t	value of Π at $x = 0$

Subscripts

x	represents that each element in the Buckley-Leverett derivation is different for each element
D	displacing fluid
d	formation dip, displaced fluid
g	gas
o	oil
ow	oil and water
t	total
w	water

CHAPTER 1

INTRODUCTION

Waterflooding is used in many oil fields due to the increasing costs in explorations, difficulty in finding large reservoirs and falling oil production rate using primary production methods.[1] Waterflooding is regarded as one of the most successful oil recovery method and is widely used all over the world in carbonate and sandstone reservoirs. Waterflooding is useful in recovering oil from a reservoir because of the ease of injecting water into the reservoir, low operating costs, the ability of water to disperse through an oil bearing formation and produce oil with high efficiency, and relative ease of availability of water.[1]

Primary production is the process of initial production of hydrocarbons from underground reservoirs accomplished by the use of natural reservoir energy.[2] According to Smith,[3] the American Petroleum Institute defines primary production as the oil, gas, or the combination of both, recovered by any method, either natural flow or artificial lift, through a single well bore. Once the reservoir is depleted of primary energy, the primary production ends. Oil and gas are displaced to production wells under primary production by fluid expansion, fluid displacement, gravitational drainage, and/or capillary expulsion.[2] In waterflooding, kinetic energy is applied to a reservoir in the form of injected water to recover additional oil, which was not possible to produce using the primary reservoir energy. Waterflooding could also be started before the primary production ceases, and involves the process of displacing oil by water.

Waterflooding has been a favorable candidate for commercial oil recovery since the mid-1900s.[4] Apart from recovering oil from the reservoir, waterflooding serves the purpose of reservoir pressure maintenance. The significance of pressure maintenance is to supplement natural reservoir energy and to improve oil-producing characteristics of the oil reservoir prior to the time that economic productive limits are reached.[5]

Any reservoir could be viewed at four levels, namely microscopic, macroscopic, megascopic and gigascopic.[6] Microscopic level is at the pore or grain level. Macroscopic level is at the core plug level. Megascopic level is at the reservoir level, which may contain large fractures and faults. Gigascopic level is as large as few reservoirs, and may contain mountains and rivers. During the oil recovery process, the distribution of immiscible phases at the microscopic level is of interest, because it influences the rate of flow, residual saturation of each phase and the microscopic displacement recovery efficiency. Moreover, the macroscopic level, viewed at the core plug level, is of interest because macroscopic displacement efficiency indicates how well the displacing fluid has contacted the oil-bearing parts of the reservoir.

The discovery of waterflooding was accidental and is dated back to 1865.[1] Since the discovery of waterflooding, numerous works have been carried out to better understand how oil is displaced by water and the factors affecting the efficient recovery of oil from the reservoir. This could be achieved by a thorough understanding of one fluid displacing another, both at the pore and core levels. Therefore, during the course of this thesis, emphasis is placed in finding literature pertaining to the factors affecting waterflood both at the microscopic and macroscopic level.

The main objective of this research project is to understand the process of water displacing oil through the porous media at the microscopic and macroscopic levels. To accomplish this objective, an extensive literature review was conducted in the area of immiscible linear displacement of oil using water. A computer application using Visual Basic® was developed to visualize the process of water displacing oil. Microsoft Excel® was used to generate a fractional flow curve and the saturation profile, which was linked to a Microsoft Access® database using the concept of linked tables.

CHAPTER 2

LITERATURE REVIEW

Life without oil would be almost unimaginable in today's industrial world. Since the discovery of crude oil by Colonel Edwin L. Drake on August 27, 1859, crude oil and its derivatives have been a major source of energy for mankind.[7] Today's world depends heavily on crude oil. An important factor for waterflooding is to increase reserve. Some primary production methods can recover only about 20% of the original oil in place, leaving behind almost 80% of the oil in the reservoir. Hence, the need of additional recovery mechanisms has attained prominent positions in the oil industry. Because only a small proportion of the oil and gas in a reservoir is producible under primary production methods, petroleum engineers develop and use various enhanced oil recovery methods that include injecting water, chemicals, gases, or steam into an oil reservoir.

Waterflooding has been a major source of oil recovery of oil since its discovery, because water is relatively inexpensive and is in plentiful supply at many producing areas. Since waterflooding has been technologically established for the past 100 years, it is a common option among operators, compared to alternative secondary drives such as immiscible gas injection.

2.1 Basic Concepts of Waterflooding

The process of waterflooding originated from the accidental admission of water from external sources onto oil sands in the Pithole city area of Pennsylvania in 1865.[1]

Intentional waterfloods were started in 1913 in Ontario, Canada. The first five spot pattern used for waterflooding started in 1924 in the Bradford field, Pennsylvania.[1] The first waterflood in Texas is reported to be at the Fry pool of Brown County in 1936.[1]

Development of a secondary waterflood was slow because it involved economic as well as geologic and engineering considerations. Early methods of waterflooding expanded with the belief that the main function of water injection was to maintain reservoir pressure. According to Frick and Taylor,[5] water-pressure maintenance is another process closely related to waterflooding. In this process, water is injected into a reservoir to supplement the energy lost by the reservoir due to primary production and to improve the oil producing characteristics of the oilfield, prior to the time of reaching economic productive limits.

Increased knowledge of concepts like capillary pressure, porosity, interfacial tension, and permeability resulted in engineers trying different injection-production patterns like line drive and five spot patterns. The five spot patterns proved to produce more oil out of the reservoir than the line drive. It was not until the early 1950s that the general applicability of waterflooding was recognized.[1] With the increasing cost of discovering new reserves, waterflooding has remained as a profitable option to petroleum engineers.

As referred by Craig,[1] the American Petroleum Institute defines secondary recovery as the oil and/or gas recovered by artificial flowing or pumping means, through the joint use of two of more well bores. According to Craft and Hawkins,[2] the use of either a natural gas or a water injection scheme is called a secondary recovery operation. Green and

Willhite[7] explain that secondary recovery, the second stage of operations, usually was implemented after primary production declined.

Once the primary production ceases, or is about to cease, water is injected into some of the wells. The wells into which water is injected are called injectors. Injected water enters the reservoir and displaces the oil towards the other wells from which oil is produced, which are called producers. Typically, there would be several producing wells surrounding an injector. The various flooding patterns used for waterflooding are shown in Figure 2.1.[1]

2.1.1 Factors to be considered While Planning a Waterflood.

In any given waterflood project, there will be certain factors such as reservoir fluid properties, reservoir rock properties, geologic stratification, faults and depth that are beyond the control of the reservoir engineer. The engineer could only vary parameters like injection fluid, injection pressure, injection rate, and well pattern. While planning an economic waterflood, the following reservoir rock and fluid properties need to be considered:

- Porosity,
- Permeability,
- Relative permeability,
- Interfacial Tension (IFT),
- Wettability,

- Capillary Pressure,
- Viscosity,
- Mobility Ratio,
- Fluid properties and relative permeability relationships,
- Continuity of reservoir rock properties,
- Magnitude and distribution of fluid saturations.

Even though certain factors like the price of oil, operating expenses, marketing considerations, and availability of fresh water play a vital role in waterflooding, these factors are not considered as part of the scope of this thesis.

2.1.1.1 Porosity

Porosity, according to Amyx, Bass and Whiting,[9] can be defined as the ratio of the void space in a rock to the bulk volume of that rock, expressed as a fraction or percent. According to them, porosity is a measure of the space available for storage of petroleum hydrocarbon. Since porosity is a direct measure of the oil storage within a reservoir, the volume of oil recovered is a function of porosity.

If a formation has higher porosity, then the formation has the ability to hold more fluids in it. According to Dyke,[10] the value of porosity could vary from less than 5 percent in a tightly cemented sandstone or carbonate to more than 30 percent in unconsolidated

sands. Further, Dyke[10] states that in order to commercially produce oil, a reservoir rock must have a porosity of 10 percent or more.

In general, as depth increases in a reservoir, the value of porosity decreases. This is because of the weight exerted by the shallower layers on the deeper layers.

2.1.1.2 Permeability

Permeability is a property of the porous medium and is a measure of the capacity of the medium to transmit fluids. Porosity and interconnection between pores are two factors that control permeability. Porosity defines the available space for a fluid to flow. Interconnection between pores defines the ease with which a fluid can flow from one pore to another.

Reservoir permeability is described as horizontal or vertical. During a waterflood, horizontal permeability is of more interest to engineers and geologists than vertical permeability, because of the necessity of connectivity between the injector and producer. While vertical permeability is of less interest, it may become important when considering water moving while bypassing oil at the top or bottom of the reservoir. According to Willhite,[7] the permeability cutoff most used in the carbonate formations of the Permian basin in west Texas is 0.1 md.

2.1.1.3 Wettability

Wettability is the tendency of one fluid to adhere to or spread on to a specific solid surface in the presence of another immiscible fluid. When two immiscible fluids come in

contact with a solid surface, one of the fluids is usually attracted more to the solid than the other. This fluid is generally called the wetting phase and the other is termed as non-wetting phase. According to Willhite,[7] wettability is explained quantitatively by examining the force balances between two immiscible fluids at the contact line between the two fluids and the solid. Generally, one of the fluids is water. As such, the contact angle measured through the water phase is the basis of measurement of the wetting phase. Contact angles less than 90° are called water-wet, and those approaching 180° are termed as oil-wet systems. When the contact angle is around 90°, then it is called intermediate wettability.

According to Smith,[3] addition of polar components like nitrogen, sulfur, or oxygen changes the film forming capability, and hence changes the wettability. He also explains that under certain circumstances chemically heterogeneous reservoir rock surfaces will have varying wettability characteristics due to the presence of some clay contents. Such wettability is called mixed wettability.

Morris and Wieland[11] carried out laboratory experiments in seventeen waterfloods in a monolayer glass bead flow cell under water-wet, intermediate wettability, oil-wet and wettability reversal conditions. Wettability reversal, according to them is achieved by changing the wettability of a rock, e.g., from oil-wet to water-wet. The authors accomplished this by changing the injection fluid from distilled water to 0.1 N hydrochloric solution. As soon as the injection took place, the contact angle changed at the fluids' interface.

They found that under water wet circumstances the oil recovery was constant and was independent of the water flow rate due to the presence of connate water. By

conducting film recordings and microscopic examination, they concluded that water tends to flow into the larger pore openings when a large hydraulic pressure gradient is applied. When small dye particles were passed through large pores at high velocities, they observed the larger pores to be more likely to experience a higher displacement rate, and oil in the smaller pores being bypassed. Once water breakthrough was achieved, oil trapped under strongly water-wet conditions were located as small islands of non-continuous nature, and water channels covering each oil patches.

When they measured the contact angle to be approximately 90 degrees, using visual measurements, indicating an intermediate wettability, the waterflood was very efficient. The residual oil saturation was noted to be extremely low compared to that obtained from water wet conditions. No oil globules were left behind in the larger pores as in the case for water-wet systems.

By increasing the concentration of octylamine, they created a strongly oil wet scenario to conduct waterfloods. Under these circumstances, the viscous fingering effect was very small. The phenomenon of numerous fingers of injected water penetrating into the oil zone is called viscous fingering. They observed the residual oil saturations to be both continuous and non continuous. The continuous oil was located in the center of the monolayer glass bead flow cell and was extended along the entire length, whereas the non-continuous residual oil was completely isolated and surrounded by water filled pore channels.

They carried out their experiments by changing the system from oil-wet to water-wet, and by varying the pH of the fluid system. While changing the system from oil-wet to

water-wet, they observed the oil being displaced from the bypassed pores which the oil-wet scenario failed to displace. They also found out that by varying the pH of the fluid system, it is possible to obtain a transient change in contact angle. Transient change here refers to the temporary change in contact angle, which could be restored once the variation in pH of the injected fluid is stopped.

2.1.1.4 Relative Permeability

Relative permeability can be defined as the ability of a porous media to conduct one fluid in the presence of other fluids. Willhite[7] defines relative permeability as an empirical method for correlating multiphase fluid flow in porous media with the saturation of the phases and the process followed in reaching a particular saturation. Relative permeability can be calculated using any of the two base permeabilities, namely:

- absolute permeability measured using air or water
- effective permeability to oil at irreducible water saturation.

In waterflooding, the most widely used base is the latter one, effective permeability to oil reservoir at irreducible water saturation, which results in an oil relative permeability of 1.0 or 100% at irreducible water saturation.

Effective permeability determined from laboratory measurements are normalized by the base permeability and therefore, the relative permeabilities are calculated as:

$$k_{ro} = \frac{k_{eo}}{k_{base}}, \qquad \text{Eq 2-1}$$

$$k_{rg} = \frac{k_{eg}}{k_{base}}, \qquad \text{Eq 2-2}$$

$$k_{rw} = \frac{k_{ew}}{k_{base}}. \qquad \text{Eq 2-3}$$

Imbibition and drainage are two terms that define the process of direction of saturation change in a waterflood operation with respect to the wetting phase. According to Craig,[1] imbibition refers to flow resulting in an increase in the wetting phase saturation. Furthermore, drainage refers to flow resulting in a decrease in the wetting phase saturation. For example, waterflooding a preferentially water-wet rock is an imbibition process, while waterflooding an oil-wet rock is a drainage process.

The wetting characteristic, either water-wet or oil-wet, is one of the factors that affect relative permeability. According to Amyx, Bass and Whiting,[9] when a rock is preferentially water-wet, water has lower mobility at a higher value of water saturation than when the rock is preferentially oil wet. Therefore, to define relative permeability, it is important to classify rocks as oil-wet or water-wet.

The rules of thumb indicating different wettability preferences are tabulated in Table 2.1.[1] When the connate water saturation is greater than 20 to 25 percent pore volume, the fluid is considered to be water-wet, and when it is less than 15 percent pore volume, it is classified as oil-wet.

Jones and Roszelle[12] proposed a graphical method to determine the relative permeability curves from displacement using an unsteady-state method. They suggested that using the unsteady method, it is impossible to obtain relative permeabilities for saturations between the initial and breakthrough values. Breakthrough in waterflooding occurs when the injected water arrives at the producer well. They plotted the oil and water

relative permeabilities as functions of water saturation, and concluded that, since all the variables were functions of cumulative injection, relative permeability is a function of cumulative injection. They then plotted the relative permeability curves using the available values, starting with the lowest water saturation. The unobtainable relative permeability curve was then calculated by interpolating the available saturation value obtained at breakthrough. Thus, they came up with a new technique using interpolation to calculate relative permeabilities for saturations between the initial and breakthrough values. The relative permeability curve plotted by them using their example data is shown in Figure 2.2. The lowest water saturation was 35% and the next highest water saturation at breakthrough was at 51.1%. In order to obtain the relative permeability values between water saturations 35% and 51.1%, the two points were joined by dotted lines and the relative permeability values were read from the graph. They concluded that by linearly interpolating the relative permeability curve on a graph, it is possible to determine the values of relative permeability that lie between the computed values and initial water saturation.

2.1.1.5 Interfacial Tension

Interfacial tension (IFT) is a fundamental thermodynamic property of an interface between two fluids and can be defined as the energy required to increase the area of the interface by one unit. Willhite[7] describes IFT as an interface between two immiscible fluids over a region few molecules thick having a limited solubility of one phase in the other. The typical units of IFT are dynes/cm or mN/m.

The concept of interfacial tension can be described by choosing a two-phase system similar to air and water. In this case, the interface is the region where the liquid phase meets the vapor phase. IFT at a phase boundary occurs because of the attractive forces between the molecules of same phase, which is larger than the one existing between molecules in the other phase. Due to the physical attraction between the molecules of the same phase, an imbalance of molecular forces occurs at the interface between the two phases. This imbalance of forces is termed as interfacial tension.

2.1.1.6 Viscosity

Viscosity is an important fluid characteristic to be considered during a waterflood. Viscosity can be defined as the internal resistance of the fluid to flow. With the increase in temperature, fluid viscosity decreases, because heating increases the distance between the molecules due to thermal expansion, thus reducing the internal resistance to flow.

Kinematic viscosity is the ratio of absolute viscosity to the density of the fluid. Kinematic viscosity (v) is mathematically represented as:

$$v = \frac{\mu}{\rho}. \qquad \text{Eq 2-4}$$

The inverse of absolute viscosity (μ) is called fluidity. With an increase of pressure, the viscosity of a fluid also increases and this is true if the hydrocarbon system is compressed above the bubble point.[9] If more than one phase exists during the compression process, the lighter constituents enter the liquid phase, and the liquid's viscosity is reduced.

2.1.1.7 Mobility Ratio

Mobility ratio is defined as the mobility of the displacing phase (λ_D) divided by the mobility of the displaced phase (λ_d). The concept of mobility ratio for a displacement process can be defined using the equation:

$$M = \frac{\lambda_D}{\lambda_d}. \qquad \text{Eq 2-5}$$

According to Willhite,[7] mobility ratio for a waterflood where piston-like flow is assumed with only water flowing behind the front and only oil flowing ahead of the front, is defined as below:

$$M = \frac{\left(\frac{k_{rw}}{\mu_w}\right)_{Sor}}{\left(\frac{k_{ro}}{\mu_o}\right)_{\bar{S}w}}. \qquad \text{Eq 2-6}$$

The above equation uses the relative permeability of water and oil obtained from the permeability/water saturation curves for a waterflood.

Mobility ratio can be evaluated in various ways, depending on the flow condition in a particular process. The important parameter while evaluating mobility ratio is at determining what saturation the mobility ratio is being evaluated.

Mobility ratio plays an important role in any displacement process by affecting macroscopic displacement efficiency (E_v), which according to Green and Willhite,[7] is a measure of how effectively the displacing fluid sweeps out the oil volume of a reservoir, both areally and vertically, as well as how effectively the displacing fluid moves the

displaced oil towards production wells. Macroscopic displacement efficiency is called volumetric displacement, also.

A mobility ratio less than one ($M < 1.0$) implies that the water velocity is less than the oil velocity and is called a stable displacement or a sharp front. When the mobility ratio is equal to one, it means that water velocity and the oil velocity are moving at the same rate through the reservoir. Furthermore, with an increase in mobility ratio, the saturation of the sharp front deteriorates, thus the front becomes unstable. This means that the injected water phase is moving faster than the oil ahead of the front. When the mobility ratio is greater than one ($M > 1$), numerous fingers of water penetrate into the oil, and this phenomenon is called viscous fingering.

In any oil recovery displacement process, the displacement efficiency (or recovery) can be considered as the product of microscopic and macroscopic displacement efficiencies.

$$E = E_D E_V . \qquad \text{Eq 2-7}$$

Microscopic displacement efficiency (E_D) refers to the mobilization of oil at the pore scale. According to Green and Willhite,[7] microscopic displacement efficiency is a measure of the effectiveness of the displacing fluid in mobilizing the oil at those places in a rock where the displacing fluid contacts the oil.

Displacement efficiency can also be defined as the ratio of the volume of hydrocarbon displaced to the initial volume of hydrocarbon pore space. Figure 2.3[7] shows the effect of mobility ratio on displacement efficiency of a linear waterflood model. The x-axis represents the cumulative water injected, and the y-axis represents the displacement

efficiency. It is evident that when M=1, the displacement efficiency is the highest. As M increases, the displacement efficiency decreases. For any waterflood process, the desired mobility ratio is less than or equal to one.

The variation of water-oil ratio with displacement efficiency for several mobility ratios is shown in Figure 2.4.[7] Willhite[7] reports that, given the same displacement efficiency, large volumes of fluid must be injected and higher water-oil ratios are produced when the mobility ratio increases.

If the mobility ratio is large, viscous fingering and an earlier breakthrough are more likely. Under such circumstances, the injected fluid sweeps a smaller area of the reservoir, resulting in a lower recovery at breakthrough.

Dyes et al.[13] carried out numerous experiments using an x-ray shadowgraph technique. They focused their study on the influence of fluid mobilities on the sweep out pattern resulting from the injection of gas or water. The period of study chosen was the production period, which followed breakthrough of the injected material. They examined the mobility ratios over a range from 0.1 to 17. Using five spot staggered, and direct line drive patterns, they concluded that ultimate oil recovery could be as much as 50% after breakthrough for these patterns.

2.1.1.8 Capillary Pressure

Capillary pressure in a porous media can be explained as the pressure difference existing between two immiscible fluids, both of which are static, in a capillary system. In general, capillary pressure can be expressed as the pressure difference between the non-

wetting phase and the wetting phase, which is a positive value in case of water wet rocks and is a negative value in case of oil wet rocks. In the case of oil-water capillary pressure system, the capillary pressure is expressed as the pressure difference between the oil phase and the water phase. Mathematically, capillary pressure is expressed as:

$$p_c = p_w - p_o . \qquad \text{Eq 2-8}$$

Allen and Puckett[14] carried out theoretical and experimental works to study the rate dependence of two-phase immiscible flow. Their work was aimed at establishing a calculation method to determine flood front shapes with high precision, to identify how saturation changed with displacement rate, and to confirm using laboratory measurements that theoretical predictions using a 1-D Lagrangian/Eulerian model and a black oil simulator were reproduced in linear core displacement tests. They compared the effects of capillary pressure on water displacing oil at core outlet to that using a simple Buckley-Leverett fractional flow performance. The general result was almost identical to that of Buckley-Leverett and is shown in Figure 2.5. The figure shows the fractional flow of water at the core outlet when the capillary pressure has a low value. It also compares the effect of capillary pressure on core outlet with that of a simple Buckley-Leverett fractional flow calculation. They observed that the when capillary pressure was greater, the difference between the two results could be large. Buckley-Leverett model is explained in more detail in section 2.1.2.1.

Yortsos and Fokas[15] developed exact solutions for a linear waterflood model including the effects of capillary pressure. Their mathematical model corresponds to a physically meaningful model of the linear waterflood process for suitable relative

permeability and capillary pressure. They modeled a waterflood to study the sensitivity to injection rate and viscosity ratios by fixing the irreducible saturation values at 0.15 and 0.0375 for oil and water, respectively. At favorable mobility ratios, capillary effects were prominent.

Residual oil saturation expressed as a function of a dimensionless group representing the ratio of viscous forces to capillary the forces is called capillary number (N_{ca}), where,

$$N_{ca} = \frac{u\mu_w}{\sigma_{ow}}. \qquad \text{Eq 2-9}$$

According to Yortsos and Fokas,[15] when the capillary number was 3.0, capillary effects were prominent, and Buckley-Leverett solution deviated from the exact results. Capillary dispersion, also called the Taylor effect, is the process of the displacing fluid being dispersed into the displaced fluid in a straight capillary. With larger values of capillary to viscous forces, the capillary dispersion affects both the saturation distribution and production characteristics. Furthermore, Yortsos and Fokas[15] suggested that their analytical model could be used to study and evaluate shock fronts, since the capillary number significantly affects both saturation distribution and production characteristics. Shock-front can be explained by considering a waterflood displacement process where a viscous fluid displaces both oil and low viscosity resident water. When the injected water miscibly displaces the resident water, the resident water forms the leading flood front. Due to the discontinuity in viscosity between the viscous and resident fluid, a second discontinuity in saturation forms at the viscous-water/resident-water boundary. This

discontinuity in saturation is termed as shock front. Figure 2.6 shows a typical shock front when there is a sudden drop in water saturation when the saturation value is equal to S_{wf}, at a dimensionless distance of x_{Df}.

2.1.1.9 Reservoir Continuity

A reservoir needs to be continuous between injectors and producers, if an injector is to displace oil to a producer. The injector and the producer need to be in the same zone in order to produce oil. Faults and other no flow barriers between injector/producer are a determent to the success of a waterflood.

A combination of analytical and interpretive techniques is used to test whether the injector and producer are in the same zone. If the samples taken from the injector and producer have same composition, then they are considered to be of the same reservoir.

2.1.1.10 Fluid Saturation

While considering a waterflood, high initial oil saturation is desirable, because a high recovery efficiency as well as high ultimate recovery is expected. If the water saturation is greater than the irreducible water saturation ($S_w > S_{wirr}$), then a sharp front may not develop.

Frick and Taylor[5] report that if the initial water saturation exceeds a critical value, then the formation of an oil bank may not take place. Above the critical value, water will be more mobile than the oil, and create viscous fingering, which will yield lower displacement efficiency. This critical water saturation can be identified on a fractional flow

curve as the tangent that cannot be formed while drawing the tangent from the irreducible water saturation.

2.1.2 Immiscible Displacement Process of Oil by Water

An immiscible displacement process can be defined as a process in which the displacing fluid does not mix in all proportions with the displaced fluid to form a single phase. Buckley and Leverett developed a theory by applying the law of conservation of mass to the one-dimensional flow of two fluids.

2.1.2.1 Buckley-Leverett Model

The theory of Buckley-Leverett[16] is the fundamental theory that governs immiscible displacement in one dimension. According to their classic work, oil displaced by water in a rock is like a leaky-piston. Based on the concept of relative permeability, they developed the theory of displacement for the physical conditions where the pressure drop is constant, and the fluids are immiscible. The assumptions made in the Buckley-Leverett model are listed below:

- A flood front exists, with only oil moving ahead of the front. Oil and water move behind the front.
- The core is a single homogenous layer.
- The cross-sectional area to flow is constant.
- Darcy's law applies for linear, steady-state flow.
- The gas saturation in front of the fluid is zero.

- Capillary and gravity effects are negligible.

Consider a core plug containing both oil and water. Using the concept of material balance, the total mass flow rate for an element dx can be represented as follows:

Mass flow rate in = Mass flow rate out + Mass accumulation.

$$q_w \rho_w\big|_x = q_w \rho_w\big|_{x+dx} + A\phi dx \frac{\partial(\rho_w S_w)}{\partial t}. \qquad \text{Eq 2-10}$$

The above equation can also be written as:

$$q_w \rho_w\big|_{x+dx} = q_w \rho_w\big|_x - \frac{\partial(q_w \rho_w)}{\partial x} dx. \qquad \text{Eq 2-11}$$

$$\frac{\partial q_w \rho_w}{\partial x} = -\frac{A\phi \partial(\rho_w Sw)}{\partial t}. \qquad \text{Eq 2-12}$$

Assuming incompressible flow, ρ_w = constant,

$$\frac{\partial q_w}{\partial x} = -\frac{A\phi \partial S_w}{\partial t}. \qquad \text{Eq 2-13}$$

$$\left.\frac{\partial q_w}{\partial x}\right|_t = -A\phi \left.\frac{\partial S_w}{\partial t}\right|_x. \qquad \text{Eq 2-14}$$

Considering the term $\frac{\partial S_w}{\partial t}$:

$$dS_w = \left.\frac{\partial S_w}{\partial x}\right|_t dx + \left.\frac{\partial Sw}{\partial t}\right|_x dt. \qquad \text{Eq 2-15}$$

Assuming a constant saturation plane such that:

$$dS_w = 0. \qquad \text{Eq 2-16}$$

The reservoir has a particular saturation at a particular time at a particular distance. Using the method of characteristics,

$$\left.\frac{\partial S_w}{\partial t}\right|_x dt = -\left.\frac{\partial S_w}{\partial x}\right|_t dx \quad . \qquad \text{Eq 2-17}$$

$$\frac{\partial S_w}{\partial t} = -\left.\frac{\partial S_w}{\partial x}\right|_t \frac{dx}{dt} \quad . \qquad \text{Eq 2-18}$$

Considering $\left.\frac{\partial q_w}{\partial x}\right|_t$ in Eq. 2-14:

$$\left.\frac{\partial q_w}{\partial x}\right|_t = \frac{\partial q_w}{\partial S_w}\left.\frac{\partial S_w}{\partial x}\right|_t \quad . \qquad \text{Eq 2-19}$$

Substituting Eq 2-18 and Eq 2-19 in Eq 2-14:

$$\frac{\partial q_w}{\partial S_w}\left.\frac{\partial S_w}{\partial x}\right|_t = A\phi\left.\frac{\partial S_w}{\partial x}\right|_t \frac{dx}{dt} \quad . \qquad \text{Eq 2-20}$$

$$\frac{\partial q_w}{\partial S_w} = A\phi\frac{dx}{dt} \quad . \qquad \text{Eq 2-21}$$

The fractional flow of water is defined as:

$$f_w = \frac{q_w}{q_t} \quad , \qquad \text{Eq 2-22}$$

$$q_w = f_w q_t \quad . \qquad \text{Eq 2-23}$$

Where q_w is the volumetric flow rate of water, and the total oil and water flow rate q_t is constant.

$$\frac{dx_{Sw}}{dt} = \frac{q_t}{A\phi}\frac{\partial f_w}{\partial S_w}\bigg|_{Sw}. \qquad \text{Eq 2-24}$$

By substituting v = dx/dt in Eq. 2.24, the velocity of the flood front is obtained.

$$v_{wf} = \frac{q_t}{A\phi}\left(\frac{\partial f_w}{\partial S_w}\right)_{Swf} \qquad \text{Eq 2-25}$$

Integrating equation 2.24 with respect to time gives the location of a particular saturation plane.

$$\int_0^{x_{sw}} dx = \frac{q_t}{A\phi}\frac{df_w}{dS_w}\int_0 q_t dt \qquad \text{Eq 2-26}$$

$$x_{Sw} = \frac{q_t t}{A\phi}\frac{df_w}{dS_w}\bigg|_{Sw} \qquad \text{Eq 2-27}$$

Substituting $W_i = q_t t$ in the above equation,

$$x_{Sw} = \frac{W_i}{A\phi}\frac{df_w}{dS_w}\bigg|_{Sw} \qquad \text{Eq 2-28}$$

The above theory of Buckley and Leverett is valid only when a sharp front exists. Buckley-Leverett equation is modeled with and no viscous fingering. For the calculation of oil rate and producing water oil ratio, three periods need to be considered namely pre-breakthrough, breakthrough, and post-breakthrough.

In the case of pre-breakthrough, the oil production rate is equal to the water injection rate and because of the assumption that the initial water saturation at the start of water injection is the same as the minimum or irreducible water saturation, the water-oil ratio is zero.

Since 1941, numerous works have been carried out to improve the Buckley Leverett model. In the Buckley Leverett model, capillary effects were not taken into account. Cardwell[17] explained that because capillarity was not accounted for on a water saturation versus distance profile (or saturation profile), certain intermediate saturations travel faster than other saturations, giving rise to triple values of water saturation for a given plane (x-distance). The triple value concept is illustrated on Figure 2.7.

From Figure 2.7, curve AGJ represents the initial water saturation versus distance. Later saturation distributions are well behaved only in the regions AB and HJ. The portions in between, calculated using Buckley-Leverett contains a portion BCDEFGH, which indicates there are three calculated saturations for each distances. This was corrected by Buckley-Leverett by drawing a vertical line CEG, from the upper branch to the lower branch of the curve, and stating the correct curve to be ABCEGHJ. Buckley-Leverett mentioned that the area enclosed by the loop CDEC was equal to the area enclosed by the loop EFGE. Welge[18] corrected some of the data going into the displacement calculation, which prevented the appearance of triple value. The corrections made by Welge was equivalent to using certain fictitious values of relative permeability values over a certain range of water saturations instead of actually measured values. Cardwell[17] argues that either the theory by Buckley-Leverett was wrong or there might have been something wrong with the experiments. Since the saturation profiles reveal the co-existence of three saturations at a single point in the linear displacement path, Cardwell[17] states this could be avoided by including the effects of capillary forces. Cardwell also states that the triple value arose from the incorrect mathematical physics chosen by Buckley-Leverett when the

saturation gradient approached infinity and occurred before the triple point. Dake[19] states that over the years, Buckley-Leverett's triple value saturation has been thought of as negligence of capillarity. Instead, it occurred because of Buckley-Leverett's absolute faith in rock relatiave permeability curves defined across the entire movable saturation range. Dake suggests that the triple value would not have arised if Buckley-Leverett were cautious while performing their computations.

Other theories about the triple values claim the use of alternative methods for solving the differential equation, instead of the 'method of characteristics' used by Buckley and Leverett. The use of the shock-front displacement concept in conjunction with their method would have nullified the effect of triple value.

Snyder and Ramey[20] developed a numerical reservoir model having a finite number of layers that communicate with each other in the wellbores and reservoir. They improved upon the work of Buckley-Leverett by including the variation of rock properties porosity, permeability, initial saturation, residual saturation, and relative permeabilities from layer to layer in a logical and consistent manner. Snyder and Ramey[20] used a modified Higgins-Leighton mathematical model to conduct their study, which involved a numerical solution to the Buckley-Leverett displacement equation, neglecting gravity and capillarity. In the stream tube model introduced by Higgins-Leighton in 1962, the assumptions made were that the streamlines were independent of the mobility ratio and that the Buckley-Leverett theory could be used to calculate the fluid displacement between adjacent streamlines. More information about the Higgins-Leighton model could be found at reference 21.

The waterflood performance of a reservoir using 10 layers was studied using the Buckley-Leverett method. Figure 2.8 and Figure 2.9 show the waterflood results when mobility ratio is equal to one. Figure 2.10 and Figure 2.11 show the waterflood results when mobility ratio is equal to ten, when the oil viscosity was increased to 40 cp. The curve, 'Buckley –Leverett Model 1' represents the Buckley-Leverett solution where all properties vary between layers. The curve, 'Buckley-Leverett Model 2' represents the Buckley-Leverett solution where only permeability varies. The constant values were equal to the average values used in the 'Buckley –Leverett Model 1,' Stiles and Dykstra-Parsons calculations. Snyder and Ramey[20] state that similar differences were earlier reported by Hiatt,[22] while comparing predictions made by Stiles and Dykstra-Parsons calculations with actual performance of water drive reservoirs. Snyder and Ramey[20] conclude that the difference is due to the combination of factors including the absolute permeability, porosity, initial saturations, residual saturations and relative permeability. Snyder and Ramey[20] claim that their numerical model, which could be applied to waterflooding and gas injection, represents the reservoir better than the Buckley Leverett model.

A numerical solution for the Buckley-Leverett equations was modeled by Sethian et al.[23] for immiscible displacement in a porous media. The main idea of their work was to accurately represent multidimensional flow. Sethian et al.[23] used the random choice method, where the generation of solution at each time step was based on the exact solution of a collection of local Riemann problems, so that the multi-dimensional flow could be represented accurately. The Riemann problem is beyond the scope of current work and could be found in more detail, under reference 24. Using the improved technique of

Sethian et al.[23] the multi-dimensional solution was obtained using a sequence of one-dimensional problems. Sethian et al.[23] used their model to study the nature of fingering instability. Sethian et al.[23] used their random choice method, their laboratory experiments were performed using five spot patterns. They found the front to be sharp, and the predicted time for breakthrough was accurate when compared to Buckley-Leverett.

Yortsos and Baomin[25] proposed the validation of Buckley Leverett theory for displacements at the macroscopic level, connecting the drainage process and the pore network using invasion percolation theory. Percolation theory deals with disordered media, where the disorder is defined by a random variation in the degree of connectivity (see Appendix A for additional details regarding percolation theory).

According to the opinion of Yortsos and Baomin[25] for the Buckley- Leverett model to be valid, the displacement process at the pore-network scale should not have viscous fingering. They also state that viscous forces do not lead to viscous fingering at smaller scales.

Langnes et al.[27] report that Roberts[28] modified the Buckley-Leverett model to be used for a layered model by making additional assumptions to the Buckley-Leverett model, namely:

- The reservoir could be represented as a series of layers.
- Water entering into each layer is directly proportional to its storage capacity (φ h).
- Cross flow does not exist between each layer.

Roberts[28] calculated the performance of each layer using the Buckley-Leverett method, and then added the recoveries obtained from each layer to obtain the total

recovery. Snyder and Ramey[20] later modified this work for application in a non-communicating layered system as follows:

- Each layer can have different initial saturations, residual saturations, and relative permeability-saturation relationships.
- Each layer can be divided into smaller cells, and calculations can be done from cell to cell, which permits closer observation of the movement of the front in each layer.
- The permeability resistance offered by each cell controls the injectivity into each cell, which varies as a function of time.

Langnes et al.[27] also reports that Johnson[29] proposed the double Buckley - Leverett technique, in a lecture at University of Southern California. This method is used in the case of hot water injection. Figure 2.12 describes the fractional flood front advance for a water-oil and water-water interface. When hot water is injected, followed by a waterflood process, a second waterfront occurs behind the oil-water interface. This second interface travels slower than the oil-water interface due to the difference in viscosity between the water-oil and water-water interface.

2.1.2.2 Frontal Advance Theory

Leverett[30] proposed the concept of fractional flow from Darcy's law for water and oil. The fractional flow equation in terms of viscosity, capillary pressure gradient, gravitational force, and water and oil relative permeability is derived below.

Capillary pressure as given by Eq 2-8 is defined as the pressure between the oil phase and the water phase. Density difference $\Delta\rho$ between the water and oil phase is given by:

$$\Delta\rho = \rho_w - \rho_o . \qquad \text{Eq 2-29}$$

The total volume flow rate, q_t, is defined as the sum of the water and oil flow rates, q_o and q_w, respectively. Mathematically:

$$q_t = q_o + q_w . \qquad \text{Eq 2-30}$$

The fraction of water flowing through the total flowing stream is given by:

$$f_w = \frac{u_w}{u_t} . \qquad \text{Eq 2-31}$$

Darcy's law for the linear flow of oil and water can be mathematically represented as:

$$q_o = -\frac{k_o A}{\mu_o}\left(\frac{\partial p_o}{\partial L} + g\rho_o \sin\alpha_d\right). \qquad \text{Eq 2-32}$$

$$q_w = -\frac{k_w A}{\mu_w}\left(\frac{\partial p_w}{\partial L} + g\rho_w \sin\alpha_d\right). \qquad \text{Eq 2-33}$$

Rearranging the above two equations,

$$q_o \frac{\mu_o}{k_o} = -A\left(\frac{\partial p_o}{\partial L} + g\rho_o \sin\alpha_d\right), \qquad \text{Eq 2-34}$$

$$q_w \frac{\mu_w}{k_w} = -A\left(\frac{\partial p_w}{\partial L} + g\rho_w \sin\alpha_d\right). \qquad \text{Eq 2-35}$$

The difference between the above two equations,

$$q_w \frac{\mu_w}{k_w} - q_o \frac{\mu_o}{k_o} = -A\left(\frac{\partial p_w}{\partial L} - \frac{\partial p_o}{\partial L}\right) - g(\rho_w - \rho_o)\sin\alpha_d . \qquad \text{Eq 2-36}$$

Rewriting the above equation by substituting Eq 2-8 and Eq 2-29:

$$q_w \frac{\mu_w}{k_w} - q_o \frac{\mu_o}{k_o} = \left(\frac{\partial p_c}{\partial L} \right) - g\Delta\rho \sin\alpha_d \,. \qquad \text{Eq 2-37}$$

By substituting Eq 2-30 into Eq 2-37:

$$q_w \frac{\mu_w}{k_w} - (q_t - q_w) \frac{\mu_o}{k_o} = \left(\frac{\partial p_c}{\partial L} \right) - g\Delta\rho \sin\alpha_d \,. \qquad \text{Eq 2-38}$$

Rewriting the above equation:

$$q_w \left(\frac{\mu_w}{k_w} + \frac{\mu_o}{k_o} \right) - q_t \frac{\mu_o}{k_o} = \left(\frac{\partial p_c}{\partial L} \right) - g\Delta\rho \sin\alpha_d \,. \qquad \text{Eq 2-39}$$

Dividing Eq 2-39 by q_t and re-arranging the equation:

$$\frac{q_w}{q_t} = \frac{\frac{\mu_o}{k_o} + \frac{1}{q_t}\left(\frac{\partial p_c}{\partial L} - g\Delta\rho \sin\alpha_d \right)}{\frac{\mu_w}{k_w} + \frac{\mu_o}{k_o}} \,. \qquad \text{Eq 2-40}$$

Substituting the definition of f_w as given by Eq 2-31 and dividing both the numerator and denominator of the right hand side of Eq 2-40 by $\frac{\mu_o}{k_o}$ gives the following form:

$$f_w = \frac{1 + \frac{k_o}{q_t \mu_o}\left(\frac{\partial p_c}{\partial L} - g\Delta\rho \sin\alpha_d \right)}{1 + \frac{\mu_w k_o}{\mu_o k_w}} \,. \qquad \text{Eq 2-41}$$

The above equation is called the general form of the fractional flow equation. Considering the displacement of oil by water in a horizontal system and neglecting the effects of capillary pressure gradient, the general fractional flow equation can be written in the following form, called the simplified form of the fractional flow equation:

$$f_w = \frac{1}{1 + \frac{\mu_w}{\mu_o}\frac{k_o}{k_w}}. \qquad \text{Eq 2-42}$$

Because relative permeability and capillary pressure are functions of the saturation alone, for a given set of rock, formation and flooding condition, the fractional flow of water, f_w, is a function of water saturation only. As the water saturation increases, the value of f_w increases with the increase in k_w and decrease in k_o.

Craig[1] reports about the effect of dip on the fractional flow curve. The effects are shown in Figure 2.13 and Figure 2.14 for a strongly water wet rock and a strongly oil wet rock. He also points out that it is possible to obtain negative values for f_w and comments about the physical significance of a negative f_w value is due to the absence of a capillary pressure term in the core or in the equation. In the presence of capillary forces, the values of f_w tend to be positive.

Furthermore, Craig[1] takes a closer look at the qualitative effect of capillary pressure gradient upon the fractional flow. He does this by separating the capillary pressure gradient (dP_c/dL) into the two components as described below:

- change of capillary pressure with water saturation, dP_c/dS_w,
- change in the water saturation gradient with length, dS_w/dL.

This is mathematically represented below:

$$\frac{\partial P_c}{\partial L} = \frac{\partial P_c}{\partial S_w}\frac{\partial S_w}{\partial L}. \qquad \text{Eq 2-43}$$

From the above expression, it could be concluded that when the water saturation gradient is low, the capillary pressure gradient is also low. Likewise, when dP_c/dS_w is low, dP_c/dL is

low. Since the water saturation decreases with distance in the direction of flow, the saturation gradient is always negative with an increase in length. As capillary pressure decreases with increasing water saturation ($dP_c/dS_w < 0$), the capillary pressure gradient tends to have a positive value, thereby increasing the value of fractional flow curve (Eq 2.41).

Maranon[31] suggested limitations of the application of fractional flow curve such that it is valid only for incompressible porous media with a linear geometry for displacement. He further suggested the addition of porosity to the calculations used for generating fractional flow curves. The basis for such a statement was because the fluid saturation depends upon the pore volume in the porous media and for immiscible fluids, the mobility for both fluids being different.

Buckley-Leverett[16] laid the foundation to the frontal advance equation in their legendary work. Later, Welge[18] determined a method to estimate the average water saturation with a simple, yet very useful concept of drawing a tangent to the fractional flow curve. This helped to calculate the oil recovery as a function of the cumulative water injected. According to Welge, the difference between the average water saturation and the initial saturation after breakthrough must be proportional to the oil recovered. Mathematically, it could be represented as:

$$Q_i f_{o2} = \bar{S}_w - S_{w2} . \qquad \text{Eq 2-44}$$

Buckley and Leverett[16] suggested the idea of balancing of the areas and Welge[18] later pointed out about the construction of a tangent to the fractional flow curve was equivalent to the balancing of the areas for determining the saturation at the discontinuity.

Welge constructed a tangent on the fractional flow curve from the initial water saturation through the breakthrough points. After drawing the above tangent, the fractional flow curve above the point of tangency was considered. A derivative was required for this portion of the curve as a function against S_w from S_{wf} to $(1-S_{or})$.

The concept of dimensionless distance is used to plot the saturation plane location vs. time as a set of straight lines, starting from the origin. The dimensionless distance (x_D) can be expressed as:

$$x_D = \frac{x}{L}. \qquad \text{Eq 2-45}$$

Dimensionless time, t_D could be expressed as:

$$t_D = \frac{q_t t}{A\phi L}. \qquad \text{Eq 2-46}$$

Using these concepts, Eq 2-27 could be re-written as:

$$x_{DS_w} = t_D f'_w. \qquad \text{Eq 2-47}$$

The saturation profile could be obtained by plotting the saturation on the y-axis and the dimensionless distance on the x-axis. The value of f'_w is scaled using the value of t_D to generate this plot. In order to calculate the average water saturation at any time after breakthrough, integration is done from x = 0 to x_D, for x_D less than or equal to x_{Dwf}.

$$\bar{S}_{wav} = \frac{\int S_w dx}{x}. \qquad \text{Eq 2-48}$$

$x_D = t_D f'_w$, where t_D is a scalar quantity.

$$\bar{S}_{wav} = \frac{\int_1^2 t_D S df'}{t_D f'} = \frac{t_D \int_1^2 S df'}{t_D f'} = \frac{\int_1^2 S df'}{f'}. \qquad \text{Eq 2-49}$$

$$\bar{S}_{wav} = \frac{\int_1^2 S df'}{f'} = \frac{S_{w2} f' - \int_1^2 f' dS}{f'} = S_{w2} - \frac{\int_1^2 f' dS}{f'} = S_{w2} - \frac{\int_1^2 \left(\frac{df}{dS}\right) dS}{f'}. \qquad \text{Eq 2-50}$$

$$\bar{S}_{wav} = S_{w2} - \frac{\int_1^2 df}{f'} = S_{w2} - \frac{f_2 - 1}{f'} = S_{w2} + \frac{1 - f_2}{f_w'}. \qquad \text{Eq 2-51}$$

$$f' = \frac{x_D}{t_D}. \qquad \text{Eq 2-52}$$

Therefore,

$$\bar{S}_{wav} = S_{w2} + \frac{t_D}{x_D}[1 - f_2]. \qquad \text{Eq 2-53}$$

At $x_D = 1$,

$$\bar{S}_{wav} = S_{w2} + t_D(1 - f_2). \qquad \text{Eq 2-54}$$

At breakthrough, i.e., at $f_2 = f_{wf}$:

$$\bar{S}_{wav} = S_{wf} + t_D(1 - f_{wf}). \qquad \text{Eq 2-55}$$

After breakthrough,

$$\bar{S}_{wav} = S_{w2} + t_D(1 - f_{w2}). \qquad \text{Eq 2-56}$$

The slope of the fractional flow curve is zero at the maximum injected fluid saturation.

$$f' = \left.\frac{df}{dS}\right|_{Sw=1-Sor} = 0. \qquad \text{Eq 2-57}$$

Before water breakthrough occurs, the amount of water injected is W_i, the maximum water saturation at this time is $\overline{S}_w = 1 - S_{or}$, and would have moved by a distance x_1. The flood front saturation, S_{wf} is located at a distance x_2 from the injector.

$$W_i = x_2 A\phi(\overline{S_w} - S_{iw}). \qquad \text{Eq 2-58}$$

$$(\overline{S_w} - S_{iw}) = \frac{W_i}{x_2 A\phi}. \qquad \text{Eq 2-59}$$

$$(\overline{S_w} - S_{iw}) = \frac{1}{\left.\frac{df_w}{dS_w}\right|_{Swf}}. \qquad \text{Eq 2-60}$$

Integrating the saturation profile,

$$\overline{S_w} = \frac{(1 - S_{or})x_1 + \int_{x1}^{x2} S_w dx}{x_2}. \qquad \text{Eq 2-61}$$

For a given volume of injected water and when $S_w \geq S_{wf}$, the above equation can be written as:

$$\overline{S_w} = \frac{(1 - S_{or})\left.\frac{df_w}{dS_w}\right|_{(1-Sor)} + \int_{1-Sor}^{Swf} S_w d\left(\frac{df_w}{dS_w}\right)}{\left.\frac{df_w}{dS_w}\right|_{Swf}}. \qquad \text{Eq 2-62}$$

Evaluating the numerator of the above equation,

$$\int_{1-Sor}^{Swf} S_w d\left(\frac{df_w}{dS_w}\right) = S_w \left.\frac{df_w}{dS_w}\right|_{1-Sor}^{Swf} - f_w\Big|_{1-Sor}^{Swf}. \qquad \text{Eq 2-63}$$

Substituting the above term in equation 2.62,

$$\overline{S_w} = S_{wf} + \frac{(1 - f_w|_{Swf})}{\left.\frac{df_w}{dS_w}\right|_{Swf}}. \qquad \text{Eq 2-64}$$

Equating Eq 2.60 and Eq 2.65,

$$\left.\frac{df_w}{dS_w}\right|_{Swf} = \frac{1 - f_w|_{Swf}}{\overline{S_w} - S_{wf}}. \qquad \text{Eq 2-65}$$

$$\left.\frac{df_w}{dS_w}\right|_{Swf} = \frac{1}{\overline{S_w} - S_{iw}}. \qquad \text{Eq 2-66}$$

Numerous works have been carried out based on Welge's[18] derivation. Mohsen[32] in 1985 proposed a new method for an approximate location of the front on the basis of mass conservation for a condition where the water saturation is greater than the residual water saturation. According to Mohsen,[32] Welge's[18] method yields the correct front location only in the special case of zero initial condition, i.e., when $S_w(x,0) = S_{wr}$ for all values of x. Mohsen[32] also proposed that the location of the tangent Welge choose was dependent on time and was a function of the initial distribution, thus, showing Welge[18] to be wrong, who stated that the point of tangency remained the same at all times.

El-Khatib[33] pointed out the above method of Mohsen[32] to be incorrect, since the initial saturation distribution calculated by Mohsen[32] was not realistic due to the discontinuity of dS_o/dx. In his opinion, in an actual scenario, S_o would always be greater than S_{wi} and the new method would produce incorrect results during the entire production history till water breakthrough. Another mistake pointed out by El-Khatib[33] is about Mohsen's[32] assumption that S_1 is always equal to S_{wi}, which would lead the initial volume of water (W_i) to become zero.

Mohsen[34] addressed the discussion from El-Khatib[33] in his next paper, describing the main objective of his previous paper[32] was to show that, for a case of non-zero initial conditions, if the front is to be located by a tangent, it must be drawn to the W_i/S_w curve and not on the f_w/S_w curve as recommended by Welge.[18] The second point made by Mohsen[34] was the redundancy for a tangent method in the absence of a triple valued situation. According to him, under such a circumstance the simple frontal advance postulated by Buckley-Leverett was sufficient.

Welge[35] in 1986 addressed this issue by responding that the modification by Mohsen[34] was unnecessary since Mohsen[34] failed to understand or include the statement present in his work which read: "because of the initial saturation (connate water) of the driving liquid, the considerations described in connection with the tangent construction now require that the tangent be drawn from a point on the fractional flow curve lying at the height of the original water saturation, rather than from the origin" (p 430). Further, Welge[35] also pointed out that there could be no sharp front if the starting water saturation was sufficiently high and no tangent construction would be possible under such a circumstance.

The issue was once again brought up by Mohsen[36] saying that he disagreed with Welge[35] about the Welge[35] method being representative in the case of non zero initial condition as well as zero initial condition. This time, he again stressed about his accuracy of the tangent being at the point of maximum slope.

Chen and Whitson[37] compared the above scenario and concluded that Mohsen's[32] method was correct for a non-uniform initial saturation distribution. They suggested the

use of Mohsen's[32] method when the front has propagated towards a distance x*, which is the distance where initial water saturation first equals the irreducible water saturation. Chen and Whitson[37] further divided the saturation front diagram into four regions, as shown in Figure 2.15, namely:

Region A – saturation discontinuities do not exist

Region B – Two point tangent methods used

Region C – Mohsen's modified Welge method

Region D – Original Welge method could also be used.

As of this writing, no other papers reinforcing the concepts about saturation front were found, which continued this discussion.

2.1.3 Factors Affecting Areal Sweep Efficiency

Areal sweep efficiency, according to Green and Willhite[7] is the area swept divided by the total reservoir area within an injected pattern. For an idealized reservoir, where the porosity, permeability and thickness stay uniform, the areal sweep efficiency can be called the pattern sweep efficiency. Under such circumstances, it is defined by Willhite[7] as the hydrocarbon pore space enclosed behind the injected fluid divided by total hydrocarbon pore space in the flooded formation within the pattern.

Injector-producer well pattern is one of the factors that control the areal sweep efficiency. Muskat[38] and Deppe[39] proposed methods for calculating injectivity for several regular well patterns with unit mobility ratios. The most successful waterflooding pattern reported by Willhite,[7] in terms of recovery, is the 5-spot pattern. The various patterns and

the injectivities suggested by Deppe[39] are illustrated in Figure 2.16. Deppe[39] approximated the pattern by first dividing them into segments of radial and linear flow and computing the total flow by summing up the radial and linear flow equations that were applicable to the individual segments. While estimating the injectivity, he divided the volume of the pattern among the producing wells of the pattern and later approximated the volume assigned to each well by regions of radial and linear flow. One assumption made by Deppe was that the flood front advanced radially in the radial regions and lineary in the linear regions before and after breakthrough was achieved. The work carried out by Deppe[39] could also be used to estimate the injectivity of irregular patterns.

According to the studies performed by Muskat[38] and Deppe,[39] as the of mobility ratio increases, the areal sweep efficiency decreases because the displacing fluid (water) travels faster than the displaced fluid (oil). This causes an inequality in velocities to develop between the two fluids, giving rise to an unstable front and viscous fingering.

Permeability anisotropy is one of the factors that affect areal sweep efficiency. Sandrea and Farouq-Ali,[40] studied the effect of permeability anisotropy. They looked at the effects of rectilinear impermeable barriers and highly permeable channels present between the injection and producers in a five-spot pattern. According to them, when an impermeable barrier has an interference modulus greater than zero, the conductivity as well as sweep efficiency of the pattern decreases. Permeability channels, in their opinion, when located along the streamlines shorten the distance between the injector and producer, causing early breakthrough.

Directional permeability is the ordered non-uniformity in which the horizontal permeability in one direction is significantly greater than the one in a perpendicular direction. Landrum and Crawford[41] studied the effects of directional permeability in various waterflooding patterns with unity mobility ratio and steady state flow. They neglected the effects of gravity and capillary effects. From their work, it was evident that by adjusting the geometry of the injector-producer arrangement, the effects of directional permeability could be minimized. Another suggestion made by the authors is that pattern dimensions should be increased in the direction of greater permeability. For a line drive and five spot pattern, the impact of directional permeability on sweep efficiency is illustrated on Figure 2.17 and Figure 2.18. Figures 2.19 and 2.20 represent the variations of production capacity under the same conditions. When the direction of permeability is observed to lie in a manner in which the direction of the maximum permeability is parallel to the line connecting adjacent injection wells, the areal sweep efficiency is said to be the maximum.

The effect of formation dip was studied by Prats et al.[42] and Matthews and Fischer[43] on a five-spot waterflood pattern with unity mobility ratio. According to them, the fluid injectivity was not affected by the dip of the formation. They improved the sweep efficiency by modifying the location of the central well (injector) to achieve equal breakthrough times from both updip and downdip wells. With the presence of gravity effects, the best method is to inject the water along the edge of the pay zone, near the base of the oil column. The gravity effects, allowing maximum sweep of the injected water, segregate oil and water.

Prats et al[42] studied the effects of irregular oil well patterns and found that the recovery with such a pattern is always lower. Their work was based on the following assumptions:

- The reservoir is thin and horizontal.
- The reservoir has uniform porosity, permeability and thickness.
- Initially, the only mobile fluid in the formation is oil.
- Mobility ratio is 1.
- Throughout the field, the injection and production rates are constant.
- Between the oil and water bank, there is a sharp boundary.

In their observation, even after the individual wells reached an economic limit of 98%, the producing wells were observed to be flowing.

According to their work, an early increase in producing WOR will occur at the producer or producers nearest to the injector, and will be offset by the late rise in producing WOR at the producer, farthest from the injector. Figure 2.21 to 2.27 could be used to evaluate multiple irregular patterns, when the irregular patterns are separated by at least one normal five spot pattern. The performance of a regular five spot pattern could be studied using Figure 2.21 to Figure 2.27. According to the Prats et al.[42] the other curves were keyed to the well diagrams included in the water-cut history figures. Prats et al.[42] used the notations D for diagonal displacement and L for lateral displacement of the wells.

Craig et al.[44] studied the effects of continued injection after breakthrough and concluded that such an injection would result in substantial increase in recovery, even in case of an adverse mobility ratio. Habermann[45] suggested that even after reaching

breakthrough, there is a substantial amount of oil left behind in the reservoir, which could be swept after breakthrough. He showed that if the mobility ratio was higher, the after breakthrough production was much more important. Figure 2.28 shows the change of breakthrough efficiency from 51% from a mobility ratio of 10 to an efficiency of 100% at a mobility ratio of 0.17.

The effects of fractures, both horizontal and vertical, play important roles in the areal sweep efficiency. Clark[46] introduced the technique of hydraulic fracturing in 1948 which increased oil production rates from wells within any type of formation. The method is useful for water as well as gas injection wells. One of the favorable factors quoted by Clark[46] is lower cost when compared to acidizing.

The effective wellbore diameter is increased by the horizontal and vertical fractures either at the injector or at producers. Landrum and Crawford[41] studied the effect of horizontal fractures and made the following conclusions:

- The effect of horizontal fractures on areal sweep efficiency depend upon the fracture radius.
- At very small fracture radius, the effect is almost unnoticeable.
- Low radius fractures can almost double injectivity.
- With the increase of radius, the effect of areal sweep efficiency is reduced.

Vertical fractures have significant effects on areal sweep efficiency. Dyes et al.[47] studied vertical fractures using five spot patterns. The findings by Dyes et al.[47] are shown in Figure 2.29 through Figure 2.32, and could be used while considering natural fracture

system. These figures could be used to plan the flooding pattern in order to reduce the impact of the fracture system.

Vertical fracture when oriented in a favorable direction has little effect on sweep efficiency. Favorable direction refers to the injector-injector fracture alignment. Once the vertical fracture is oriented in an unfavorable direction, the breakthrough areal sweep efficiency decreases with increasing fracture length. In other words, fracture orientation is more important than fracture length. Simmons et al.[48] reported that a fracture length of about 1/3 the distance between injector and producer affected breakthrough efficiency regardless of orientation.

Frailey et al.[49] used a reservoir simulation method using historic field data to determine the fracture orientation and possible effects on volumetric sweep efficiency. They point out that an injection well must be fractured before breakthrough to use the time for breakthrough as a parameter to identify fracture orientation. They used a single-layer homogenous model and a five-layer heterogeneous layer model to study the effect of fracture orientation. According to their results, it is necessary to know the degree of heterogeneity of a reservoir before conducting the analysis, because an injector without a fracture in homogenous reservoir appeared similar to an injector with a fracture in a heterogeneous reservoir.

2.1.4 Factors Affecting Vertical Sweep Efficiency

Because non-uniform permeabilities prevail in a reservoir, the injected fluid moves as an irregular front, moving readily in the high permeable sector, than the less permeable

sector. Vertical sweep efficiency can be defined as the ratio of the cross sectional area contacted by the injected fluid to the cross sectional area enclosed in all layers behind the injected fluid front.

The main factors affecting vertical sweep efficiency are below:

- gravity segregation due to density difference,
- mobility ratio,
- vertical to horizontal permeability variation,
- capillary forces.

Gravity segregation occurs when large density differences prevail between the injected water and displaced oil that are significant enough to induce flow in the vertical direction even while horizontal flow is the principal direction. Under circumstances of the injected fluid being less dense than the displaced fluid, gravity segregation occurs and the injected fluid overrides the displaced fluid. Such segregation is called gravity override. The opposite condition when the displaced fluid is denser than the injected fluid, again gravity segregation occurs which is termed as gravity underride. Gravity override and underride is illustrated in Figure 2.33. During a waterflood operation, water being generally denser than oil moves down below oil. According to Willhite,[7] injecting relatively higher rates of water could reduce gravity segregation under such conditions.

Spivak[50] carried out reservoir simulation to determine the factors affecting gravity segregation in a 2-phase, secondary recovery displacement process. Based on his results, Spivak[50] states that gravity segregation increases by:

- increasing permeability, either in the vertical or horizontal direction,

- increasing the fluid density difference,
- increasing the viscosity ratio.

According to Spivak,[50] gravity segregation decreases by:

- increasing the flow rate,
- increasing level of viscosity for a given viscosity ratio.

Wyckoff et al.[51] studied waterflood patterns using a technique involving the use of electrolytic models and blotters soaked in an electrolyte for tracing the approximate shape of the flooded zone between the injector and producer. While tracing the advancement of water into an oil horizon using both line drives and five spots, Wyckoff et al.[51] also considered the effects of gravity segregation. According to Wyckoff et al.,[51] because water has a higher density than oil, it has a tendency to move preferentially through the bottom of the formation.

Craig et al.[52] conducted a laboratory study using scaled reservoir models to understand gravity segregation in frontal drives. Craig et al.[52] used a laboratory flow test model for both line drive and five spot patterns. Dyed fluids were used to track the motion of the injected fluids and covered the range of injection rates normally used for field applications. According to their results of the model studies, when capillary effects are neglected and flow rate is reduced, the oil recovery rate is low. Permeability distribution of the reservoir is another factor that affects the oil recovery rate. Their findings indicate that oil recovery at breakthrough is largely affected by fluid segregation caused by the variation in rock properties than by gravity segregation.

Gravity underride or override is enhanced when the mobility ratio is greater than unity. Green and Willhite[7] reported that whenever gravity effects are important and the mobility ratio is unfavorable, vertical sweep could be affected by both the tendency of the displacing fluid to flow into the gravity tongue and the superposition of viscous fingers onto the gravity tongue.

The effect of mobility ratio on relative injectivity in a liquid saturated radial system is shown in Figure 2.34. The relative injectivity, according to Craig,[53] is defined as the ratio of the injectivity index at any time to that at the start of injection in a liquid-filled reservoir. When the mobility ratio M is one, the relative injectivity is a constant. When M is less than one, the injectivity decreases with an increasing flood-front radius. Injectivity gradually increases when M is greater than one. The relative injectivity become equal to mobility ratio during breakthrough.

Craig, Geffen, and Morse[44] in their classic paper, presented a technique for predicting oil recovery performance from five-spot patterns using modifications from Buckley-Leverett and frontal advance equations. They said that from an areal sweep perspective, mobility ratios less than unity is favorable. Another observation made was that the injected fluid mobility constantly decreases from the injection-well towards the flood front at breakthrough.

Gaucher and Lindley[54] used a three-dimensional, five-spot, two-layered model by scaling capillary, gravitational and viscous forces, to study the rates of recovery with different viscosity oils. They observed that oil recovery efficiency was dependent upon the degree of distribution of permeability stratification. They obtained highest recovery when

the upper layer was almost twice as permeable as the lower sand. Figures 2.35 and 2.36 shows the observed flood fronts for two water injection rates were higher at three different cumulative pore volumes injected, when the higher permeable layer was on top. Gaucher and Lindley[54] believe that for the case when the upper sand was more permeable, high viscous pressure gradients controlled the shape of the front, both at higher and lower injection rates. The most effective results were observed when 1.0 pore volumes were injected at lower rates, since a larger portion of the tight sand was contacted by water. The reason for such increased rates of water injection was due to the tendency for viscous fingering in the horizontal plane. Recovery was observed to decrease with increased rate of water injection and higher viscosity oil.

When the more permeable layer was at the bottom, it was observed that a vertical front was formed at the bottom of the model, which developed subsequently due to gravity segregation into a thin long layer. The authors believed that, oil was produced due to the combination of capillary imbibition of water into the oil bearing sand and displaced oil by the viscous pressure gradients.

2.1.5 Factors Affecting Volumetric Sweep Efficiency

Willhite[7] defines volumetric sweep efficiency (E_V) as the product of the areal (E_A) and vertical (E_I) sweep efficiencies. In other words, volumetric sweep efficiency is the product of the fraction of the reservoir cross section that has been displaced by the injected water (E_A) and the fraction of the reservoir area within the vertical portion of the reservoir that has been swept (E_I) to residual oil saturation.

The effects of change in fluid injectivity, mobility ratio and permeability variation on volumetric sweep efficiency at breakthrough was studied by Craig,[53] using a single-zone model derived from a 24 layered model. According to Craig,[53] the volumetric sweep efficiency at breakthrough decreases when the permeability variation increases. Permeability variation (V) is defined as

$$V = \frac{\bar{k} - k_{\sigma}}{\bar{k}} \quad . \qquad \text{Eq 2-67}$$

Figure 2.37 shows the volumetric sweep efficiency for a five spot pattern with no initial gas saturation. Craig[53] found that the largest effect of mobility ratio (for any permeability variation) on breakthrough sweep efficiency was between M = 0.1 and M = 10.0 and the greatest effect was observed near M = 1.0. Figures 2.38 through 2.39 show the volumetric sweep efficiency at water breakthrough with initial gas saturation. When the initial gas saturation increases, the volumetric sweep efficiency at breakthrough at lower permeability variation tends to flatten out. When water is injected continuously, volumetric sweep efficiency continues to increase until the maximum sweep efficiency is reached. Higher volumetric sweep efficiency at water breakthrough gives a sign of an increased sweep for any injected fluid volume after breakthrough.

Craig[53] concluded that mobility-reducing techniques are less attractive for reservoirs with increasing heterogeneity and for reservoirs with increased initial gas saturation. He concludes that there was no advantage for waterfloods having natural mobility ratios of 0.1 or less, because for a five-spot pattern, the breakthrough volumetric sweep efficiency has a major effect only when the mobility ratio is between 1 and 10.

2.2 Flow through Porous Media

Flow through porous media is one of the most complicated fluid flow processes, when compared to regular flow methods like flow through pipes, because it involves numerous unknown factors. In order to understand the process better, it is desirable to know details about the pore, porous media and the fluids flowing through them.

Pores, usually measured in terms of microns, are void spaces that are distributed in a random fashion through the porous material. Voids that are extremely small are called molecular interstices and extremely large voids are called caverns. Pores fall intermediate between the molecular interstices and caverns. The pores within a porous medium could be either interconnected or non-interconnected. Interconnected pores allow the flow of fluids through them, while non-interconnected pores do not.

Pore spaces are classified under many classes.[55] A single porous media may contain many classes of pore spaces. In general, pores are classified into voids, capillaries, and force spaces. Voids are classified by the fact that they only have a significant effect upon the forces and motion of fluids acting upon their inner walls. The walls of capillaries do have a significant effect upon the forces and motions of fluids acting upon them, but do not bring the molecular structure of the fluid into evidence. Force spaces are pores that bring molecular structure of the fluid into evidence.

One of the well-defined geometrical properties of a pore is the porosity, which is the ratio of the void space to the bulk volume. Specific internal area is another geometrical quantity, which is the ratio of the internal area of the pore to the bulk volume of the pore.

Apart from the above classification, pores are sub-classified as ordered or disordered and dispersed or connected. Bear[55] has an additional pore classification called dead end pores, which have a narrow, single connection to the interconnected pore space where no continuous flow takes place between them.

In order to clearly define the geometry of a pore, it is highly desirable to be able to estimate the size of the pore in a porous medium. Scheidegger[55] states that the pore system of a porous medium forms a very complicated surface, which is geometrically difficult to describe. He states that it is not possible to find any simple parameter or simple function, which describes the surface of a pore and therefore will not be able to encompass all properties of a pore.

A pore diameter can be defined if a pore has a tubular shape. The diameter of the pore can then be called as 'pore diameter.' The cross section could vary since the pores converge and diverge. Therefore, it is difficult to specify a largest or smallest diameter of a pore.

Ryder[57] explains the fundamental operation in all oil recovery as, oil is pushed, pulled or dragged from a position in a pore by water, gas, capillary forces or gravity. He therefore stressed on the fundamental problem of an oil producer as to how to profitably remove most oil from each microscopic pore. Ryder[57] conducted laboratory observations under a microscope and concluded that water displacing high oil saturations tend to produce more oil. He also observed that while gas was displacing oil under pressure, the interfacial tension prevented the gas from bypassing the oil through the constrictions (in this case, the pore throats with smaller diameter). Ryder[57] observed that oil particles were

being displaced to the producing wells, unless they were trapped in some dead-end pores. The oil remaining in such dead end-pores, in his opinion, constituted the unproduced 'residual oil saturation.'

Arriola et al.[58] conducted laboratory experiments to study the trapping and mobilization of oil drops in a capillary of square cross section, since non circular pore constructions provide the possibility of provide the possibility of the wetting phase bypassing a trapped oil drop. According to their results, trapping of an oil drop in a water-wet rock occurred when the drop became hydrodynamically stable in a pore. In other words, an oil droplet is said to be stable when the drag forces exerted by the flowing water on the oil drop are unable to overcome capillary forces associated with the size of a particular pore throat.

Mohanty et al.[59] explained in detail about the mechanism of displacement and entrapment of oil at the pore level. According to them, the factors affecting movement of oil at the pore level are controlled by the pore geometry and fluid properties. Pore geometry, according to them is the shape of the pore. They considered the case of a water-wet pore and explained the menisci of oil-water system. In their opinion, there are two types of menisci: head menisci and neck menisci.

Head menisci, according to Mohanty et al.[59] are concave towards oil and its Gaussian curvature (see Appendix B) is positive. These kinds of menisci tend to occupy wider regions of pore spaces and are often referred to as the pore body. Neck menisci, according to them are saddle shaped with its gaussian curvature negative. Neck menisci constitute the pore throats. Figure 2.40a shows an oil-water interface for a single pore, and

Figure 2.40b shows a pore model in terms of head menisci and neck menisci. Apart from the above head and neck menisci, they also referred to draping menisci, which are grooves, pits and pockets. Pressure connection is not provided in such case. Pressure connection is illustrated in Figure 2.40b within the wetting phase.

The oil trapped inside a pore has a stable energy configuration under static equilibrium. To displace an oil globule trapped within a porous media, the oil globule needs to be unstable. When the external conditions are changed, the interfacial configuration loses its stability and tends to move to an adjacent pore. Detailed study about stability analysis of head and neck menisci is discussed in reference 59.

Whenever oil is displaced by water in a porous media, two kinds of phenomenon are observed during the literature review, namely:

- Haines' Jump Phenomenon,
- Snap-off Phenomenon.

2.2.1 Haines' Jump Phenomenon.

Castor and Somerton[61] explain Haines Jump as a phenomenon that could be described as any sporadic configurational instabilities which accompany the displacement of a fluid interface from a porous media. To understand the above statement, consider a fluid being displaced by another fluid through a capillary tube with varying cross section. A two-fluid meniscus which moves towards the narrower end of the capillary from the wider end due to capillary pressure difference, jumps back towards the widen end as the saturation of the wetting phase decreases. The occurrence of such a phenomenon in a

porous media is termed as Haines jump and is illustrated in Figure 2.41. This phenomenon was first observed by Haines[62] in 1930. According to Haines,[62] a two-fluid meniscus advances through an irregular pore in a series of advancements. Between the advancements, the meniscus creeps forward a short distance, until instability develops and the next advancement occurs.

Oh and Slattery[63] carried out several laboratory experiments using a capillary tube model to study the recovery of residual oil by a low interfacial tension waterflood. During their studies, they used a single irregular pore partially filled with oil to carry out the investigation of interfacial tension. From their study, it was evident that the most efficient displacement of residual oil was possible from a water wet porous structure or an intermediate wet (partially wet with oil and water). An advantage with intermediate wettability, pointed out by the authors, is that all residual oil could be displaced if the interfacial tension is low enough. With an oil-wet porous media, all oil spreads out as a film on the pore wall, which makes it difficult to displace.

Figure 2.42 illustrates a model pore containing a segment of residual oil. The residual oil trapped inside the pore is isolated as a blob occupying neighborhood pores. Figure 2.43 shows the sequence of motion of a large oil segment moving through a water-wet pore over a ring of water trapped on the wall of the pore. As the oil segment moves over the trapped ring of water, there is a discontinuity in the oil movement. Figure 44 indicates the movement of a smaller water segment while being displaced through a water-wet pore. The isolated spherical drop is moving from left to right, when the pressure difference is large enough. The oil segment squeezes through the pore throat and returns to

its original shape in the next pore. When the pressure difference is not large enough, this oil segment gets trapped within the pore.

Figure 2.45 shows the sequence of motion, as a large oil segment moves through and oil-wet pore, leaving behind a portion of oil, as it advances from left to right. Oil is trapped, while moving through the pores and the volume of the initial oil segment is reduced during the motion. Figure 2.46 explains the process of movement of a smaller oil segment under oil-wet conditions. The shape of the oil segment changes while moving through the pore-throat, and a portion of the oil segment adheres to the walls of the pore. Figure 2.47 shows the pressure drop required to hold an oil segment while moving from left to right, as a function of the position of its trailing interface. Haines jump is indicated on the figure.

2.2.2 Snap-Off Phenomenon

While an oil drop moves through a constriction into a pore filled with the wetting phase, which is either oil or water, part of oil drop breaks off into a smaller droplet and moves ahead of the primary drop. This mobilization phenomenon is termed as snap-off.

Pickell et al.[64] first observed the snap-off phenomenon in 1966. They used a laboratory model to study the pore structure and degree of fluid interconnections at various saturations. They found that the interface between two liquids in a porous medium could be viewed as curved with the non-wetting liquid always on the side containing the center of the smallest radius of curvature, as shown by Figure 2.48b. Figure 2.48(a) represents the smaller radius and Figure 2.48(b) represents the larger radius. Figure 2.48 (a) and 2.48(b)

each have two radii of curvature, where r_a represents the smaller radius of curvature and r_b represents the larger radius of curvature. They suggested the use of the Laplace expression below to relate capillary pressure and the curvature of the interface:

$$P_c = \sigma\left[\left(\frac{1}{r_a}\right)+\left(\frac{1}{r_b}\right)\right] \qquad \text{Eq 2-68}$$

where σ is the interfacial tension between the two immiscible fluids, in this case, oil and water.

They examined the injection and withdrawal of oil through a single pore, which had triangular cross-section represented by Figure 2.49. They observed the injection pressure rise to a maximum value while the oil front was forced through the narrowest point. When the injection was continued, the pressure reduced because of the increase of radius of curvature. The resulting reduced pressure noted at this point did not support the smaller effective radius of curvature at the narrowest part of the pore throat and the configuration of the interface at that point was observed to change, pinching the oil. This process was named as snap-off process.

They also studied how capillary forces were involved in the displacement of oil by water. In their opinion, with water-wet rocks and a reasonably low oil/water viscosity ratio, capillary forces are involved in the displacement process.

Roof[65] used a single pore with circular cross section, which he called a doughnut-hole pore, to study the snap-off phenomenon. He studied the conditions required to separate oil emerging from water-wet formations. He observed as water enters the water-wet pore, a very thin layer of water remains between the oil and the wall of the pore.

Roof[65] agrees with Pickell et al.[64] about the fundamental equation of capillarity, which relates the capillary pressure difference across the interface to the interfacial tension and the principal radii.

The observations made by Roof[65] are shown in Figure 2.50. From these figures. he observed that for a circular cross sectional pore, the oil drop needs to protrude beyond the throat for a distance of at least seven times the pore throat radius before snap-off occurred. He explained this as oil needs to have a passageway into the throat to permit the snap-off process.

Roof[65] also observed the formation of a collar of water around the oil in the pore throat. The formation of this water collar was necessary before snap-off occurred. In his observation, if a water collar was formed and the protrusion of oil was retracted below the minimum length of seven times the pore throat radius, the collar disappeared.

Another finding by Roof[65] was that snap-off in circular cross-sectional pores occurred relatively slowly when compared to other cross-sections because water could not flow readily into the collar. Non-circular cross-sectional pores allowed water to bypass the oil drop and helped form the collar rapidly.

Arriola et al[58] conducted laboratory experiments to study the trapping and mobilization of oil drops in a capillary of square cross section. According to their results, snap-off was found to be occurring at the pore throat. The instability of oil drop was observed at the interface between the oil and flowing water, which became large enough to initiate rupture at the oil-water interface. Their results were slightly different from that of Roof[65] about the snap-off process, since the formation of a collar around the oil drop was

not observed. They also found that by using a square cross-sectional capillary tube, about 94% of the non-wetting phase occupied the flow area in a water-wet capillary tube and the bypassing phenomenon described by Roof[65] occurred through the remaining 4% of the flow area. A marginal stability curve was created by them to define stable and unstable regions and is shown in Figure 2.51. The x and y coordinates of the graph are distance, and the dimensionless quantity $P_C R_1/\sigma$ respectively.

Arriola et al[58] observed the velocity of displaced oil drops to be slightly less than the average injected water velocity. Literature about velocity of oil movements through porous media could be found elsewhere.[66,67]

2.3 Visual Basic

The following section of this thesis is written with the intention that the reader is already familiar with some basic knowledge about computer terminology. In order to gain additional knowledge about Visual Basic, it is highly recommended to refer other books.[68,69] The introductory information provided about Visual Basic 6.0 in this thesis is intended to help the reader understand about the phrases commonly used by the author while developing the application package and used in Chapter 3.

Visual Basic is a powerful programming language used to create Windows based applications. A Visual Basic program is written specifically for Windows 98 or Windows NT operating system using the Visual Basic Development System. Visual Basic is one of the products created by Microsoft ® Corporation, for creating and publishing interactive information.

Visual Basic contains various sources for help designed for first time users, intermediate users and advanced users. It contains complete reference information about menu commands, icons, tools, variables, and functions. It also contains step-by-step instructions for accomplishing common task like creating an application. In order to find the procedure required to accomplish a particular task, choose Help > Index, click on the Find tab, and type the topic name.

OLE[70] is defined as Microsoft's framework for a compound document technology. Briefly, a compound document is something like a display desktop that can contain visual and information objects of all kinds. Some examples are: text, calendars, animations, sound, motion video, 3-D, continually updated news, and controls. Each desktop object is an independent program entity that can interact with a user and communicate with other objects on the desktop. Part of Microsoft's ActiveX technologies, OLE takes advantage and is part of a larger, more general concept, the Component Object Model (COM) and its distributed version, DCOM). An OLE object is necessarily a component (or COM object), also. Table 2.2 explains some main concepts in OLE and COM.

ActiveX is Microsoft's new name for its OLE technology. Some ActiveX components, along with Visual Basic version 6.0 were used for generating an application in this thesis. ActiveX controls are explained in detail in reference 70.

2.4 Microsoft Excel

Microsoft Excel, commonly known as Excel, is a spreadsheet program from Microsoft Corporation, and is part of their Microsoft Office suite of productivity tools for

Microsoft Windows and Macintosh. Excel is one of the most widely used spreadsheet in the world.

A spreadsheet is a type of application program, which manipulates numerical and string data in rows and columns of cells. The value in a cell can be calculated from a formula, which can involve other cells. A value is recalculated automatically whenever a value, on which it depends upon, changes. Different cells may be displayed with different formats. An essential feature of a spreadsheet is the copy function (often using the mouse to drag-and-drop). A rectangular area may be copied to another area, which is a multiple of its size. Spreadsheets usually incorporate a macro language, which enables third-party writing of worksheet applications for commercial purposes. Excel spreadsheets are widely used in business and universities.

Excel cells are represented using letters and numbers. The cell B10 represents the column B and row ten. In order to specify a range of numbers, the variables are specified using both the first and last cell, separated by a colon. A10: A35 represents the range of cells between A10 and A35, both inclusive.

An Excel spreadsheet was used for computational purposes of the fractioanl flow curve and during the development of a computer program for this thesis. The details are explained in Chapter 3.

2.5 Microsoft Access

Microsoft Access, commonly known as Access is a relational database product available for the Windows platform. A database is a collection of data that is organized so

that its contents can easily be accessed, managed, and updated. A relational database is a collection of data items organized as a set of formally described tables from which data can be accessed or reassembled in many different ways without having to reorganize the database tables. Each table (which is sometimes called a relation) contains one or more data categories in columns. Each row contains a unique instance of data for the categories defined by the columns.

Access is part of the Microsoft Office Suite, and was used during the development of a relational database for the current thesis. Chapter 3 explains more detail about the use of a database.

Table 2.1

Rules Of Thumb Indicating Different Wettability Preferences[1]

SL.#.		WATER-WET	OIL-WET
1	Connate water saturation	Usually greater than 20 to 25 percent Pore Volume	Generally less than 15 percent pore volume, frequently less than 10 percent
2	Saturation at which oil and water relative permeabilities are equal	Greater than 50 percent water saturation	Less than 50 percent water saturation
3	Relative permeability to water at maximum water saturation, (floodout)	Generally less than 30 percent	Greater than 50 percent and approaching 100 percent

Table 2.2

Some Main Concepts in OLE and COM[70]

Concept	What it is
OLE	A set of APIs to create and display a (compound) document
Document (compound document)	A presentation of different items in an "animated desktop"
Item (object; also called a component)	An element in a document, such as an animated calendar, a video window, a sound player, a sound file...
Container or container application	The program entity that holds a document or a control
Server or server application	The program entity that holds an item within an OLE container
Embedding	Adding the source data for an item to a document; use the Paste command in a container application
Linking	Adding a link to the source data for an item to a document; use the Paste Link command in a container application
Visual editing	Activating an item that is embedded in a document and "editing" it
Automation	Having one container or server application drive another application
Compound files (structured storage)	A standard file format that simplifies the storing of (compound) documents; consists of storages (similar to directories) and streams (similar to files)
Uniform Data Transfer (UDT)	A single data transfer interface that accommodates drag-and-drop; clipboard; and dynamic data exchange (DDE)
Component Object Model (COM)	Provides the underlying support for OLE items (objects) and ActiveX controls to communicate with other OLE objects or ActiveX controls
ActiveX control	An item (object) that can be distributed and run on top of a COM
Microsoft Foundation Class (MCF) library	A set of ready-made classes or templates that can be used to build container and server applications

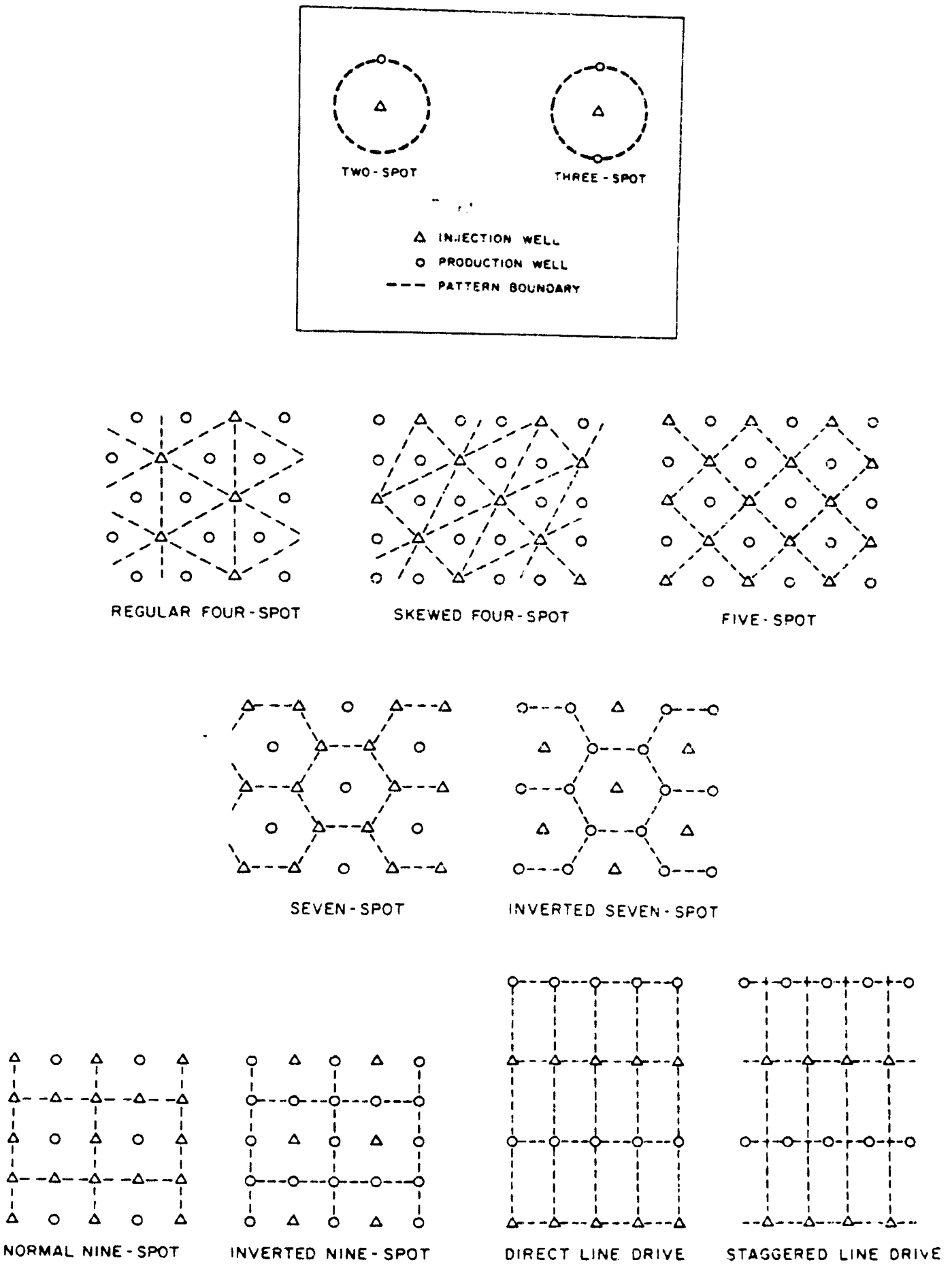

Figure 2.1. Various Waterflooding Patterns

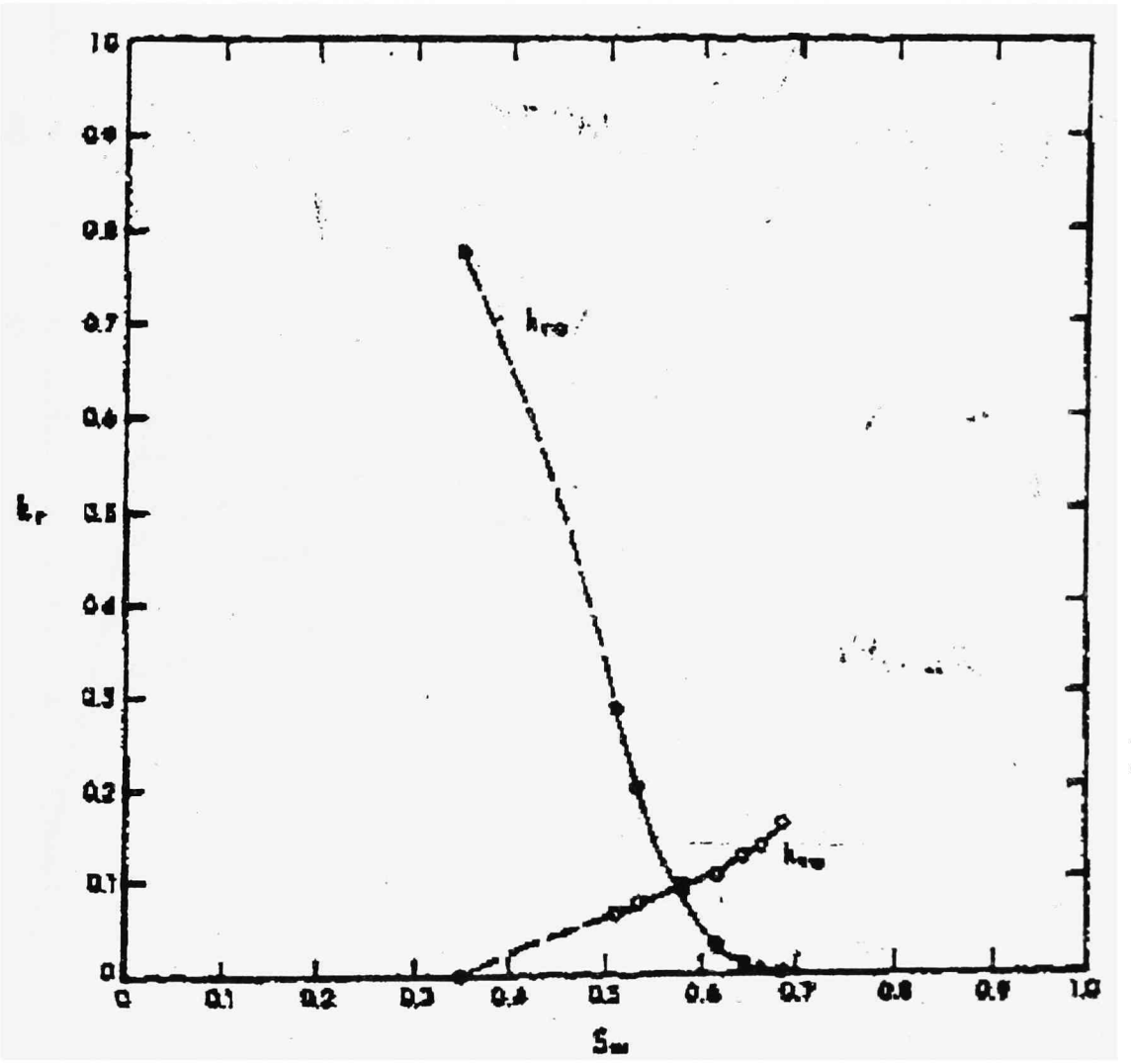

Figure 2.2. Relative Peermeability curves

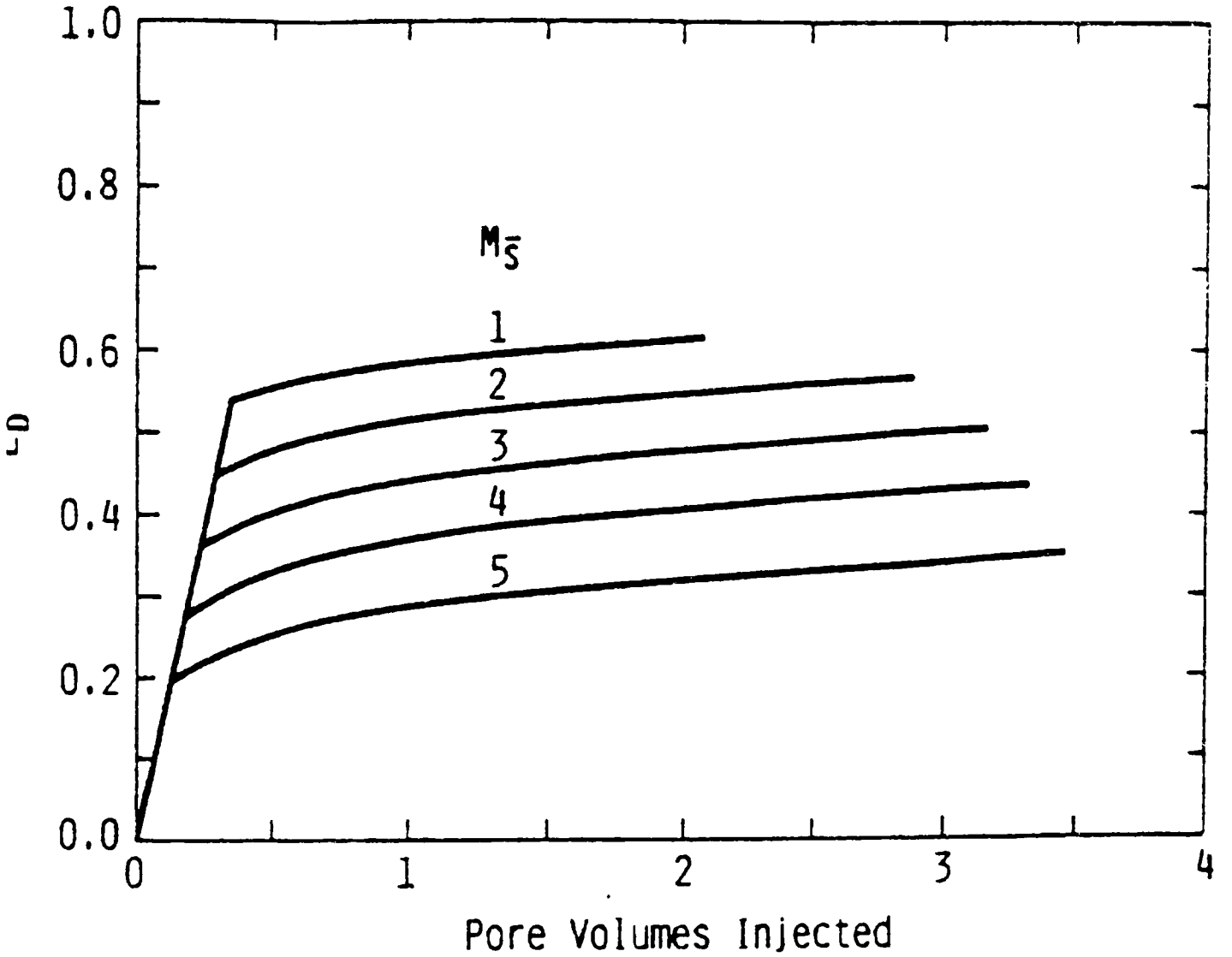

Figure 2.3. Effect of mobility ratio on displacement efficiency of a linear waterflood.

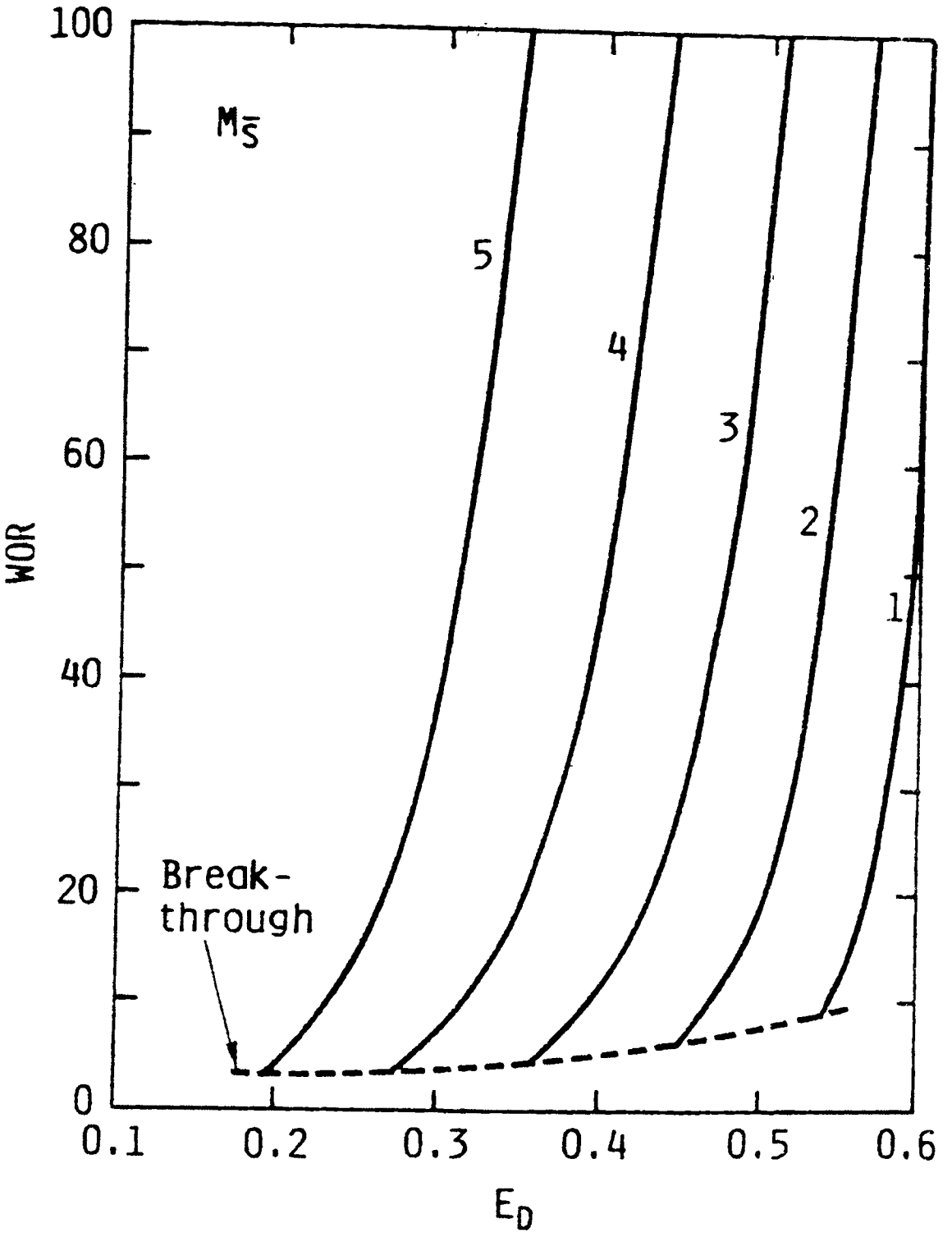

Figure 2.4. Variation of WOR with displacement efficiency for several mobility ratios.

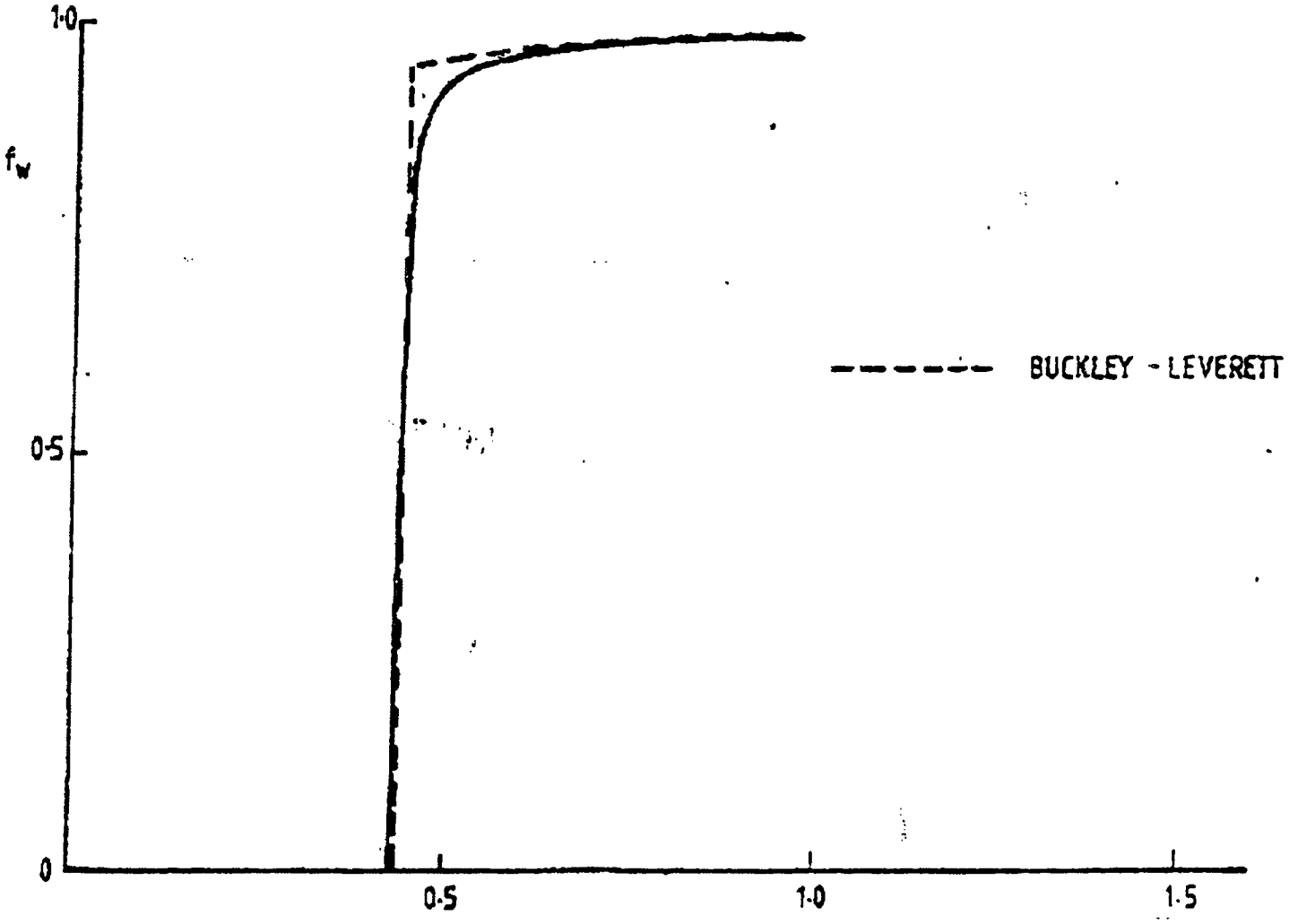

Figure 2.5. Fractional flow of water at core outlet.

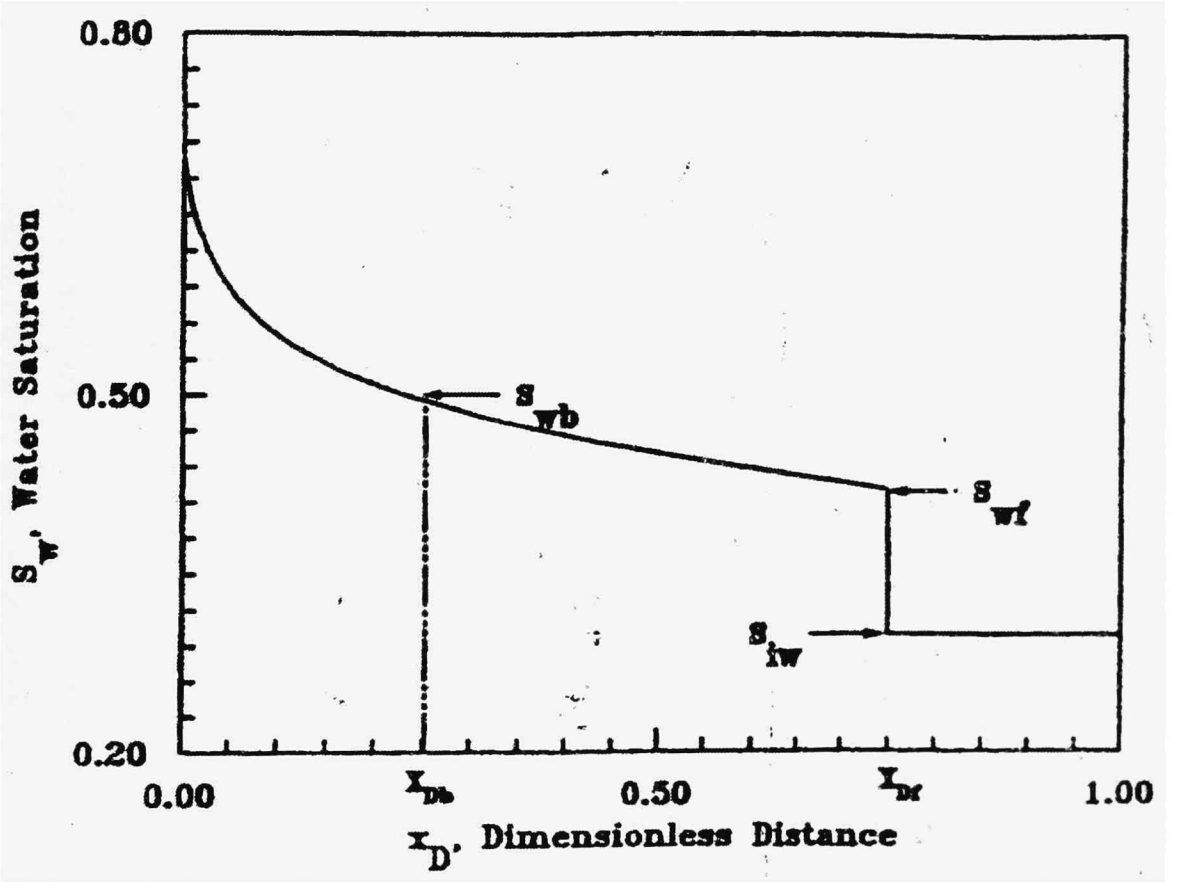

Figure 2.6. Saturation profile showing interstitial water displaced by the injected fluid.

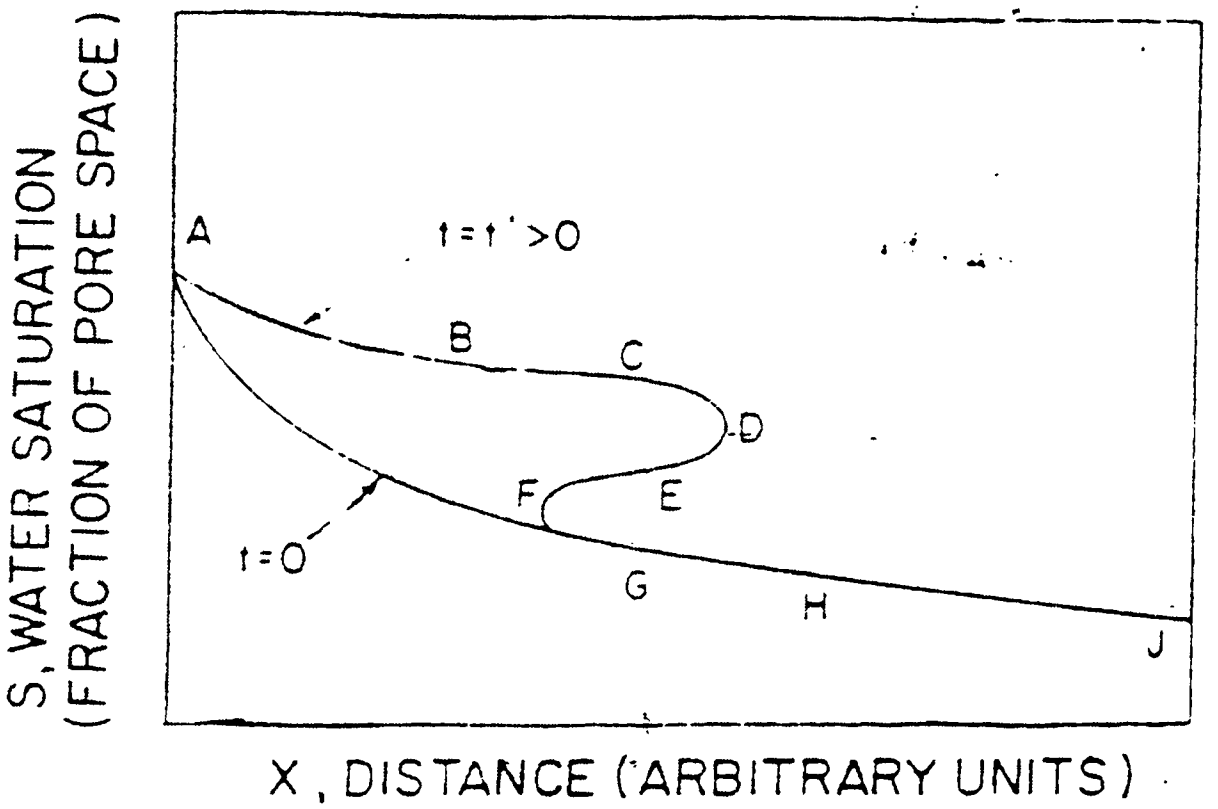

Figure 2.7. Triple-value concept.

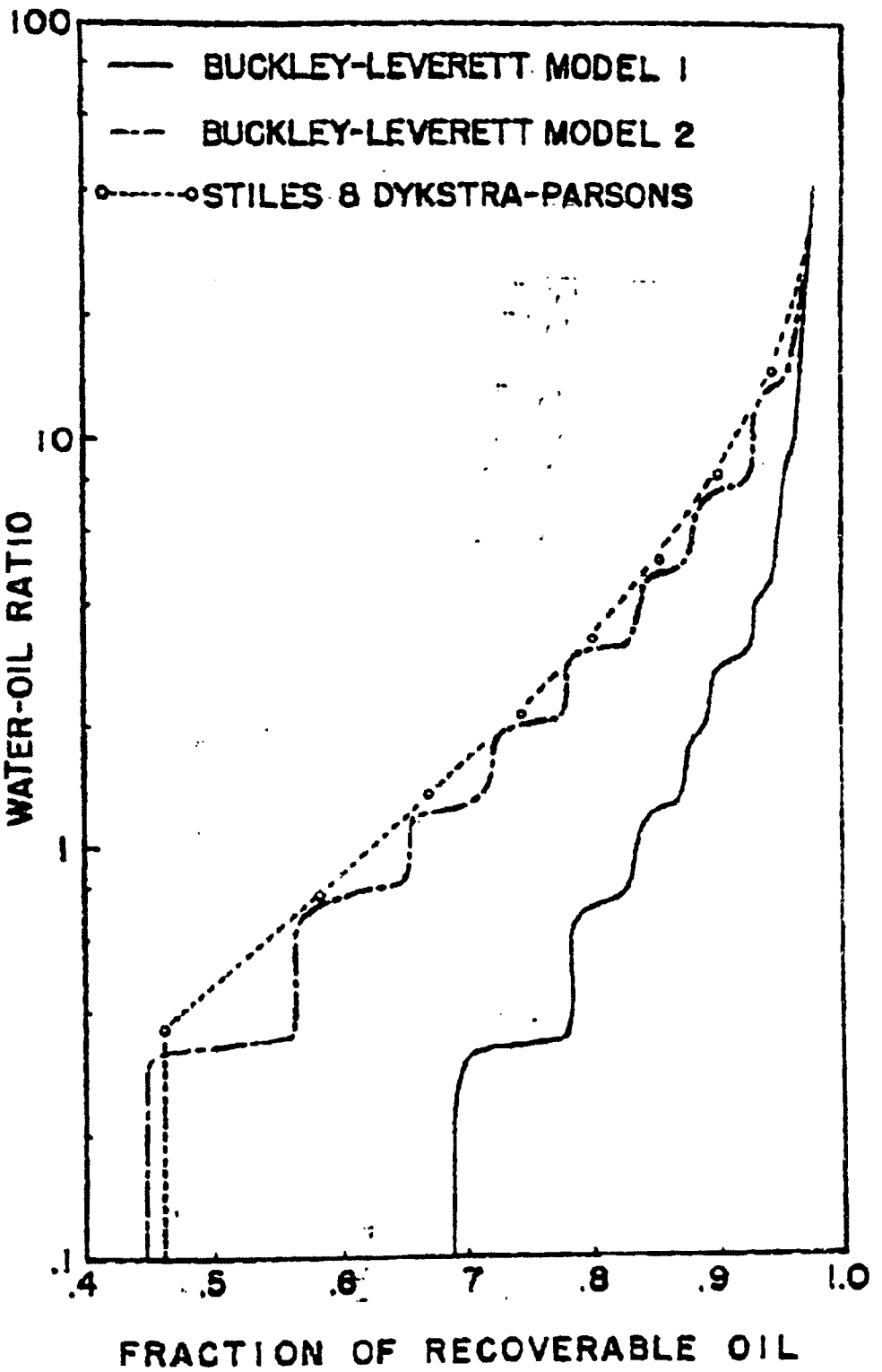

Figure 2.8. Waterflood case B (M = 1), Recovery versus WOR.

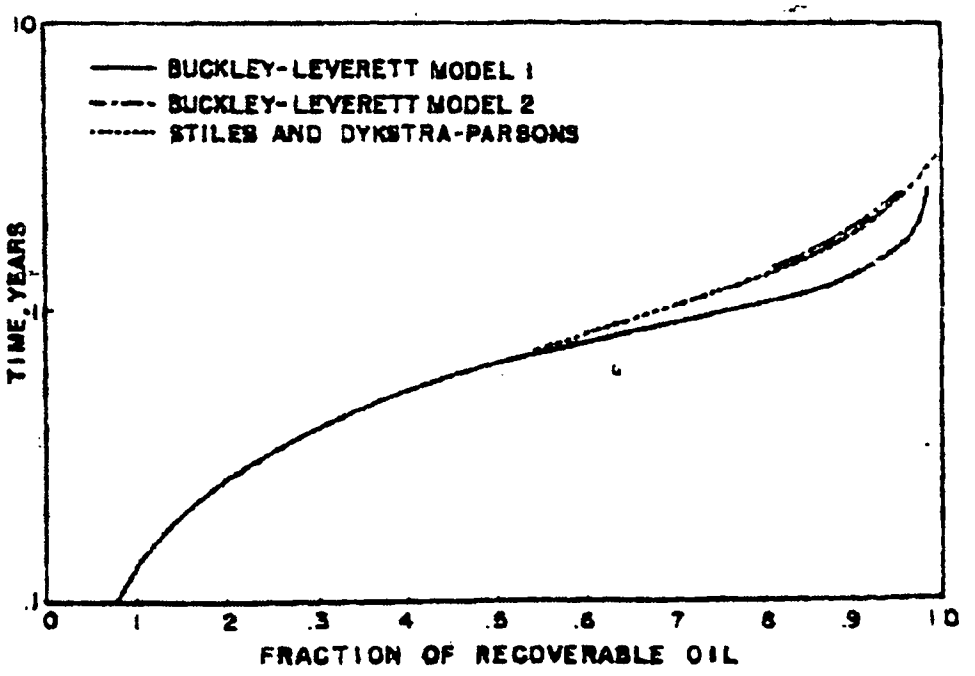

Figure 2.9. Waterflood case B (M = 1), Recovery versus Time.

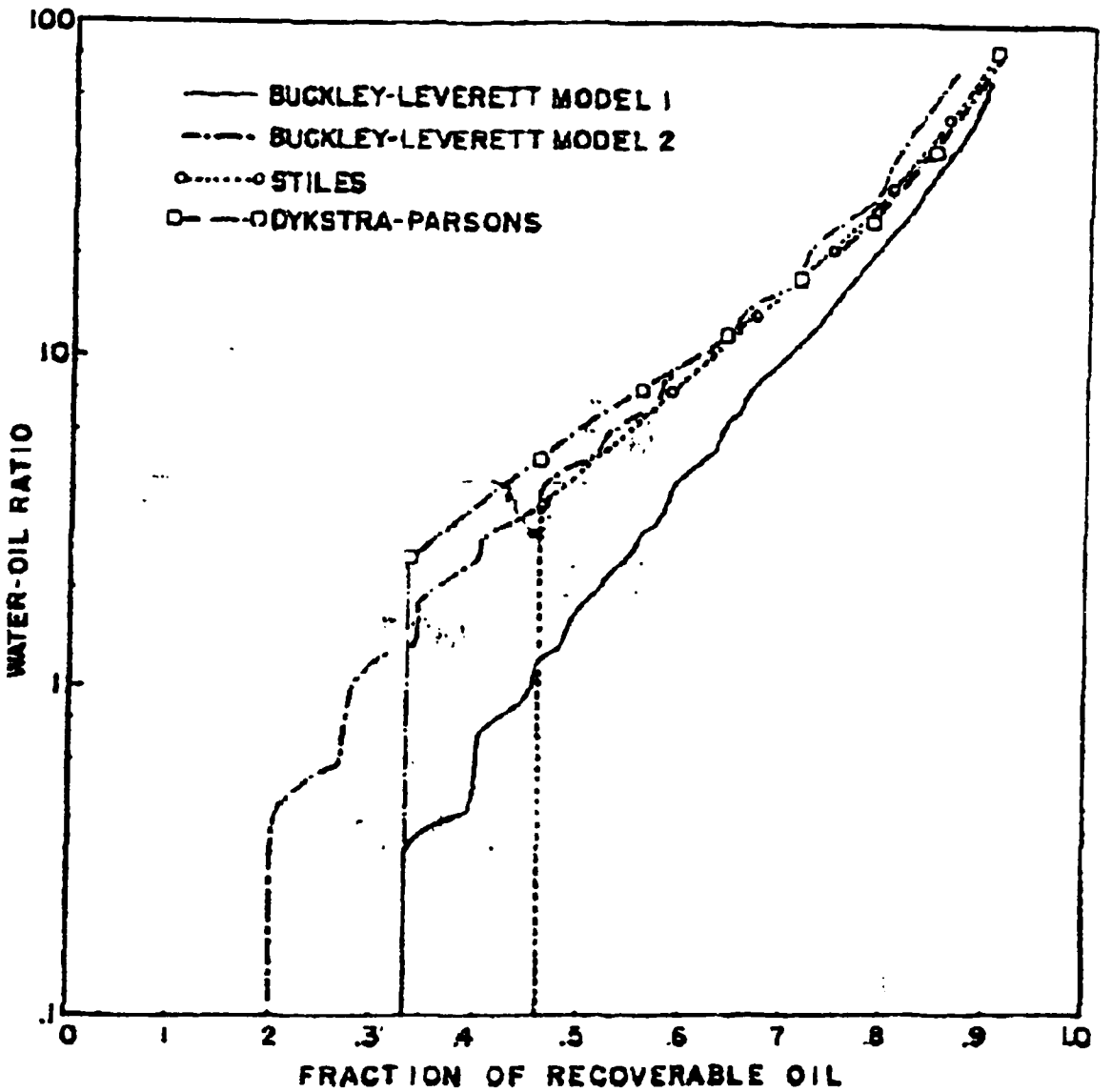

Figure 2.10. Waterflood case C (M = 10) Recovery versus WOR.

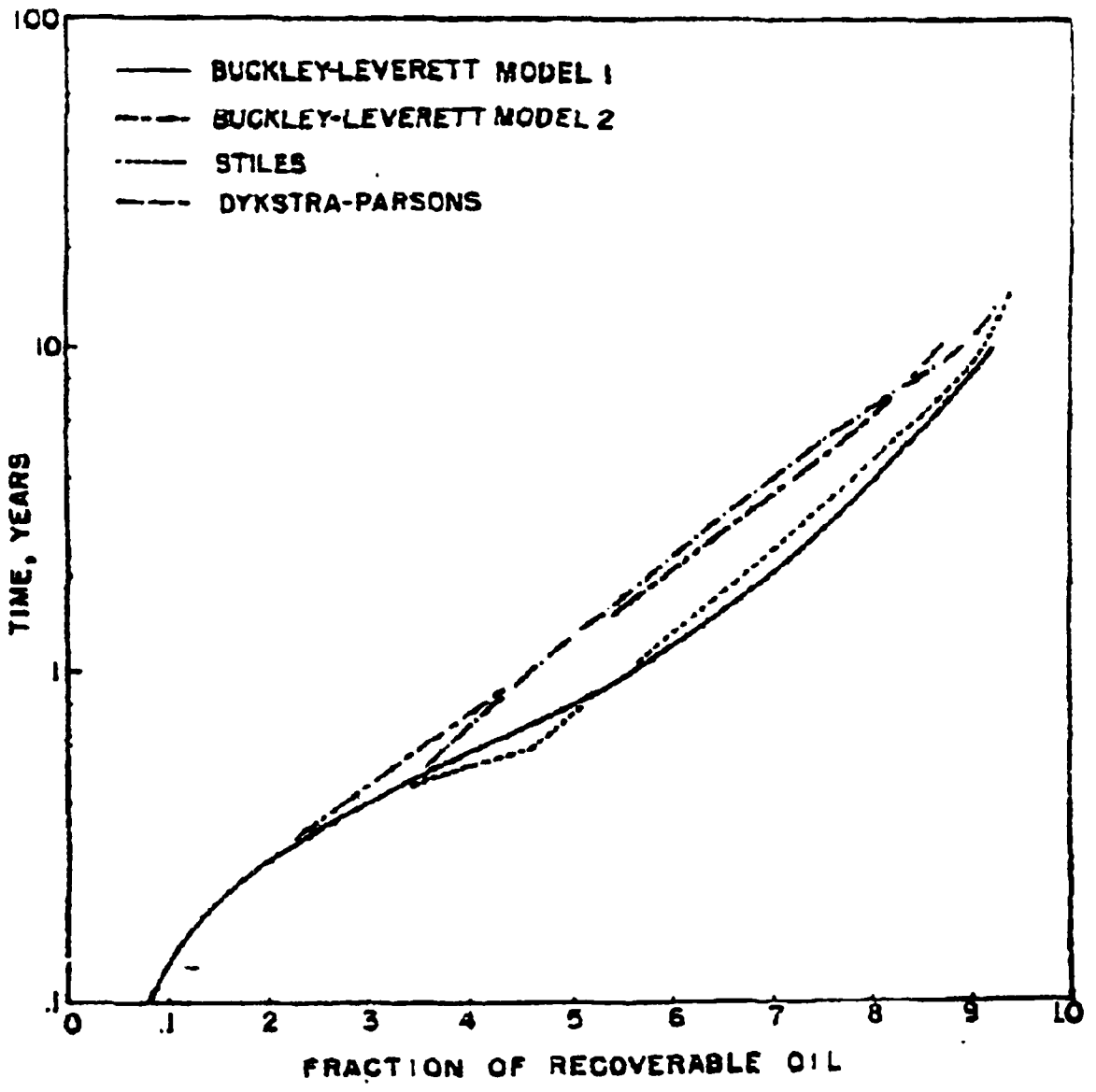

Figure 2.11. Waterflood case C (M = 10) Recovery versus Time.

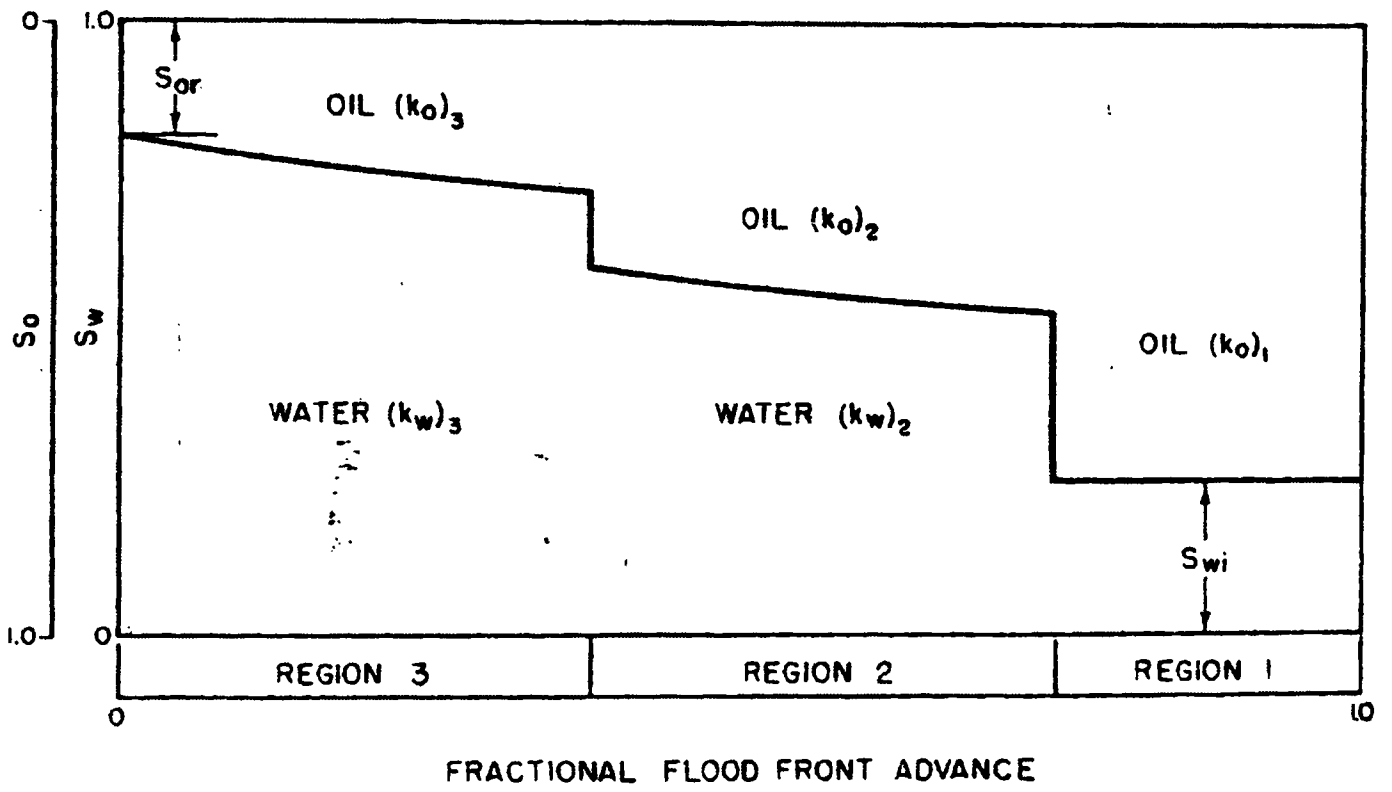

Figure 2.12. Partial frontal displacement with two fronts and two movable phases behind each front.

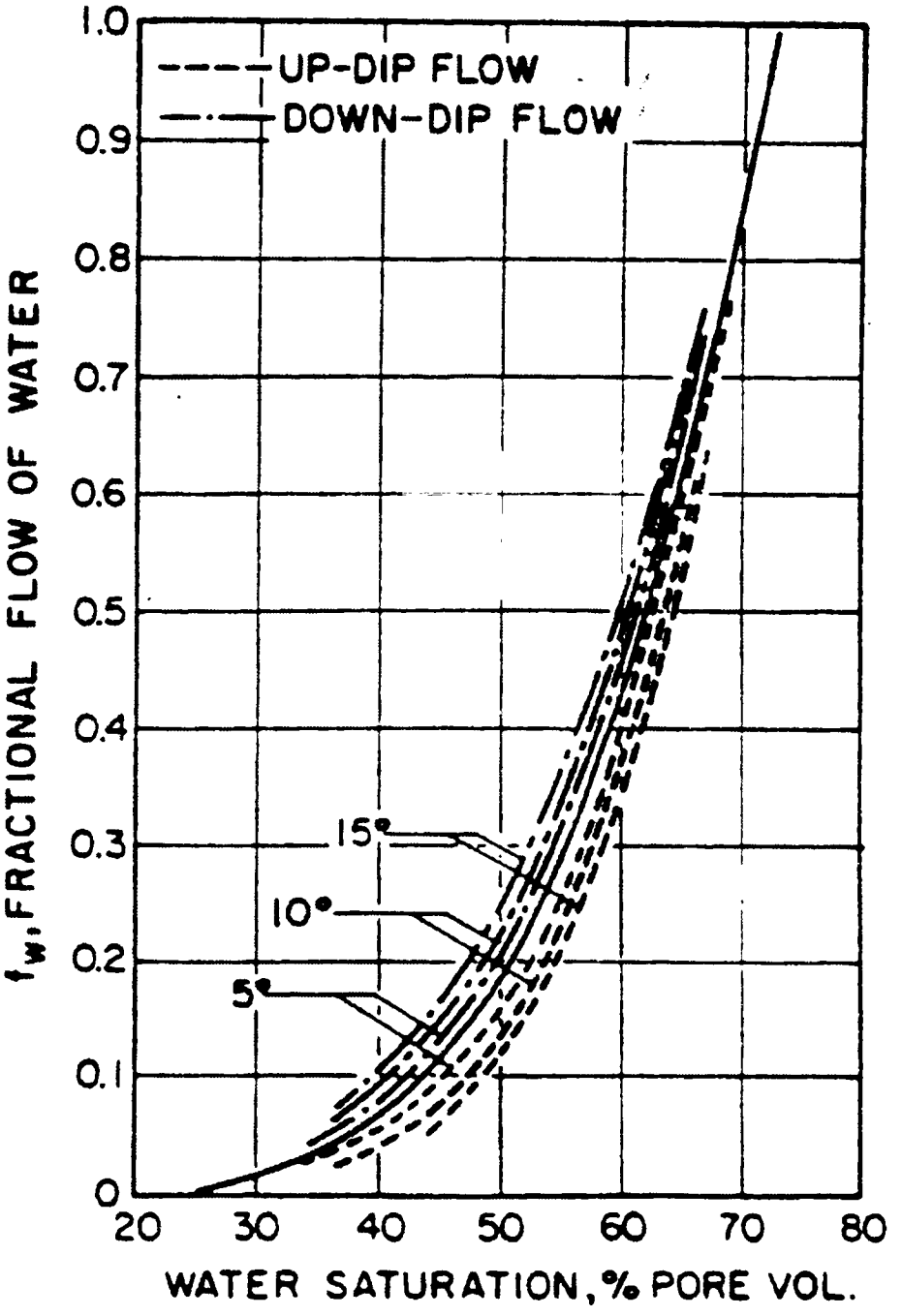

Figure 2.13. Effect of formation dip on fractional flow curve, strongly water-wet rock.

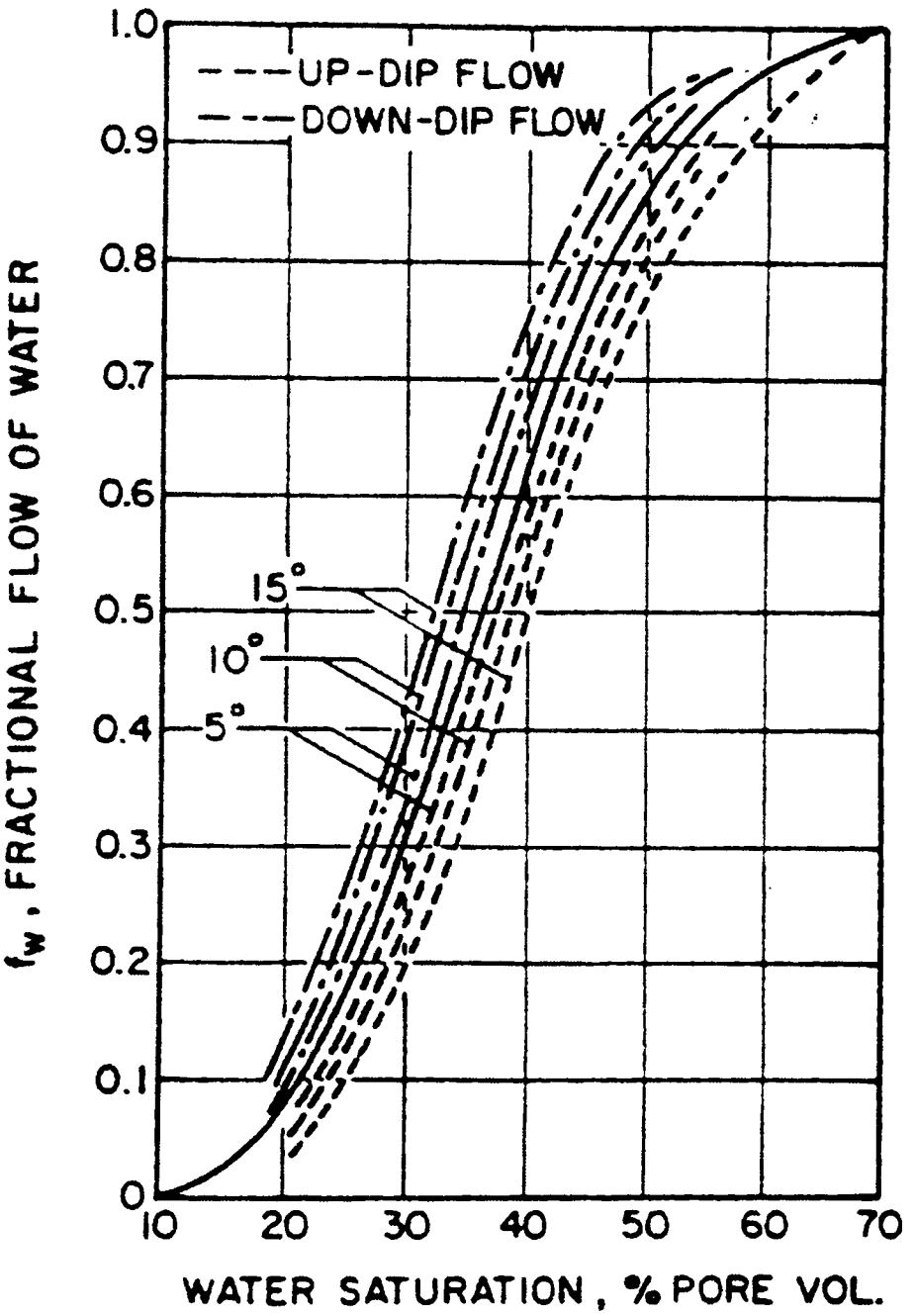

Figure 2.14. Effect of formation dip on fractional flow curve, strongly oil-wet rock.

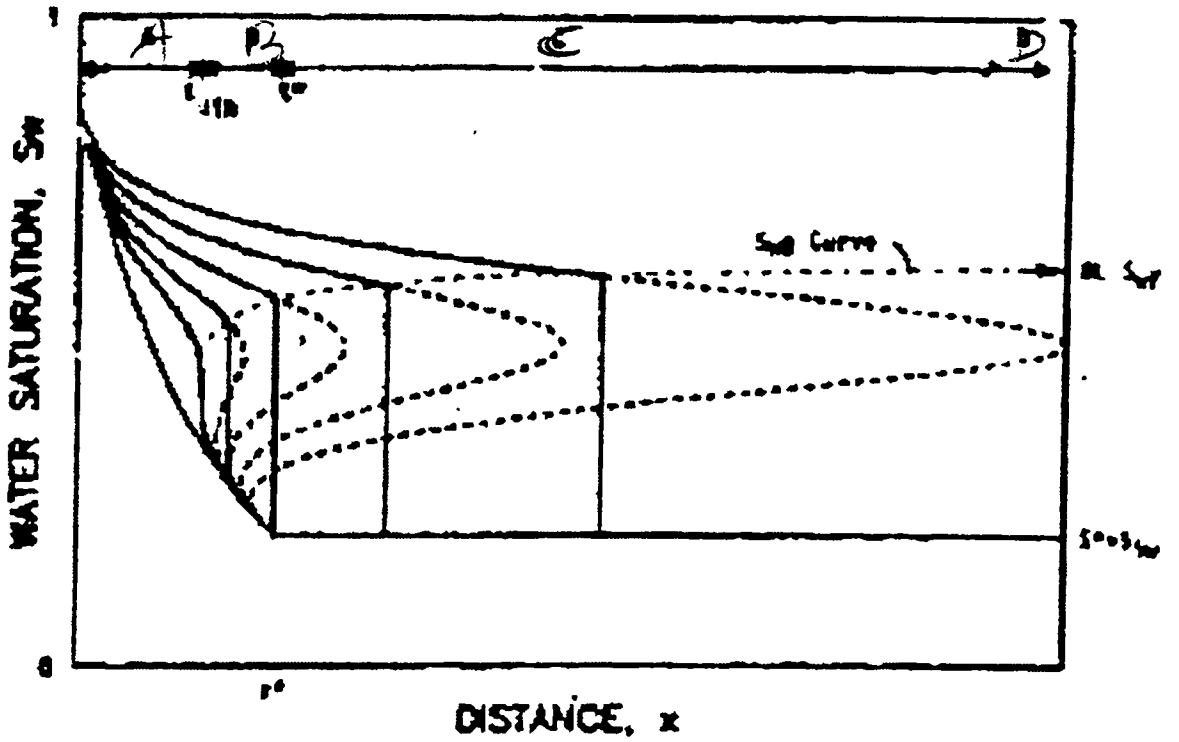

Figure 2.15. Saturation front

Solid line indicates symmetry pattern of infinite well network.
Dashed line indicates symmetry element of infinite well network.

Code: ○ Injection Wells, ● Producing Wells

DIRECT LINE DRIVE

$$i = \frac{0.001538\,\lambda h \Delta P}{\log \frac{a}{r_w} + 0.682\frac{d}{a} - 0.798}$$

$$\frac{d}{a} \geq 1$$

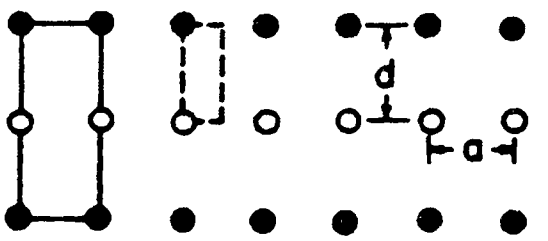

STAGGERED LINE DRIVE

$$i = \frac{0.001538\,\lambda h \Delta P}{\log \frac{a}{r_w} + 0.682\frac{d}{a} - 0.798}$$

$$\frac{d}{a} \geq 1$$

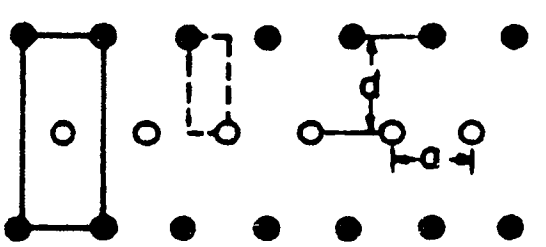

FIVE-SPOT

$$i = \frac{0.001538\,\lambda h \Delta P}{\log \frac{d}{r_w} - 0.2688}$$

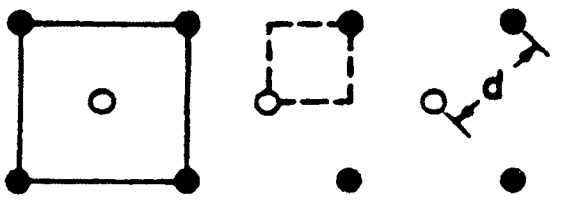

SEVEN-SPOT

$$i = \frac{0.002051\,\lambda h \Delta P}{\log \frac{d}{r_w} - 0.2472}$$

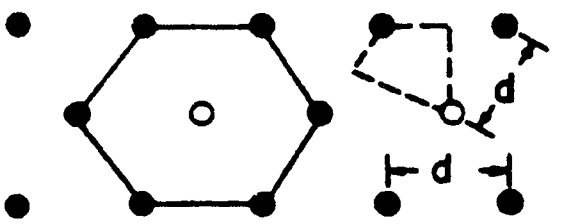

Figure 2.16. Injectivities for regular patterns for mobility ratio equal to one.

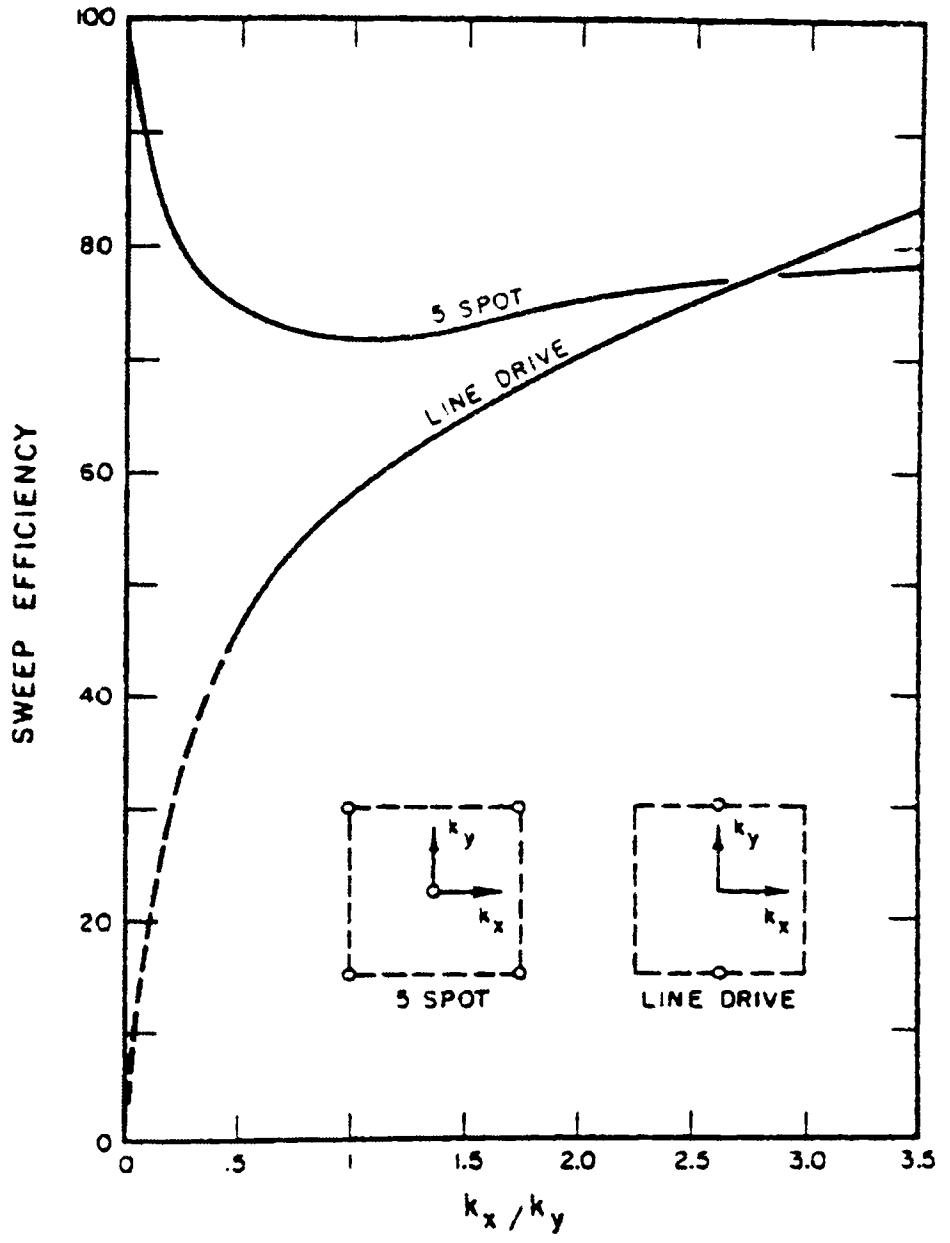

Figure 2.17. The effect of directional permeability on sweep efficiency.

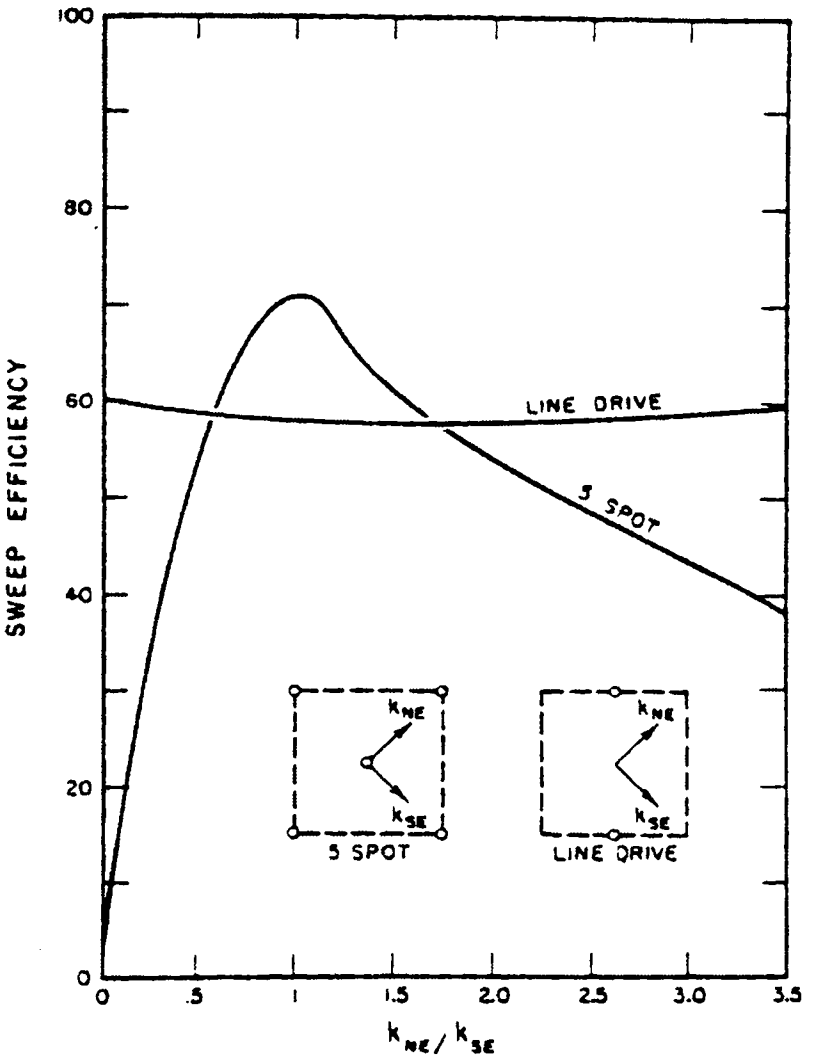

Figure 2.18. The effect of directional permeability on sweep efficiency.

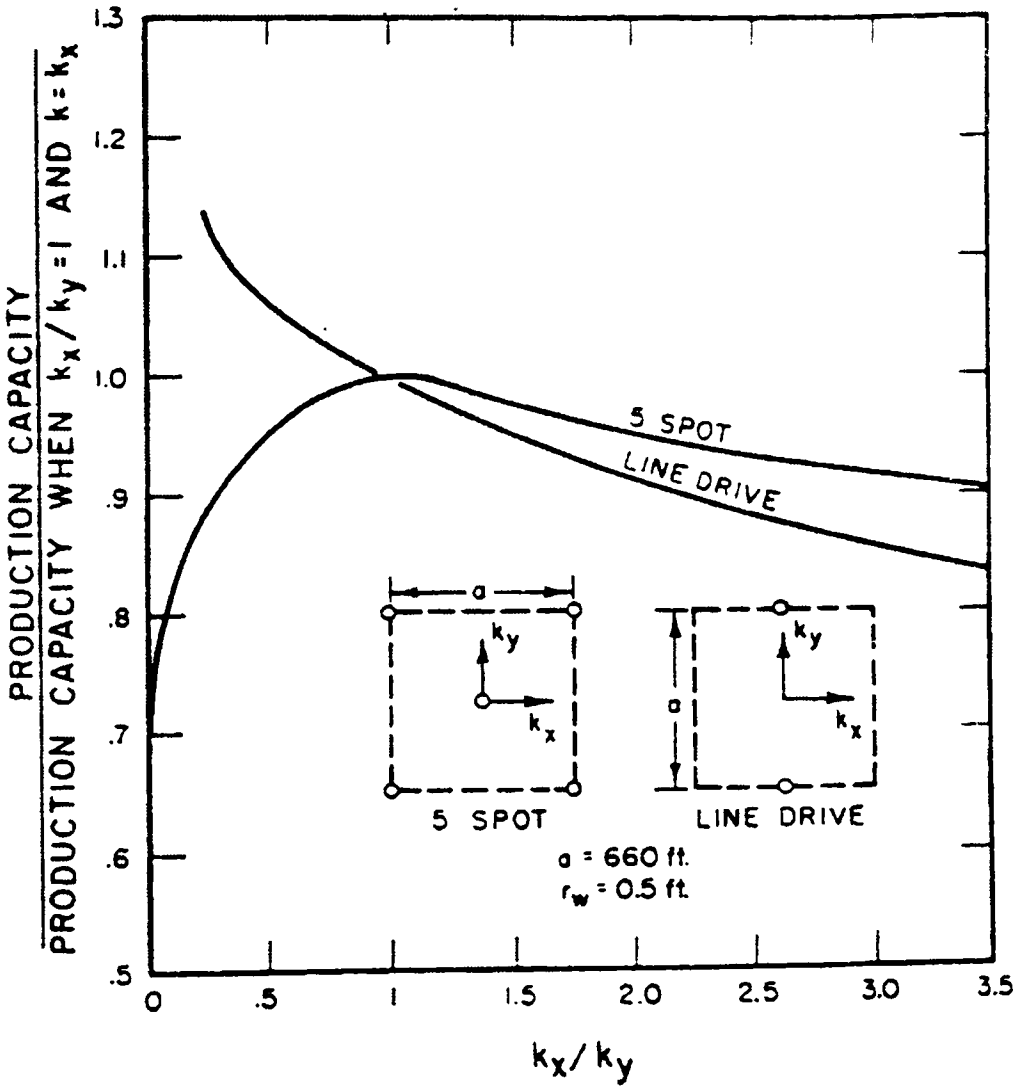

Figure 2.19. The effect of directional permeability on production capacity.

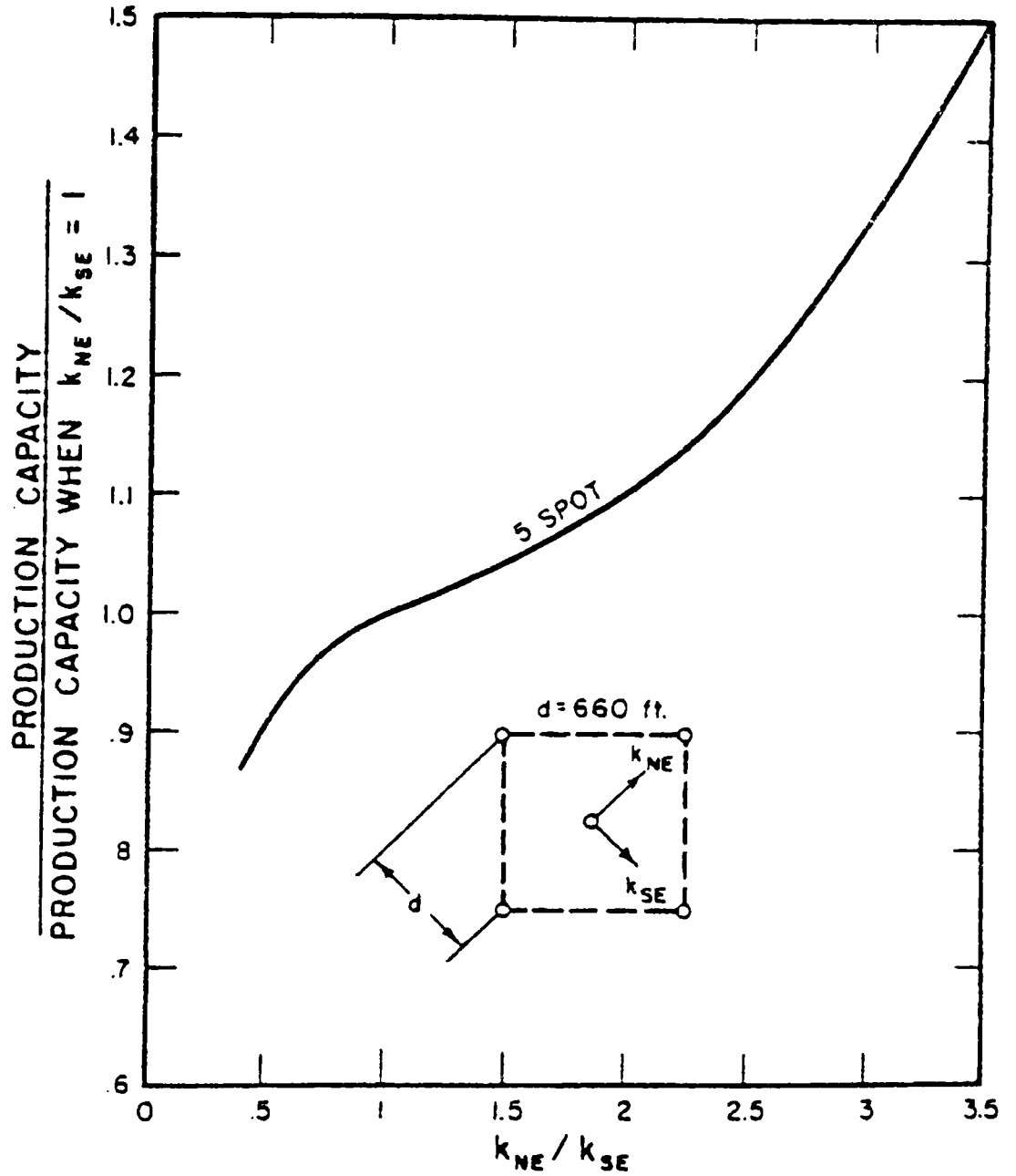

Figure 2.20. The effect of directional permeability on production capacity.

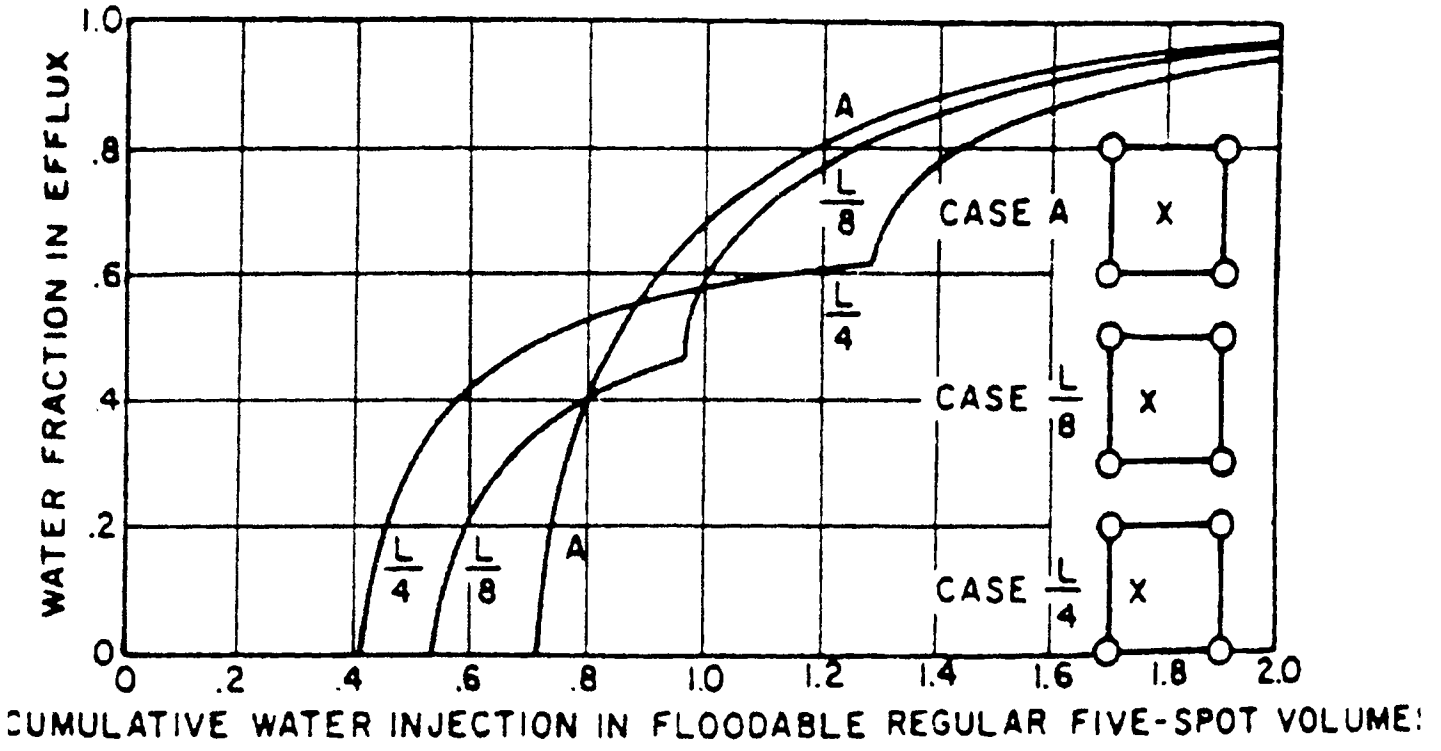

Figure 2.21. Water-cut history of a laterally displaced production well.

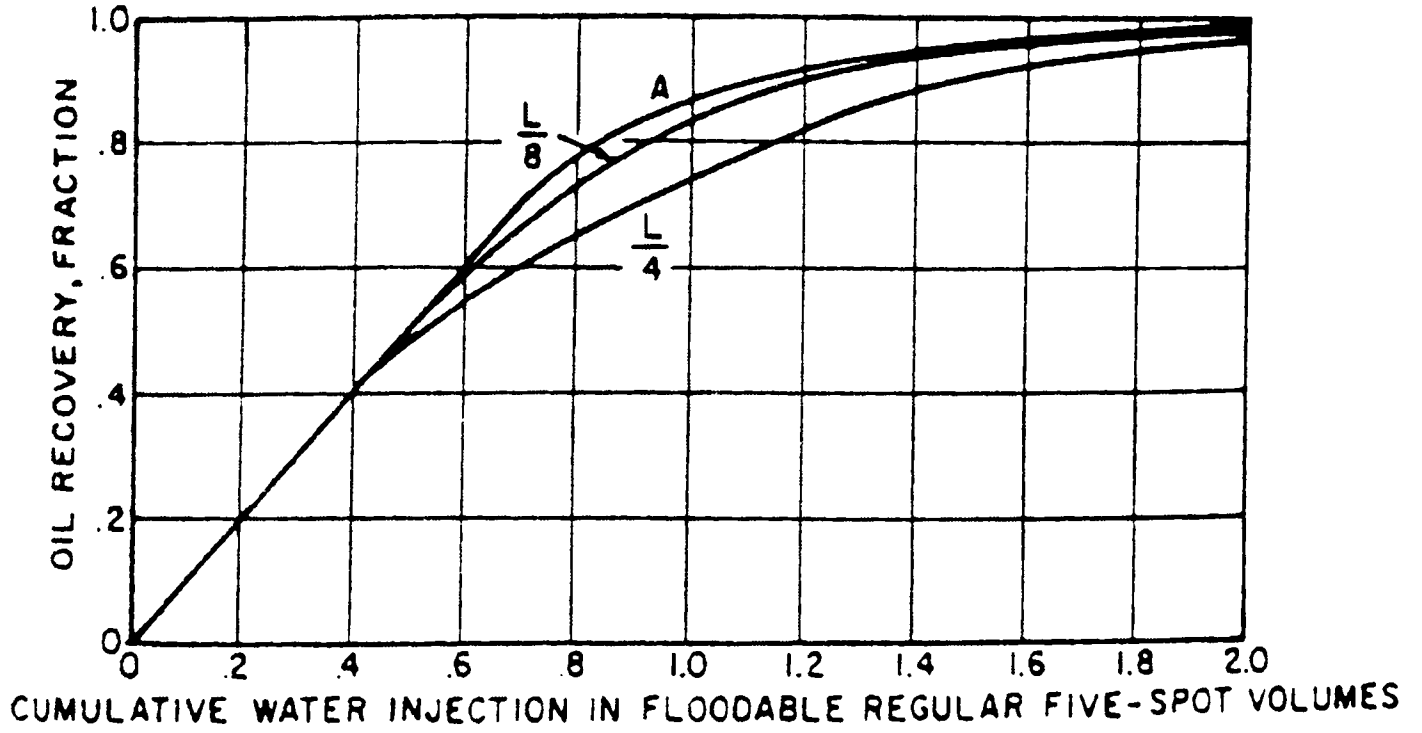

Figure 2.22. Oil production history of a laterally displaced production well.

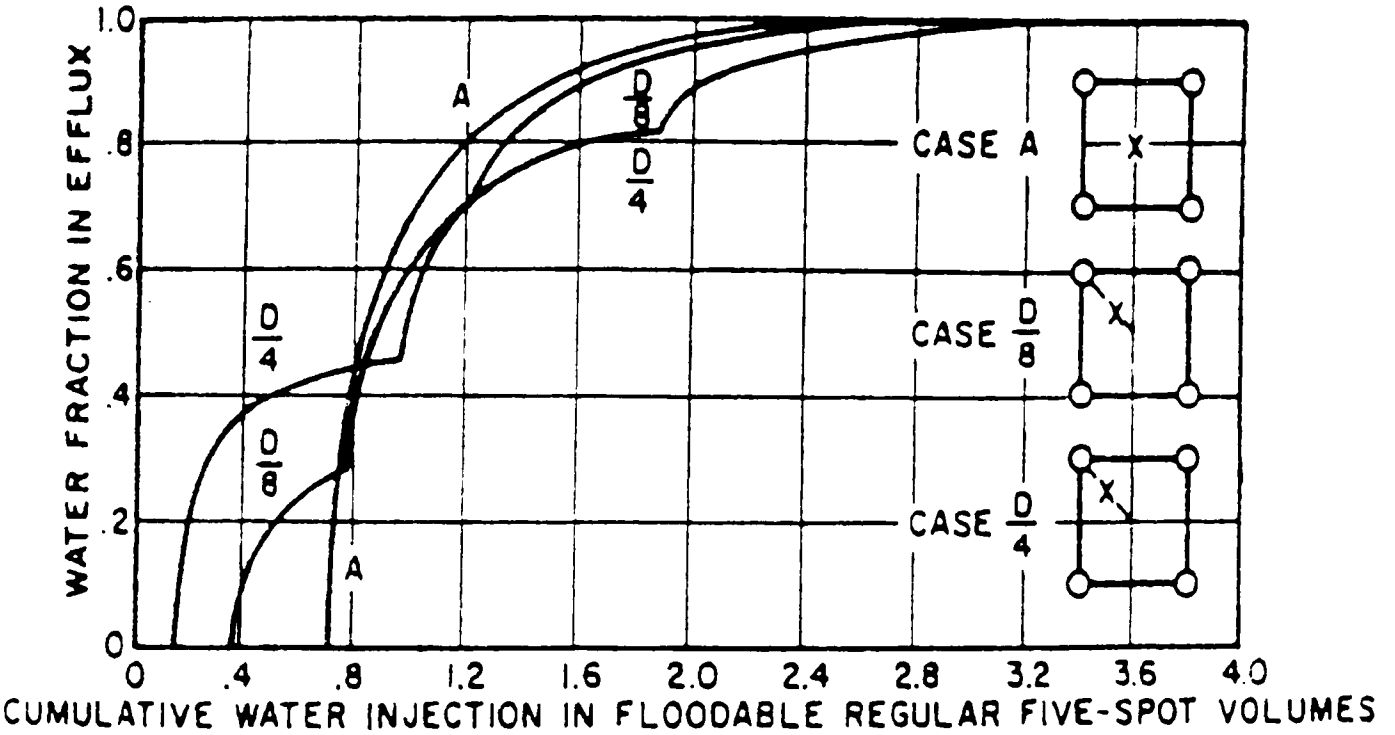

Figure 2.23. Water-cut history of a diagonally displaced production well.

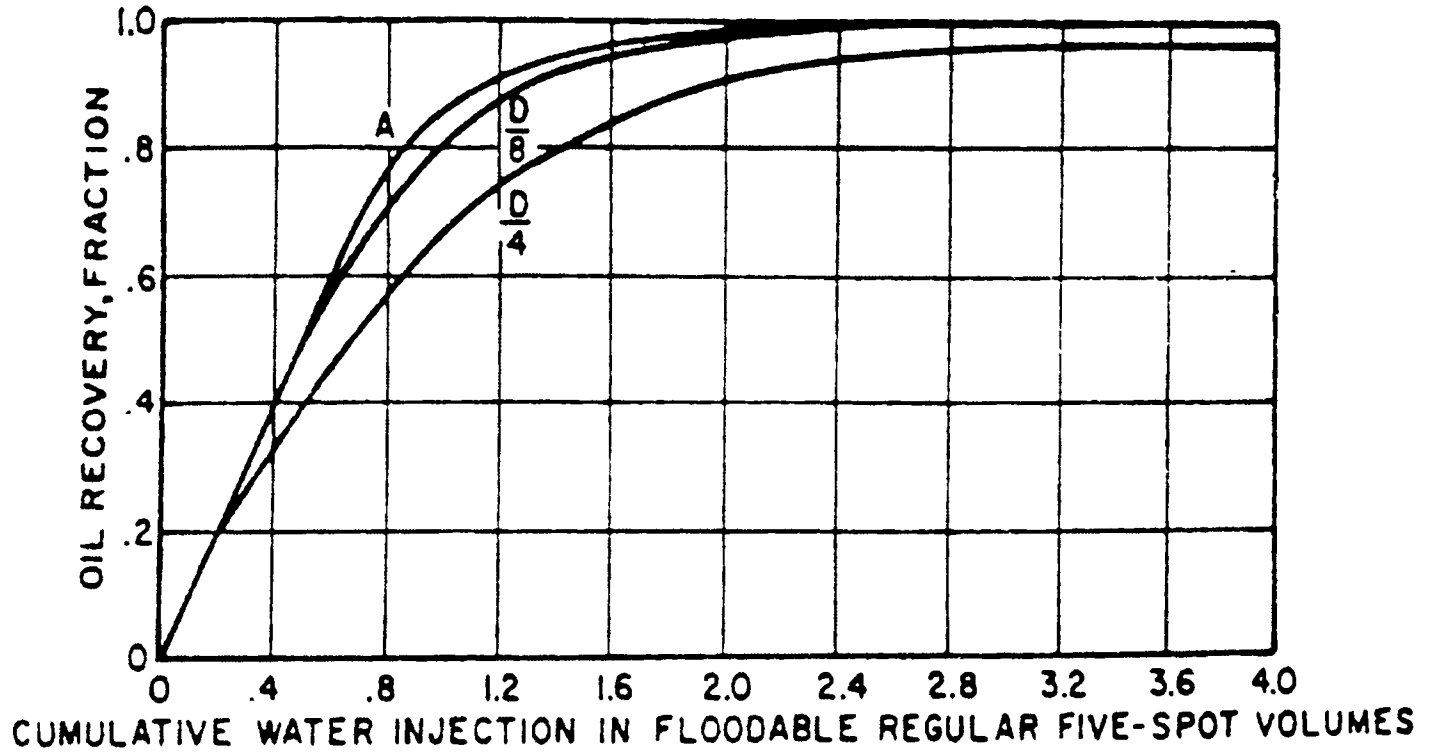

Figure 2.24. Oil production of a diagonally displaced production well.

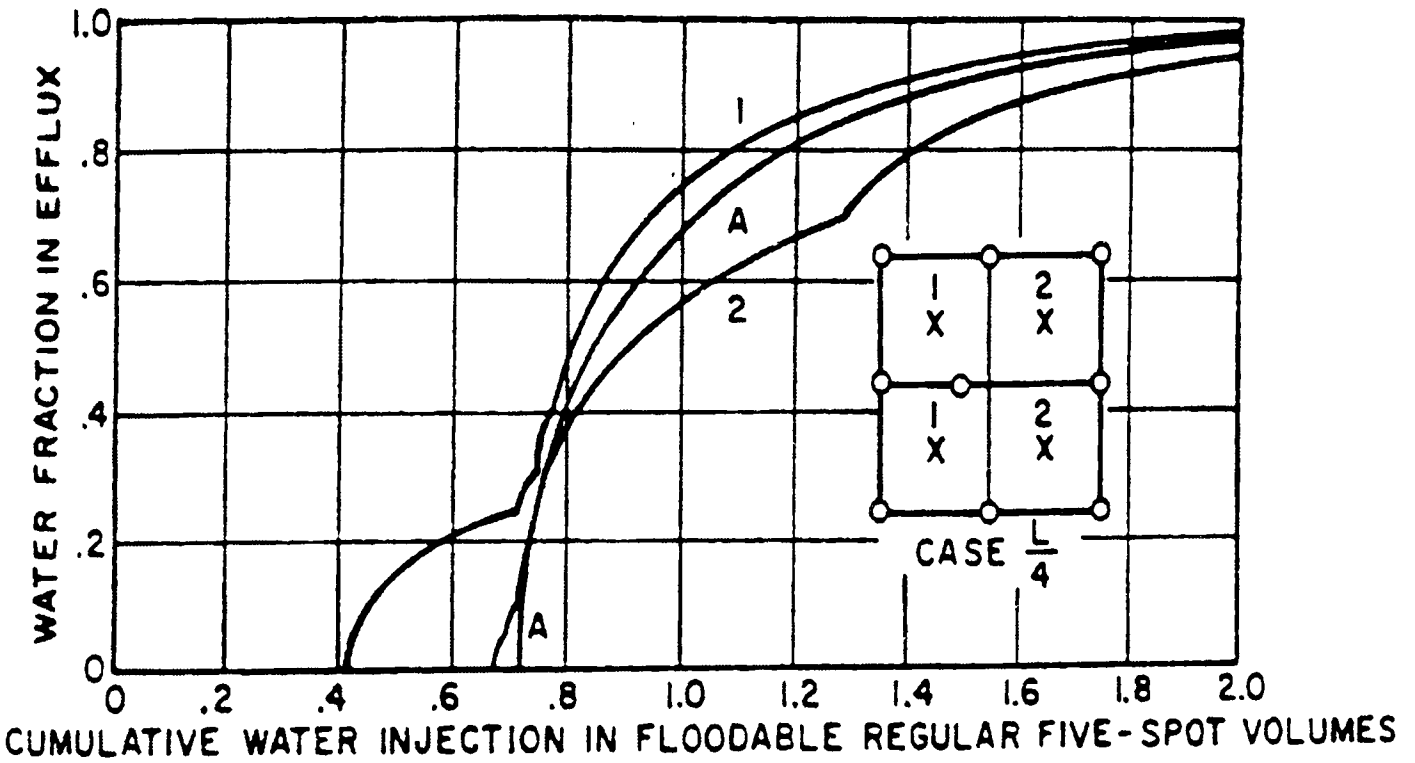

Figure 2.25. Water-cut history of five-spot pattern surrounding laterally displaced production well.

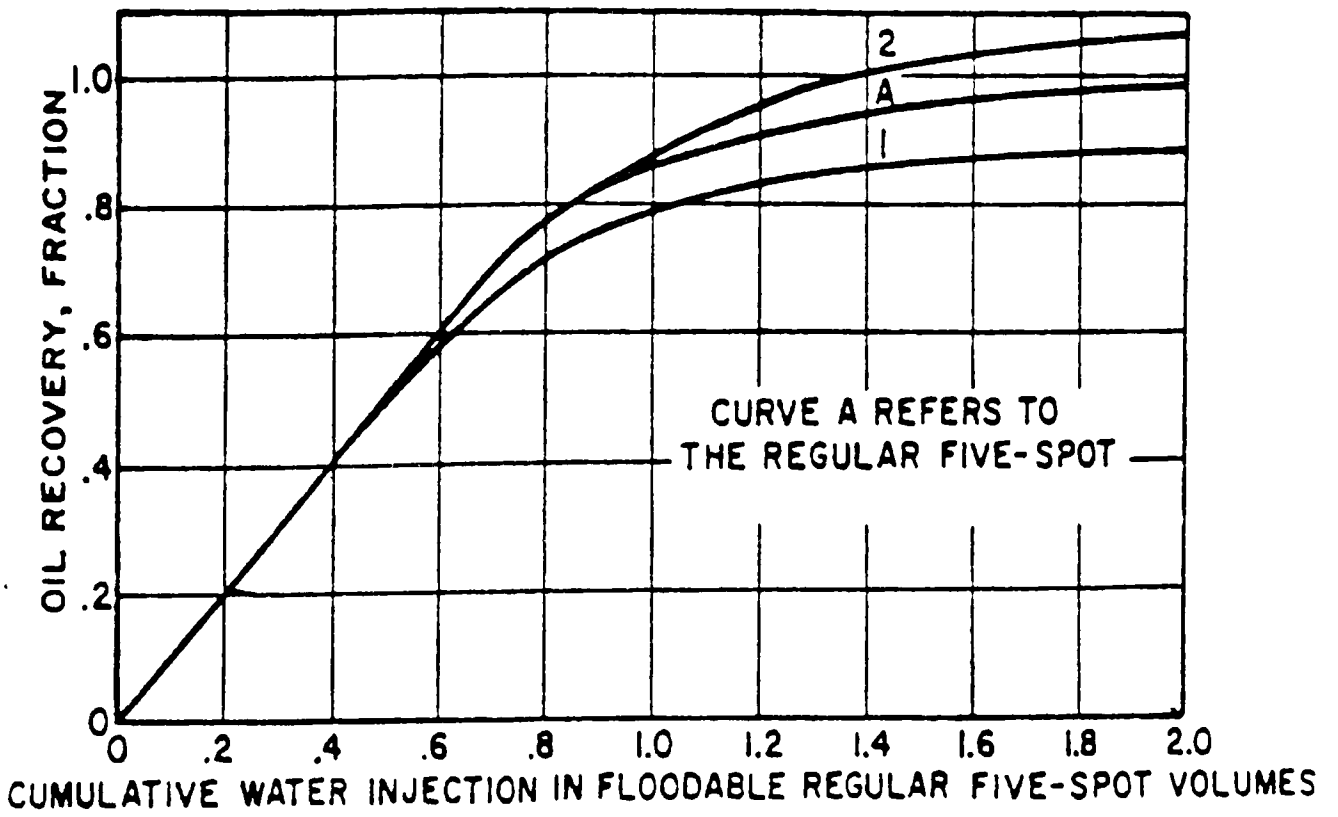

Figure 2.26. Water-cut history of five-spot pattern surrounding laterally displaced injection well.

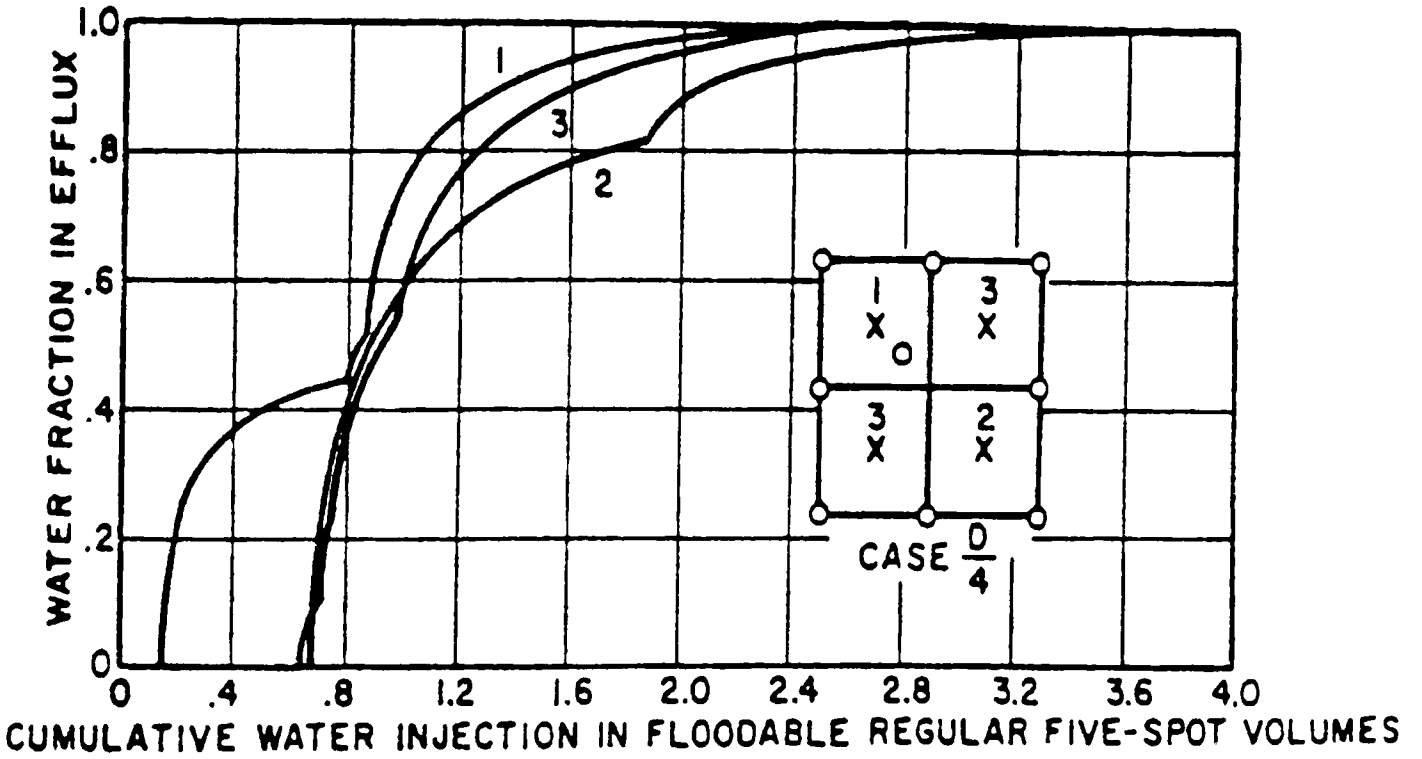

Figure 2.27. Water-cut history of five-spot pattern surrounding diagonally displaced injection well.

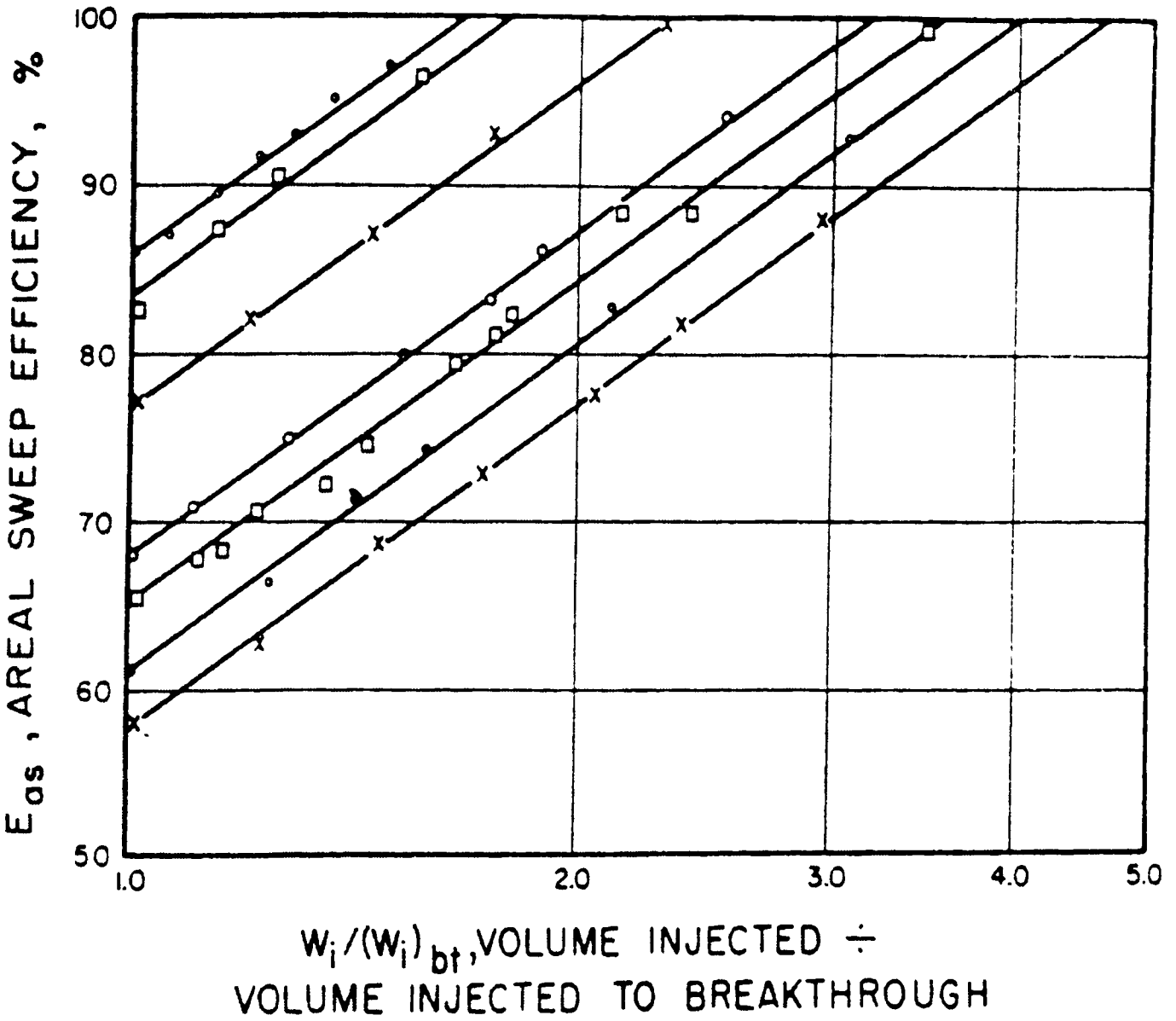

Figure 2.28. Increase in areal sweep efficiency after breakthrough.

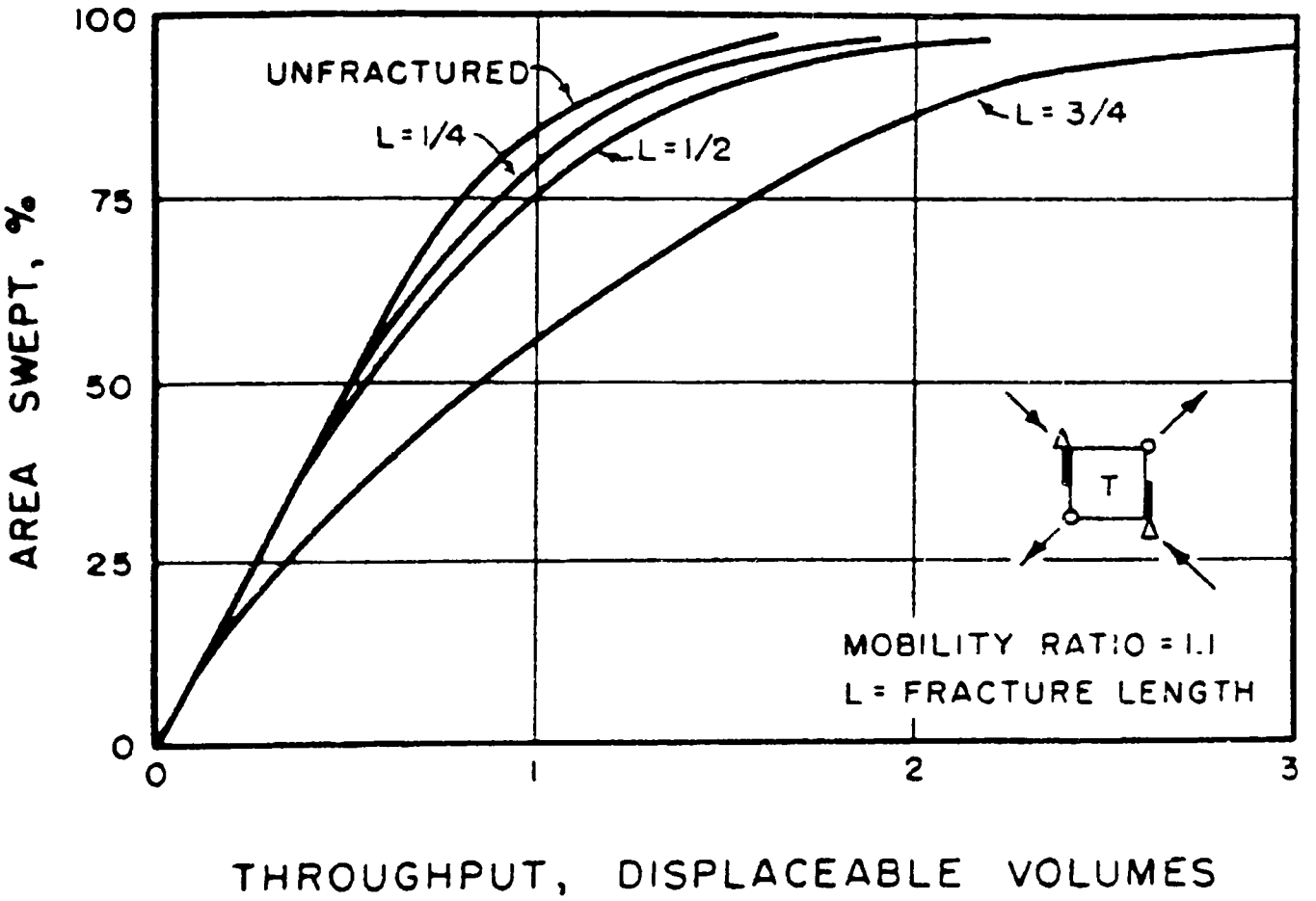

Figure 2.29. Sweep-out with vertical fracture of favorable direction

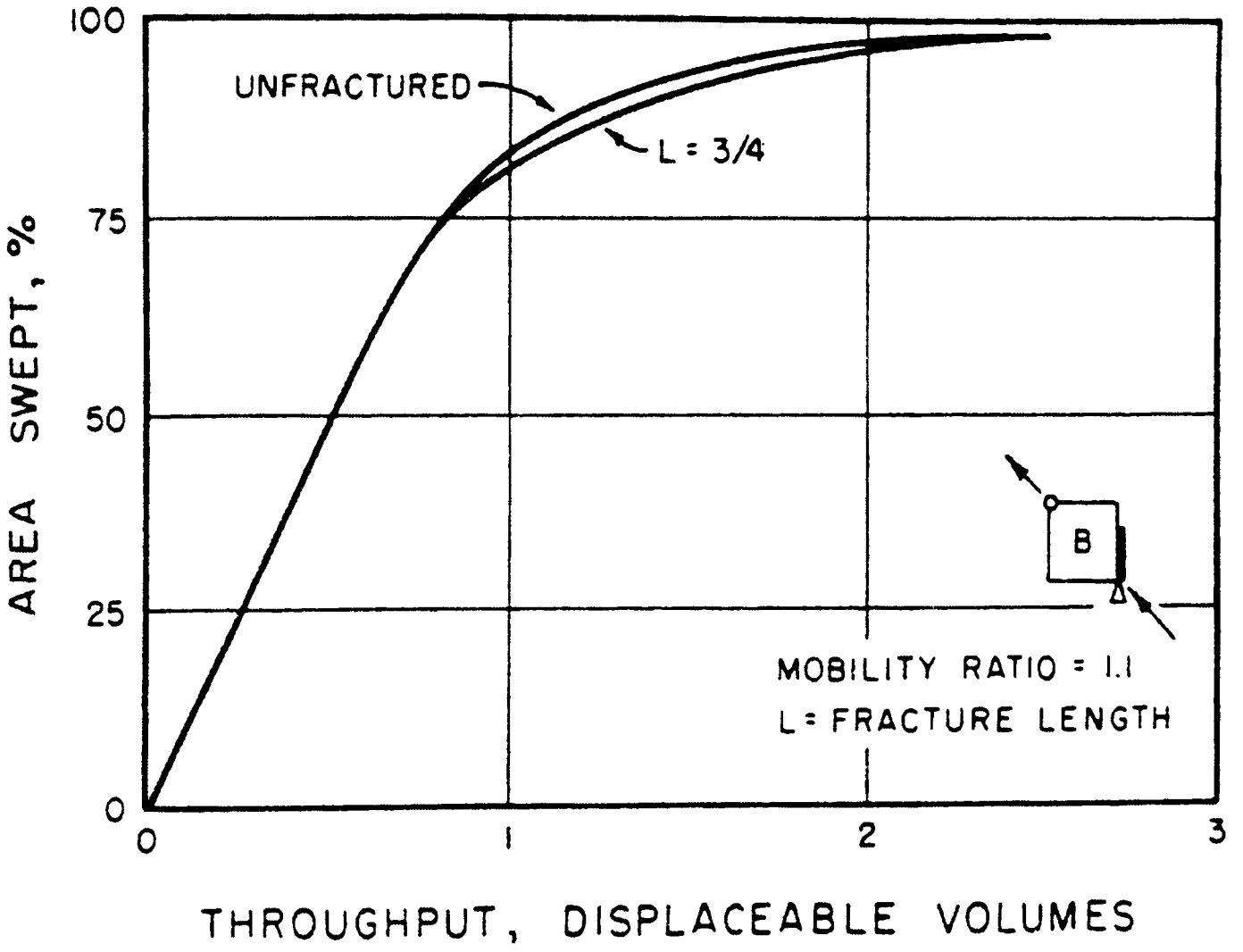

Figure 2.30. Sweep-out with vertical fracture having unfavorable directions.

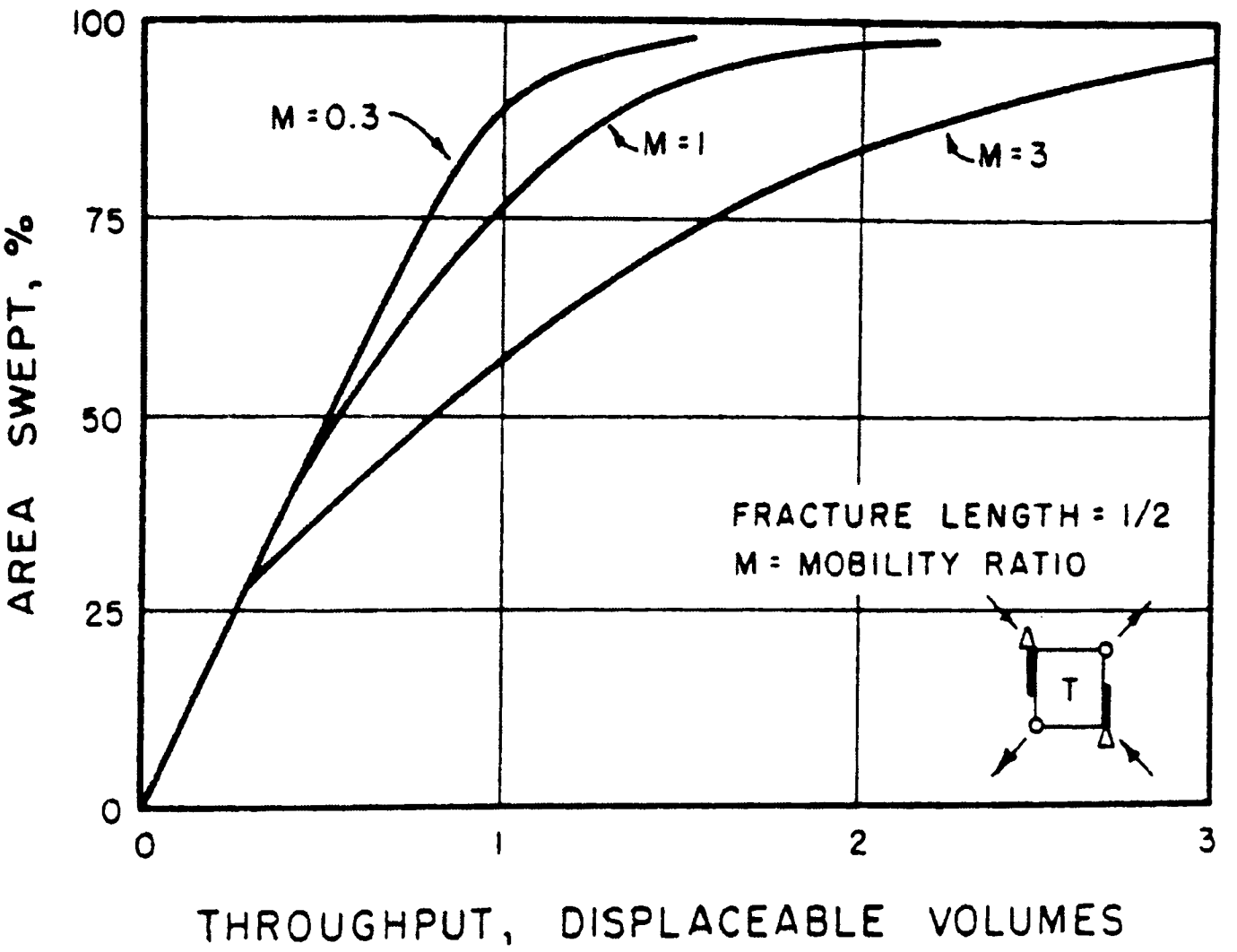

Figure 2.31. Influence of mobility ratio and fracture on % area swept.

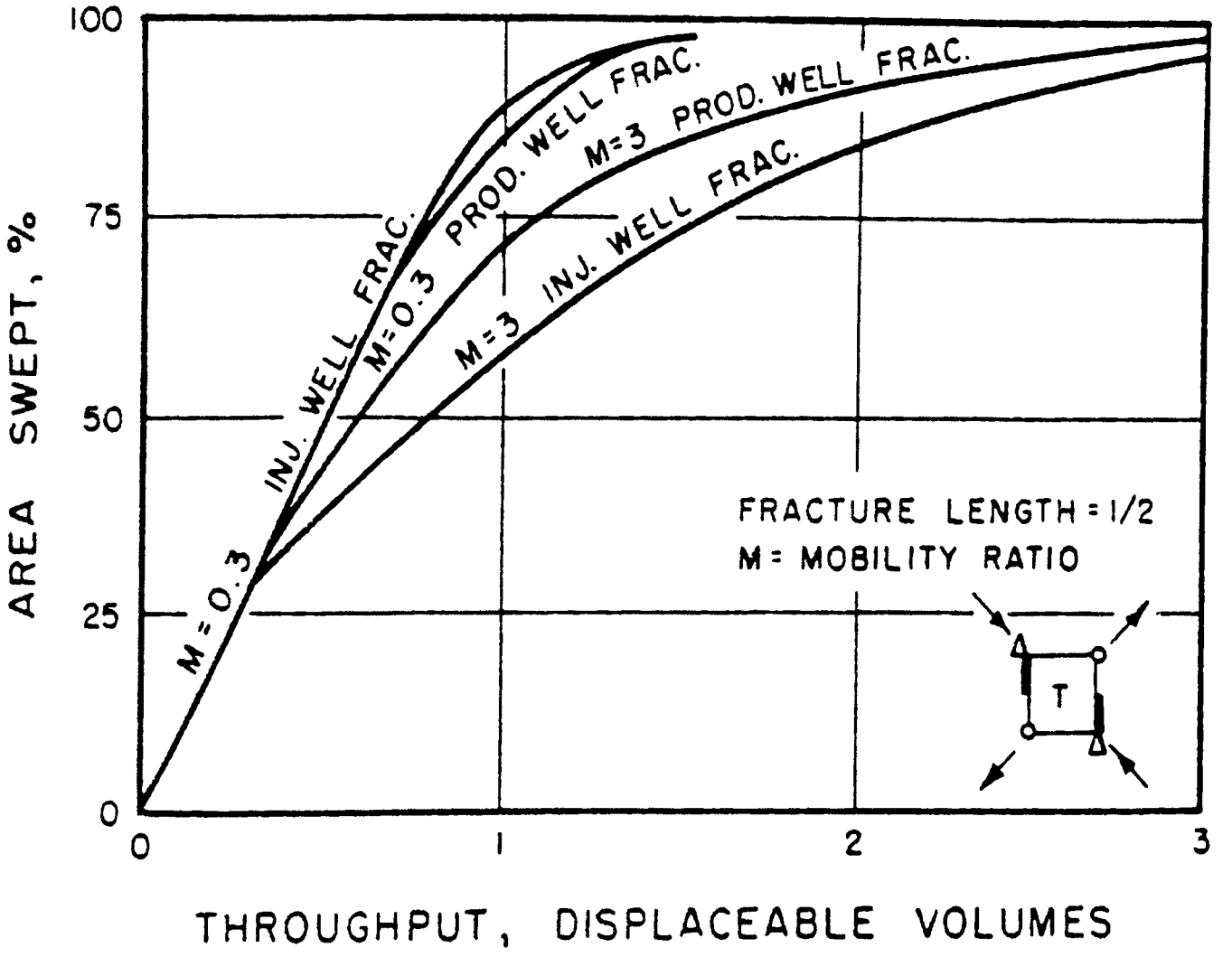

Figure 2.32. Influence of injection or production well fracture on % area swept.

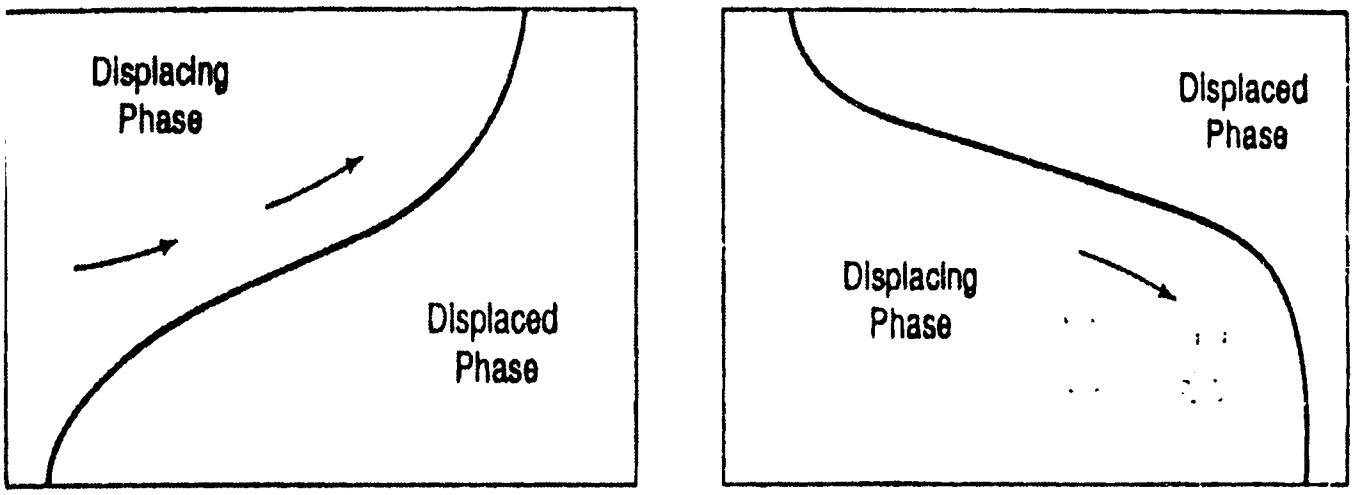

(a) Gravity Override $\rho_D < \rho_d$

(a) Gravity Underride $\rho_D > \rho_d$

Figure 2.33. Gravity segregation in displacement processes.

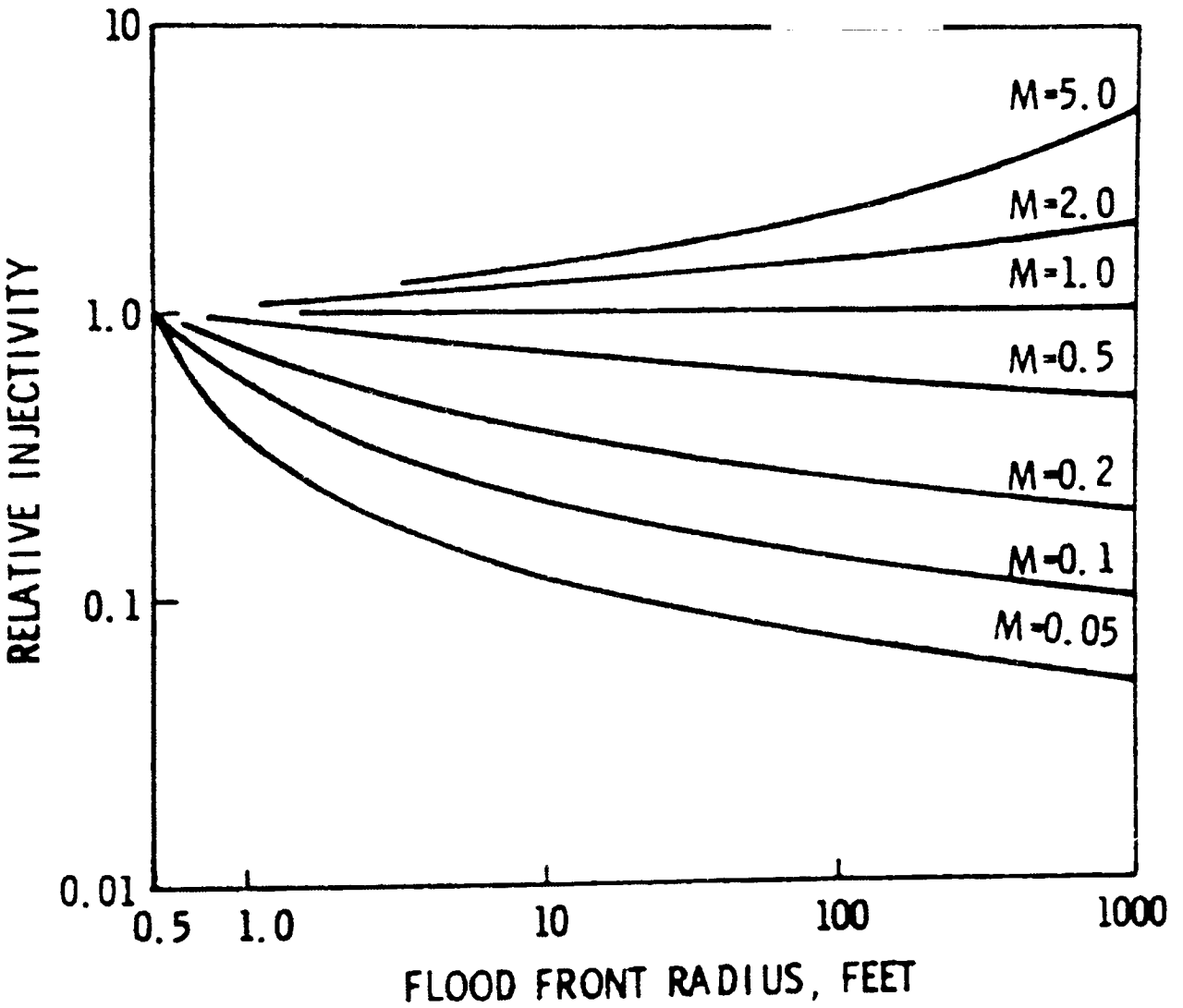

Figure 2.34. Variation in fluid injectivity in liquid-saturated redial system.

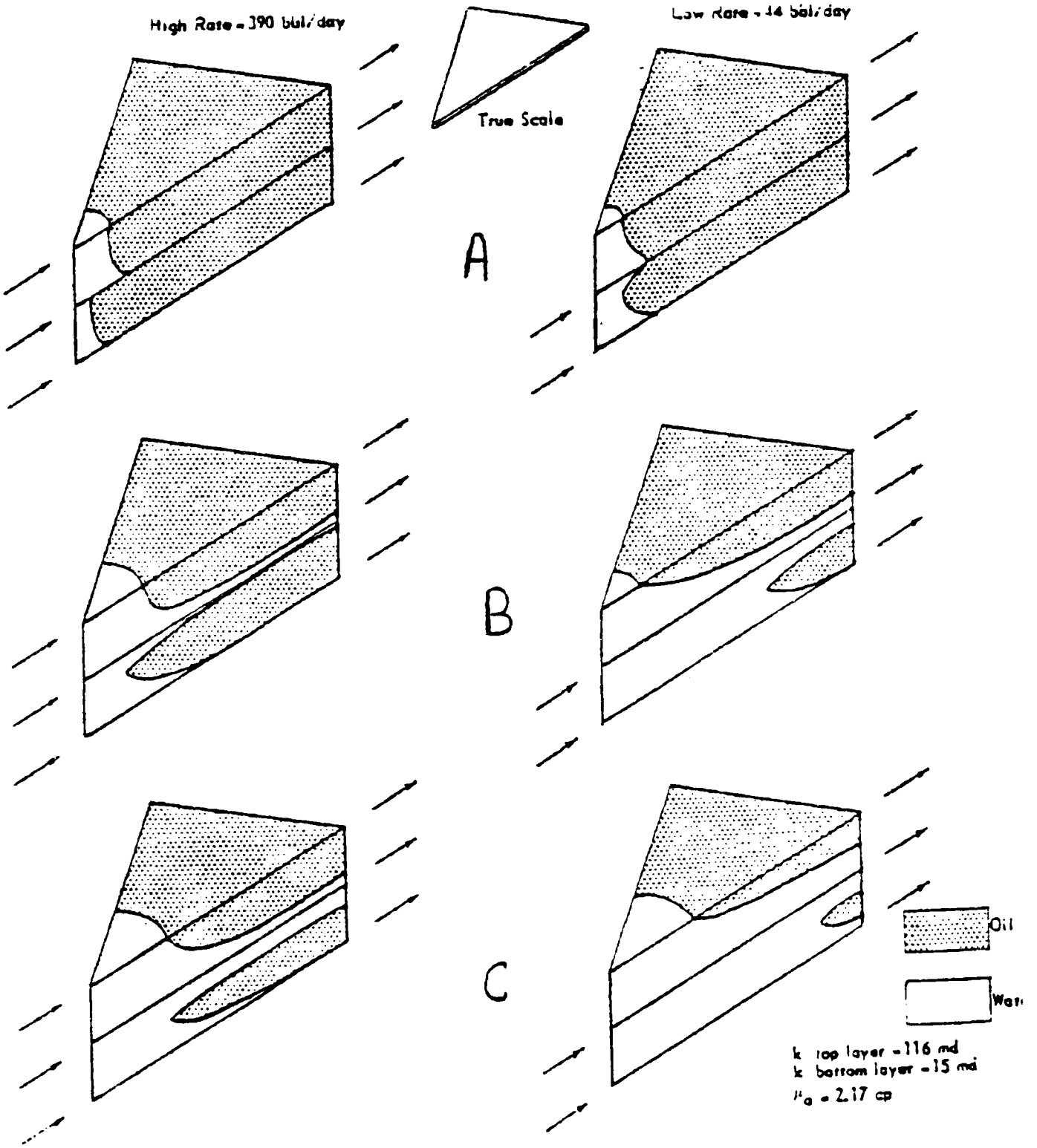

Figure 2.35. Observed flood fronts.

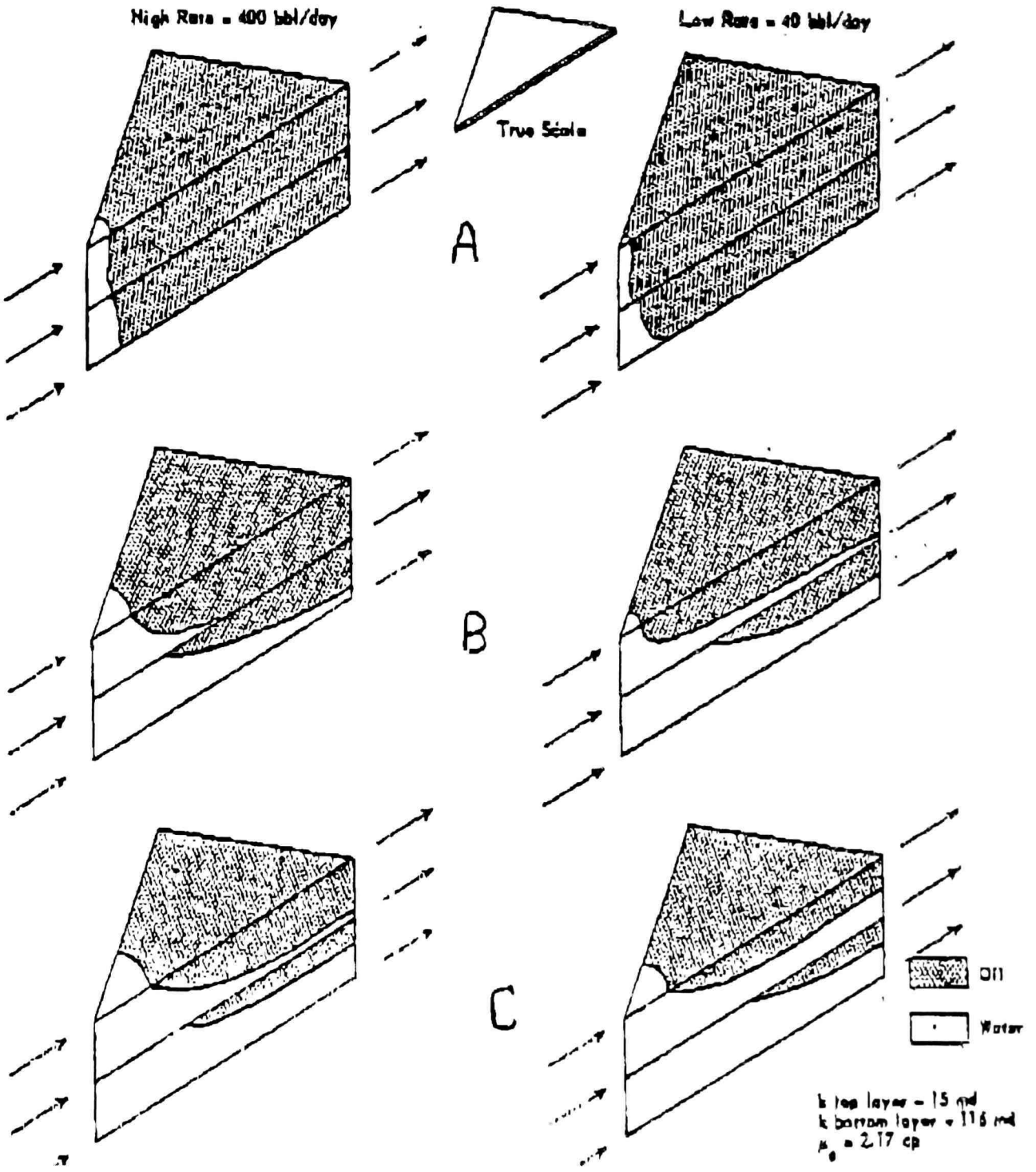

Figure 2.36. Observed flood fronts.

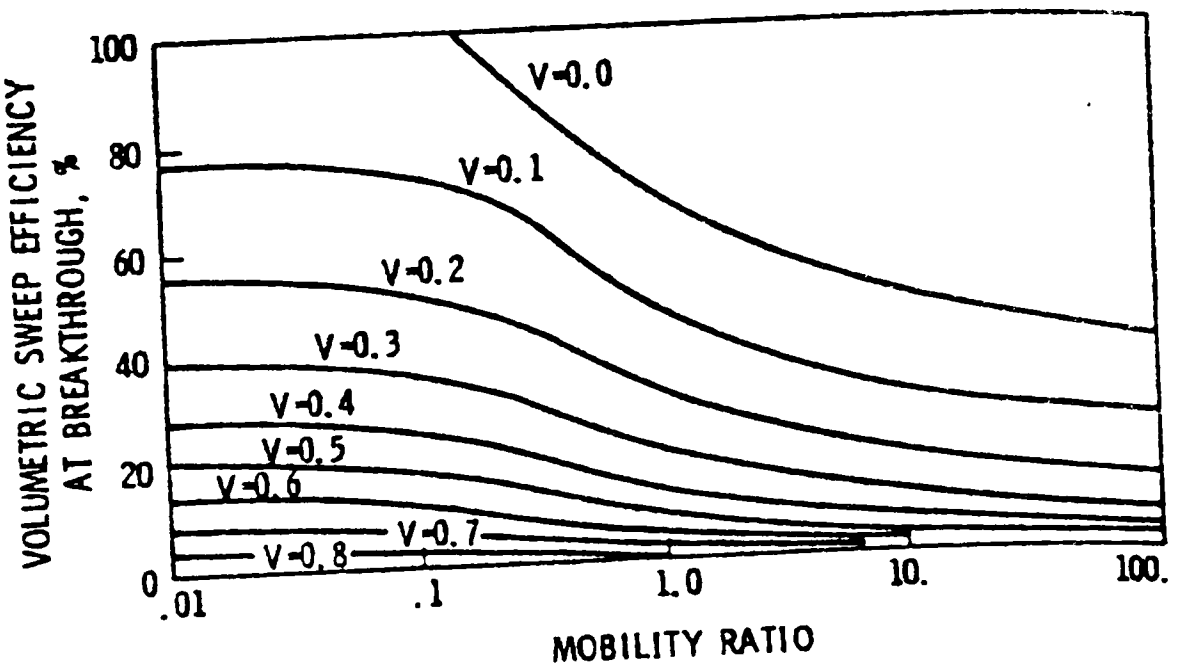

Figure 2.37. Volumetric sweep efficiency at breakthrough, five-spot pattern; zero initial gas saturation.

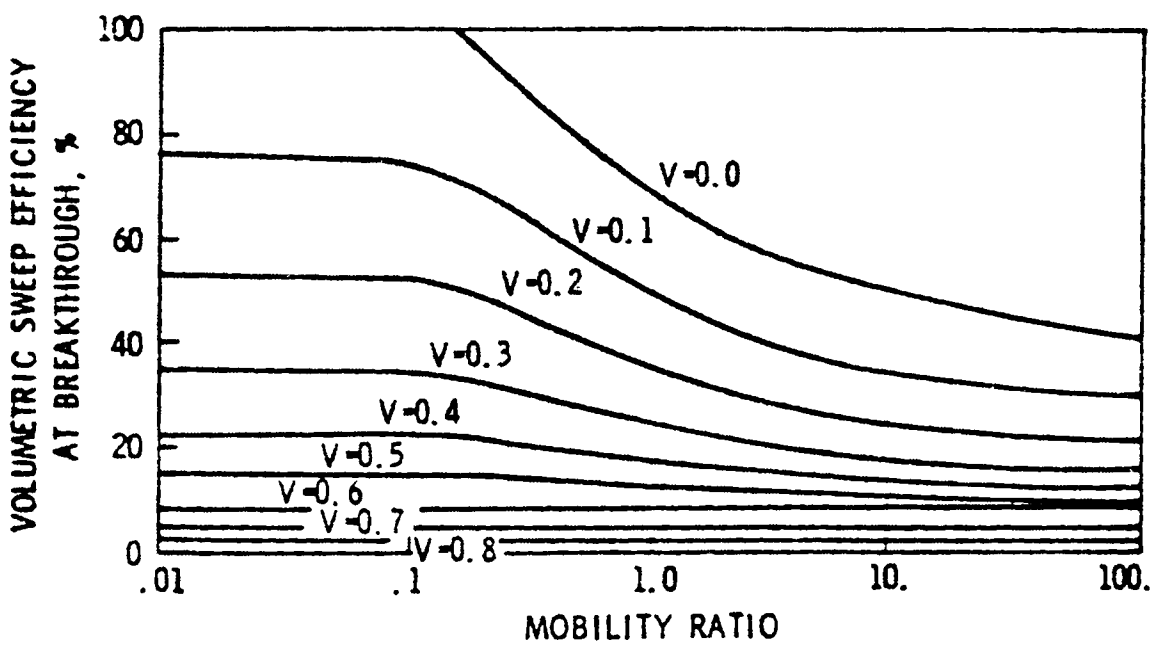

Figure 2.38. Volumetric sweep efficiency at breakthrough, five-spot pattern; initial gas saturation = 10% PV.

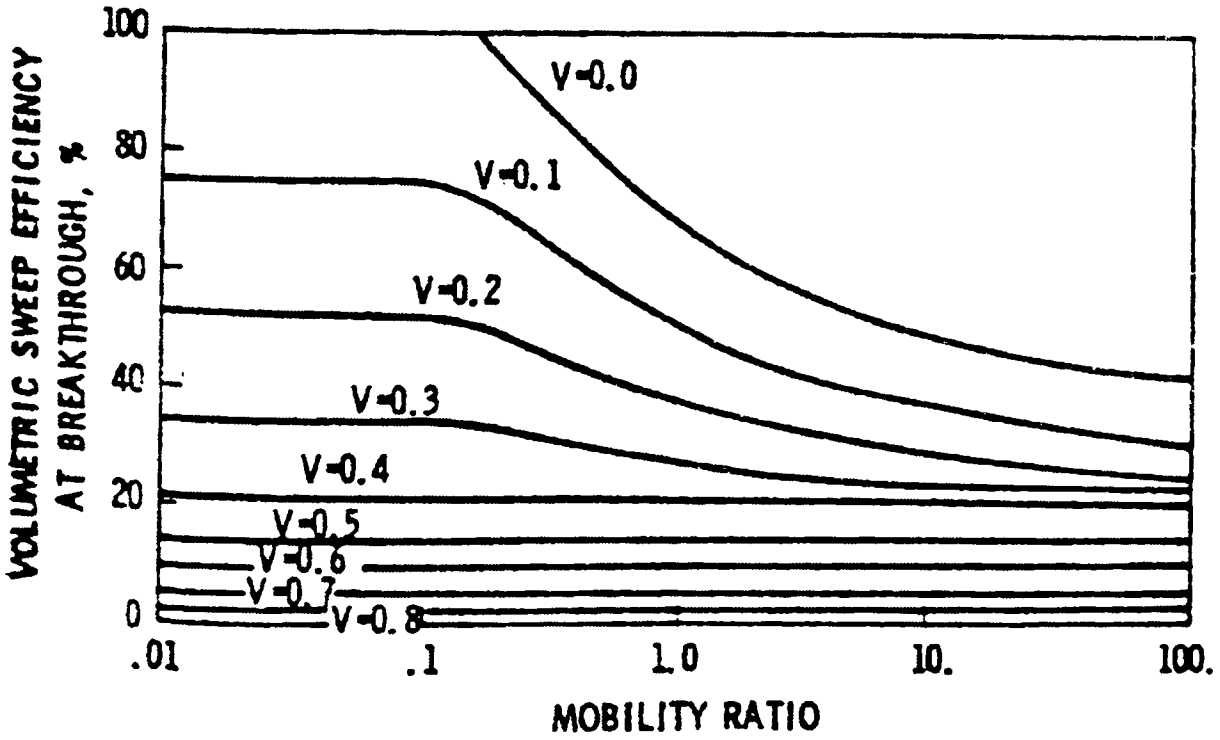

Figure 2.39. Volumetric sweep efficiency at breakthrough, five-spot pattern; initial gas saturation = 20% PV.

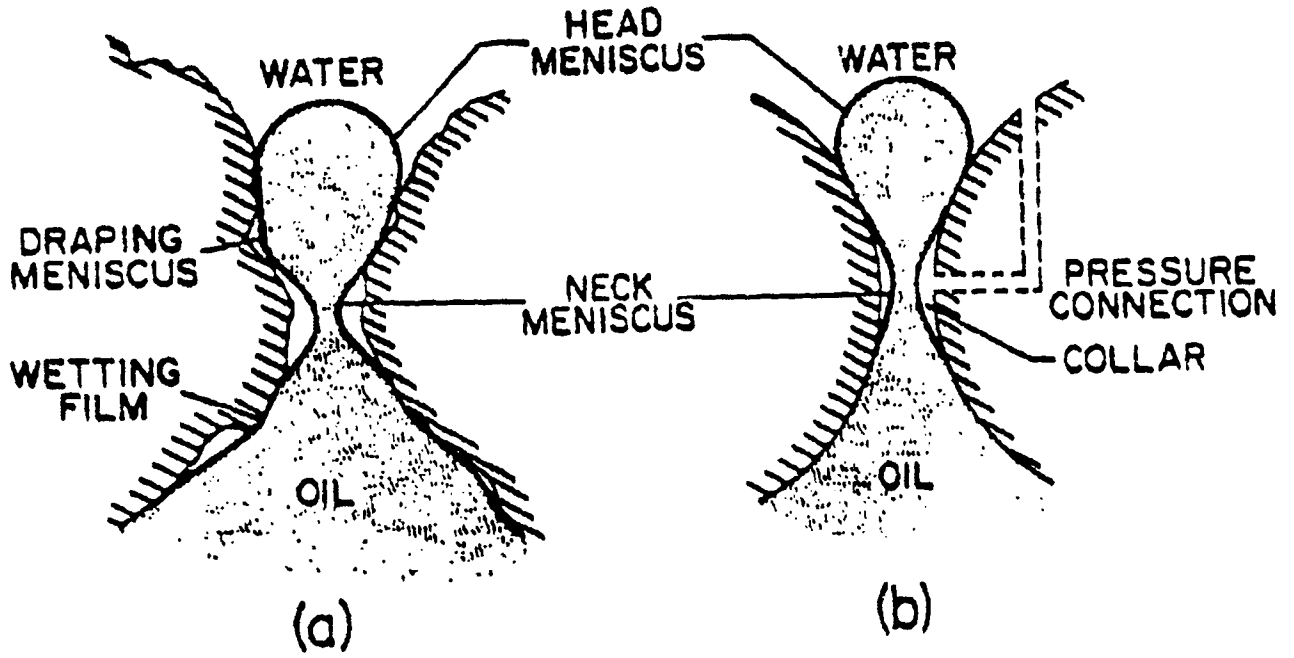

Figure 2.40. Displacement and entrapment of oil at pore level.
(a) water-oil interface in a pore
(b) model in terms of head menisci, a neck menisci and a pressure connection.

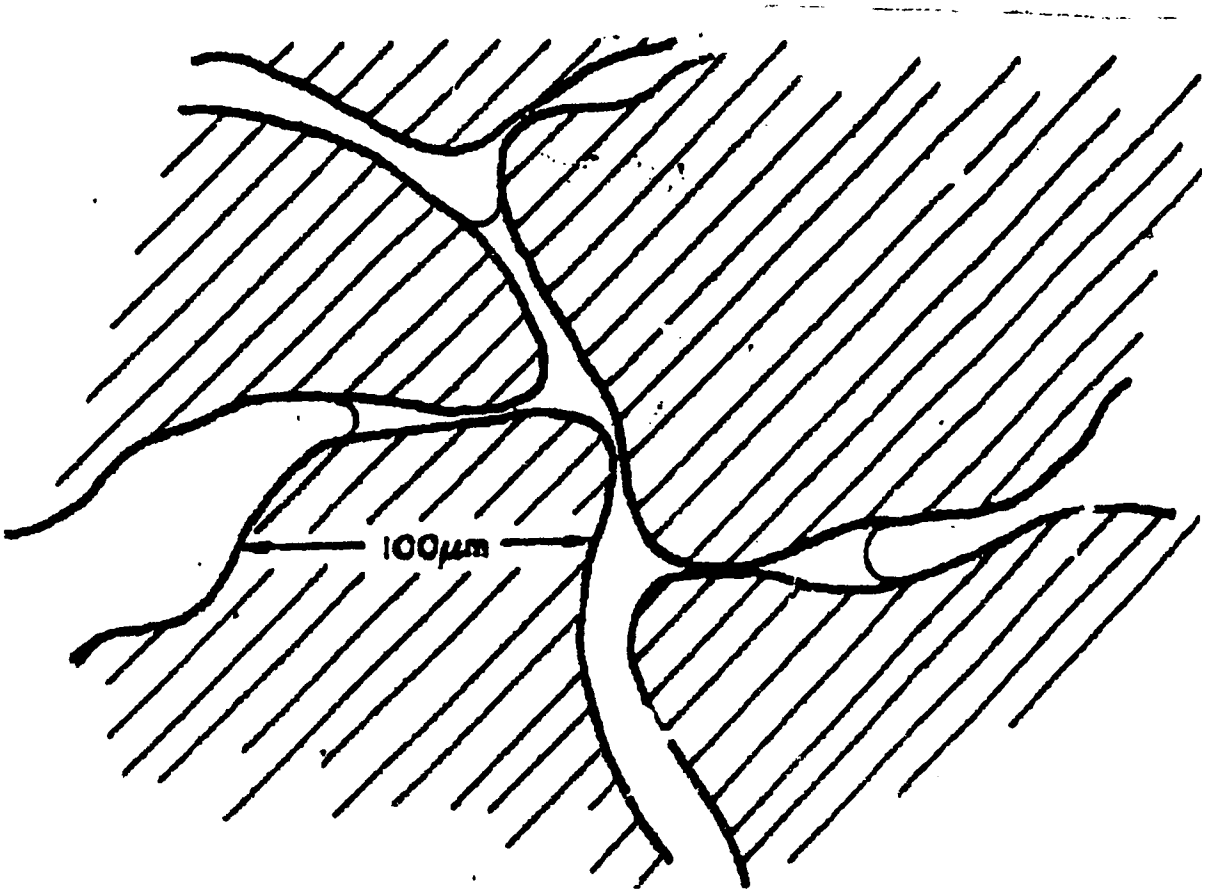

Figure 2.41. Haines' jump phenomenon occurring in the microscopic, tortuous flow channels of a porous medium.

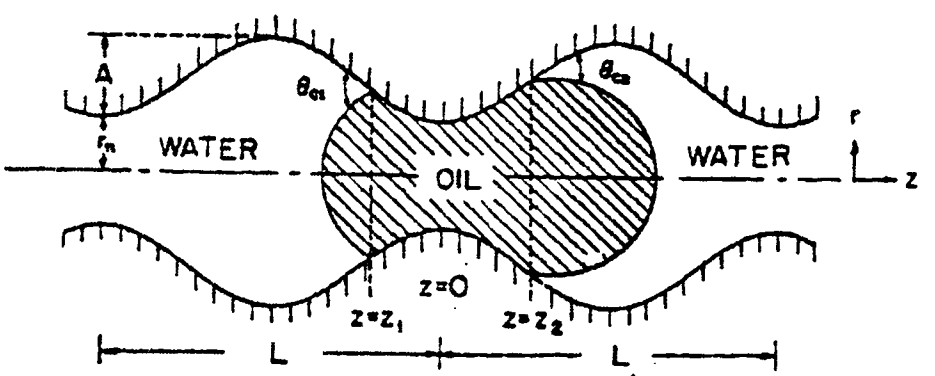

Figure 2.42. Sequence of static configurations as an oil segment

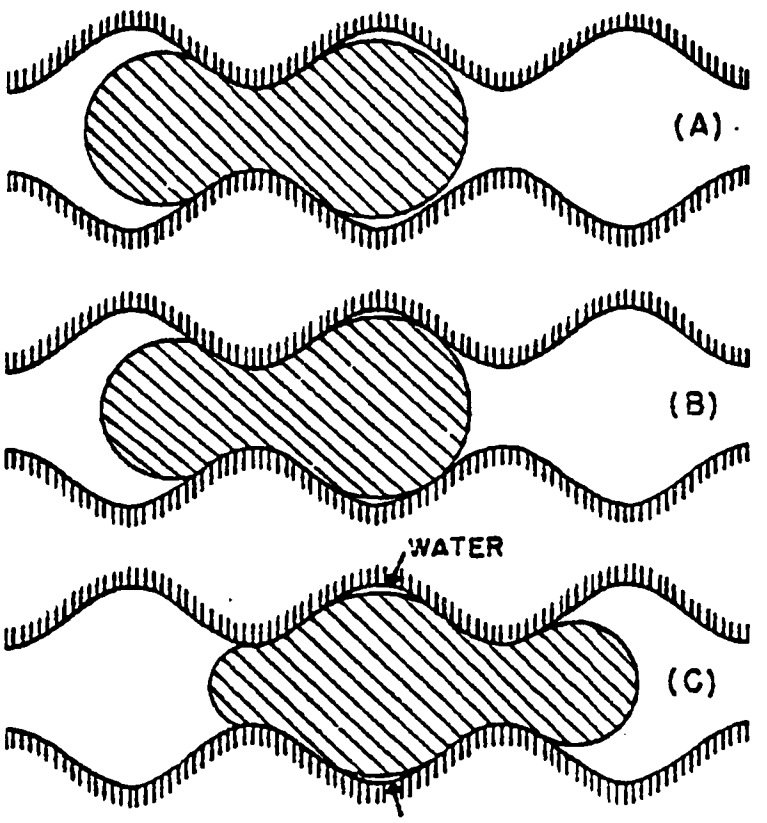

Figure 2.43. Sequence of static configurations as an oil segment moves through a water-wet pore over a ring of water trapped on the wall of the pore.

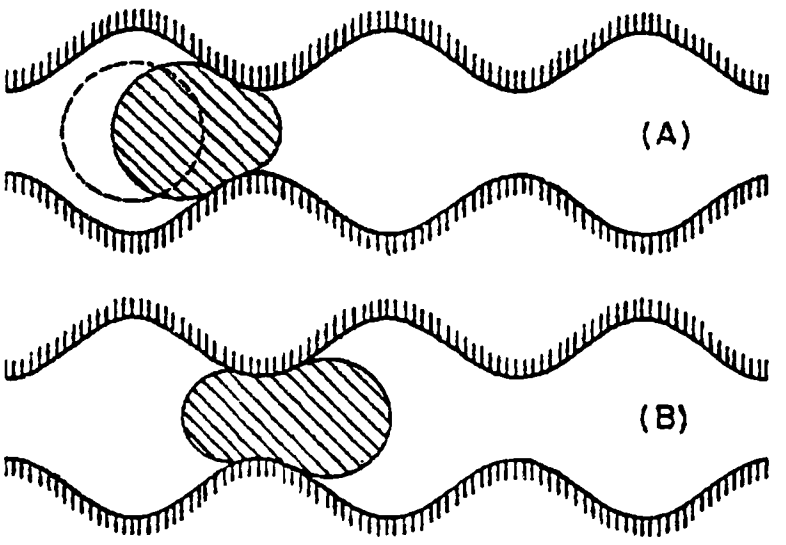

Figure 2.44. A small oil segment may be trapped in the form of a spherical drop as it is displaced through a water-wet pore.

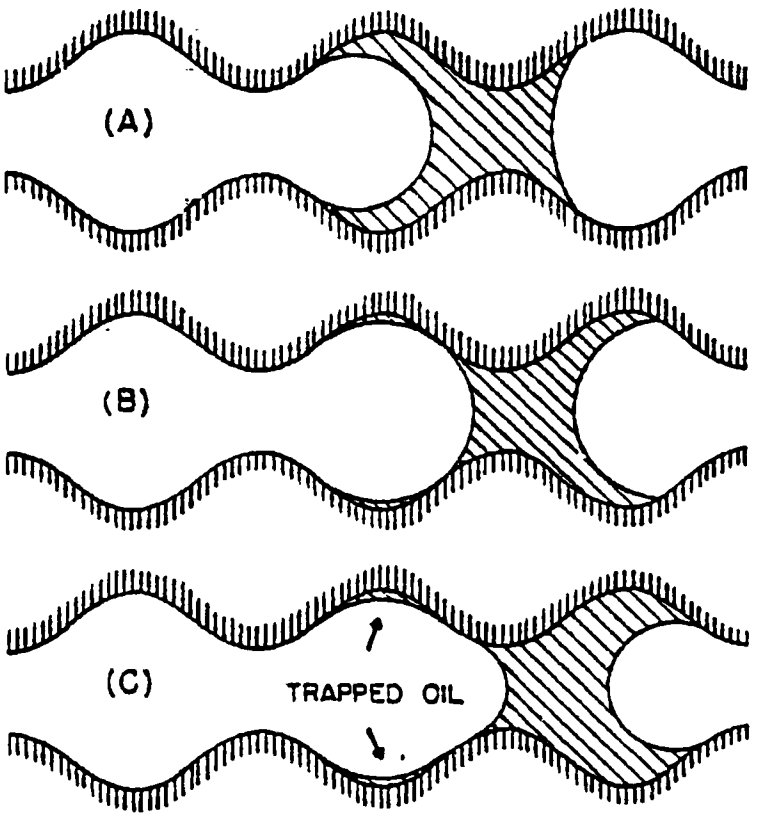

Figure 2.45. Sequence of static configurations as an oil segment moves through an oil-wet pore, leaving a portion of itself behind trapped on the wall.

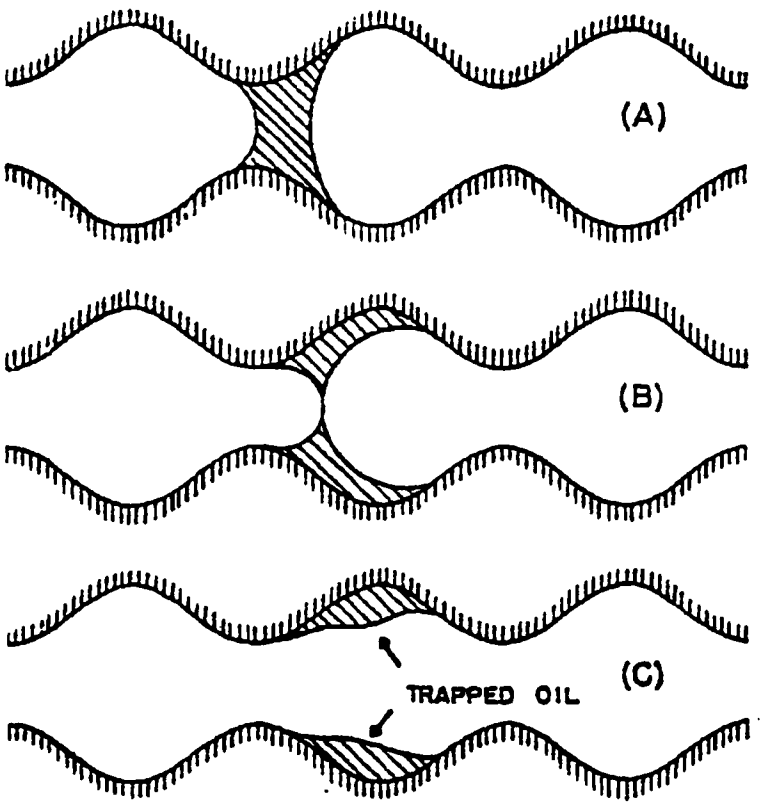

Figure 2.46. A smaller oil segment cannot assume a static configuration at all positions in an oil-wet pore. It will be trapped on the wall of the pore.

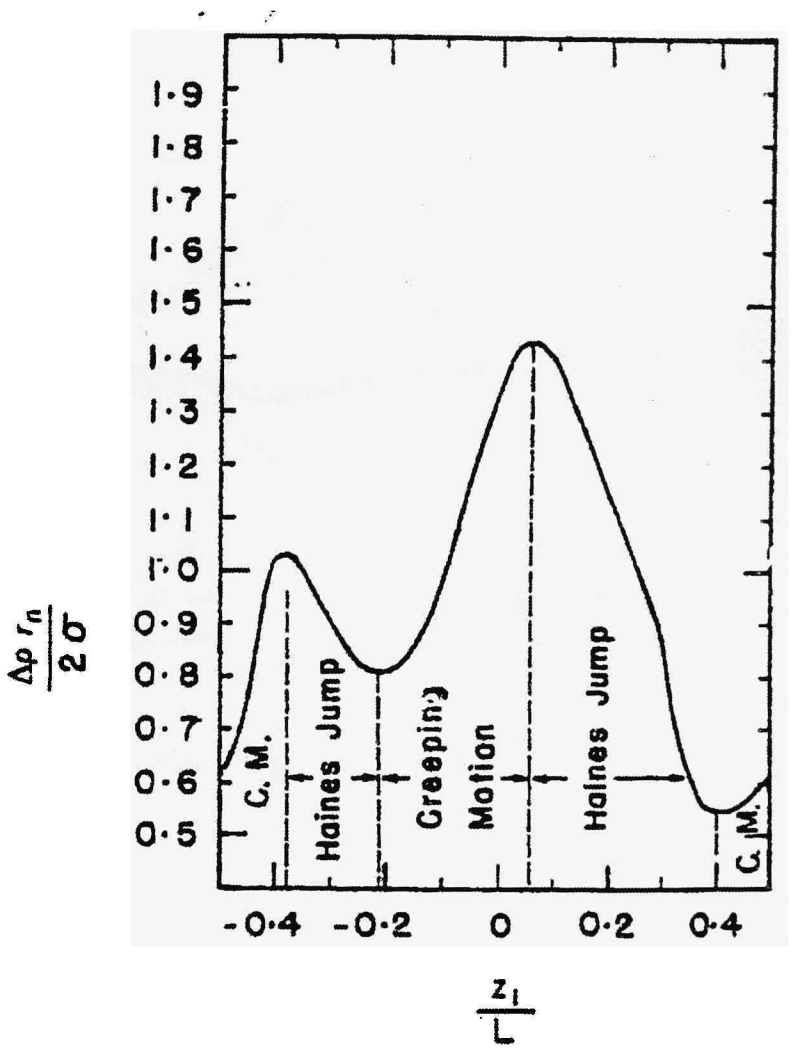

Figure 2.47. Haines jump

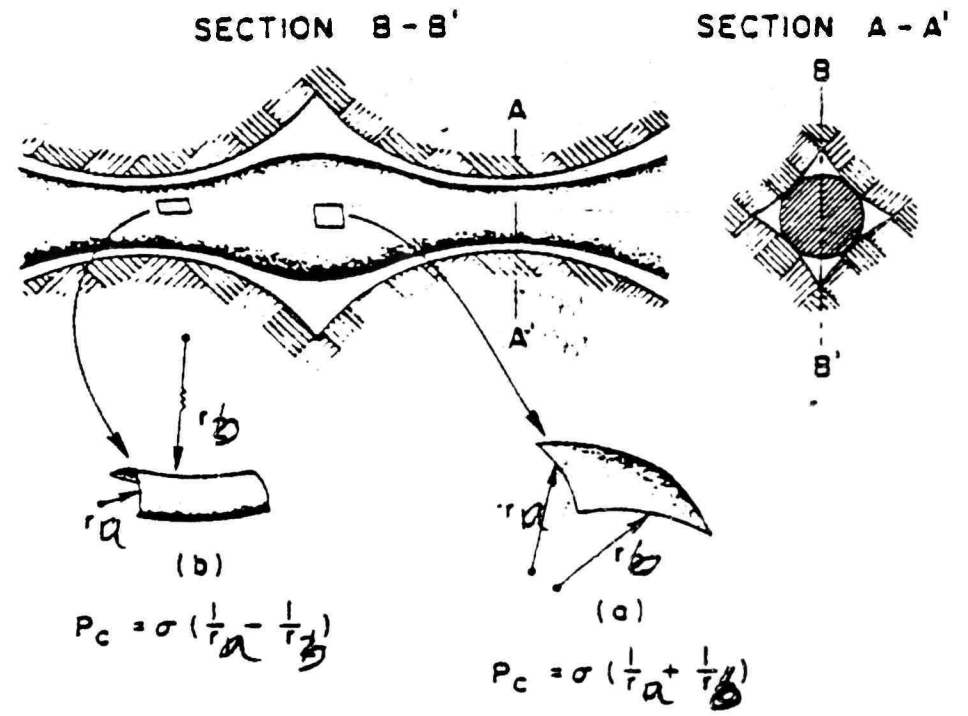

Figure 2.48. Two types of interfacial curvature

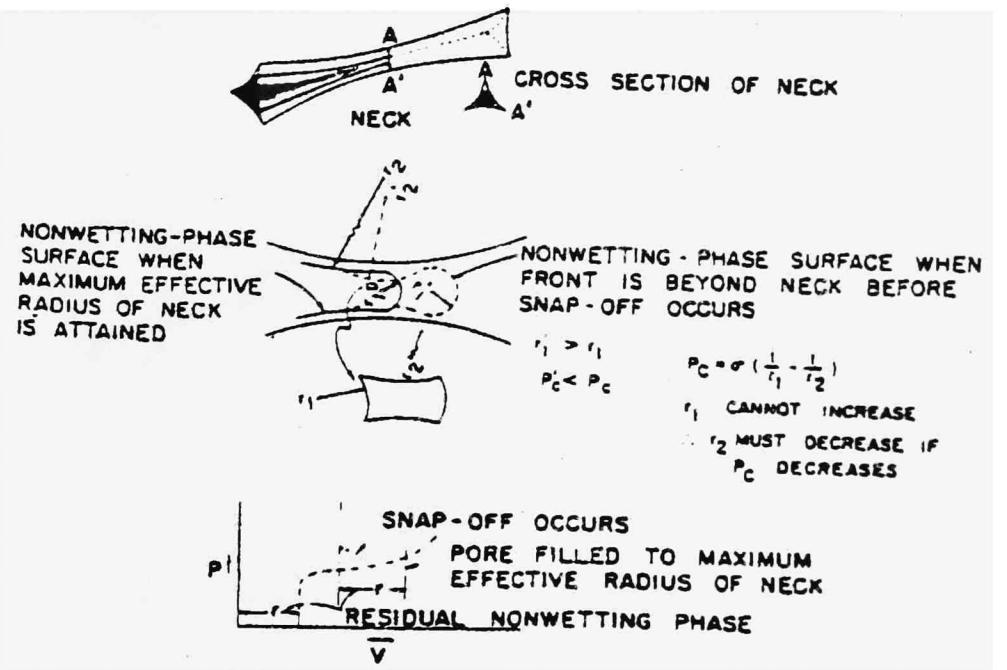

Figure 2.49. Schematic representation of non-wetting-phase injection through restricted opening and subsequent trapping.

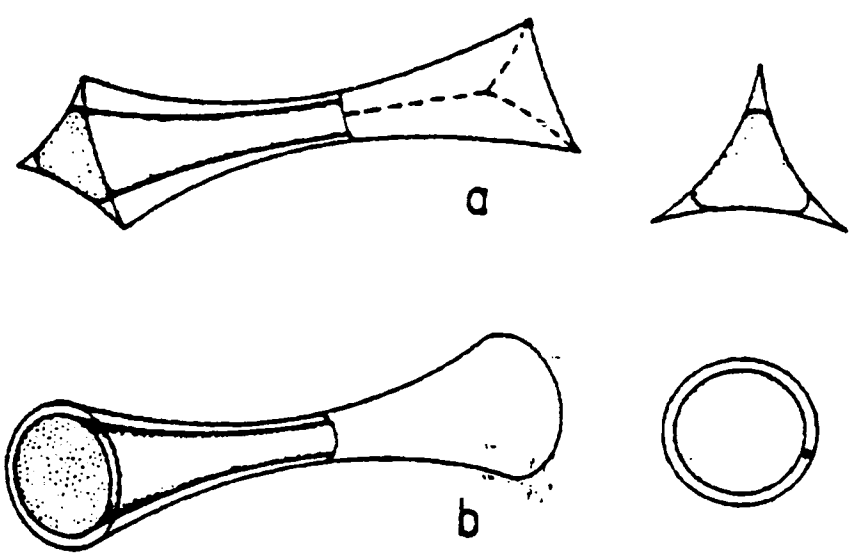

Figure 2.50. Pore Geometry

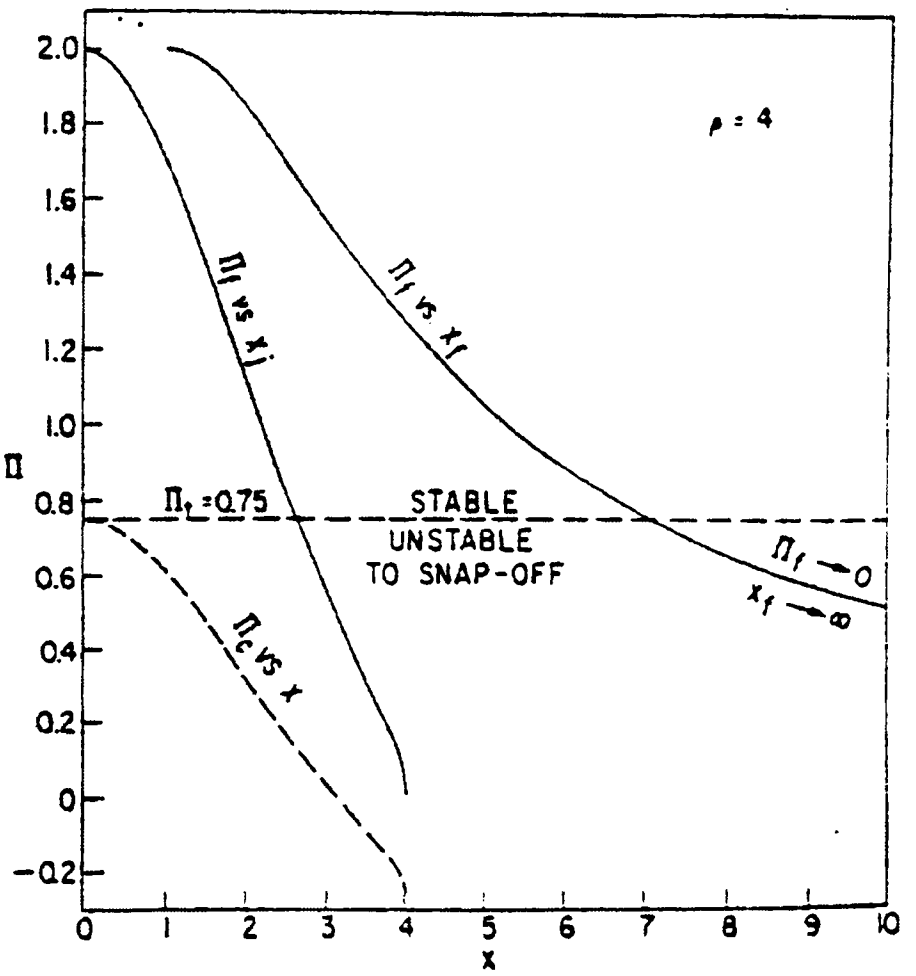

Figure 2.51. Stable and unstable region for snap-off

CHAPTER 3

METHODOLOGY

The Buckley-Leverett Model was used in this thesis for modeling the linear, immiscible displacement of oil by water. In order to visualize the microscopic and macroscopic movement of oil through a porous media, a computer program was developed. This chapter discusses the method followed in developing the computer program.

The following sequence was used to achieve the objective of this thesis, stated in the introduction of this manuscript.

1. Create a fractional flow curve in Microsoft Excel, using the rock and fluid properties from example 3.5 of Green and Willhite.[7]
2. Automate the tangent drawn from the initial water saturation and passing through the breakthrough point on the fractional flow curve. This helps to view a tangent on the fractional flow curve, created with any set of core data.
3. Create a saturation profile (S_w vs. x_D), to view saturation distribution at the macroscopic level.
4. Create microscopic views using PowerPoint for the movement of oil through pores. These views are later used in conjunction with the macroscopic views to make the saturation profile interactive.
5. Develop a computer program using Visual Basic 6.0, Access 97, Excel 97 and PowerPoint 97. Excel and Access are linked to Visual Basic, using the ActiveX

technology so that any modification in the Excel spreadsheet reflects in the Access database.

3.1 Creation of Fractional Flow Curve

In order to create the fractional flow curve, the Buckley-Leverett model was used to model the waterflooding process. Core data, listed in Table 3.1,[7] was used to create the fractional flow curve. The difference between the initial water saturation (S_{iw}) and ($1-S_{or}$) was divided into 50 equal increments. (The number of divisions was randomly chosen to be relatively high in order to approximate the fractional flow curve via linear interpolation, but not too high to be computationally tedious.) This is represented by S_w in column 2 of Table 3.2.

The fractional flow of water, f_w, represented by column 3 of Table 3.2, was calculated using the equation:

$$f_w = \frac{S_{wD}^n}{\left[S_{wD}^n + A(1-S_{wD})^m\right]}. \qquad \text{Eq 3-1}$$

The derivative of fractional flow with respect to saturation, represented by f'_w (column 4 of Table 3.2), was calculated using this expression:

$$f'_w = \frac{\partial f_w}{\partial S_w} = \frac{AB\left[nS_{wD}^{n-1}(1-S_{wD})^m + mS_{wD}^n(1-S_{wD})^{m-1}\right]}{\left[S_{wD}^n + A(1-S_{wD})^m\right]^2} \qquad \text{Eq 3-2}$$

where A and B were constants:

$$A = \frac{\alpha_1 \mu_w}{\alpha_2 \mu_o} \qquad \text{Eq 3-3}$$

$$B = \frac{1}{(1 - S_{or} - S_{iw})}. \qquad \text{Eq 3-4}$$

The dimensionless time, t_{D2}, was entered in column 5. When water saturation S_{w2} arrives at the end of the linear system, t_{D2} is given by:

$$t_{D2} = \frac{1}{f_w'}. \qquad \text{Eq 3-5}$$

Average water saturation, represented by column 6 of Table 3.2, was calculated using the equation:

$$\bar{S}_w = S_{w2} + t_D(1 - f_{w2}). \qquad \text{Eq 3-6}$$

The dimensionless water saturation, S_{wD}, represented by column 7 on Table 3.2, was calculated as follows:

$$S_{wD} = \frac{S_w - S_{iw}}{1 - S_{or} - S_{iw}}. \qquad \text{Eq 3-7}$$

Using the data tabulated in the Table 3.2, a plot of saturation of water vs. fractional flow of water (S_w vs. f_w) was created and is shown in Figure 3.1 (f_w vs. S_w).

3.2 Drawing an Automated Tangent to the Fractional Flow Curve

"Automated tangent" is defined as the tangent automatically created, starting at the initial water saturation and passing through the point of maximum slope on the fractional flow curve,

In order to determine the water saturation and fractional flow of water at water breakthrough at the outlet of the linear system, an automated tangent was drawn from the

initial water saturation (S_{iw}) to the point of maximum slope on the fractional flow curve. The intersecting point of the tangent on the fractional flow curve is the breakthrough point.

The automated tangent to the fractional flow curve was created by finding the maximum slope of the fractional flow curve. The final value (50^{th} value) of initial water saturation was ($1-S_{or}$), where S_{or} was the residual oil saturation entered in Table 3.1. The value of initial water saturation (S_{iw}) from Table 3.1 was the first value of water saturation, S_w. In this case, $S_{iw} = S_w$. The difference between the final and first value of water saturation was divided into fifty equal parts and entered into column 1 of Table 3.2.

To determine the x and y coordinates of the point with maximum slope, the first step was to find the slope of each point on the fractional flow curve. The slope of each point on the fractional flow curve at and before breakthrough was calculated using the expression:

$$Slope = \frac{df_w}{dS_w} = \frac{f_w}{S_w - S_{iw}}. \qquad \text{Eq 3-8}$$

The maximum value of slope was found using the MAX function of Excel. MAX returns the largest value in a set of values. The exact syntax for the MAX function is:

MAX (number1, number2, number3…).

This could be written as MAX (A1:A10), where A1 is the first cell and A10 is the last cell to be considered for finding the maximum. The maximum value of the slope was calculated by the expression:

Maximum Slope =MAX (D101:D149)

The MAX result was place in a cell – in this case, cell H100.

After determining the maximum slope of the fractional flow curve, the value of maximum slope was matched up with those in Table 3.2. The MATCH function of Excel was used for this purpose. The MATCH function returns the relative position of an item in an array that matches a specified value in a specified order. The syntax for Excel function MATCH is as follows:

MATCH (*lookup_value, lookup_array, match_type*).

Match_type is the number -1, 0, or 1. *Match_type* specifies how Excel matches *lookup_value* with values in *lookup_array*. A *Match_type* of –1 is used to find the smallest value that is greater than or equal to *lookup_value*. A *Match_type* of 1 is used to find the largest value that is less than or equal to *lookup_value*. A match type of 0 is used to find the first value that is exactly equal to the *lookup_value*. In this case, a *Match_type* of 0 was used, since the goal was to match the exact value of saturation (S_w) corresponding to the maximum value of slope. The specified value to be matched in this case was the maximum slope.

In order to determine the saturation and the fractional flow of water at the maximum slope, the INDEX function of Excel was used. The INDEX function returns the value of an element in a table or an array, selected by the row and column number indexes. The syntax for the INDEX function is given below:

INDEX (array, row_number, column_number).

The MATCH and INDEX function were used together to obtain the saturation S_w as:

INDEX (B100:B148, (MATCH (H99, D100:D148,0))).

To obtain the value of fractional flow of water, corresponding to the maximum slope, MATCH and INDEX functions were used together again, as follows:

INDEX (C100:C148, (MATCH (H99,D100:D148,0))).

The water saturation and fractional flow values corresponding to the maximum slope values were automatically copied to a new location, using Excel's formula function, *Cell Reference*. The water saturation and fractional flow values were the x and y coordinates, respectively, necessary to determine the point through which the tangent was meeting the fractional flow curve.

3.3 Creation of Macroscopic View

The macroscopic view, or the saturation profile, is a graph of all the saturations (S_w) plotted against dimensionless distance (x_D). The data required to create the macroscopic views, namely, water saturation (S_w) and the derivative of fractional flow values (f'_w) were obtained from Table 3.2. Table 3.3 holds the consolidated and required information to plot a saturation profile. Data from the saturation profile corresponding to a dimensionless time, when water saturation reaches the end of the linear system ($x_D = 1$), i.e., when

$$t_D = t_{D2} \qquad \text{Eq 3-9}$$

An explicit value of dimensionless distance is required to create the macroscopic view. A provision was made to input any desired value of dimensionless distance and observe the shape of the macroscopic view. Such a provision was made on the Excel spreadsheet called 'Table 1'. This could be achieved by entering the value of dimensionless distance (x_D) in percentage in the specified cell in sheet named 'Table 1'.

Table 3.3 was constructed to represent a dimensionless distance as entered by the user. For example, if the user requires to view the saturation profile at 75% (x_D=0.75). Table 3.3 automatically retrieves the S_w and f'_w values from Table 3.2 and displays the dimensionless distance at 75%. The saturation entries in Table 3.3 started with 1-S_{or} and gradually reduced in steps to reach the breakthrough saturation, and finally the initial water saturation. This saturation reduction in steps was done to show the decrease in water saturation to the flood front. Corresponding values for the fractional flow derivative (f'_w) were entered into Table 3.3. The final dimensionless distance (x_D) entry in Table 3.3 was 1, which represented a dimensionless distance of 100%. Moreover, x_D = 1 is the case if the front is at the producer.

A graph representing the macroscopic view was plotted using the values in Table 3.3. The macroscopic view was divided into ten regions, by dividing the dimensionless distance (x_D) into ten equal parts from zero to one. The basis for dividing the dimensionless distance into ten equal parts was to enable visualization in steps of 10% water saturation.

3.4 Creation of Microscopic Views

Microscopic views were created with the aim of representing a pore at a given saturation distribution and dimensionless distance. The pore images were constructed using Microsoft Paint® from within PowerPoint®. The process used to construct the pores is described below.

A blank presentation window was opened in PowerPoint®, and using the drawing toolbar, located at the bottom of the screen, "Auto shapes > Lines > Scribble" was selected, as shown in Figure 3.2. This was done to draw the curvature of the pore body and pore throats, as shown in Figure 3.3. The oval button, located on the drawing toolbar, was clicked and the mouse was pointed to the center of the pore construct to draw an oval, representing the oil phase, as shown in Figure 3.4. The rectangle button was used to draw a rectangle around the above-mentioned construct, as shown in Figure 3.5. The textbox button, located on the drawing toolbar was used to name each of the regimes- Oil, Water and Porous Media, as shown in Figure 3.6.

This image (Figure 3.6) was selected by choosing "Edit > Select All". The selected image was copied and pasted into Paint®, as shown in Figure 3.7, to enable coloring. The colored image was copied and pasted back into another PowerPoint slide, and was saved, as shown in Figure 3.8. This procedure was repeated to construct each of the pores, with different saturations.

Pore 1 (Figure 3.9) and Pore 2 (Figure 3.10) represent the water saturation regimes of 5-10% and 11-20%, respectively. Pore 3 (Figure 3.11) and Pore 4 (Figure 3.12) represent water saturation regimes of 21-30% and 31-40%, respectively. Pore 5 (Figure 3.13) and Pore 6 (Figure 3.14) represent water saturation regimes of 41-50% and 51-60%, respectively. Pore 7 (Figure 3.15) and Pore 8 (Figure 3.16) represent water saturation regimes of 61-70% and 71-80%, respectively. Pore 9 (Figure 3.17) and Pore 10 (Figure 3.18) represent water saturation regimes of 81-90% and 91-95%, respectively. The

constructed pore images were embedded into saturation profile using the Object Linking and Embedding (OLE) technique.

3.5 Linking Excel to Access

In order to create the graphs of fractional flow curve, automated tangent, and the saturation profile, the graphs required the data to be populated from a database. Access was chosen as a database, due to its popularity and ease of availability, and the superior interface between Microsoft products. Data from the Excel spreadsheet was used to populate the Access database by linking Excel and Access so that any change of value in the Excel tables would be reflected in the Access database.

For each database table, Access required the source data from Excel to be generated from a different Excel sheet. Five Access database tables were required to be created to:

- plot the fractional flow curve
- plot the fractional flow curve with tangent
- create the macroscopic views
- identify the microscopic view to be displayed
- generate the fractional flow curve with derivative (to be used for further enhancements).

These data were copied from the existing tables (Tables 3.2 and 3.3) and copied to a new location using Excel's Reference Cell function. The new Excel sheets were named TA, TB, TC, TD and TE. Whenever data was modified in the parent tables (Table 3.2 – 3.3), the corresponding child tables (on sheets TA, TB, TC, TD and TE) gets updated to

reflect current data. This was achieved by writing a macro in the Excel spreadsheet. Updated data was transferred to Access tables named TableA, TableB, TableC, TableD, and TableE.

3.6 Linking Visual Basic to Excel and Access

Visual Basic was used to make the microscopic views interactive. In computer language, interactivity is the sensory dialog that occurs between a human being and a computer program. An example of an interactive computer program is a computer game. An executable is a file that contains a program, which is a particular kind of file capable of being executed or run as a program in the computer. In a Disk Operating System (DOS) or Windows operating system, an executable file usually has a file name extension of .bat, .com, or .exe.

The flowchart used for creating the necessary logic for the Visual Basic program is shown in Figure 3.19. The Visual Basic Program displays the fractional flow curve, the automated tangent, the breakthrough points, the macroscopic views and the microscopic views. By clicking on the macroscopic view, the user can visualize the corresponding microscopic views. The Visual Basic program also allows the user to view or modify the input parameters. The flowchart explains the various logical steps involved while executing the program.

When the Visual Basic program starts, it requires the location of the Excel and Access files as input. This is achieved by providing browse buttons in the software, where the user can navigate and locate the required files. The program was created such that only

Excel files (files with extension .xls) will be displayed during Excel file selection. Similarly only Access files (files with extension .mdb) will be displayed during Access file selection. Once the Excel and Access files are chosen, the Visual Basic program automatically links itself in the background.

The next stage is a processing stage. The program, based on the user's selection, processes the next screen. The choices available to the user are:

- View existing data
- Compute and Save
- Get Breakthrough Points
- View Fractional Flow curve
- View Fractional Flow and Tangent
- View Saturation profile
- Exit.

If the user requests to "View existing data," the program displays the corresponding values from the Excel sheet. "Compute and Save" makes new changes to the Excel file. "Get Breakthrough Points" displays the breakthrough water saturation and the breakthrough fractional flow of water. "View Fractional Flow curve" displays the fractional flow curve. "View Fractional Flow and Tangent" displays a tangent along with the fractional flow curve. "View Saturation profile" displays the macroscopic view, and "Exit" closes the program.

If the user requires to exit the program, the Visual Basic program first confirms if the action is necessary or not. If the user selects "Yes", then the program again confirms it

any data needs to be saved. Based on the user's selection, the program saves the data or not, and exits the program. If the user chooses "No" while exiting, the previous output results are displayed, and the program returns to the main screen.

3.6.1 Procedure for Creating a Visual Basic Executable

The procedure described below is used to create a standard executable in Visual Basic to achieve the interaction required between the user and the executable. A standard executable in Visual Basic can be executed on any windows operating system. The Visual Basic development environment was opened to create a new project file by navigating the controls Start | Programs | Microsoft Visual Studio 6.0 | Microsoft Visual Basic 6.0, as shown in Figure 3.20 (this location may vary on other computers, if Visual Basic was installed on another location that the default location). A window called 'New Project' appeared, as shown in Figure 3.21. In order to create an executable, a 'Standard EXE' type was selected and the Open button was clicked. A standard executable could be executed on any computer containing the Windows operating system.

A blank form, called Form1 appeared in the Visual Basic development environment, as shown in Figure 3.22. Form1 houses the Visual Basic controls required for the user inputs. The required reference libraries were included to the project by going to Project | References, as shown in Figure 3.23. The window that appears is shown in Figure 3.24. The reference library allows the selection of another application's objects that needs to be available in the code by setting a reference to that application's object library.

The following reference objects were included with the project, when the reference window appeared:

- Visual Basic for Applications
- Visual Basic runtime objects and procedures
- Visual Basic objects and procedures
- OLE Automation
- Microsoft Access 8.0 Object Library
- Microsoft Excel 8.0 Object Library

The first three reference objects Visual Basic for Applications, Visual Basic runtime objects and procedures, and Visual Basic objects and procedures are necessary for running Visual Basic. OLE Automation is a way to work with an application's objects from another application or development tool. The OLE Automation helps to work with the objects present in Microsoft Access and Microsoft Excel. OLE Automation is an industry standard and a feature of the Component Object Model (COM). By including the reference objects, Microsoft Access 8.0 Object Library and Microsoft Excel 8.0 Object Library, the features in Microsoft Access and Microsoft Excel are made available within the programming environment.

The Visual Basic Project Explorer window displays a list of all the forms, modules, and classes included in the program. A new module was created in the Visual Basic Project explorer window, by clicking Add | Module. This procedure is indicated by Figure 3.25. The variables declared at the module level are available throughout the project.

The project properties Project Name and Project Description were set by clicking the menu Project | Project1 Properties, as shown in Figure 3.26. The window titled Project1 - Project Properties appeared, as shown in Figure 3.27.

A new form was added as the title page. This form is shown in Figure 3.28. Controls like labels and command buttons were placed on the form. The labels were captioned to read the required text. The command button was captioned to display "OK". Code was written below the command button so that by clicking the OK button, the present screen was closed and the next form called Browse appeared.

The form Browse shown in Figure 3.29 has command buttons, text box and labels placed on the form. Code was written such that the first command button would display only the Excel files, and the second command button would display only the Access files. Code for the command button OK was written such that it would close the form Browse and display the form called Input Data.

The form Input Data shown in Figure 3.30 has controls, command buttons, labels, text boxes, frame, and menu items placed on the form. The labels were captioned appropriately to read the data retrieved from the Excel spreadsheet. The command buttons were labeled to indicate the action to be performed by the program. The frame contained all the labels and text boxes for clarity and grouping. The menu items used the same captions as the command buttons. Code was written such that the operation performed when the user clicked the menu items or the command buttons were the same.

The code for the command button "View Existing Data" retrieved the data from the Excel spreadsheet, called Table1. The Rock and Fluid Properties are displayed in Table

3.1. The data contained in the spreadsheet was retrieved in a 'read-only' format and was achieved with OLE Automation.

The code for the command button "Compute and Save" was written such that the program checked if any of the fields were changed by the user, and the corresponding value was updated in the Excel spreadsheet, Table1. The program would also display a list of properties modified by the user, since the last modification. The program also checks if any of the fields are left empty. A message would appear to the user indicating the field was empty and would prompt the user to input the necessary value. The new values would then be entered into the Excel spreadsheet. Whenever the input parameters were changed by the user, code was written to update the Access tables as well. Therefore, the Access Tables TableA, TableB, TableC, TableD, and TableE were updated.

The code for the command button "Get Breakthrough Points" was written such that it would display the form Breakthrough Points without closing the form Input Data. The data required to calculate the breakthrough points were also displayed on the form Input Data. The form Breakthrough Points is shown in Figure 3.31. Labels and a command button were placed on the form Breakthrough Points. When the form was displayed, the breakthrough points were read from the Excel spreadsheet, called Table1. The data was obtained in a read-only format using OLE Automation. The code for the command button "OK" closed the form Breakthrough Points and returned to the form Input Data.

The code for the command button "View Fractional Flow Curve"displayed the form, Fractional Flow Curve, shown in Figure 3.32. A graph object was placed on the form along with a command button. The data required to populate the fractional flow

curve was obtained from the Access database called TableB. The command button was captioned Close, and code was written to close the form Fractional Flow Curve and return to the form Input Data. Upon closing the form Fractional Flow Curve, the connection to the Access database was terminated.

The code for the command button "Fractional flow and Tangent" was similar to that of the command button "View Fractional Flow Curve" but contained additional data to create the tangent to the fractional flow curve. The form used to display the fractional flow curve and the tangent is the same. The data required to populate the graph was obtained from the Access database called TableC. When the form Fractional Flow and Tangent was closed using the command button captioned Close, the connection to the database was also terminated.

The code for the command button "View Saturation Profile" displayed the values obtained from the Excel spreadsheet Table1 and the form Dimensionless Distance. The form Dimensionless Distance is shown in Figure 3.33. A label, textbox and a command button were placed on the form Dimensionless Distance. The command button captioned OK used the value of the dimensionless distance entered in the textbox and supplied this value to the Excel spreadsheet called Table1. The spreadsheet performed the necessary calculations and updated the values in the Access Database called TableD. The code would then close the form Dimensionless Distance and display the form Saturation Profile. The form Saturation Profile is shown in Figure 3.34. The form Saturation Profile contained a graph object similar to the one used by the form Fractional Flow Curve. The data required to draw the saturation profile was obtained from the Access Database called TableD. The

command button captioned OK was coded such that it would terminate the database connection and close the form Saturation Profile.

The graph object was made sensitive to the computer mouse movements, such that when the mouse was placed over the graph, the mouse icon would change its shape from arrow to a hand. The user could then click on that region and the appropriate microscopic view would appear in a new window. Code was written to locate the mouse co-ordinates when it was placed over the macroscopic image. When the mouse was on the data points of the macroscopic views, the shape of the mouse was programmed to change into a hand. Upon clicking of the mouse when it appeared as a hand, the Visual Basic program calculated the average water saturation at that location, and displayed the appropriate microscopic view.

The code for the command button, Exit would prompt the user, whether to save any information or not, before quitting the application. Upon selecting the corresponding button, the program executes as directed.

The methodology discussed in this chapter was followed to create a fractional flow curve, automated tangent, and the macroscopic view using Excel. Microscopic views were created and linked to the macroscopic views. Both the microscopic and macroscopic views were displayed to the user using Visual Basic for ease of learning. Code to the magnitude of approximately 3000 lines was written to meet the requirements. The Excel spreadsheet contained macros on each of the child tables to transfer data to the tables in Access database.

Table 3.1

Rock and Fluid Properties

Property	Symbol	Value	Units
Porosity	ϕ	0.2	
Initial water saturation	S_{iw}	0.3	
Residual oil saturation	S_{or}	0.3	
Oil viscosity	μ_o	40	cp
Water viscosity	μ_w	1	cp
Oil formation volume factor	B_o	1	bbl/STB
Water formation volume factor	B_w	1	bbl/STB
Constant in relative permeability equation	α_1	0.8	
Constant in relative permeability equation	α_2	0.2	
Exponent in relative permeability equation for oil	m	2	
Exponent in relative permeability equation for water	n	2	
Parameter defined by Eq 3-3	A	0.1	
Parameter defined by Eq 3-4	B	2.5	

Table 3.2

Average Water Saturation Calculations

1	2	3	4	5	6	7	8	9	10
Sl.#	S_w	f_w	f'_w	t_{D2}	Average S_w	S_{wD}	K_{ro}	K_{rw}	F_{wo} (bbl/bbl)
1	0.3000	0.0000	0.0000	0.0000	0.3000	0.0000	0.8000	0.0000	0.0000
2	0.3082	0.0043	1.0762	0.1895	0.4968	0.0204	0.7677	0.0001	0.0043
3	0.3163	0.0178	2.2311	0.2084	0.5210	0.0408	0.7360	0.0003	0.0181
4	0.3245	0.0408	3.4043	0.2274	0.5426	0.0612	0.7050	0.0007	0.0425
5	0.3327	0.0732	4.5262	0.2463	0.5609	0.0816	0.6747	0.0013	0.0790
6	0.3408	0.1144	5.5269	0.2653	0.5757	0.1020	0.6451	0.0021	0.1291
7	0.3490	0.1630	6.3473	0.2842	0.5869	0.1224	0.6161	0.0030	0.1947
8	0.3571	0.2174	6.9471	0.3032	0.5944	0.1429	0.5878	0.0041	0.2778
9	0.3653	0.2757	7.3095	0.3221	0.5986	0.1633	0.5601	0.0053	0.3807
10	0.3735	0.3361	7.4410	0.3411	0.5999	0.1837	0.5331	0.0067	0.5062
11	0.3816	0.3967	7.3668	0.3600	0.5988	0.2041	0.5068	0.0083	0.6575
12	0.3898	0.4559	7.1242	0.3790	0.5960	0.2245	0.4811	0.0101	0.8380
13	0.3980	0.5126	6.7553	0.3979	0.5919	0.2449	0.4561	0.0120	1.0519
14	0.4061	0.5660	6.3013	0.4168	0.5870	0.2653	0.4318	0.0141	1.3040
15	0.4143	0.6154	5.7988	0.4358	0.5819	0.2857	0.4082	0.0163	1.6000
16	0.4224	0.6606	5.2777	0.1895	0.4868	0.3061	0.3852	0.0187	1.9464
17	0.4306	0.7016	4.7605	0.2101	0.4933	0.3265	0.3628	0.0213	2.3508
18	0.4388	0.7384	4.2630	0.2346	0.5001	0.3469	0.3412	0.0241	2.8223
19	0.4469	0.7712	3.7957	0.2635	0.5072	0.3673	0.3202	0.0270	3.3715
20	0.4551	0.8004	3.3642	0.2972	0.5144	0.3878	0.2999	0.0301	4.0111
21	0.4633	0.8263	2.9711	0.3366	0.5217	0.4082	0.2802	0.0333	4.7562
22	0.4714	0.8491	2.6166	0.3822	0.5291	0.4286	0.2612	0.0367	5.6250
23	0.4796	0.8691	2.2993	0.4349	0.5365	0.4490	0.2429	0.0403	6.6392
24	0.4878	0.8867	2.0170	0.4958	0.5439	0.4694	0.2252	0.0441	7.8254
25	0.4959	0.9021	1.7668	0.5660	0.5513	0.4898	0.2082	0.0480	9.2160
26	0.5041	0.9156	1.5459	0.6469	0.5587	0.5102	0.1919	0.0521	10.8507
27	0.5122	0.9274	1.3512	0.7401	0.5660	0.5306	0.1763	0.0563	12.7788
28	0.5204	0.9377	1.1799	0.8475	0.5732	0.5510	0.1613	0.0607	15.0620
29	0.5286	0.9467	1.0294	0.9715	0.5803	0.5714	0.1469	0.0653	17.7778
30	0.5367	0.9546	0.8971	1.1147	0.5873	0.5918	0.1333	0.0701	21.0250

Table 3.2 (continued)

1	2	3	4	5	6	7	8	9	10
Sl. #	Sw2	f_{w2}	f'_{w2}	t_{D2}	Average S_w	S_{wD}	K_{ro}	K_{rw}	F_{wo} (bbl/bbl)
31	0.5449	0.9614	0.7809	1.2806	0.5943	0.6122	0.1203	0.0750	24.9307
32	0.5531	0.9674	0.6788	1.4732	0.6011	0.6327	0.1080	0.0800	29.6605
33	0.5612	0.9726	0.5891	1.6975	0.6078	0.6531	0.0963	0.0853	35.4325
34	0.5694	0.9770	0.5102	1.9599	0.6144	0.6735	0.0853	0.0907	42.5391
35	0.5776	0.9809	0.4408	2.2684	0.6209	0.6939	0.0750	0.0963	51.3778
36	0.5857	0.9843	0.3798	2.6333	0.6272	0.7143	0.0653	0.1020	62.5000
37	0.5939	0.9871	0.3259	3.0680	0.6334	0.7347	0.0563	0.1080	76.6864
38	0.6020	0.9896	0.2785	3.5905	0.6394	0.7551	0.0480	0.1140	95.0694
39	0.6102	0.9917	0.2367	4.2252	0.6453	0.7755	0.0403	0.1203	119.3388
40	0.6184	0.9935	0.1997	5.0064	0.6511	0.7959	0.0333	0.1267	152.1000
41	0.6265	0.9950	0.1671	5.9836	0.6567	0.8163	0.0270	0.1333	197.5309
42	0.6347	0.9962	0.1383	7.2310	0.6621	0.8367	0.0213	0.1400	262.6562
43	0.6429	0.9972	0.1128	8.8654	0.6674	0.8571	0.0163	0.1469	360.0000
44	0.6510	0.9981	0.0902	11.0811	0.6726	0.8776	0.0120	0.1540	513.6111
45	0.6592	0.9987	0.0703	14.2281	0.6775	0.8980	0.0083	0.1613	774.4000
46	0.6673	0.9992	0.0526	19.0065	0.6824	0.9184	0.0053	0.1687	1265.6250
47	0.6755	0.9996	0.0370	27.0495	0.6870	0.9388	0.0030	0.1763	2351.1111
48	0.6837	0.9998	0.0231	43.2572	0.6915	0.9592	0.0013	0.1840	5522.5000
49	0.6918	1.0000	0.0109	92.1296	0.6958	0.9796	0.0003	0.1919	23040.0000
50	0.7000	1.0000	0.0000			1.0000	0.0000	0.2000	

Table 3.3

Saturation Profile Data

S_w	f'_w	x_D
0.7	0	0
0.683673	0.023118	0.003285
0.659184	0.070283	0.009988
0.634694	0.138293	0.019653
0.618367	0.199745	0.028385
0.602041	0.278516	0.039579
0.577551	0.440832	0.062646
0.561224	0.589097	0.083715
0.536735	0.897095	0.127484
0.520408	1.179939	0.167679
0.487755	2.016958	0.286626
0.455102	3.364216	0.478082
0.422449	5.27768	0.75
0.3		0.75
0.3		1

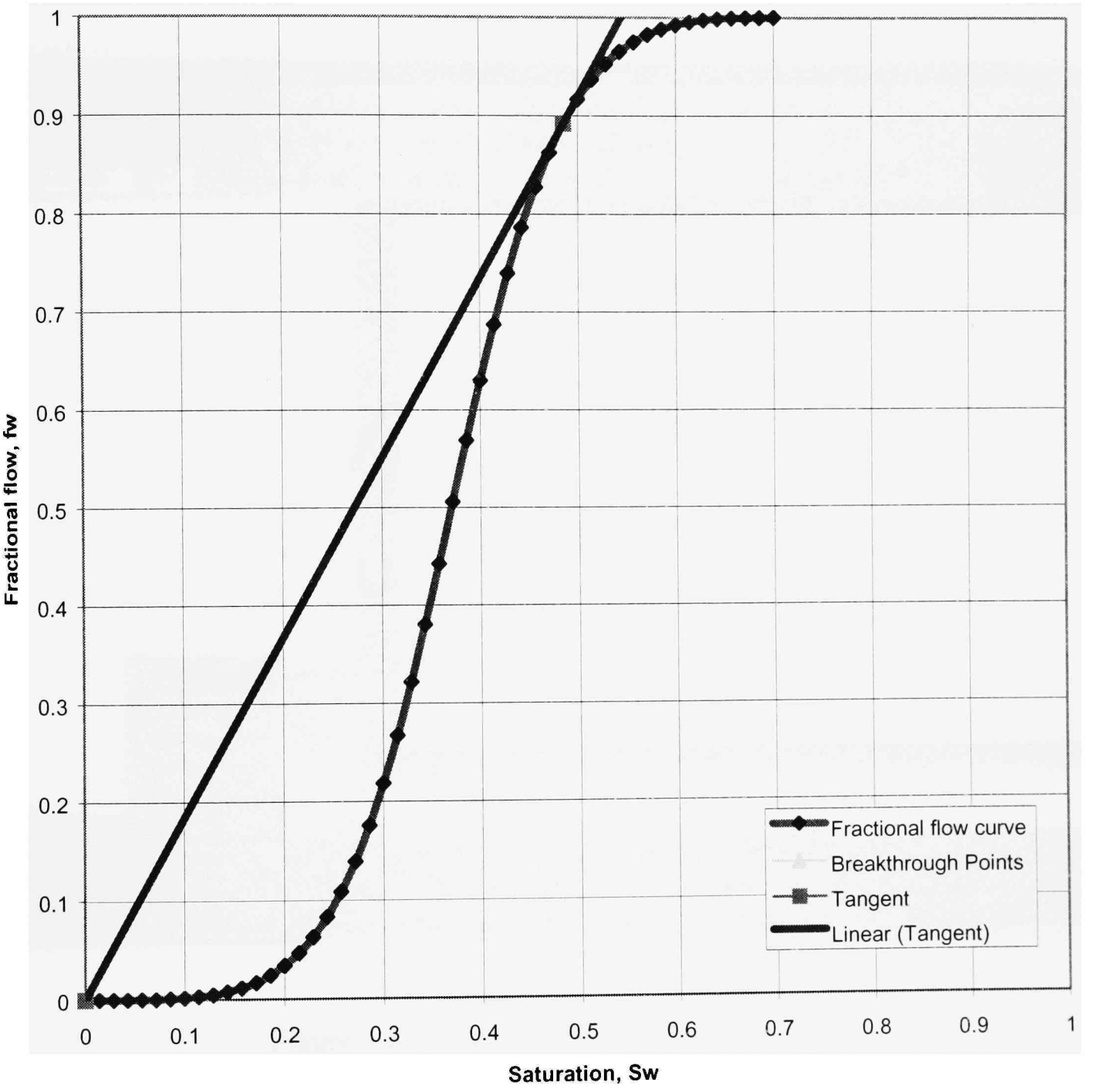

Figure 3.1. Fractional Flow Curve

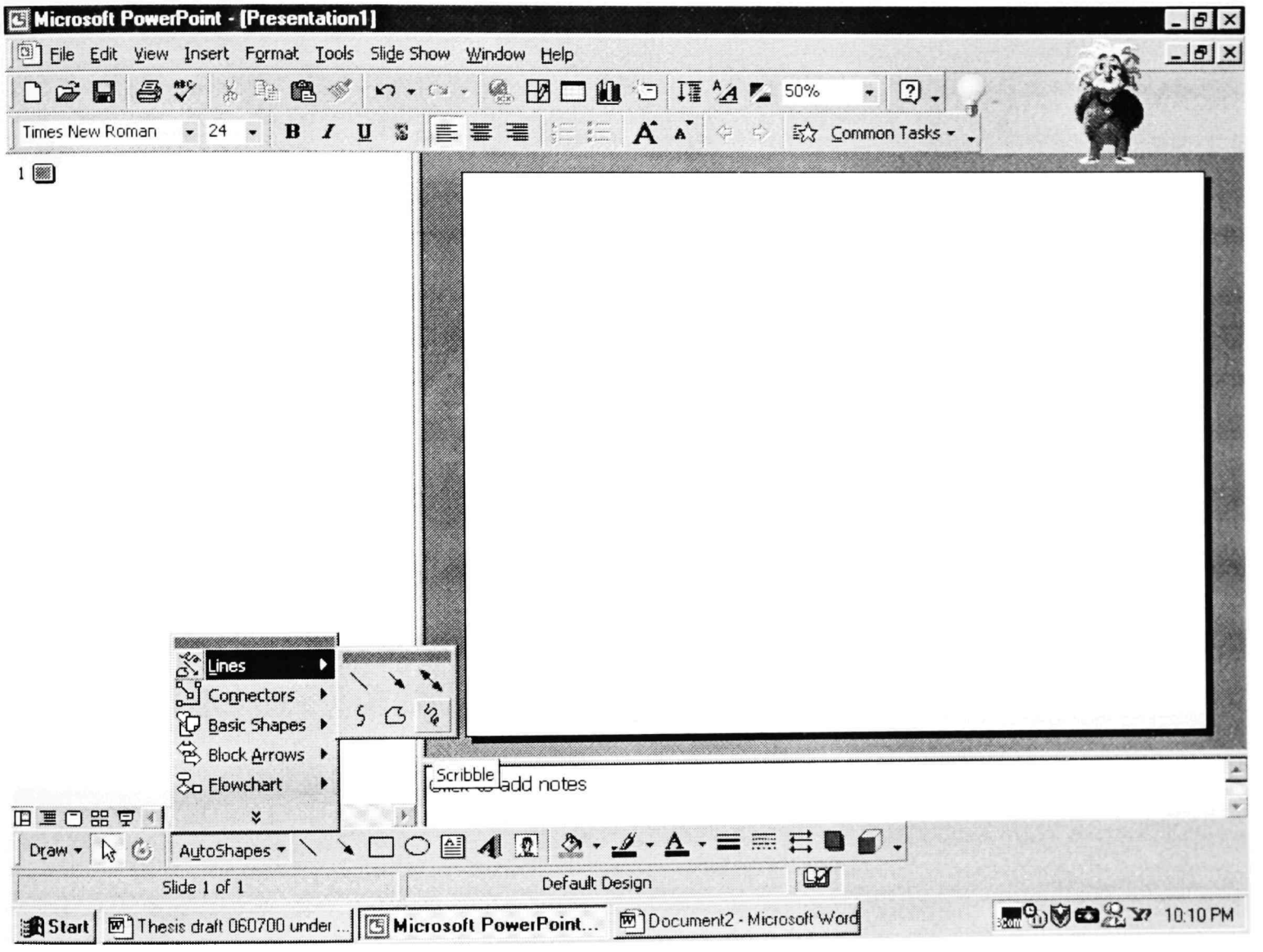

Figure 3.2. Construction of a Pore Curvature

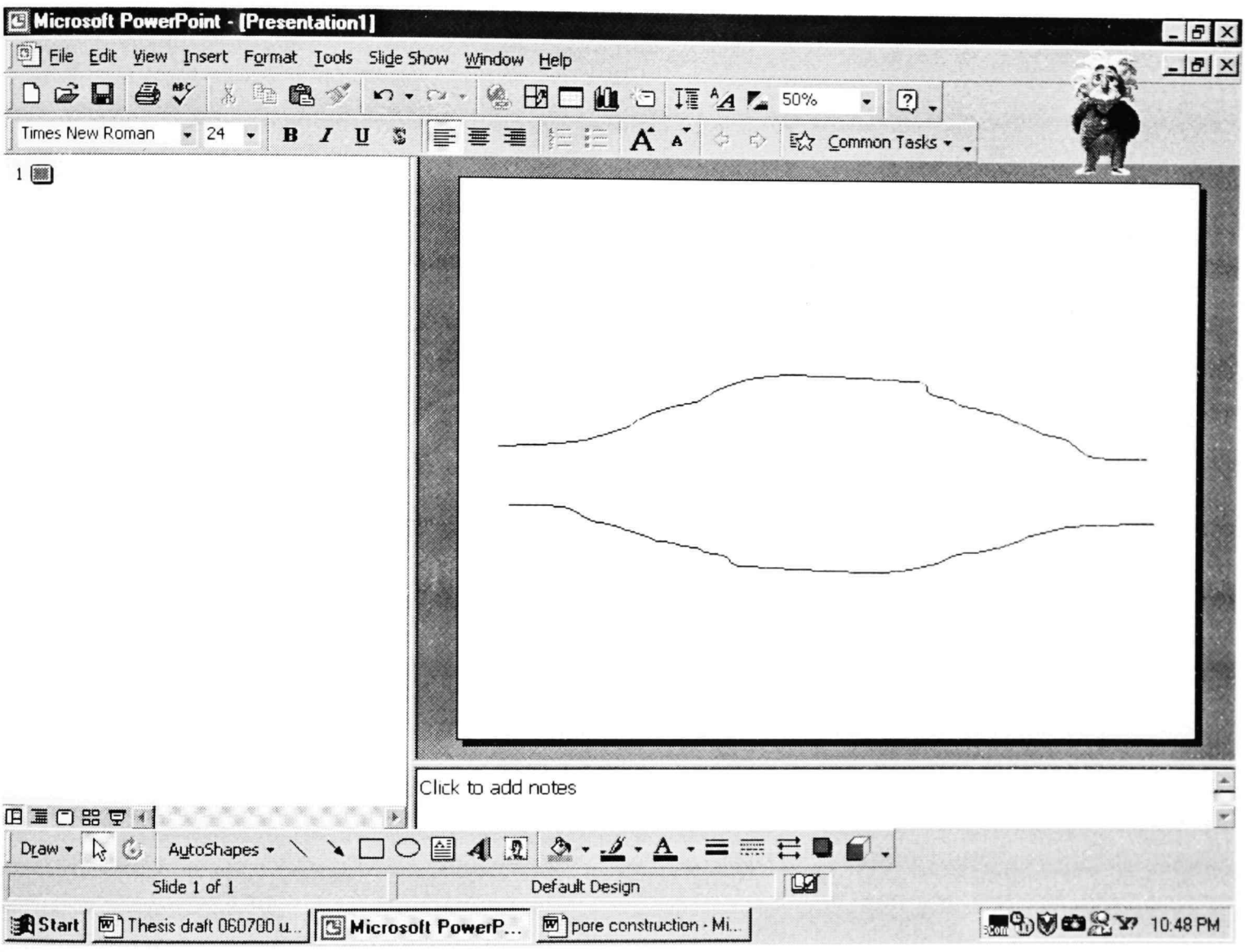

Figure 3.3. Construction of the pore body

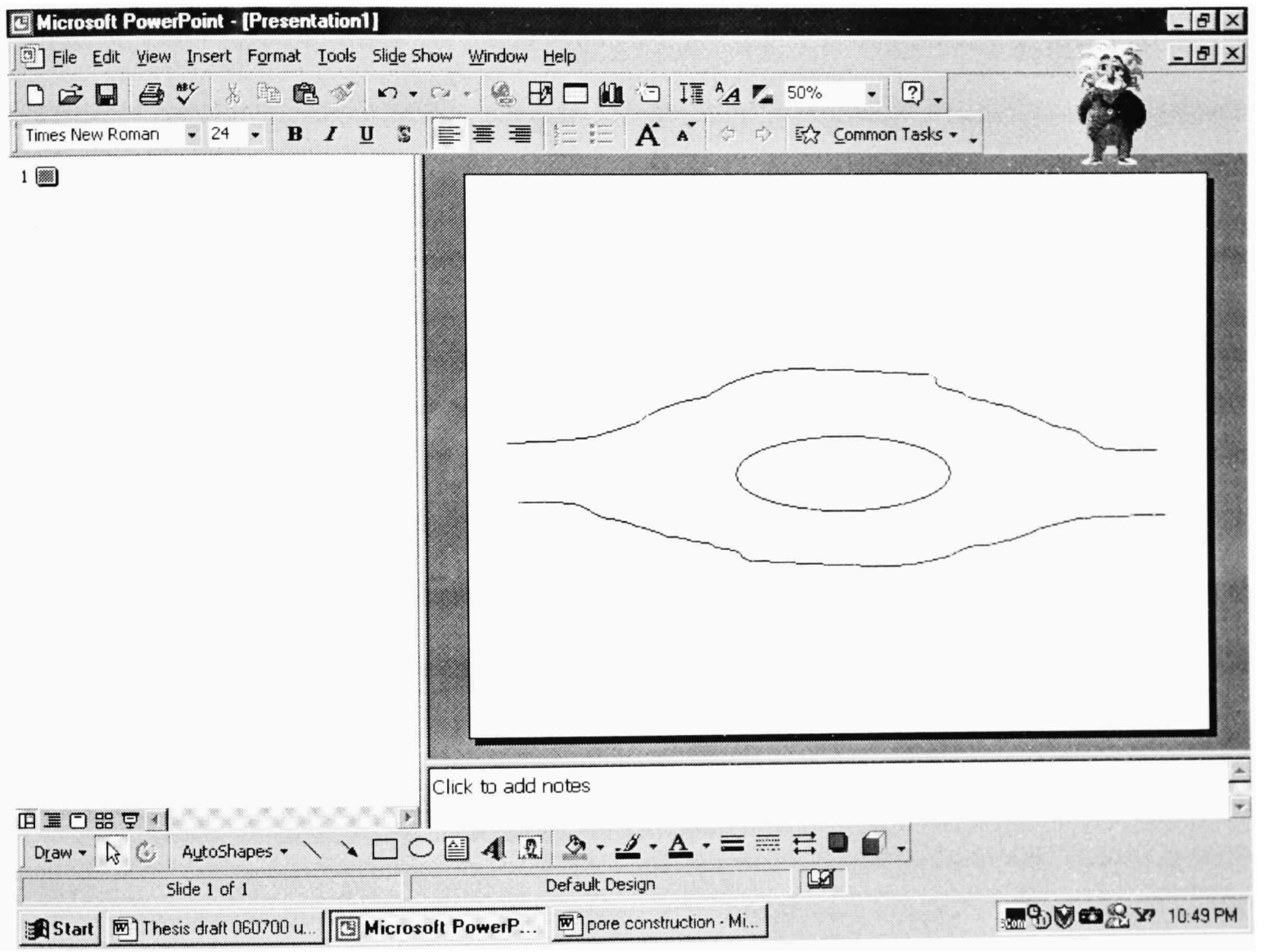

Figure 3.4. Construction of an Oil Phase

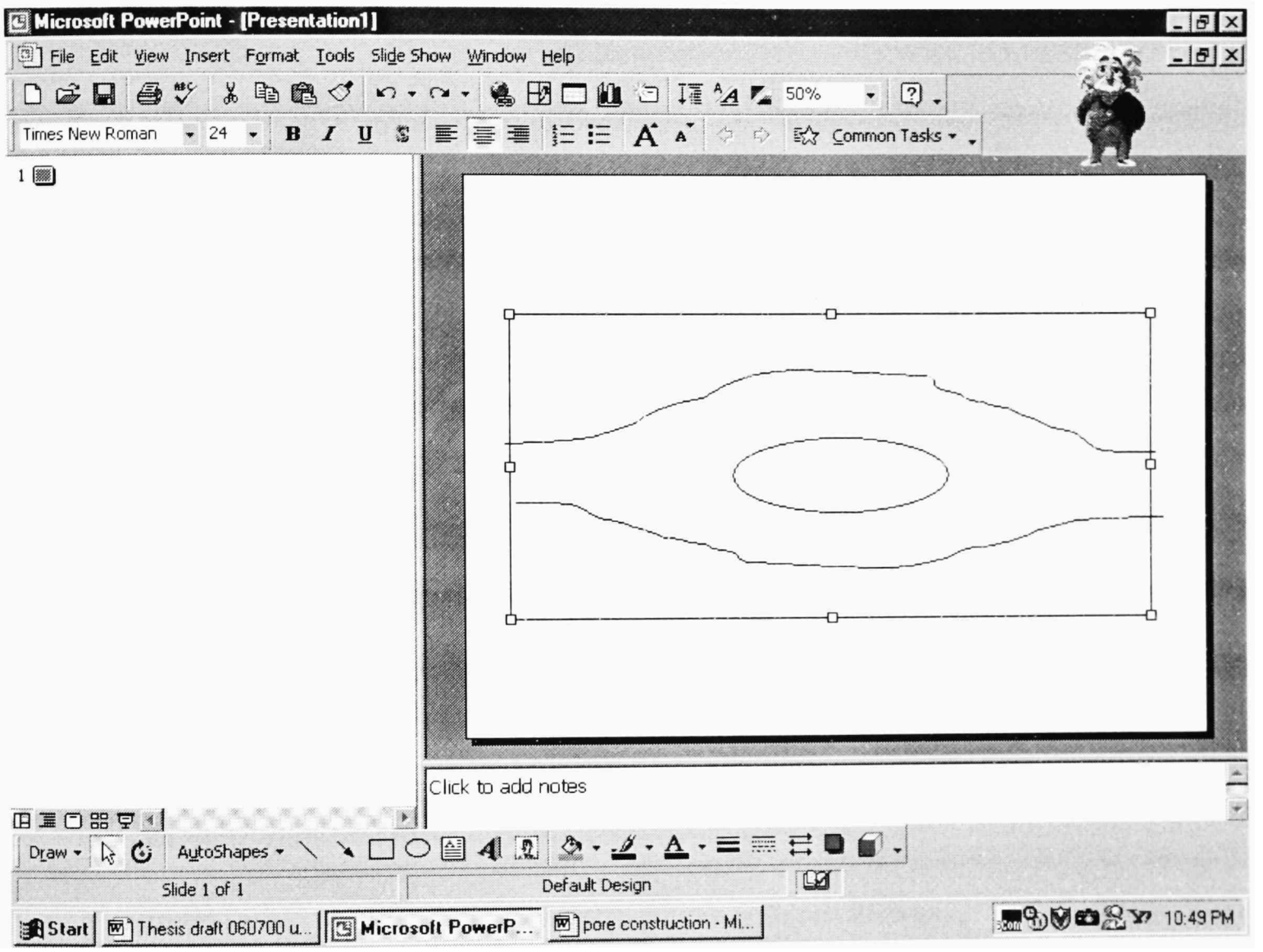

Figure 3.5. Drawing of a Rectangle Around the Porous Media Surrounding the Pore

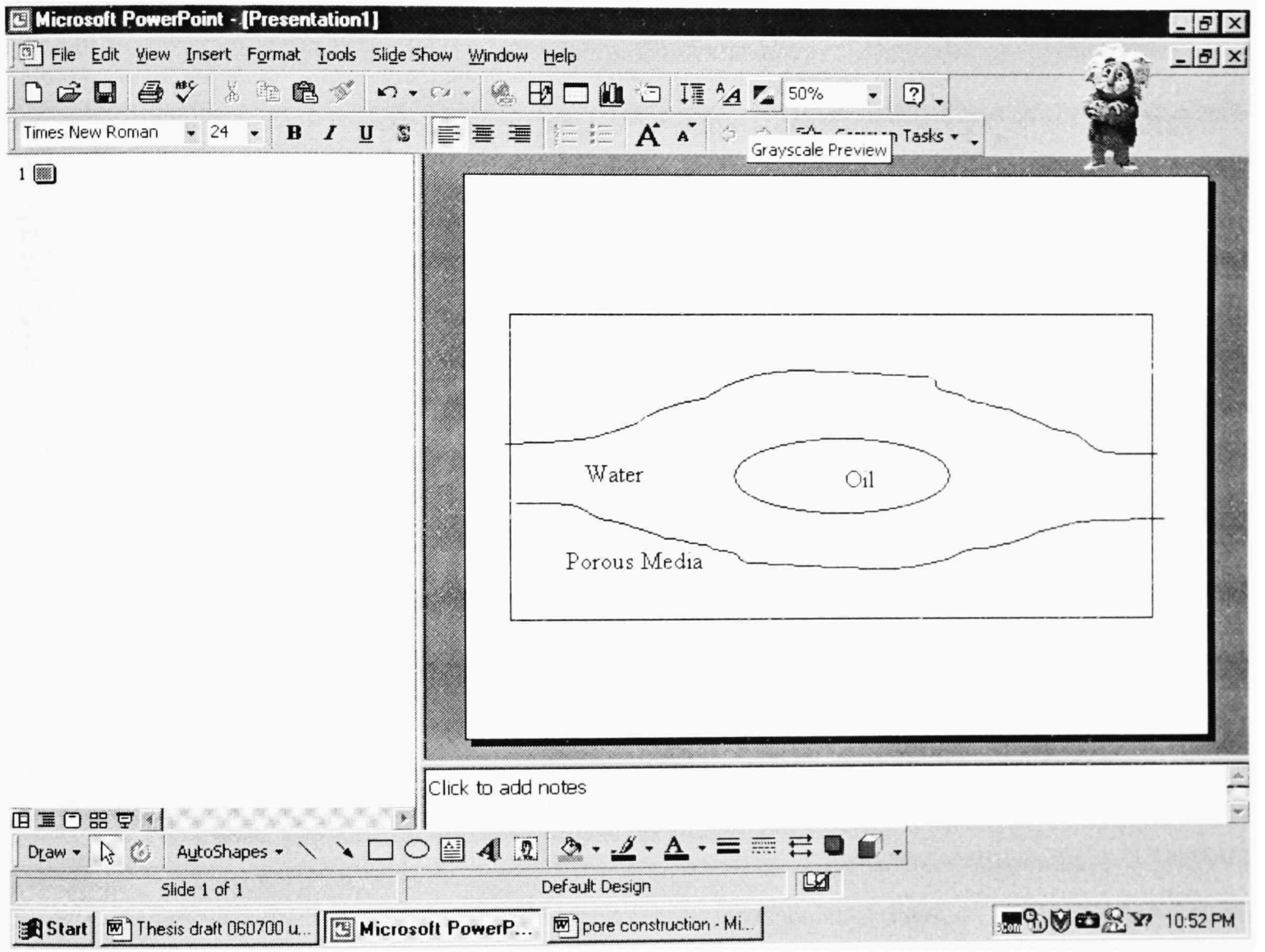

Figure 3.6. Pore, Identifying Oil, Water and Porous Media

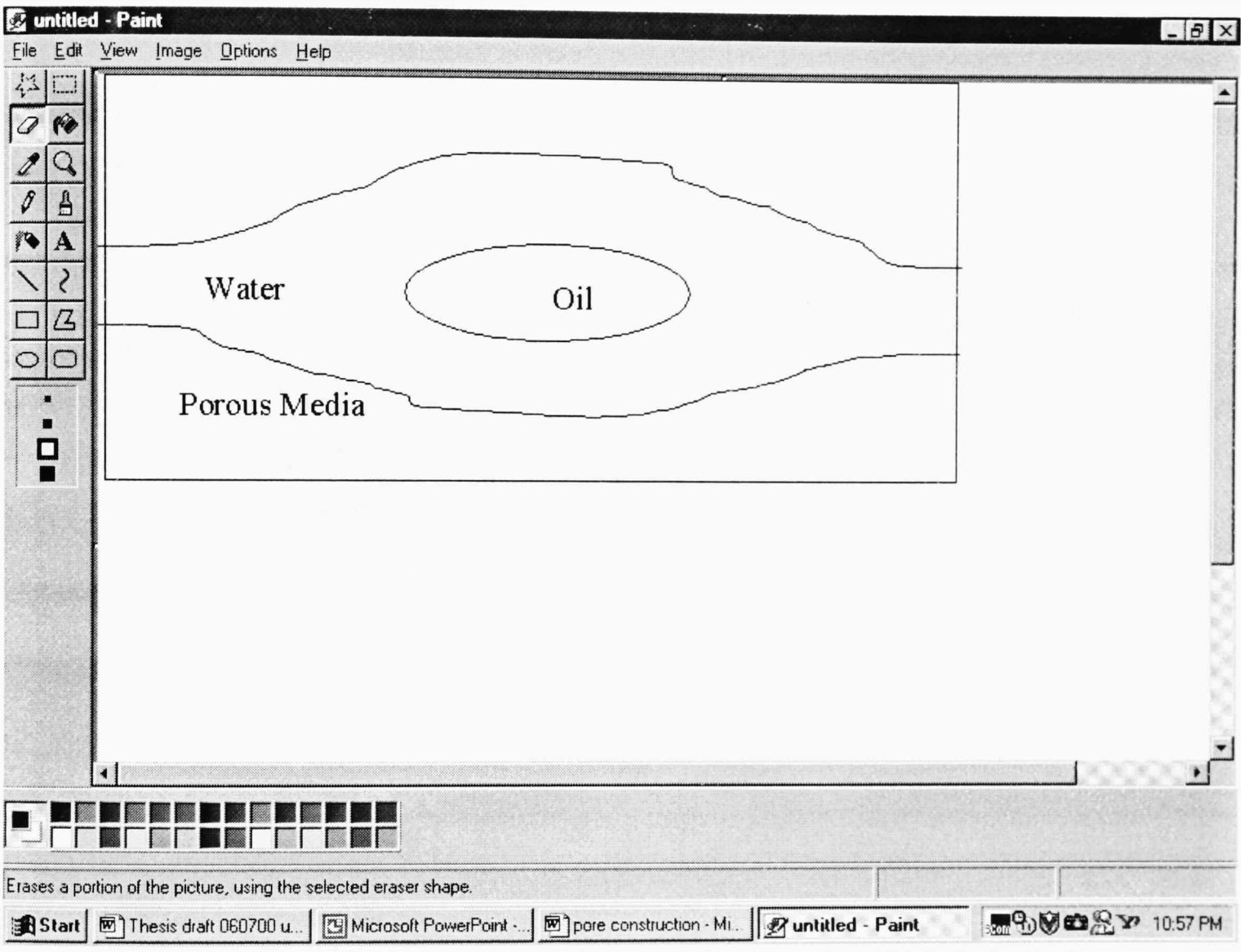

Figure 3.7. Copied Image in Paint®

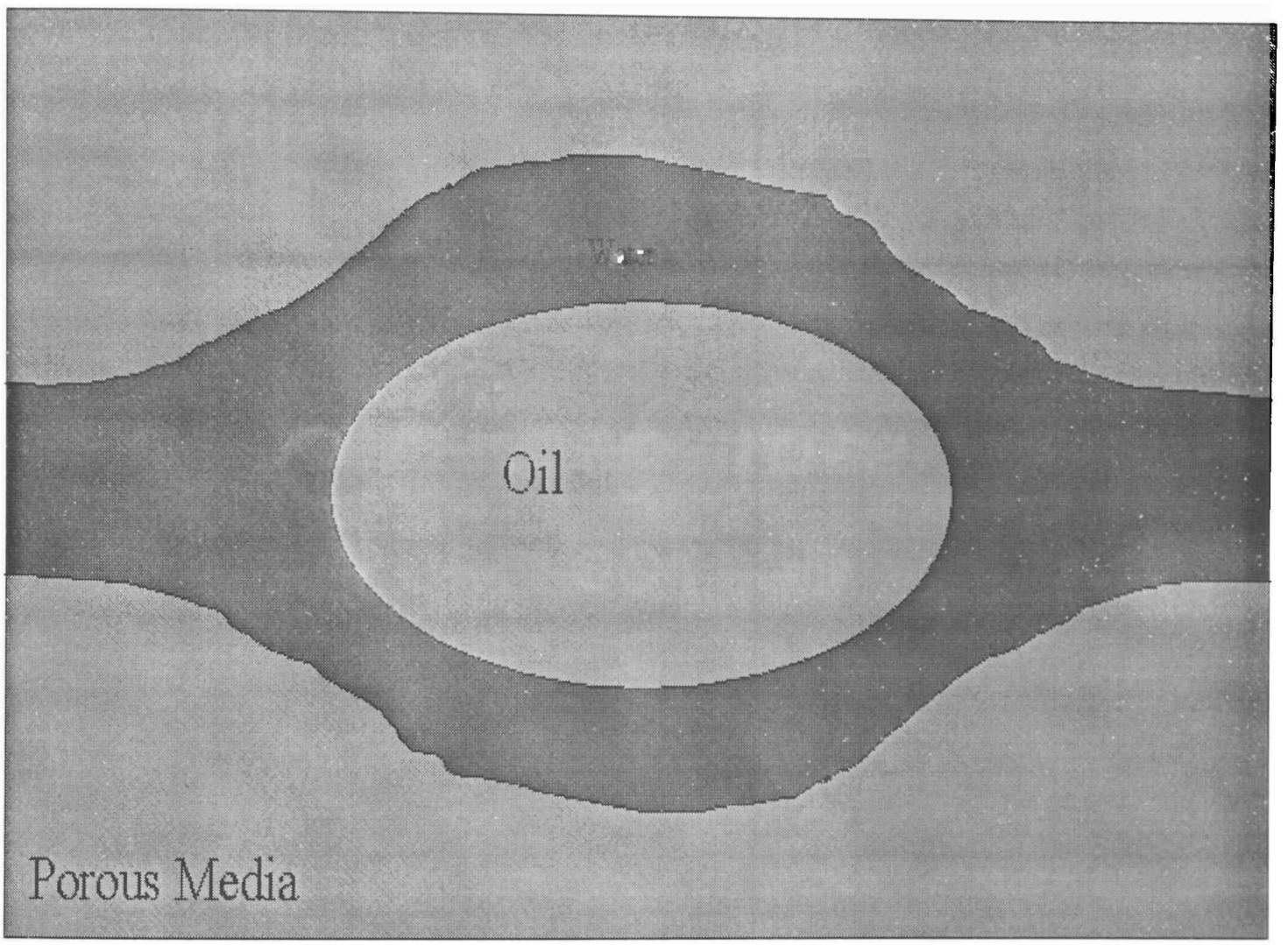

Figure 3.8. Colored Pore Image

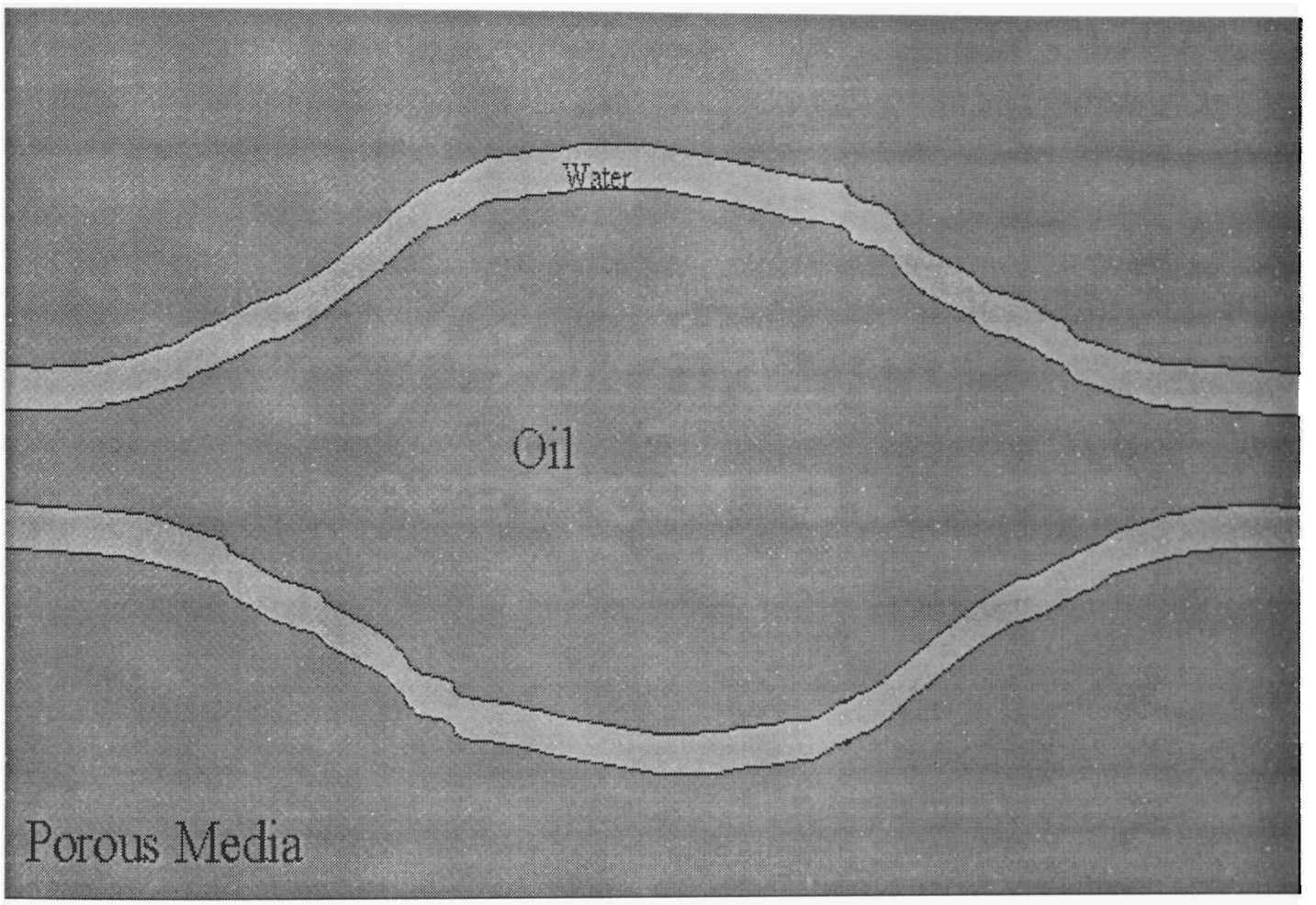

Figure 3.9. Pore 1 Water Saturation = 5-10%, Oil Saturation = 95-100%

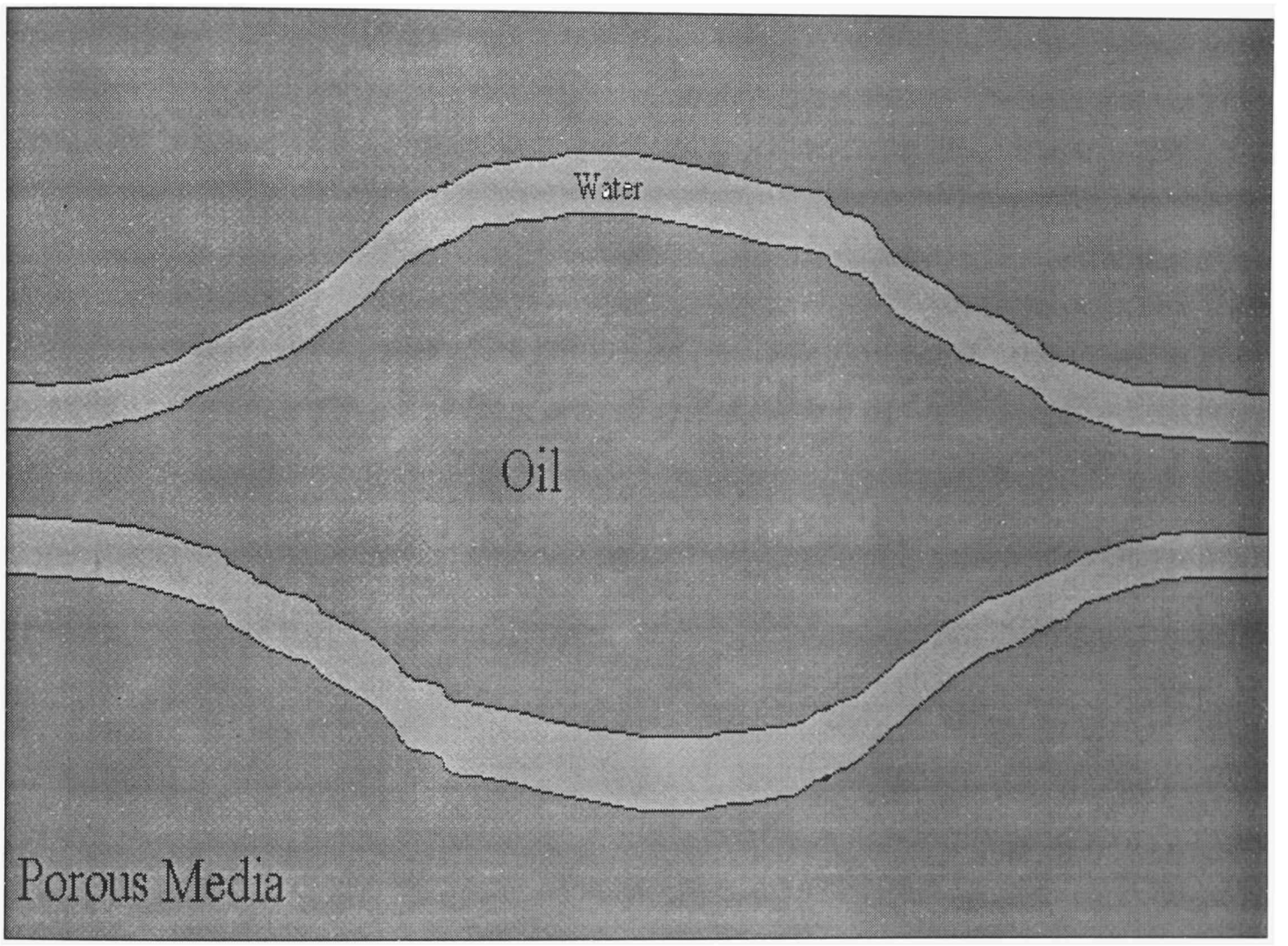

Figure 3.10. Pore 2 Water Saturation = 11-20%, Oil Saturation = 80-89%

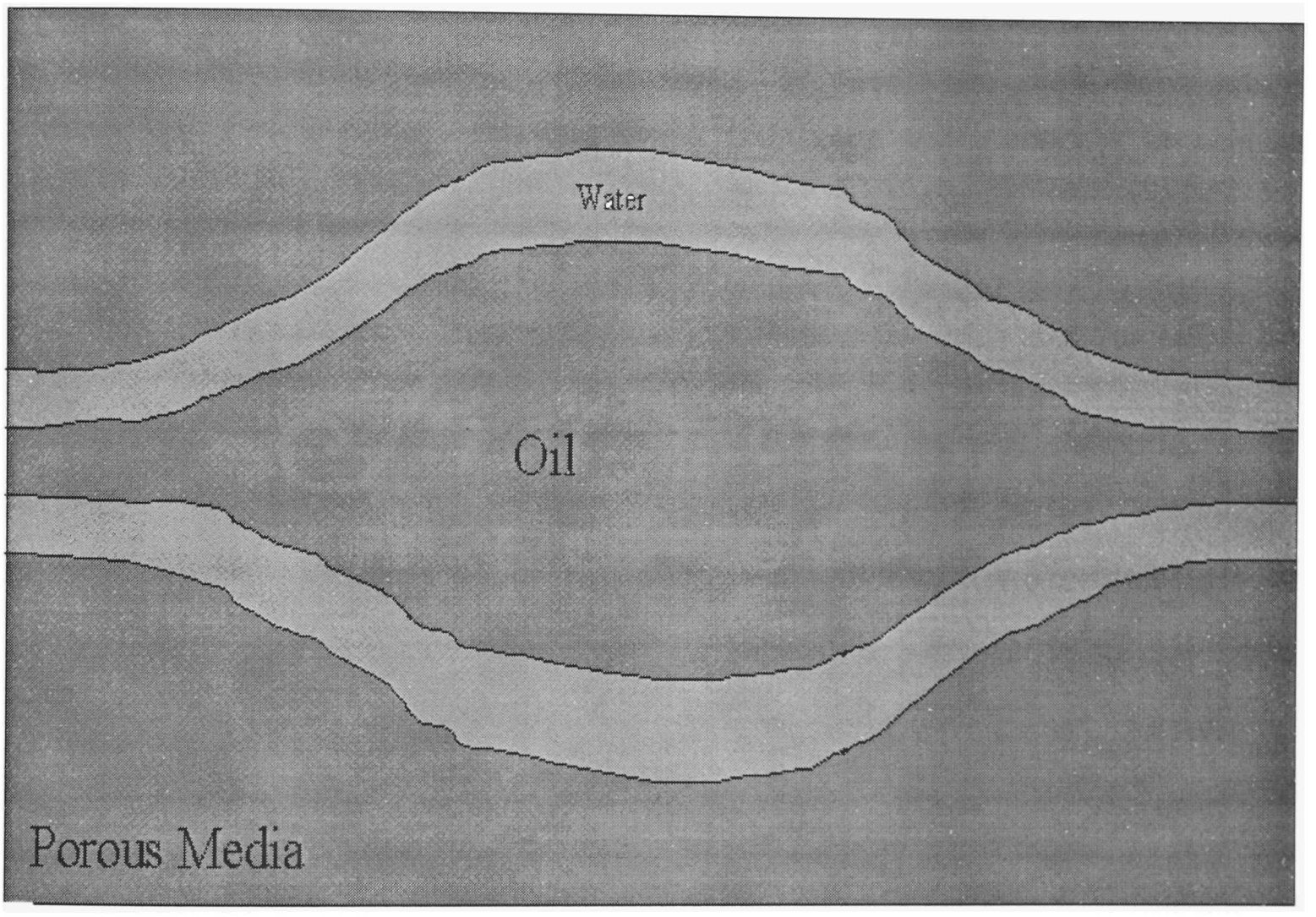

Figure 3.11. Pore 3 Water Saturation = 21-30%, Oil Saturation = 70-79%

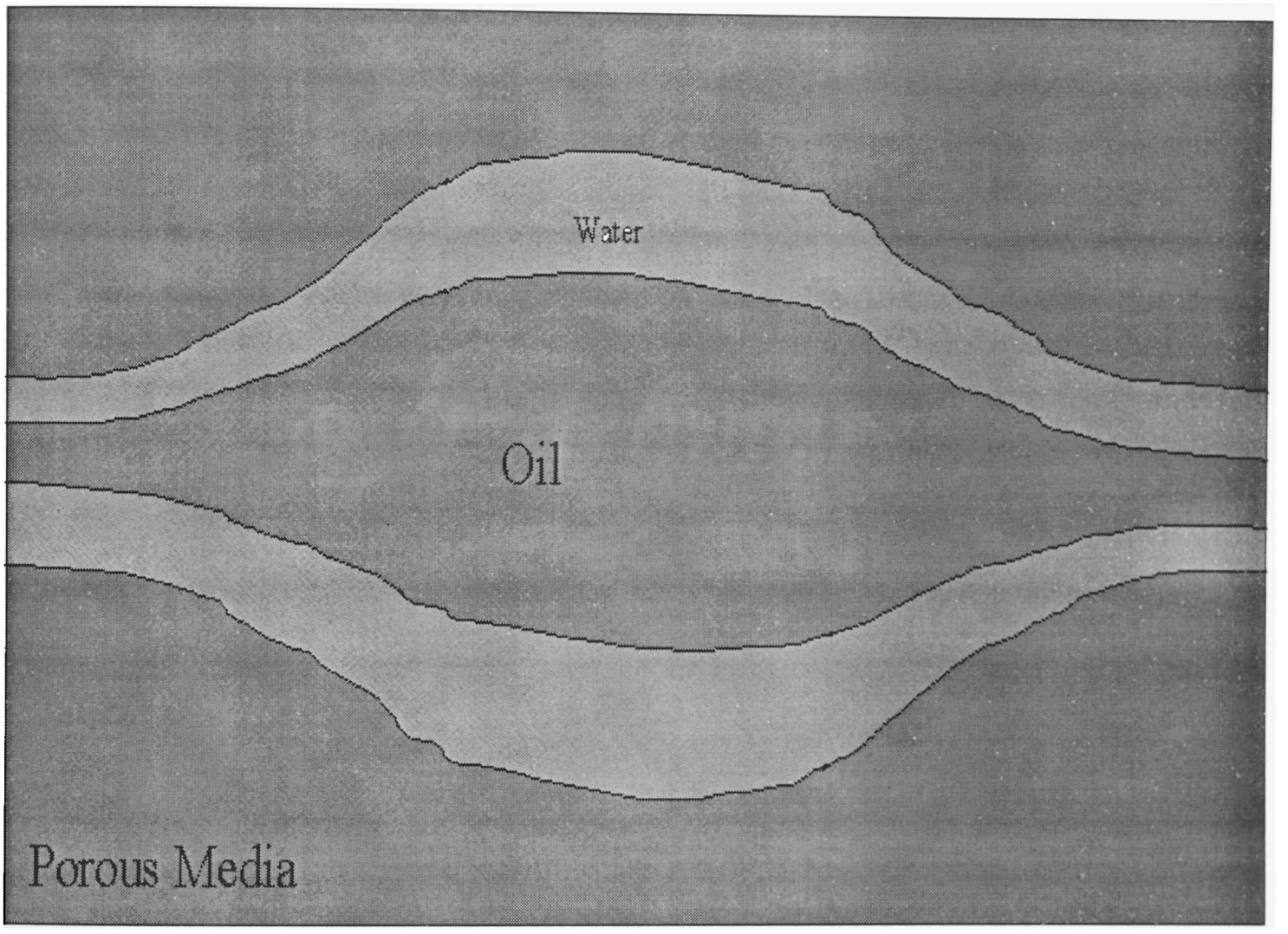

Figure 3.12. Pore 4. Water Saturation = 31-40%, Oil Saturation = 60-69%

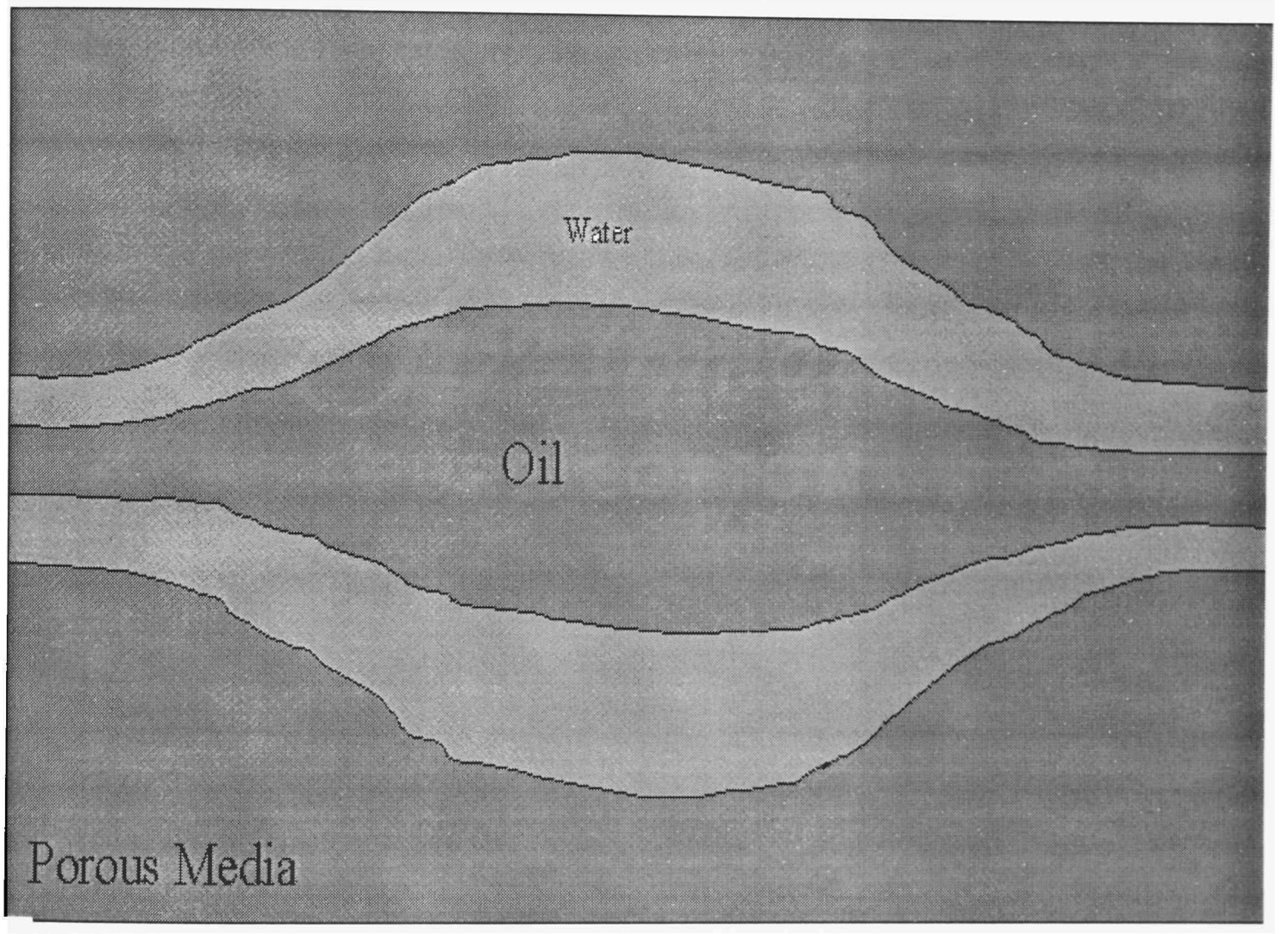

Figure 3.13. Pore 5. Water Saturation = 41-50%, Oil Saturation = 50-59%

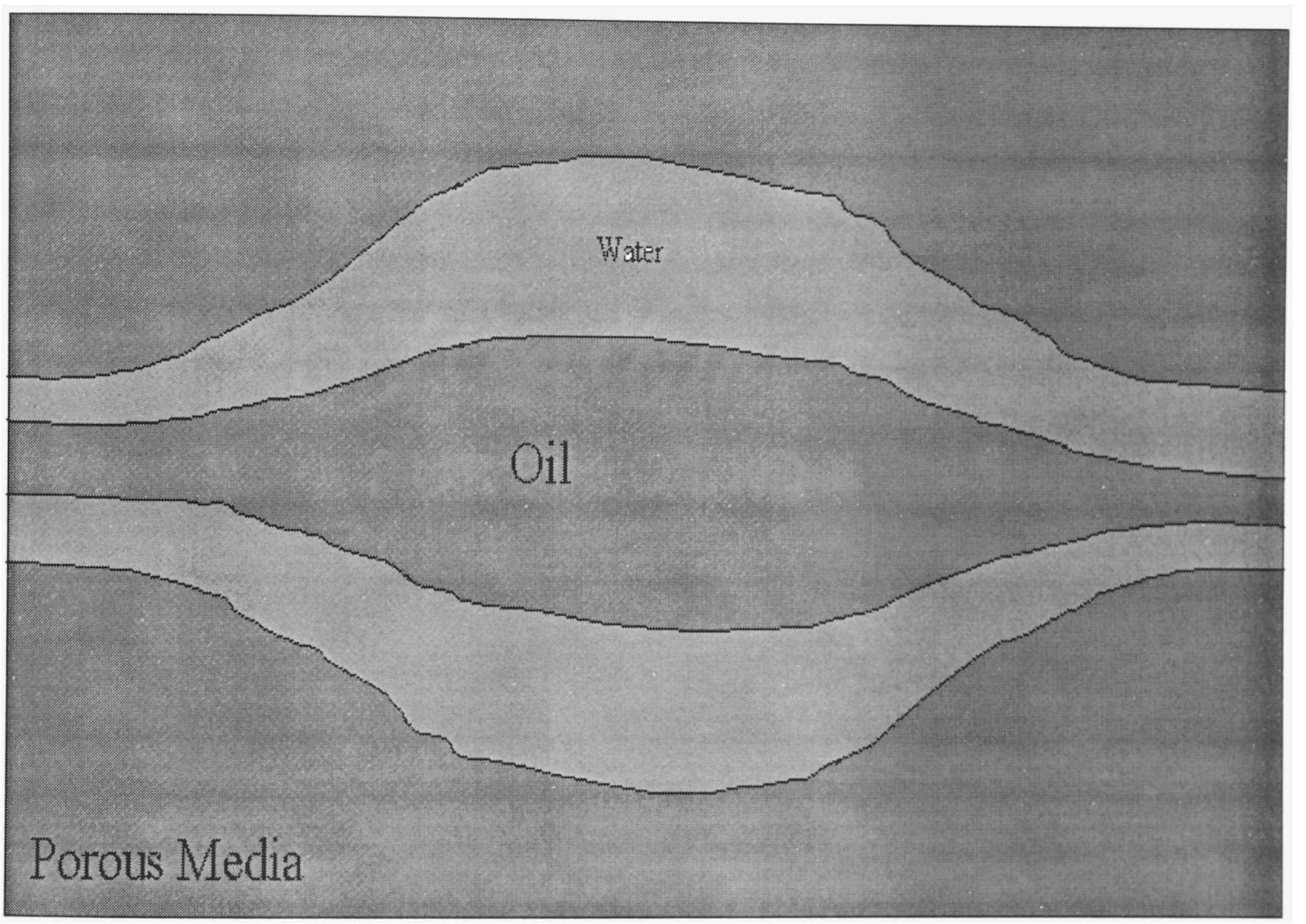

Figure 3.14. Pore 6. Water Saturation = 51-60%, Oil Saturation = 40-49%

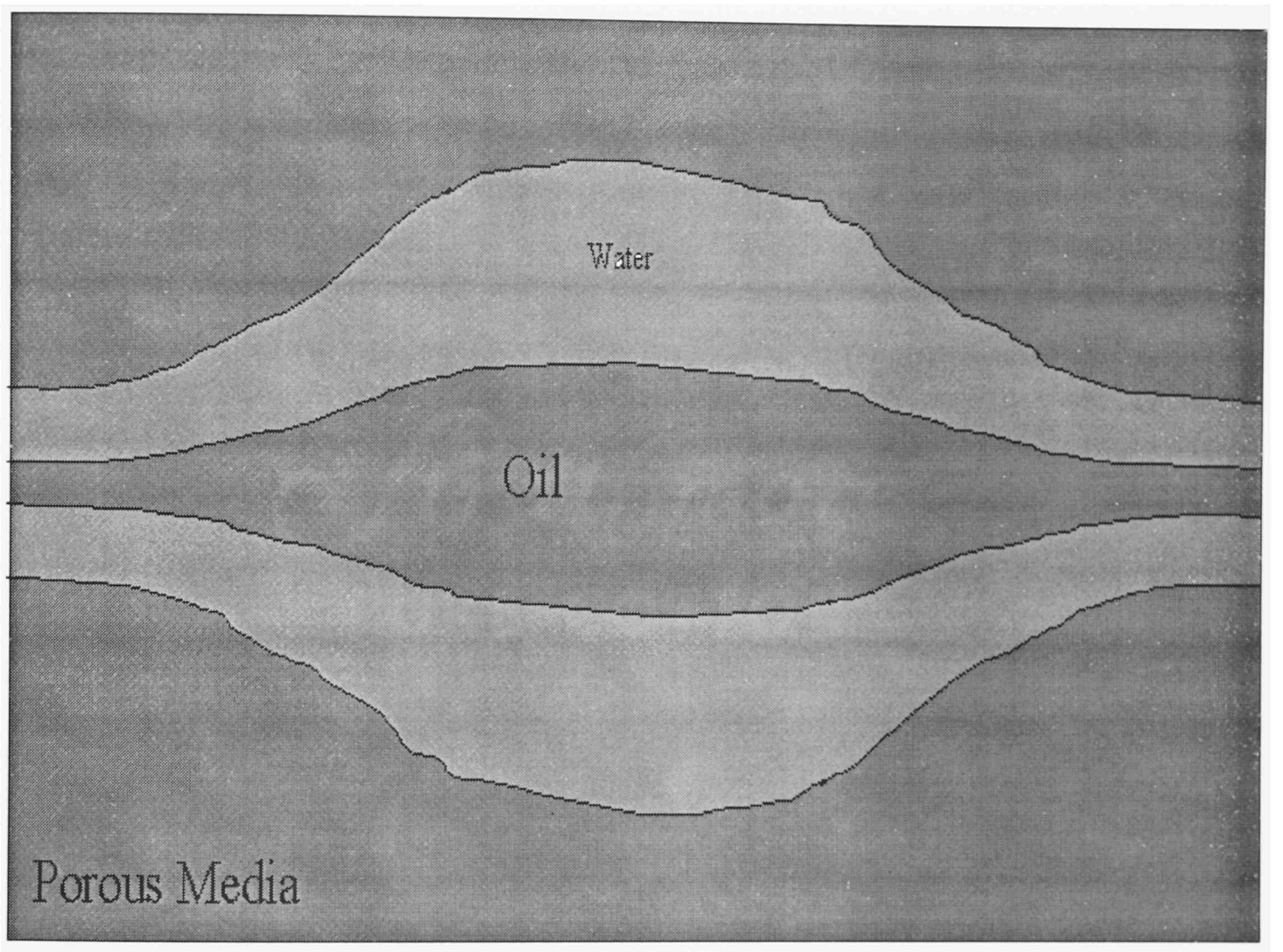

Figure 3.15. Pore 7. Water Saturation = 61-70%, Oil Saturation = 30-39%

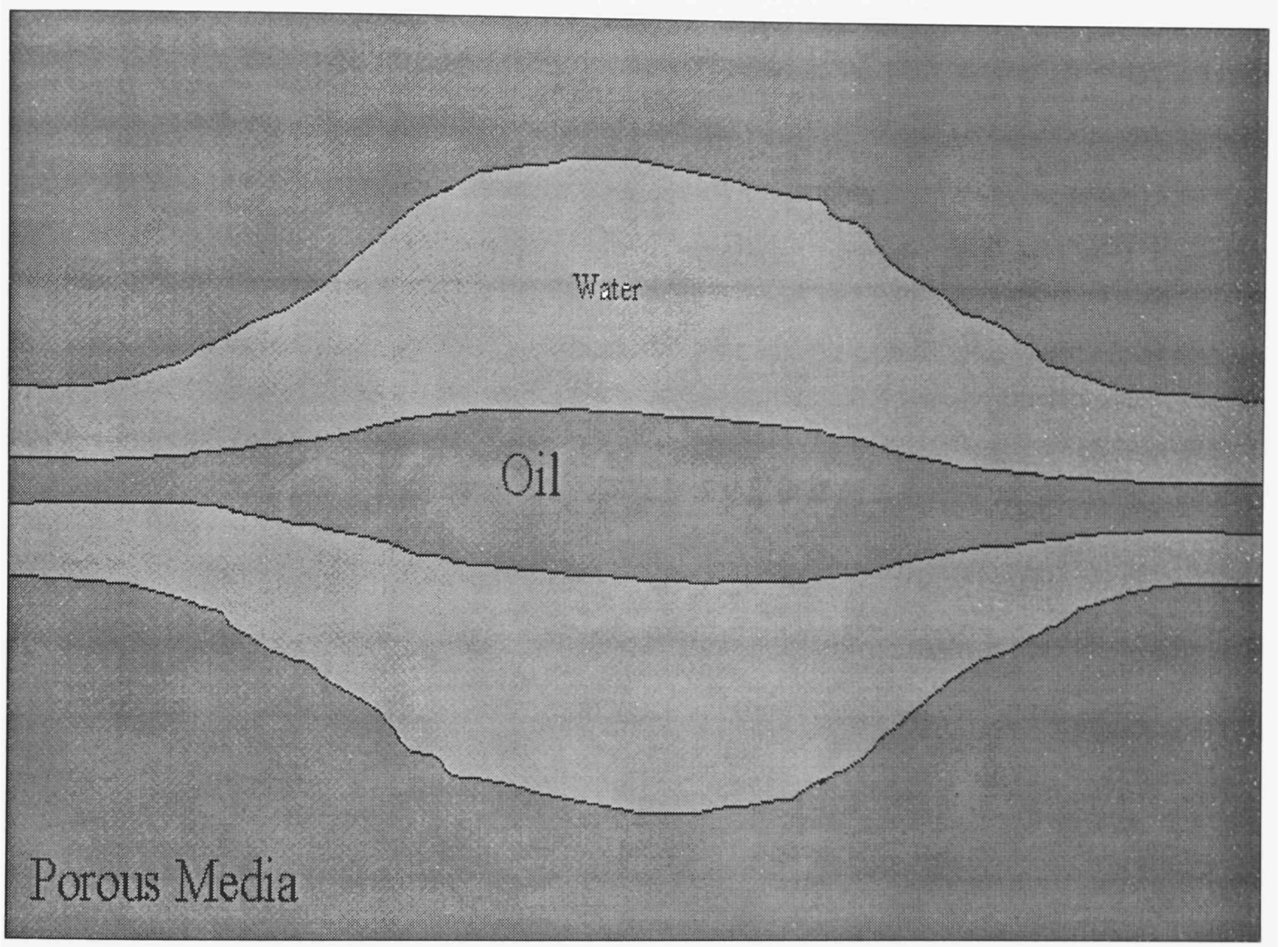

Figure 3.16. Pore 8. Water Saturation = 71-80%, Oil Saturation = 20-29%

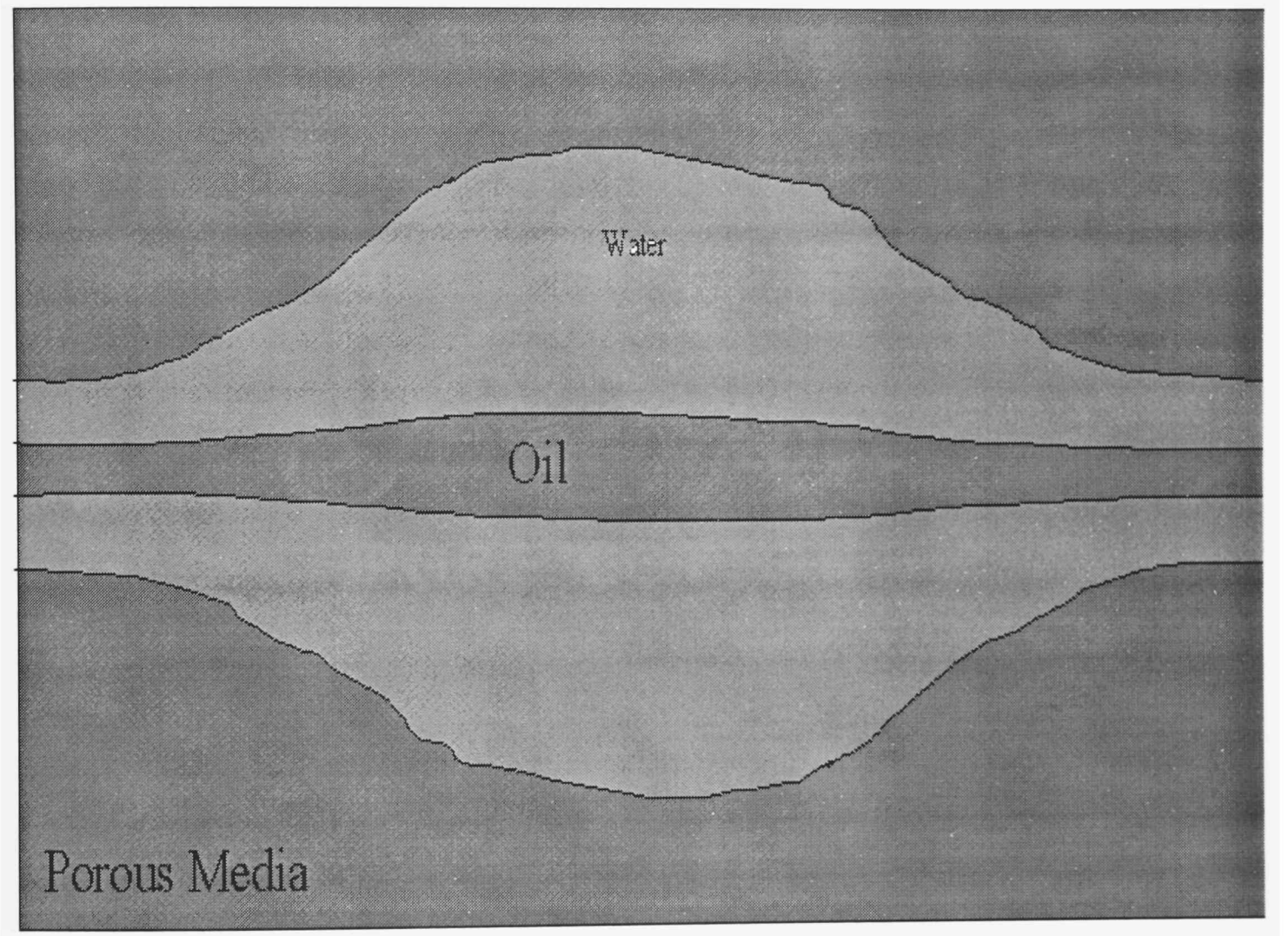

Figure 3.17. Pore 9. Water Saturation = 81-90%, Oil Saturation = 10-19%

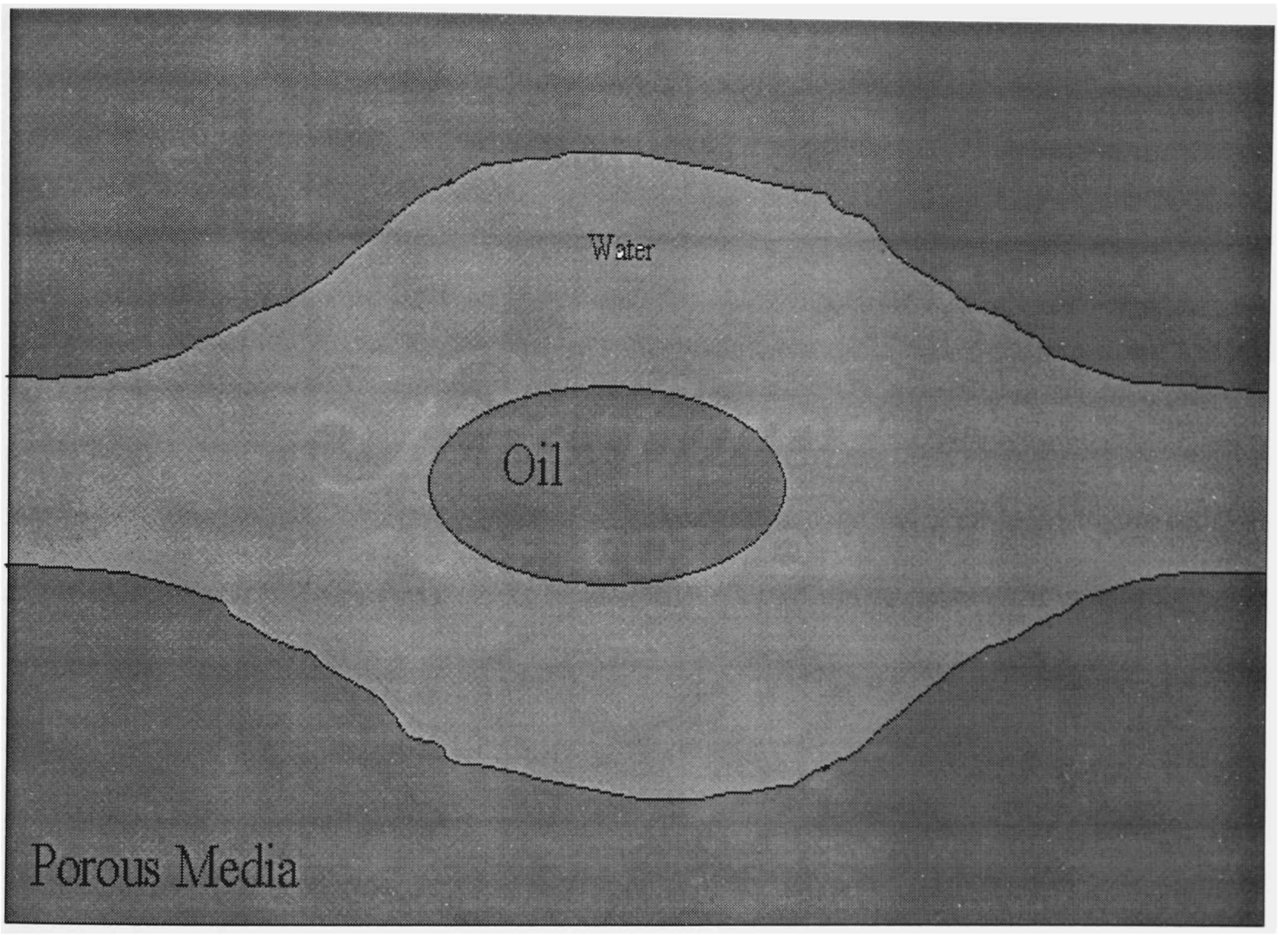

Figure 3.18. Pore 10. Water Saturation = 90-95%, Oil Saturation = 5-10%

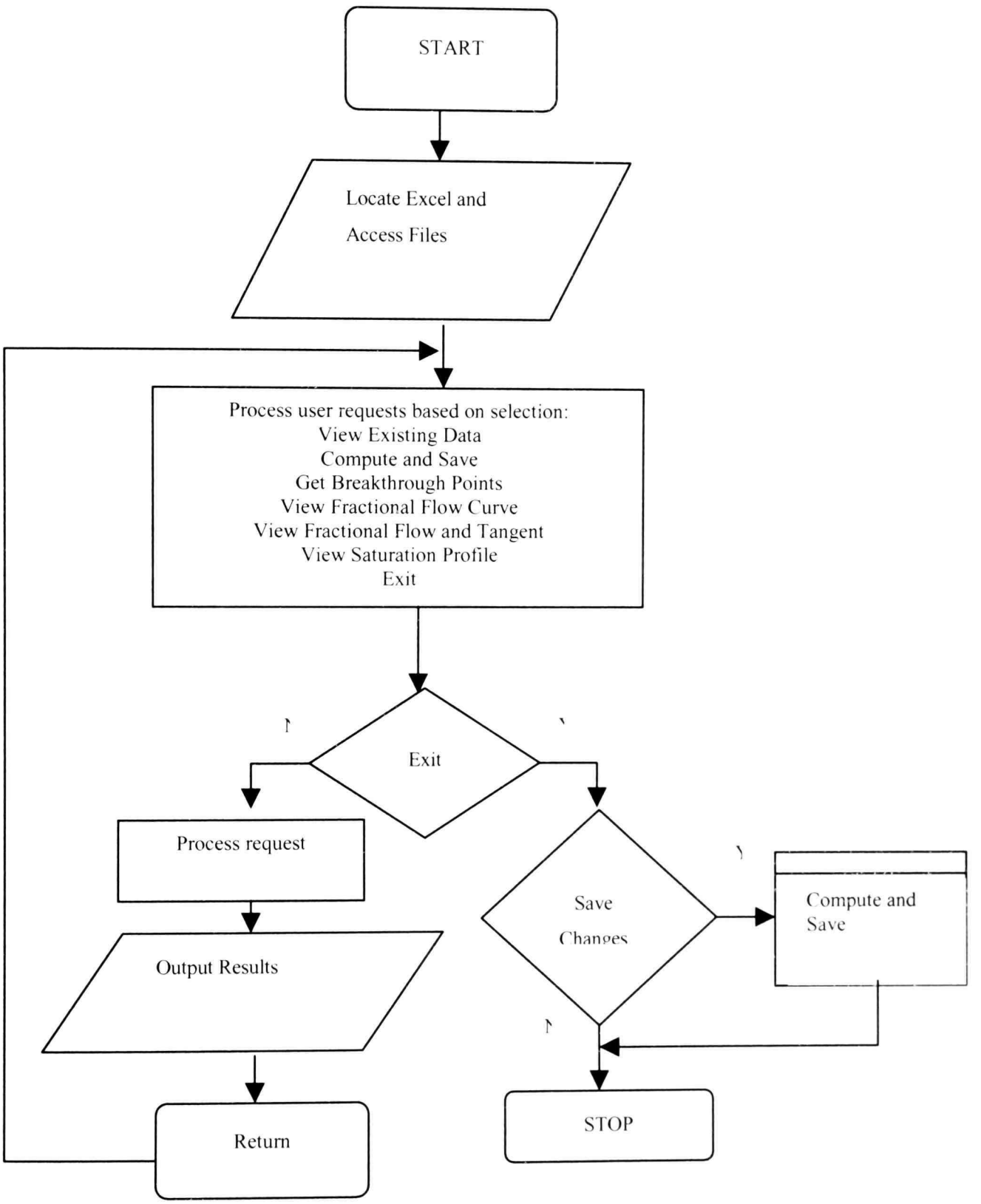

Figure 3.19. Flowchart of the Visual Basic Program

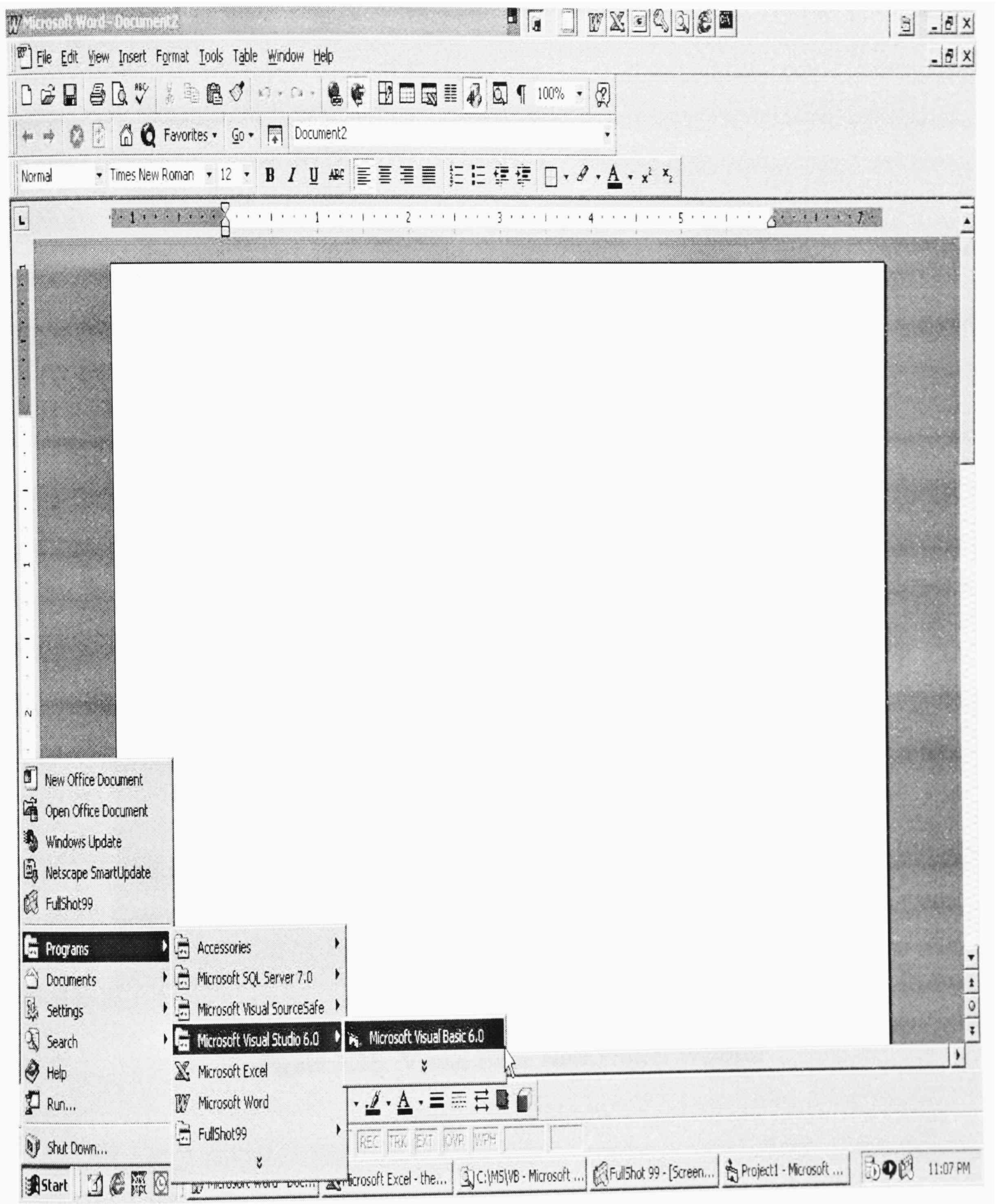

Figure 3.20. Opening the Visual Basic Development Environment.

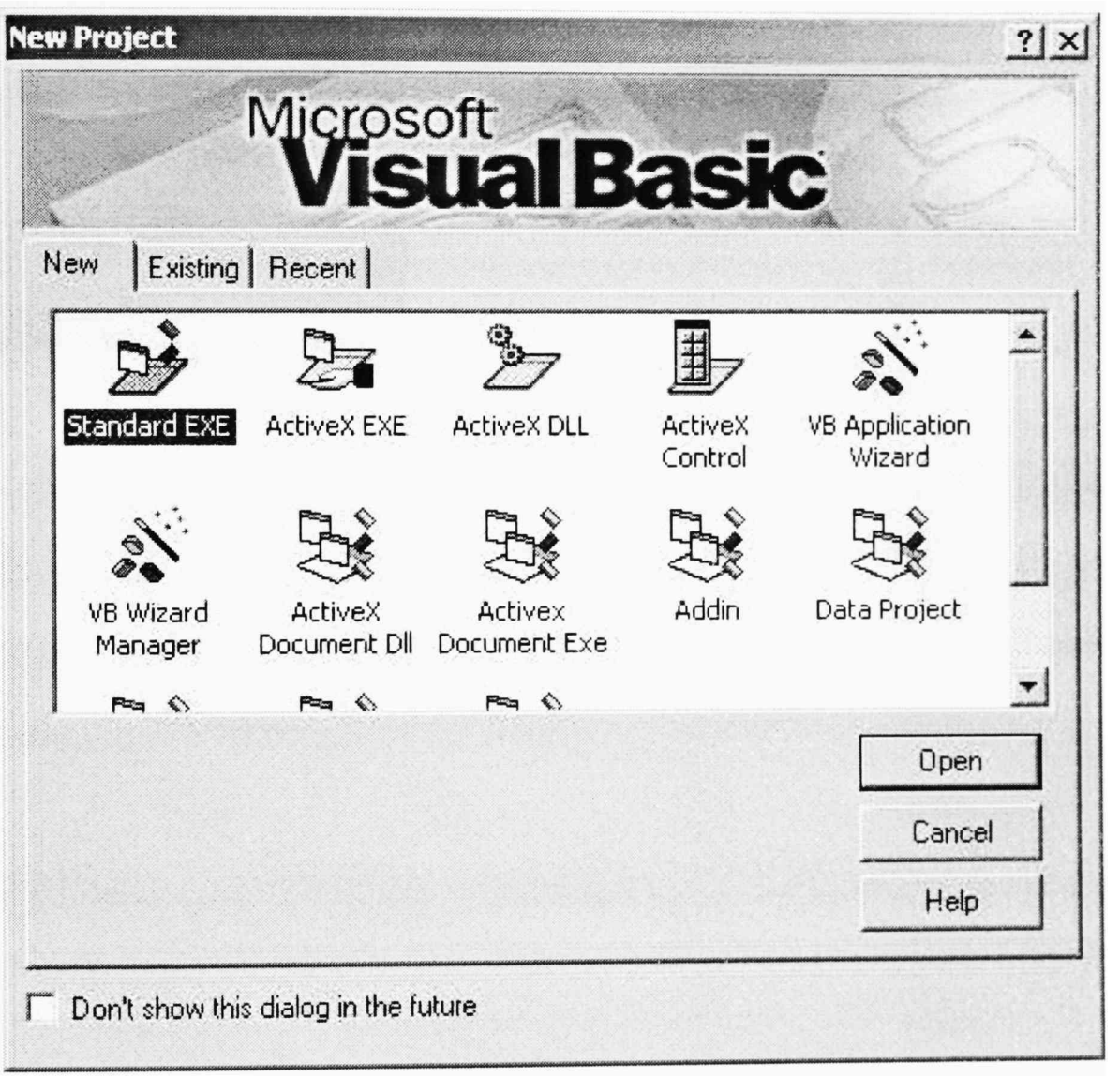

Figure 3.21. Visual Basic New Project Window

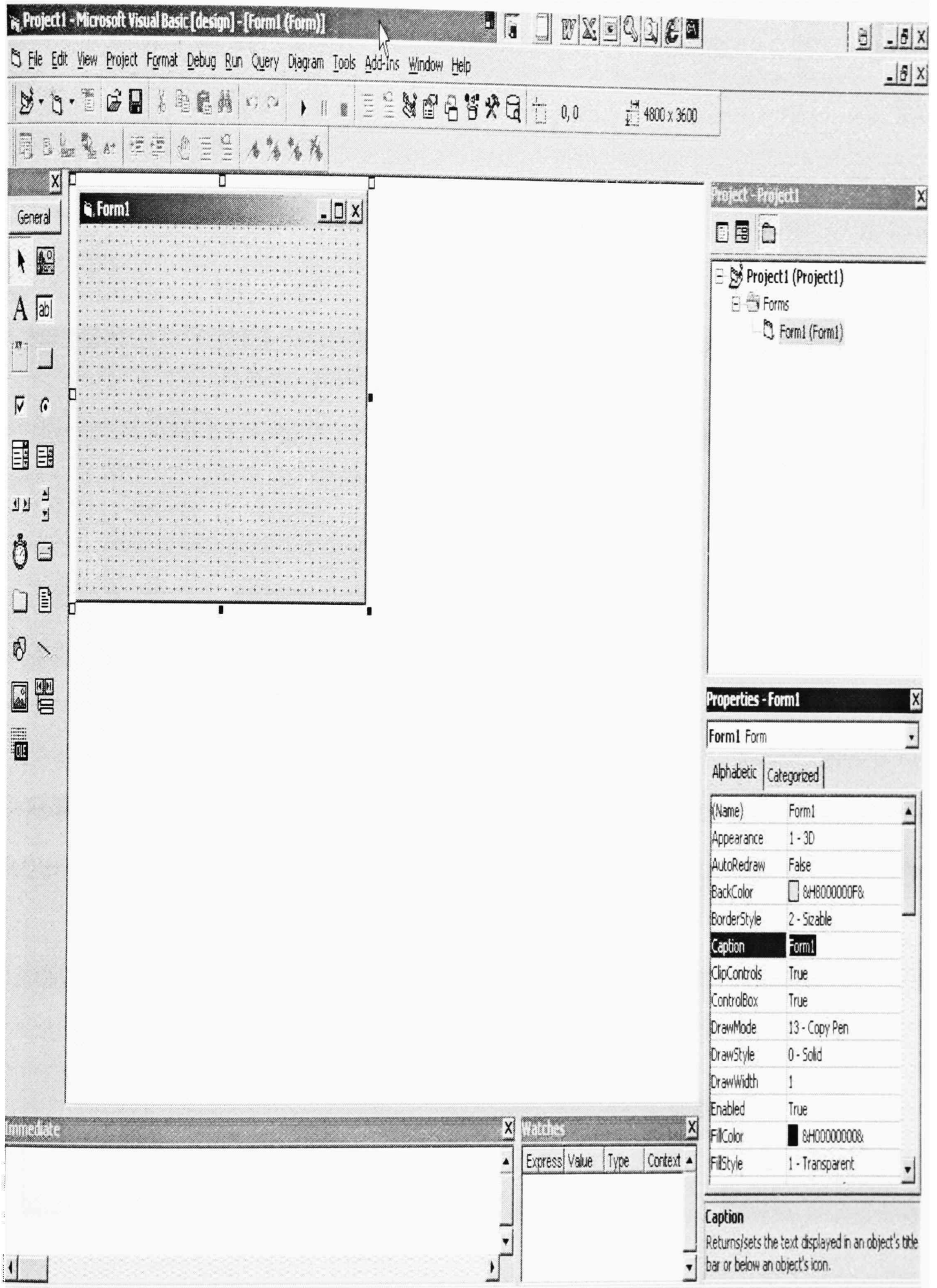

Figure 3.22. Visual Basic Form1 Window

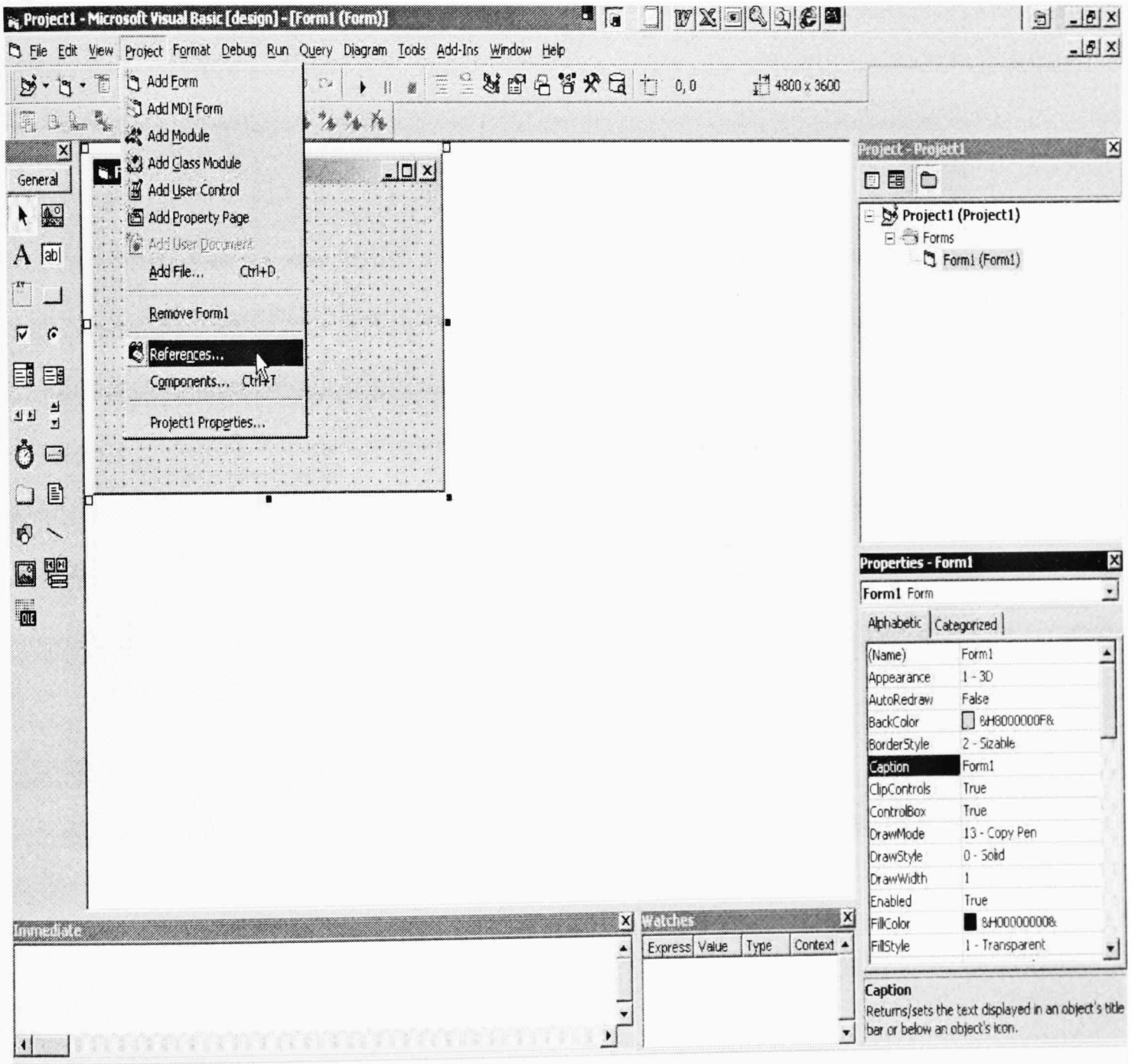

Figure 3.23. Visual Basic Project References Menu.

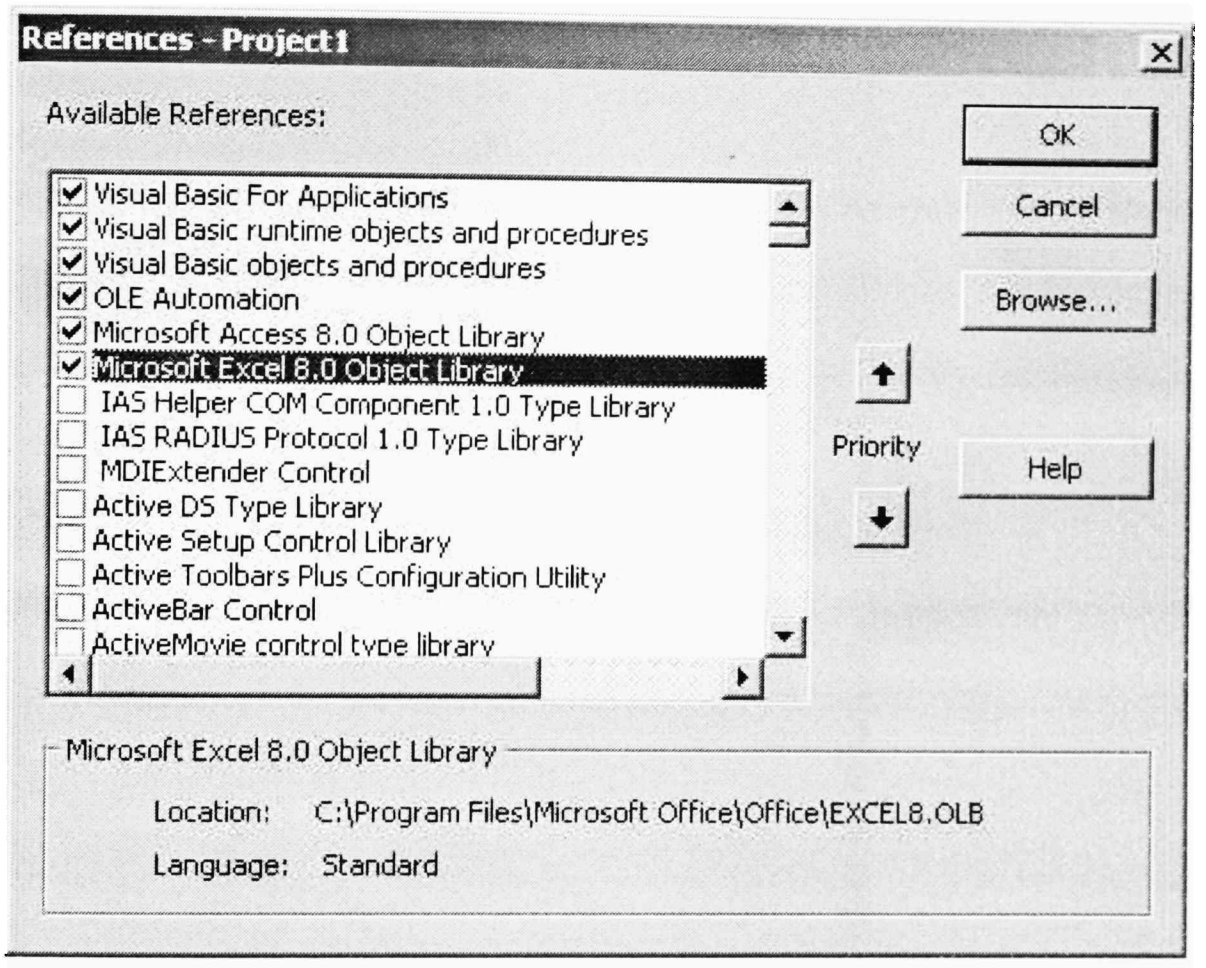

Figure 3.24. Visual Basic Project References

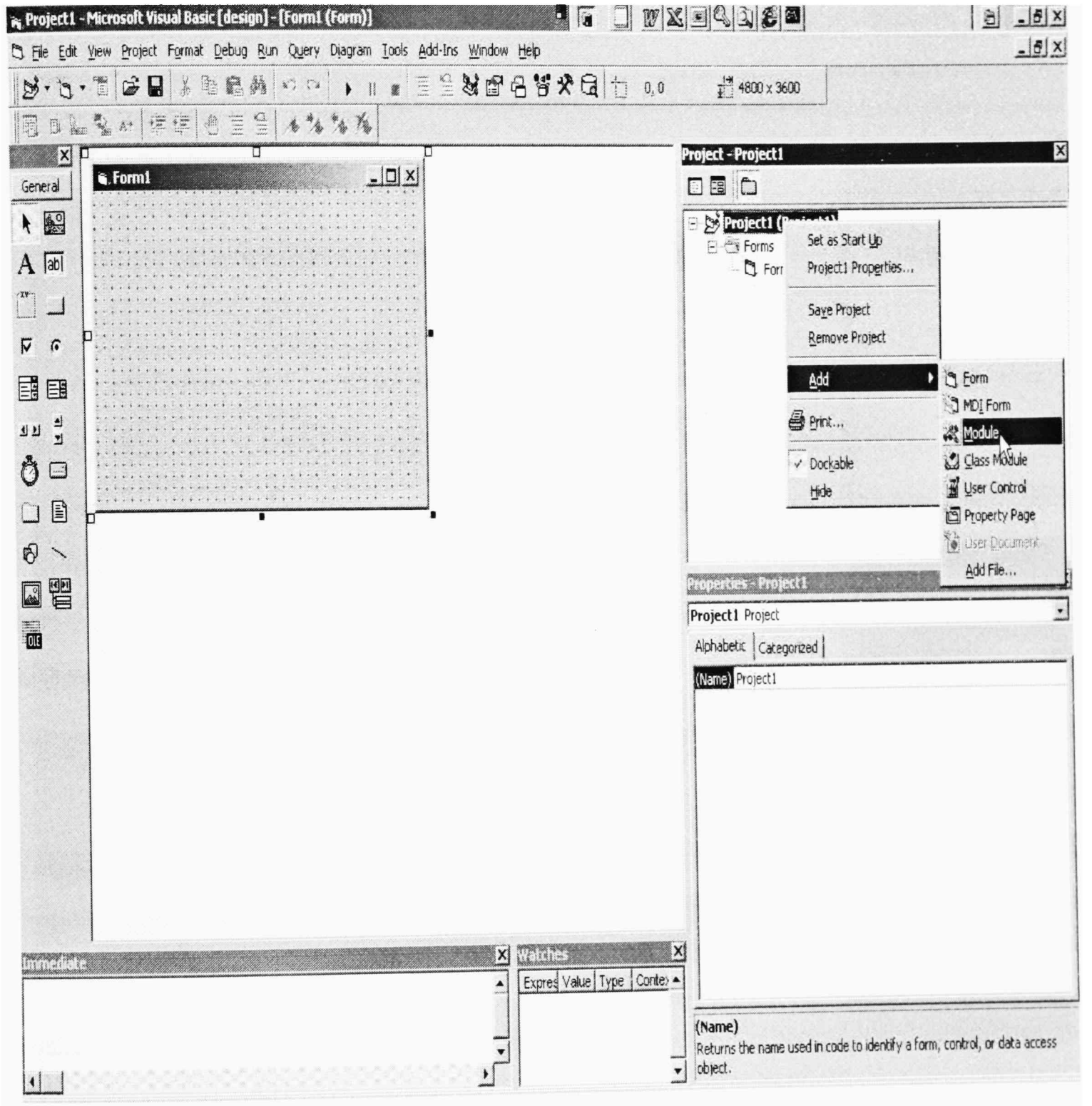

Figure 3.25. Adding a New Module to the Visual Basic Project

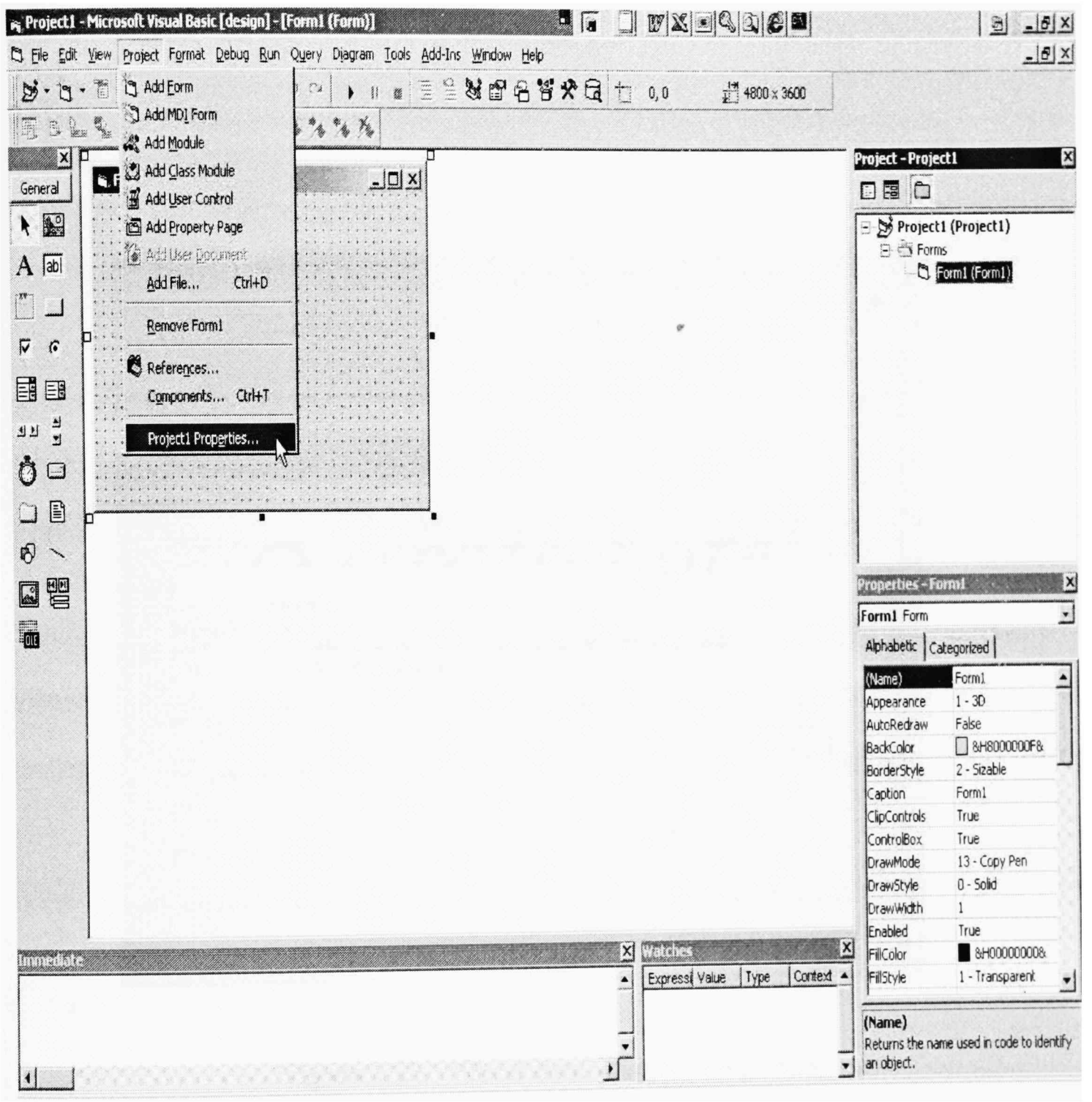

Figure 3.26. Visual Basic Project Properties Menu

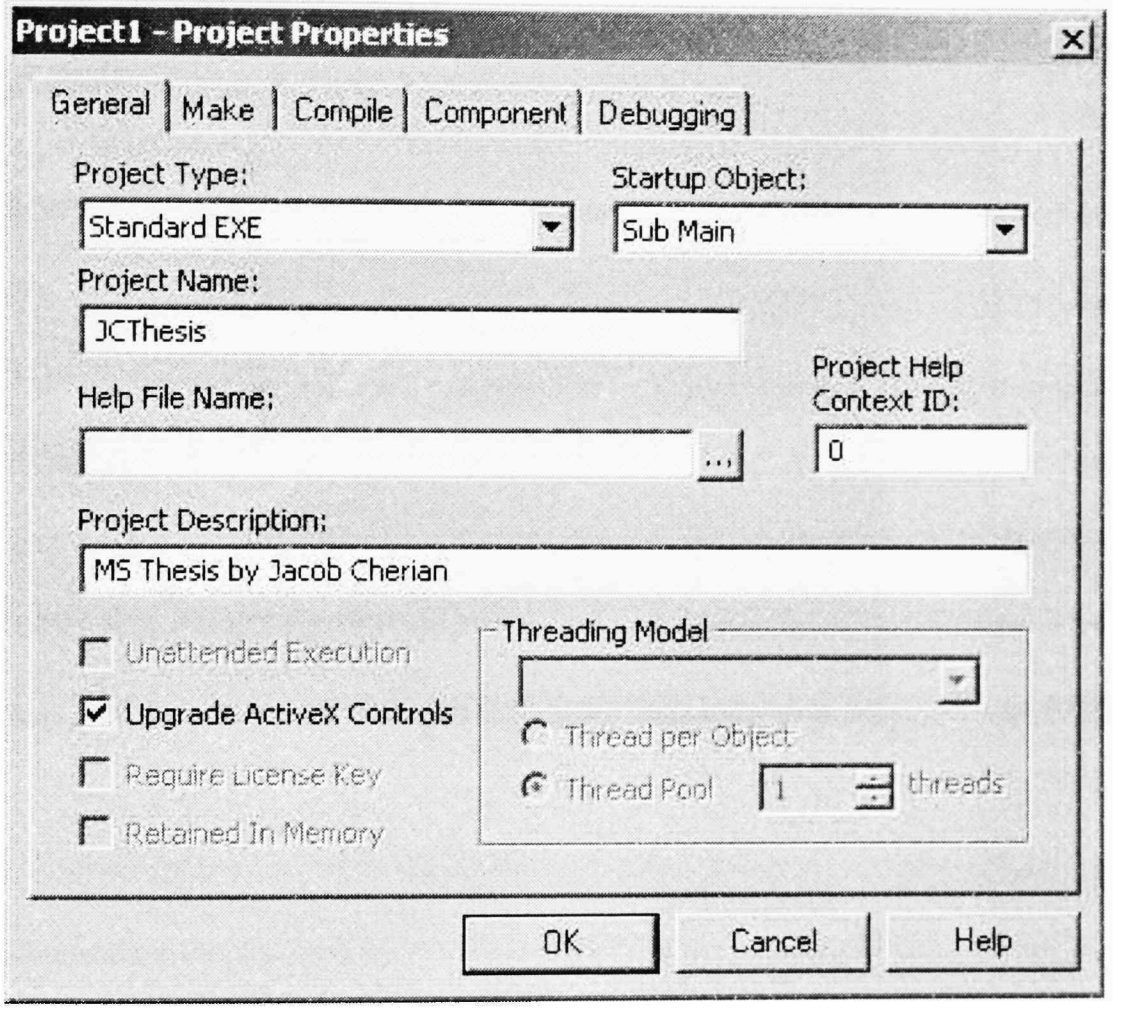

Figure 3.27. Visual Basic Project Properties

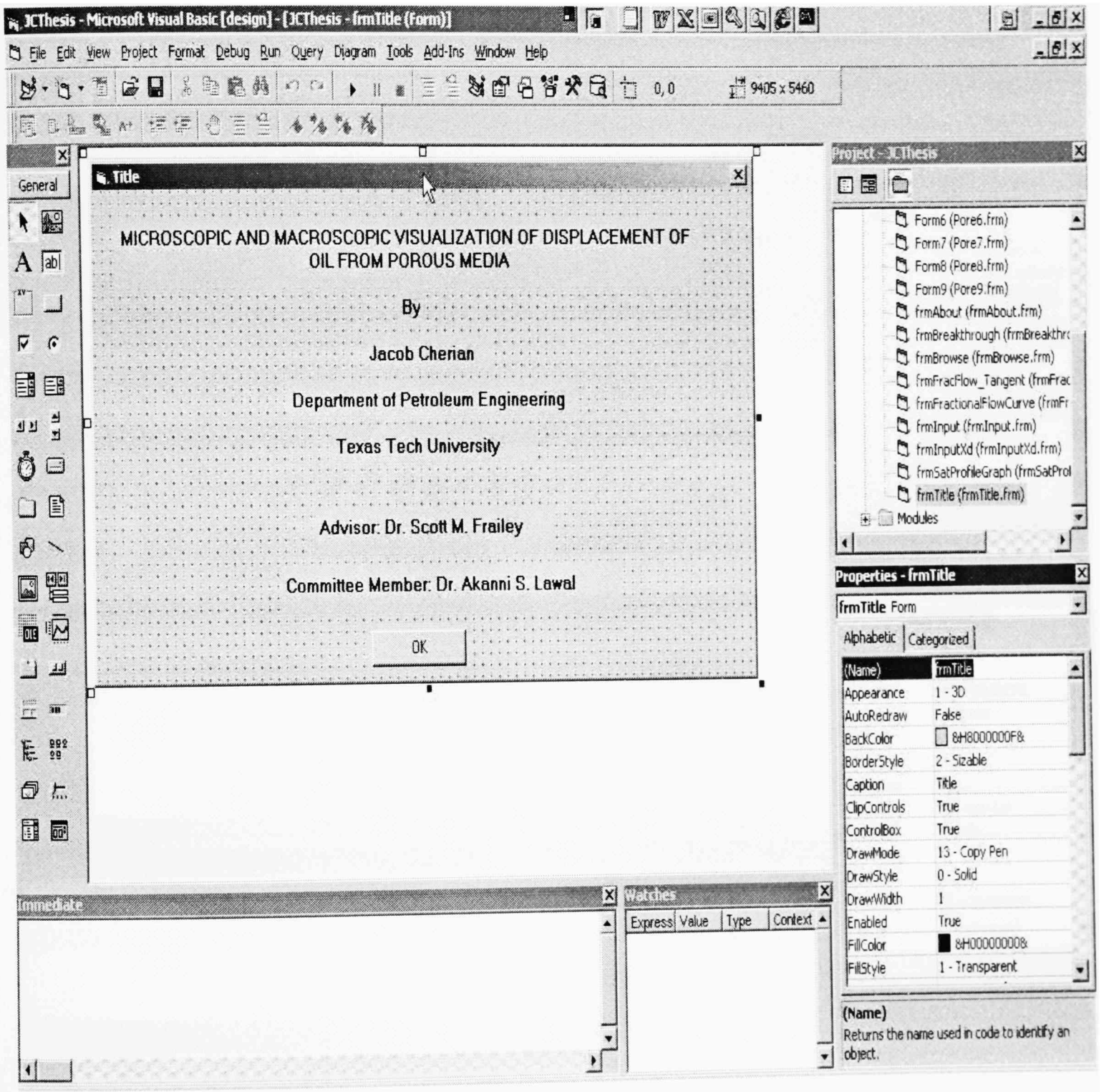

Figure 3.28. Title Page of the Visual Basic Project

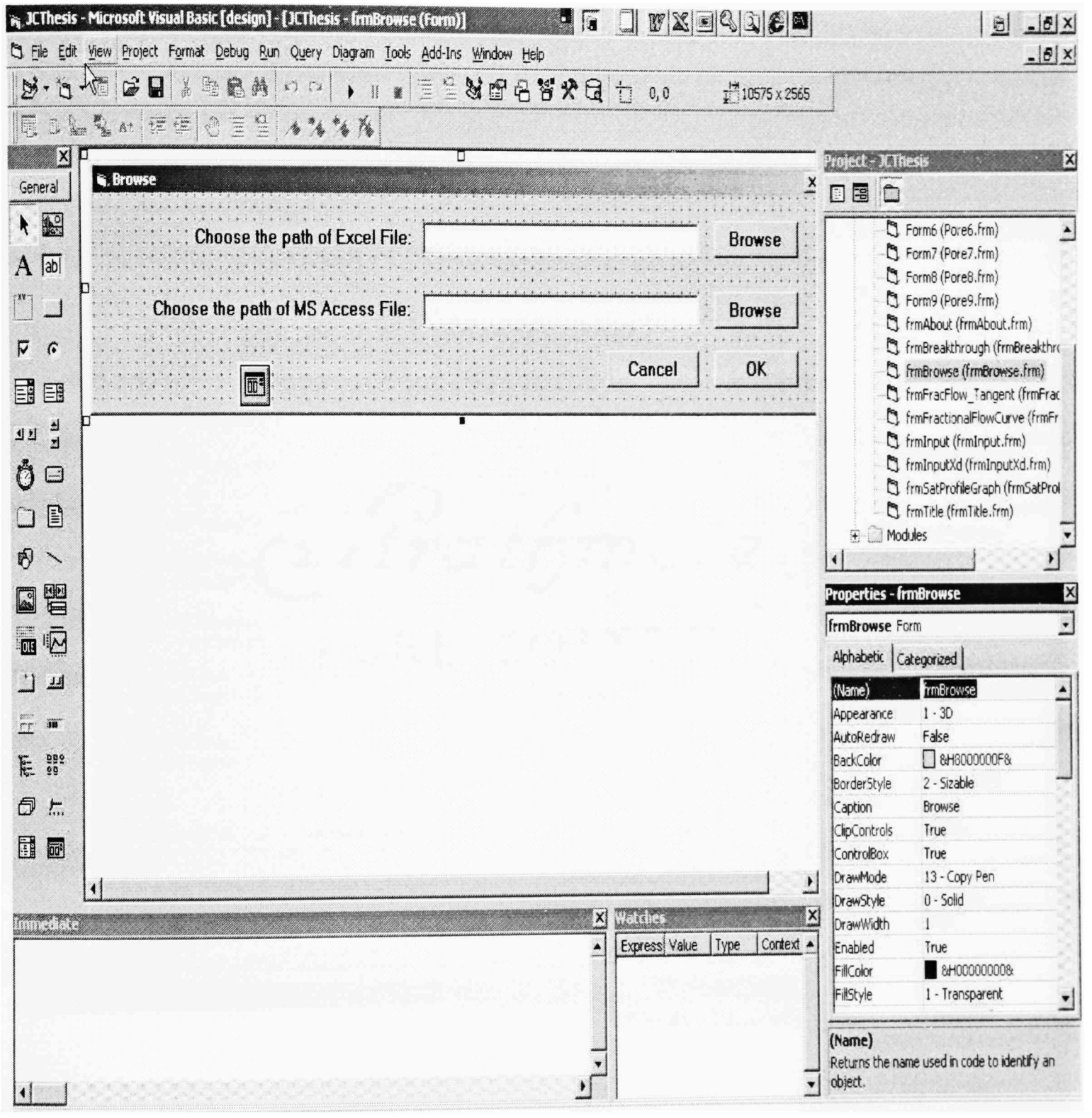

Figure 3.29. Browse Form of the Visual Basic Project

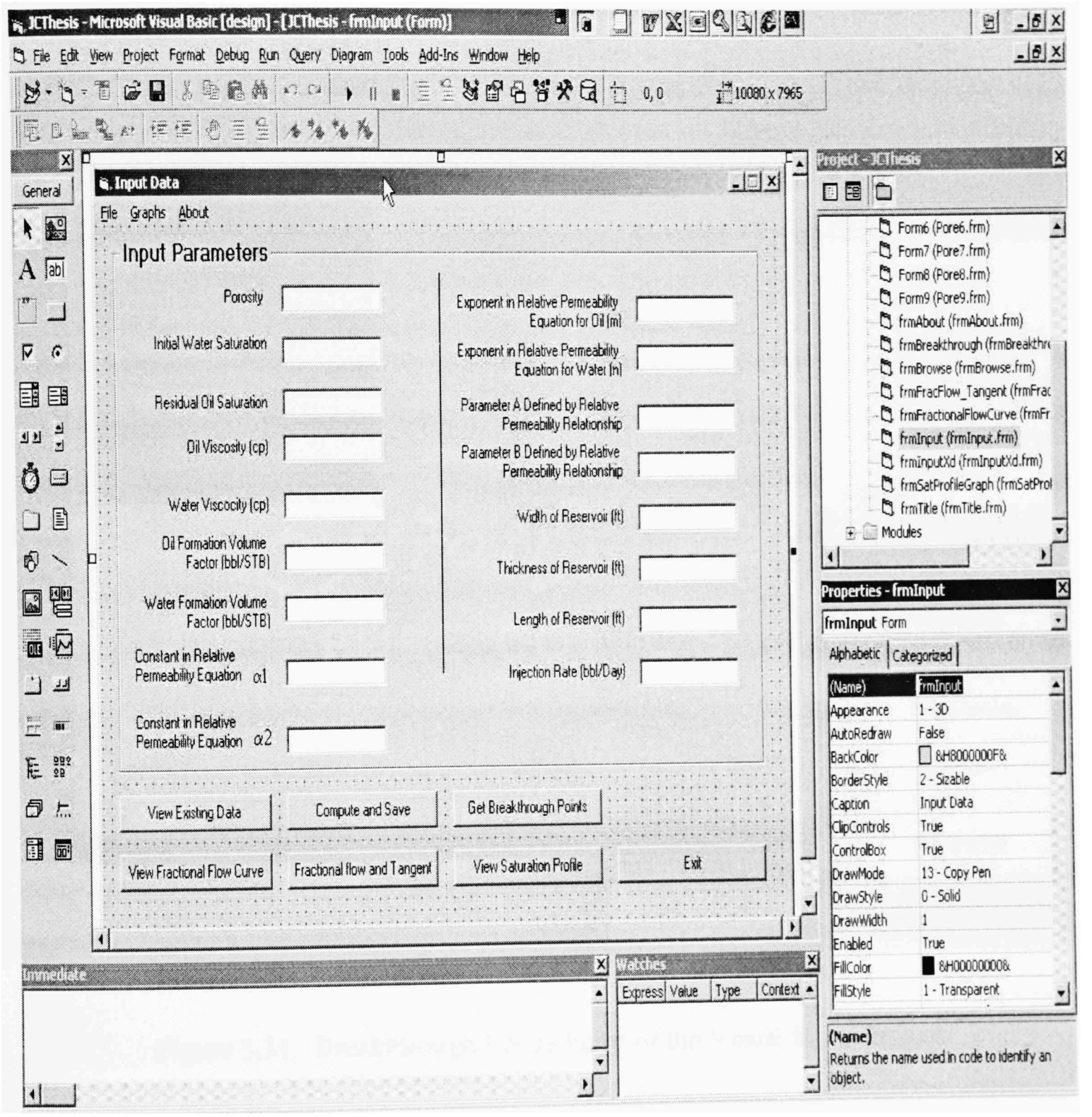

Figure 3.30. Input Data Form of the Visual Basic Project

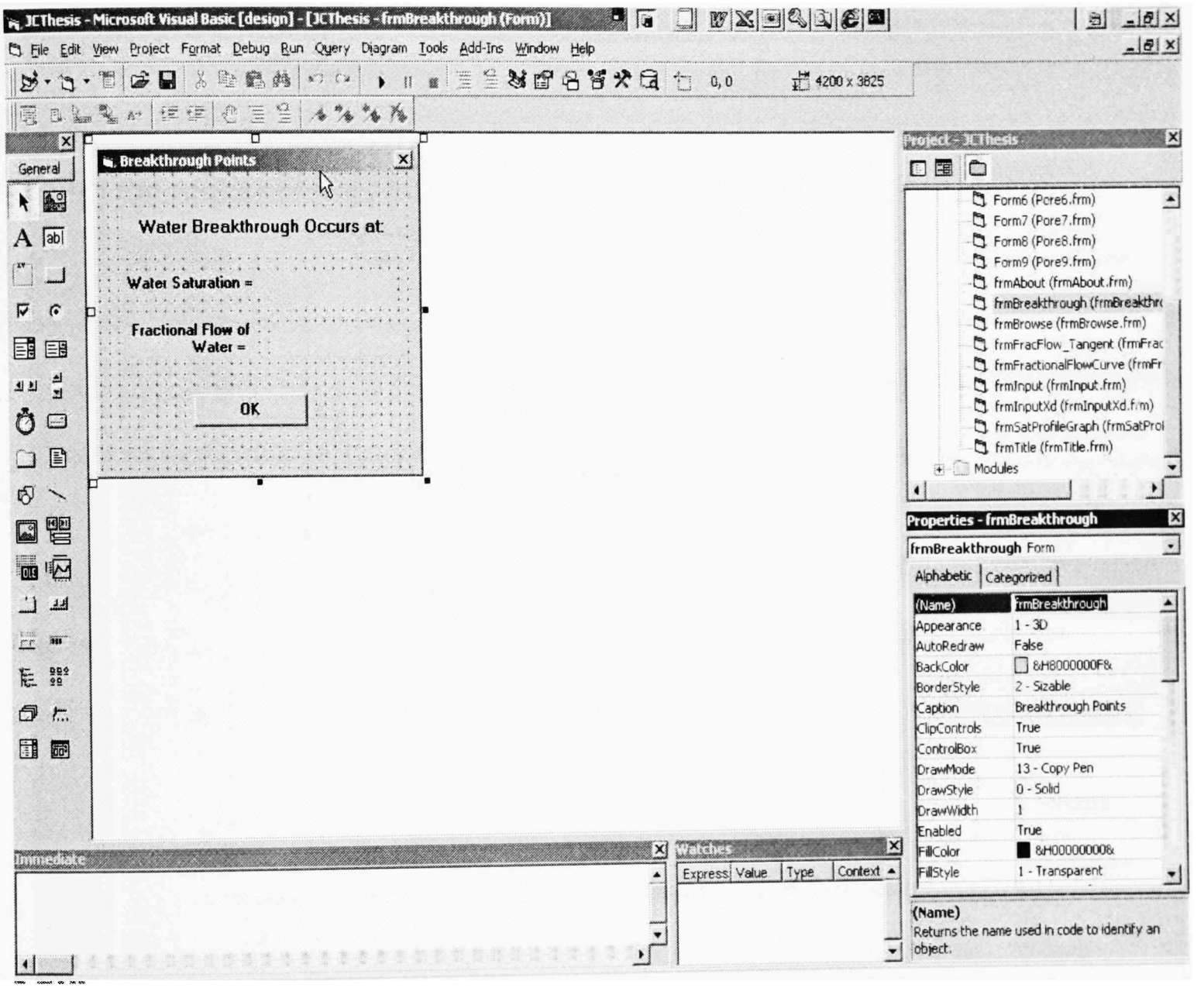

Figure 3.31. Breakthrough Points Form of the Visual Basic Project

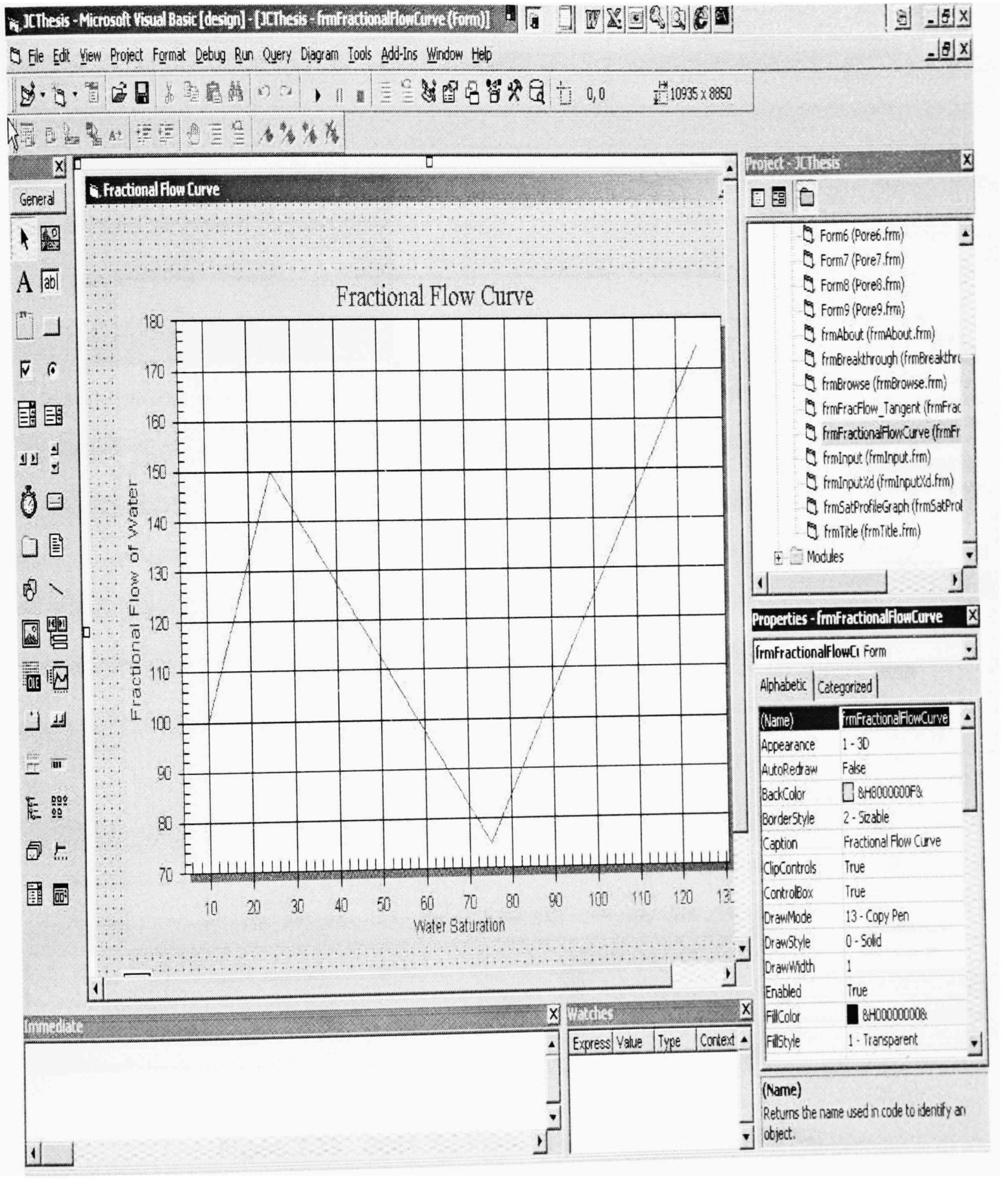

Figure 3.32. Fractional Flow Curve Form of the Visual Basic Project

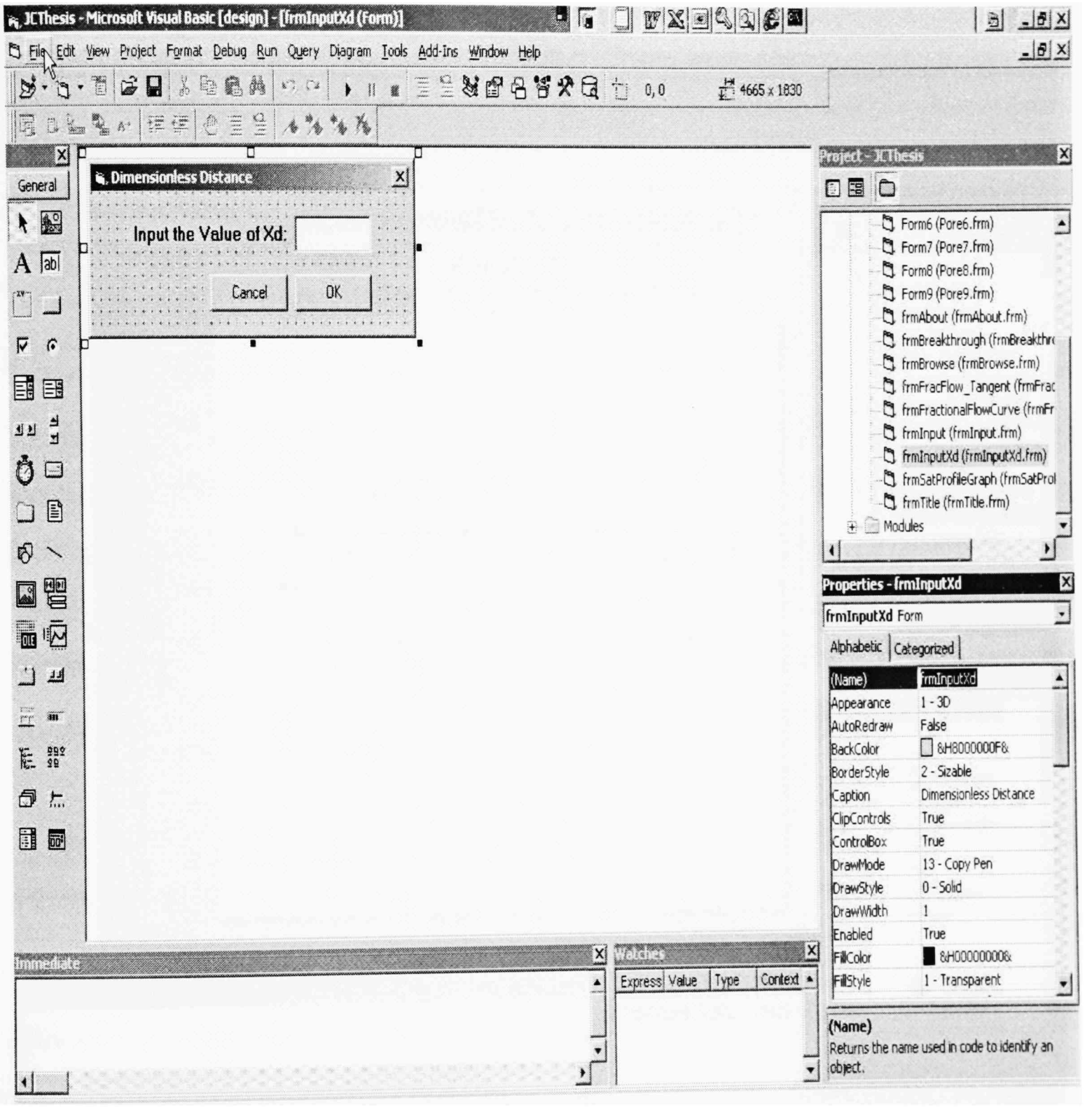

Figure 3.33. Input Xd Form of the Visual Basic Project

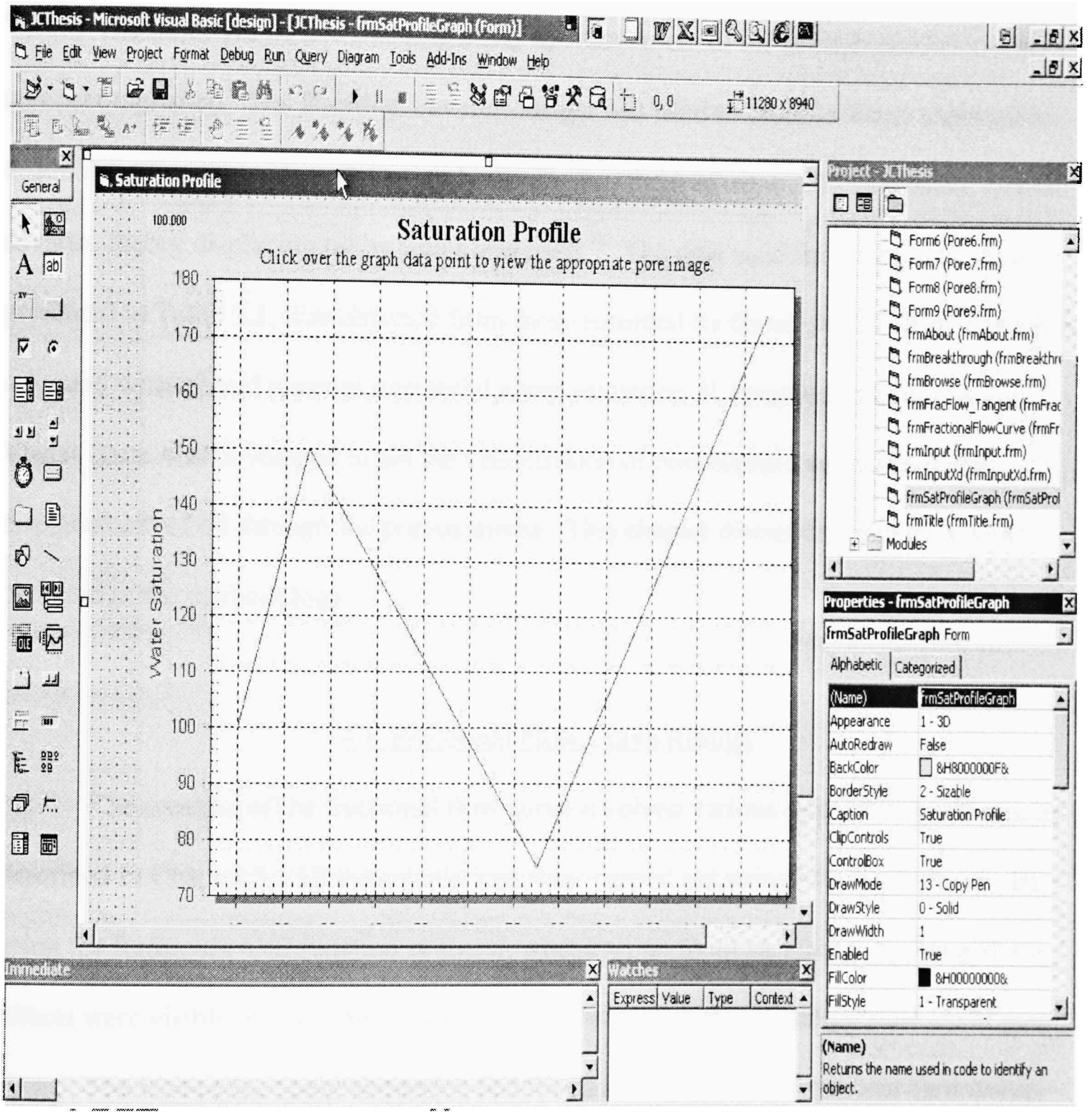

Figure 3.34. Saturation Profile Form of the Visual Basic Project

CHAPTER 4

DISCUSSION OF RESULTS

The objective of this study, to study the movement of oil through porous media, was accomplished. The Buckley-Leverett Model was used to model a linear immiscible displacement process. In order to study the displacement of oil in a linear system, frontal advance theory displacing oil by water was used.[18] The data used for the present study. presented in Table 3.1, was obtained from those recorded by Green and Willhite[7] for a core saturated with oil and water at interstitial water saturation. A computer program using Visual Basic was developed to aid the visualization of microscopic and macroscopic displacement of oil through the porous media. This chapter discusses about the results obtained in the methodology.

4.1 Fractional Flow Curve Results

The creation of the fractional flow curve involved various steps of calculations, as described in Chapter 3. All the calculations were carried out using Microsoft Excel. By using the Reference Cell function of Excel, whenever an input variable was changed. the effects were visible on the entire spreadsheet, as well as on the fractional flow curve graph.

The irreducible water saturation had the most effect on the fractional flow curve, because relative permeability is a function of water saturation. When the irreducible water saturation was increased in steps of 10% for a given set of input parameters. the breakthrough water saturation value advanced by a constant value. The breakthrough

fractional flow value remained the same. Figure 4.1 shows the fractional flow curves when the water saturation was varied from 0.1 to 0.5. The starting point of the fractional flow curve was observed to shift, based on the initial water saturation.

By observing Eq 2-42, it is evident that the fractional flow is a function of relative permeability of both oil and water. For a given set of oil/water relative permeability, if the relative permeability of water increases, water saturation increases, and the relative permeability of oil decreases. If the oil viscosity is high, then the fractional flow of water increases. Alternately, if the water viscosity is high, the fractional flow of water decreases.

The residual oil saturation had a similar effect on the fractional flow curve. When the residual oil saturation was increased by maintaining lower water saturation, the fractional flow curve became steeper. When the residual oil saturation was increased in steps of 10% for a given set of input parameters, the breakthrough water saturation decreased in constant steps, and the breakthrough fractional flow of water remained constant. Figure 4.2 shows the fractional flow curves when the residual oil saturation was varied from 0.1 to 0.5. The end point of the fractional flow curve was observed to shift, based on the value of residual oil saturation.

Other factors which affect the fractional flow curve which include formation permeability, dip of the reservoir, etc. are not discussed here. The current method of creating the fractional flow curve using Excel spreadsheet made it possible to change the input parameters on the spreadsheet and to subsequently visualize the shape of the resultant fractional flow curve (figures created using the Visual Basic program are discussed in a

later section). This method was found to save time by not constructing the fractional flow curve all over, which enhanced learning.

4.2 Results of Creating an Automated Tangent

The objective at this stage was to create an automated tangent to the fractional flow curve. The automated tangent started at the initial water saturation and passed tangentially through the breakthrough points of the fractional flow curve. The program is capable of detecting the maximum slope of the fractional flow curve, and plotting the tangent, accordingly. Figure 4.3 shows the automated tangent when the water saturation is 0.1 and the residual oil saturation is 0.4. When the input parameter in Table 3.1 is varied by the user, the shape of the fractional flow curve changes, the tangent adjusts itself to start from the initial water saturation and to pass through the breakthrough points. This was achieved with the help of cross-linking each cell of the spreadsheet, using the Excel functions like MAX, MATCH and INDEX. Figure 4.4 shows the fractional flow curve, and the automated tangents when the water saturation is maintained at 0.2 and the residual oil saturation are varied from 0.2 to 0.4. The automated tangents start at the initial water saturation and pass through the breakthrough points. The automated tangent is helpful in visualizing the breakthrough points on the fractional flow curve.

The parameter that has the most effect on water breakthrough points is water saturation. When the water saturation was high, the breakthrough occurred relatively earlier, than when the water saturation was low. For a given set of input parameters, when the water saturation was 0.3, breakthrough occurred at a water saturation of 0.6265. When

the water saturation was decreased to 0.1, the breakthrough water saturation was observed to be 0.5897.

4.3 Results of Creating Macroscopic View

The S_w vs. x_D plot constructed using the values tabulated in Table 3.3, is called the macroscopic view, or the saturation profile. Table 3.3 was constructed using the S_w and f'_w values from Table 3.2, and the dimensionless distance (x_D) values were created between 0 and 1. The saturation region was divided into 10 equal parts to represent 10% saturation intervals. By having 260 data points on the S_w vs. x_D plot, there was at least one point within each of the saturation intervals.

The macroscopic view created using the water saturation and the dimensionless distance was adequate in viewing the saturation distribution along the one dimensional reservoir. The saturation distribution could be viewed for various dimensionless distances (x_D). This is achieved by changing the x_D values in Table 3.1. When the x_D value is changed, values in Table 3.3 are changed automatically, thus changing the macroscopic view.

Mobility ratio has the most impact on the macroscopic view. In general, for oil with low viscosity, if M is less than or equal to one, the waterflooding is said to be efficient in terms of recovery such that, all of the movable oil is recovered by the injection of an equivalent volume of water.

The macroscopic view has a water saturation value $1-S_{or}$ at the injector and the water saturation gradually decreases along the dimensionless distance towards the

producer, until the breakthrough water saturation value is reached. At the breakthrough saturation point, the value of dimensionless distance is the same entered by the user in Table 3.1. A sharp change in the saturation value that represents the waterflood front is visible in the macroscopic view, and the water saturation continues to remain at the initial water saturation value, to the producer.

Figure 4.5 represents the macroscopic view at $S_{iw} = 0.3$, $S_{or} = 0.3$, and $x_D = 0.5$. The macroscopic view starts with a water saturation of 0.7 and gradually decreases to a breakthrough water saturation of 0.4224, and then drops down to the initial water saturation of 0.3. It is visible from Figure 4.5 that the water saturation at the injector is higher and gradually decreases towards the producer. This also means that the oil saturation remains higher towards the producer and lower towards the injector. When the velocity of the flood front saturation exceeds or is equal to the velocity of the initial saturation, an oil bank is formed. When the mobility ratio is favorable, a piston like displacement is observed with no gradual decrease in saturation. The breakthrough saturation is determined by the location of the tangent on the fractional flow curve, drawn from the initial water saturation point, and as long as the tangent could be drawn to the curve, a saturation discontinuity exists. The breakthrough saturation is identified on the macroscopic view (Figure 4.5) as the location on the curve where the sharp drop in saturation occurs, when water saturation is 0.5.

The Visual Basic program prompts the user to enter the dimensionless distance while viewing the macroscopic view. The value entered by the user is transferred to the

Excel spreadsheet, and the appropriate macroscopic view is displayed to the user. Thus, the user does not have to open the Excel spreadsheet to view the macroscopic view.

The macroscopic view aided in the visualization of the saturation distribution at the reservoir level. Since the macroscopic view changed its shape based on the dimensionless distance input by the user, the required amount of automation was achieved in the case of macroscopic view.

4.4 Results of Creating Microscopic Views

Microscopic views are the visual representation of the pores at various saturations. By examining the macroscopic view it is evident that when water is injected, the water saturation inside the pores increases, and displaces the oil trapped within the pores.

Microscopic views were created with the aim of representing a pore at a given saturation distribution and x_D. Since the macroscopic view was divided into 10 saturation regions, it was appropriate to include at least 10 pores representing each saturation region (Figures 3.9 to 3.18). The pores created in this case were two-dimensional.

During the creation of the microscopic views, along the direction of fluid flow, a circular cross section of the pores is assumed. A plane perpendicular to the circular cross section in the direction of flow is assumed to be of a semi-elliptical shape with pore throats. Figure 4.6 represents a two-dimensional pore, where the brown color indicates the porous media, the blue color represents water, and the dark green color represents oil.

The microscopic view is embedded in the macroscopic view using Object Linking and Embedding (OLE) technique. The macroscopic view consists of 260 points, and these

points are sensible to the computer mouse. When the user places the mouse over these points and clicks, calculations are performed to determine the average water saturation within a 10% dimensionless distance (x_D). Based on the results of this calculation, a microscopic pore image is displayed to the user. For example, if the average water saturation within a 10% dimensionless distance is 32%, then a macroscopic view within 31-40% saturation is displayed. Thus, embedding the microscopic views within the macroscopic view provides visual understanding of the saturation distribution of a reservoir as well as the pore body. Displaying the microscopic view from the macroscopic image after determining the average water saturation within a 10% dimensionless distance automated the selection of an appropriate microscopic view. Displaying a macroscopic and microscopic view is discussed in section 4.6.

4.5 Results of Linking Excel to Access

The Excel spreadsheet is linked to Access to transfer data to plot graphs and the average saturation. The graphs populated using these data are the fractional flow curve, the automated tangent, and the macroscopic view, as shown in Figures 4.7-4.9. The average saturation values are used to display microscopic view. Transfer of data from Excel to Access is necessary, since the graphs require the data to be populated from a database instead of a spreadsheet. The updated values from the Access database are used to plot the graphs. Thus, any change in the input parameter or spreadsheet calculation is updated in the Access database, and is reflected on the corresponding graphs.

4.6 Results of Linking Visual Basic to Excel and Access

The primary objective of this section is to facilitate the user interface to the Visual Basic program without the necessity of opening Excel spreadsheets. This was achieved by using a Visual Basic program. The initial screen of the program is displayed in Figure 4.10. At the start of the Visual Basic application, the program requires the location of the Excel and Access files. The window seeking the location of the Excel and Access database is shown in Figure 4.11. The user can browse to the location of these two files, and the program automatically links the Excel spreadsheet with the Access database in the background. Linking of the two files was necessary in order to update the access database with the results of the Excel spreadsheet.

Figure 4.12 displays the main screen of the program. From this screen, the user can navigate as desired. By clicking the button "View Existing Data" displays the contents of Table 3.1 from the Excel spreadsheet, as shown in Figure 4.13. After the modifications are done, the user can modify the contents of Excel spreadsheet by clicking on the button "Compute and Save" located on the main screen. A pop up window displays the list or parameters modified by the program in the Excel spreadsheet, as shown in Figure 4.14. The modified values are updated in the Excel spreadsheet, and necessary calculations are performed to compute the water breakthrough values, plot the fractional flow curve, draw the automated tangent, and plot the macroscopic view. The computed results are transferred and stored in the Access database to be used with the Visual Basic program.

Based on the entries made by the user in Table 3.1 through the Visual Basic program, breakthrough water saturation and fractional flow values are displayed to the user

by clicking on the button "Get Breakthrough Points." Figure 4.15 displays the breakthrough points when this button is clicked.

Plotting the fractional flow curve, constructing an automated tangent to the fractional flow curve, and creating the macroscopic view are achieved using the data stored in the Access database, as described in section 4.5. In order to view the fractional flow curve, the user needs to click the buttons "View Fractional Flow Curve", and the fractional flow curve is displayed in Figure 4.7. To view the fractional flow curve and tangent, the button "Fractional flow and Tangent" is used, and the display is shown in Figure 4.8. The button "View Saturation Profile" requires an input parameter from the user as shown in Figure 4.16. The saturation profile displayed is shown in Figure 4.9.

Data from the Access database also provides the information to display the appropriate microscopic view. To view the microscopic view, the user needs to point the computer mouse on the saturation profile at the upper boundary of the oil region (green region). The computer mouse arrow changes into the shape of a hand, indicated by a red circle in Figure 4.17. Upon clicking the hot spot (area where the mouse pointer changes shape from an arrow to a hand), the microscopic view is displayed, as shown in Figure 4.18.

The Visual Basic application provides the necessary interactive environment where the user can visualize the microscopic and macroscopic views. The user can visualize the change in the fractional flow curve and the breakthrough points by modifying the input parameters. The program allows the user to navigate with ease and minimal user-intervention.

The Visual Basic program allows the user to view multiple windows at the same time. Thus, the user can view the fractional flow curve, the macroscopic view, and the microscopic view at the same time. Data saved through the Visual Basic program is stored in the Excel spreadsheet and is displayed to the user the next time.

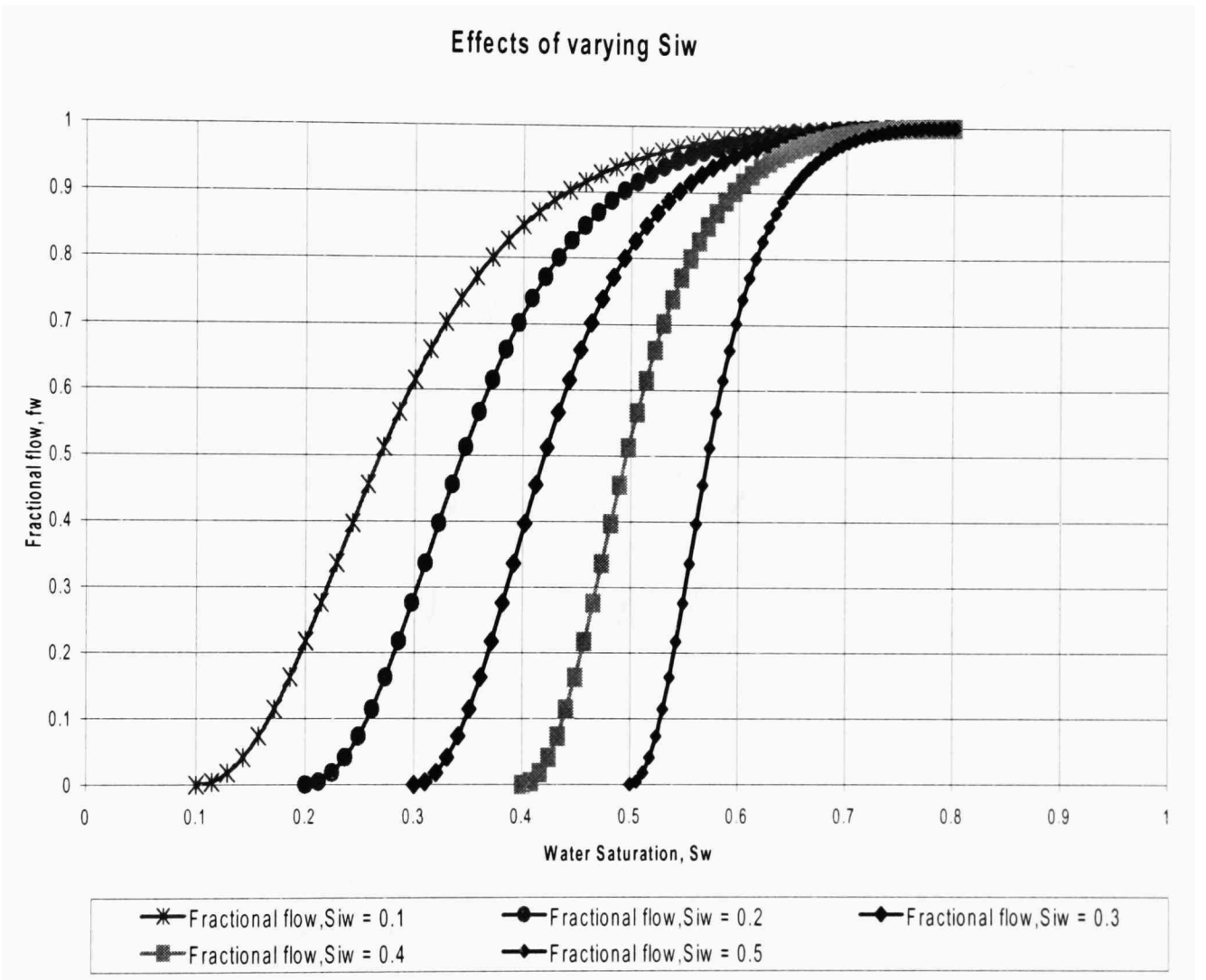

Figure 4.1. Fractional flow of water with varying Siw

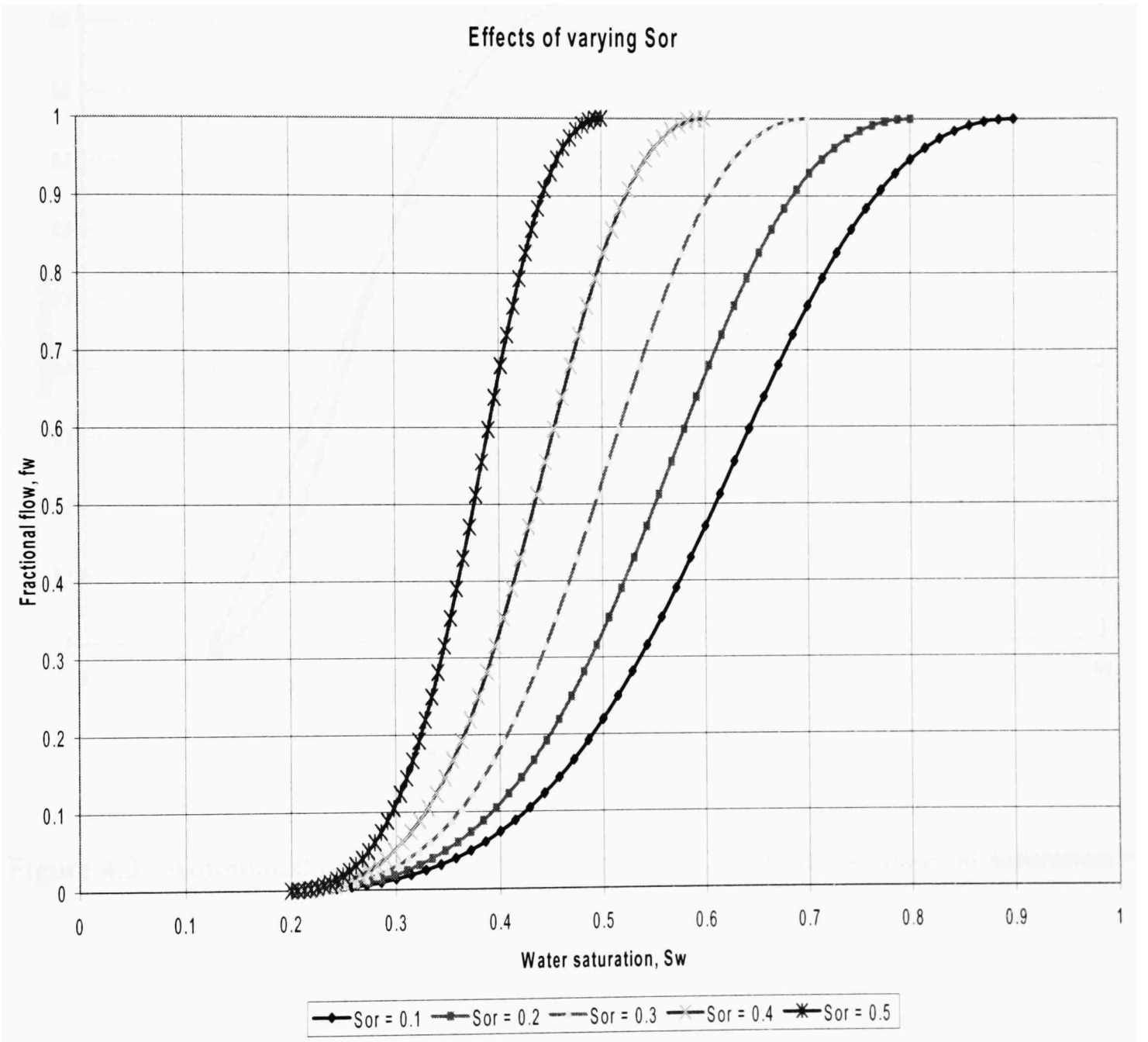

Figure 4.2. Fractional flow of water with varying Sor.

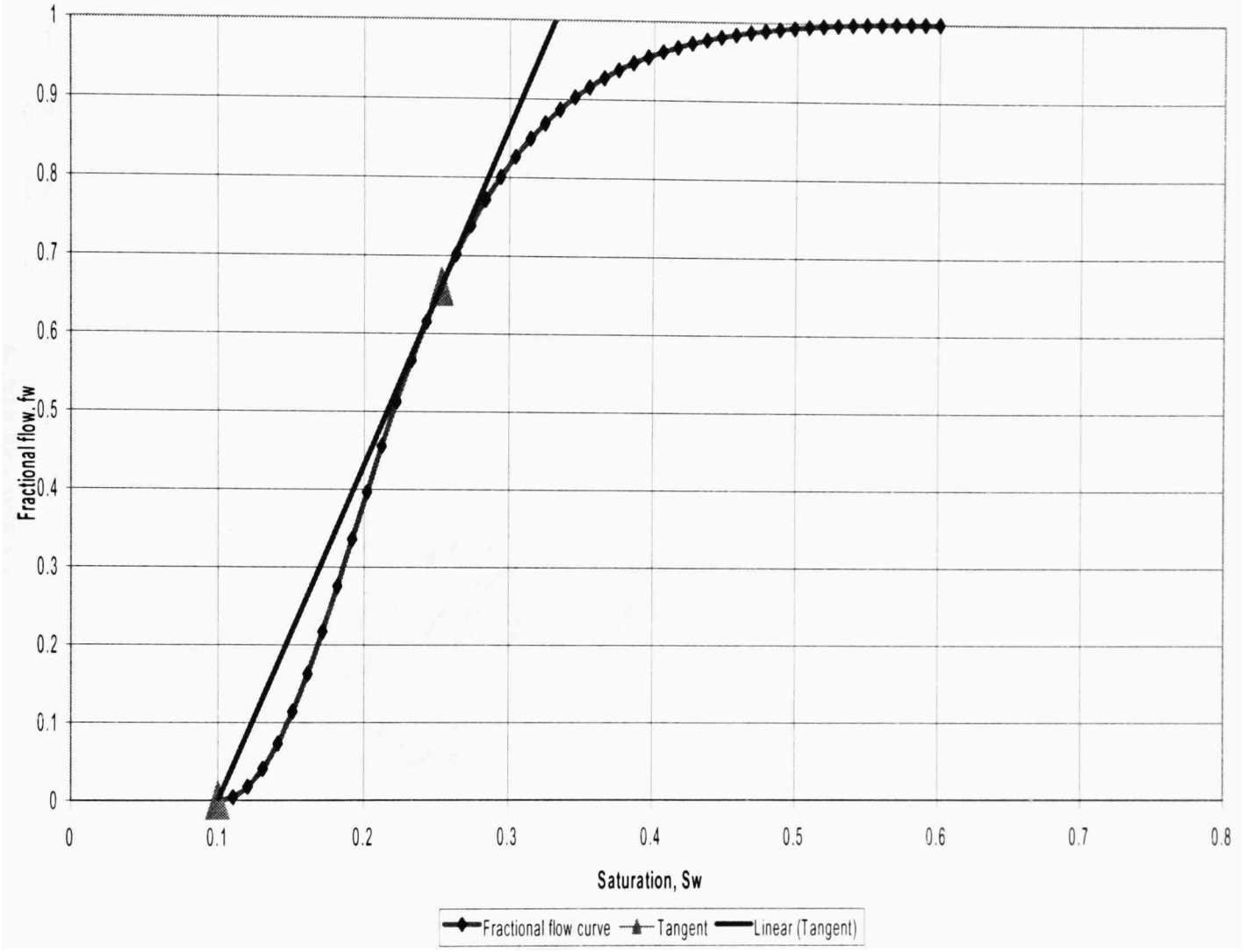

Figure 4.3. Automated tangent when water saturation = 0.1 and residual oil saturation = 0.4.

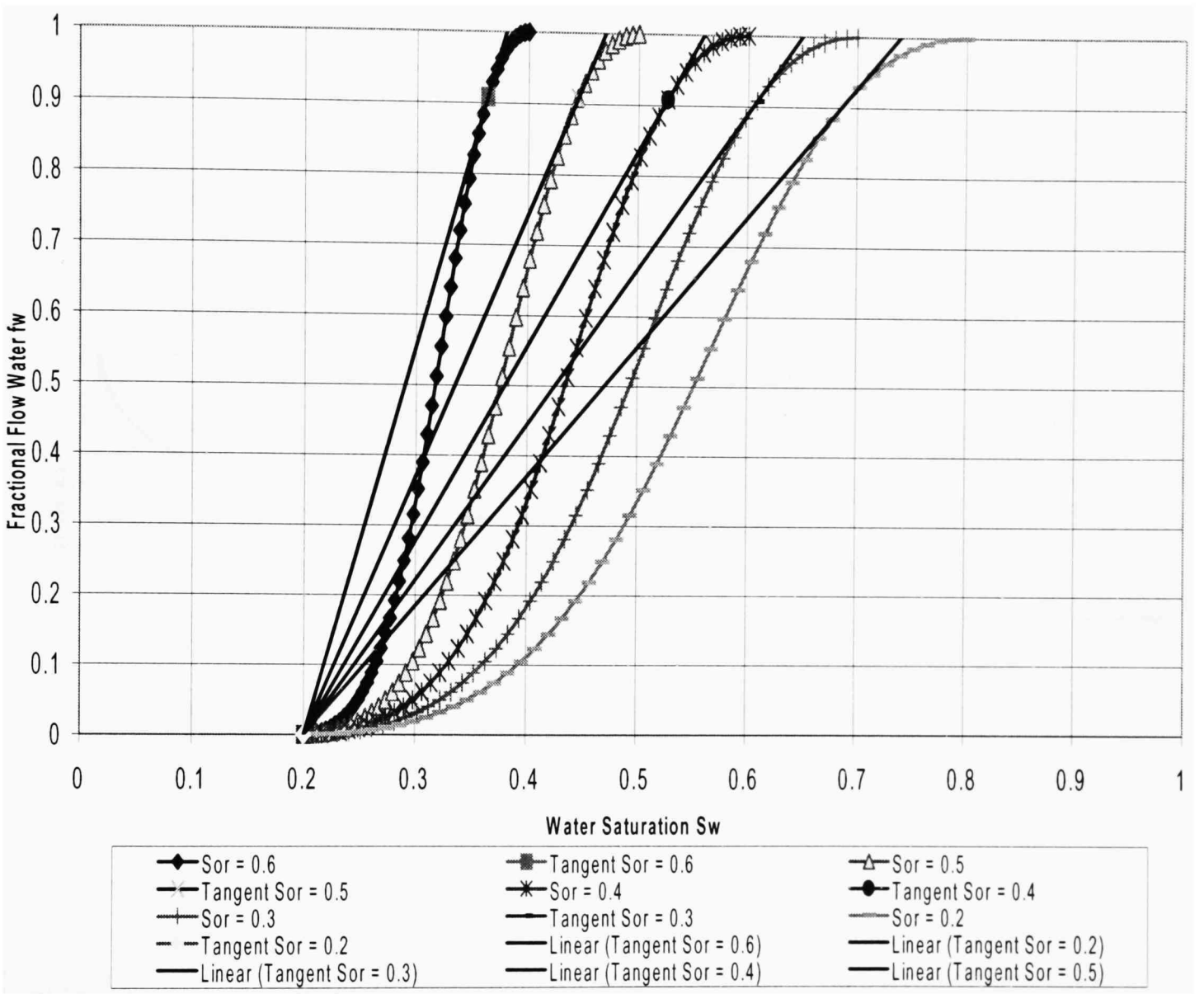

Figure 4.4. Automated tangents when water saturation = 0.2 and residual oil saturation = 0.2 to 0.6.

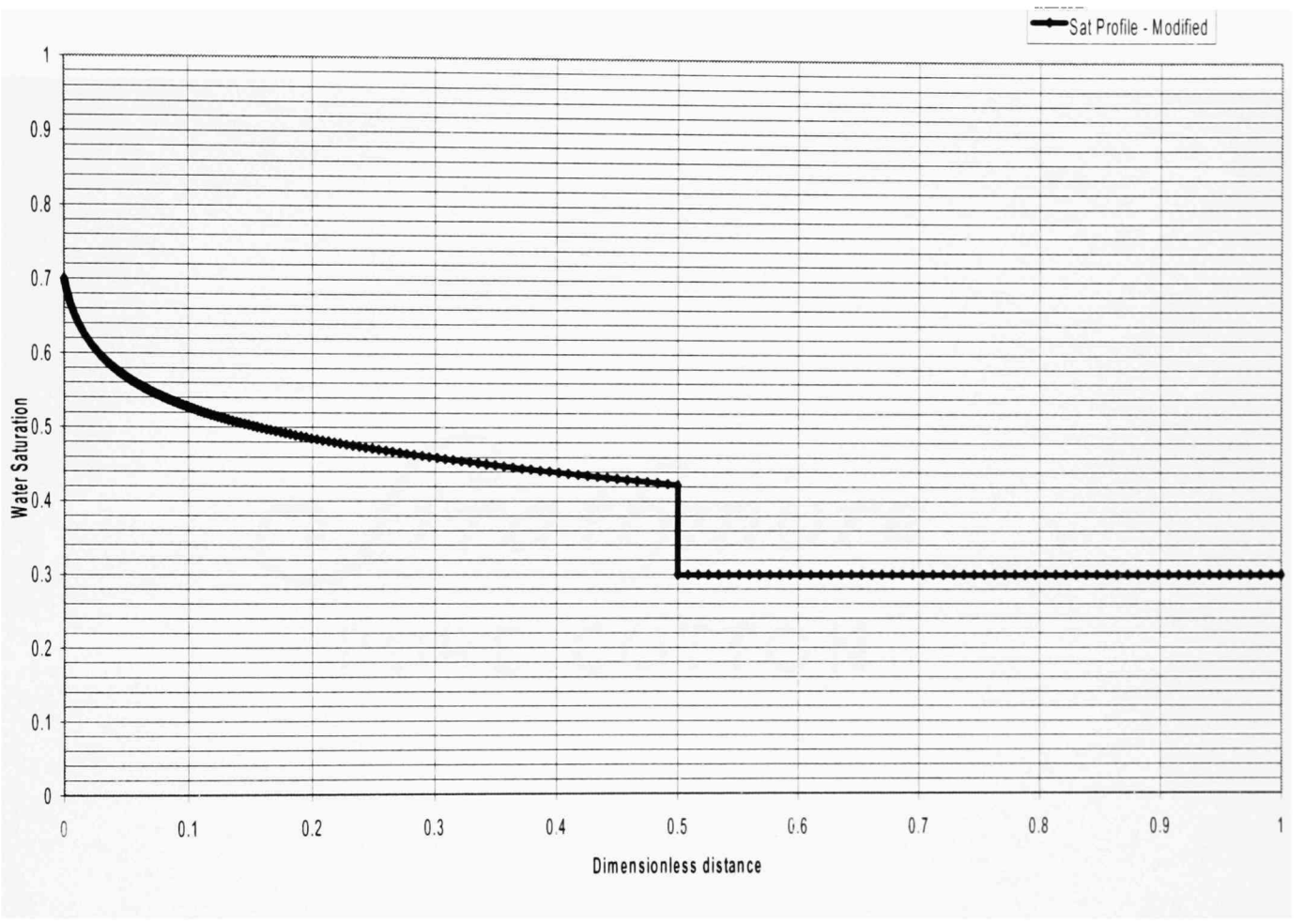

Figure 4.5. Macroscopic view when water saturation = 0.3, residual oil saturation = 0.3 and dimensionless distance = 0.5.

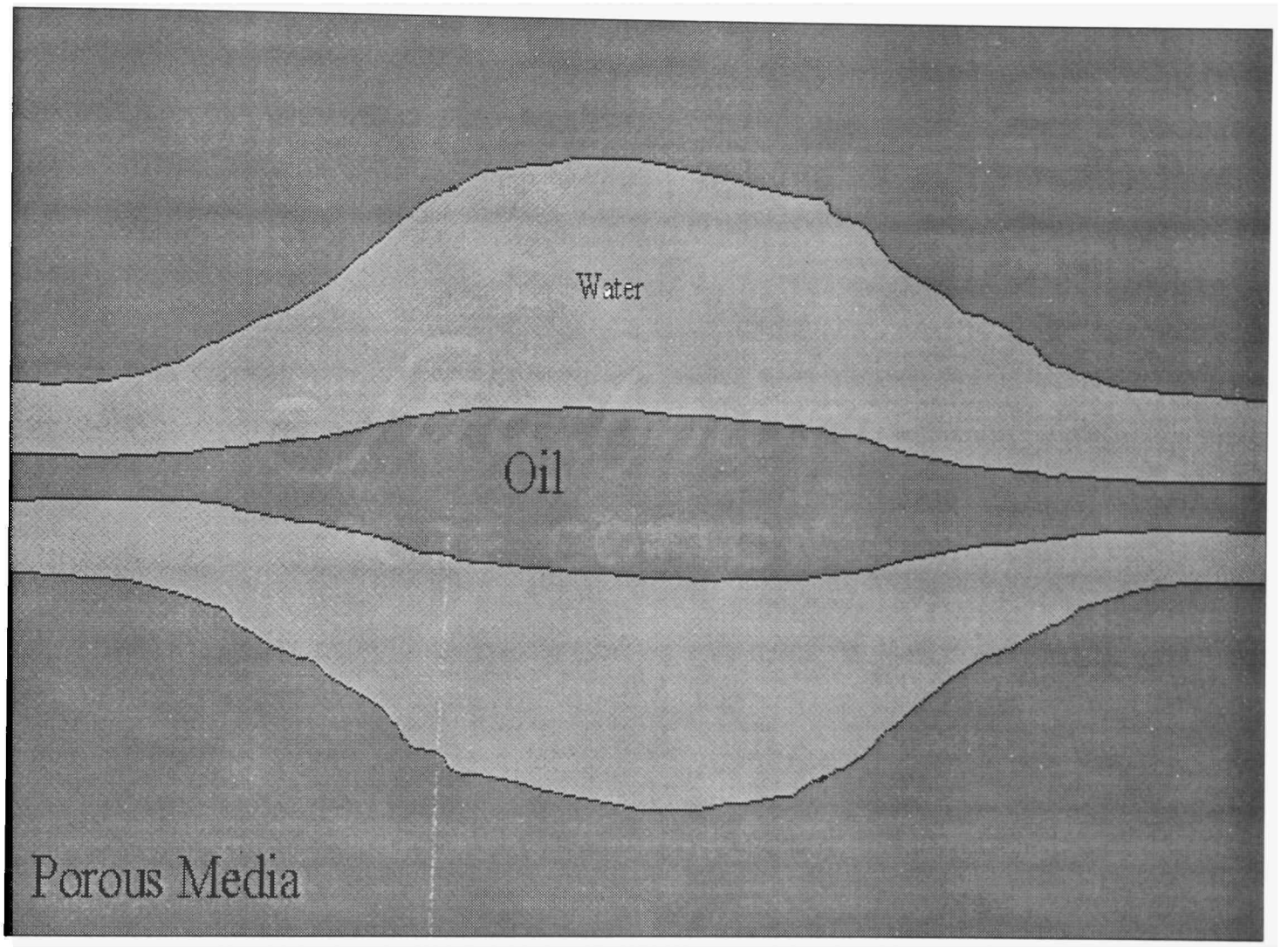

Figure 4.6. A two-dimensional pore

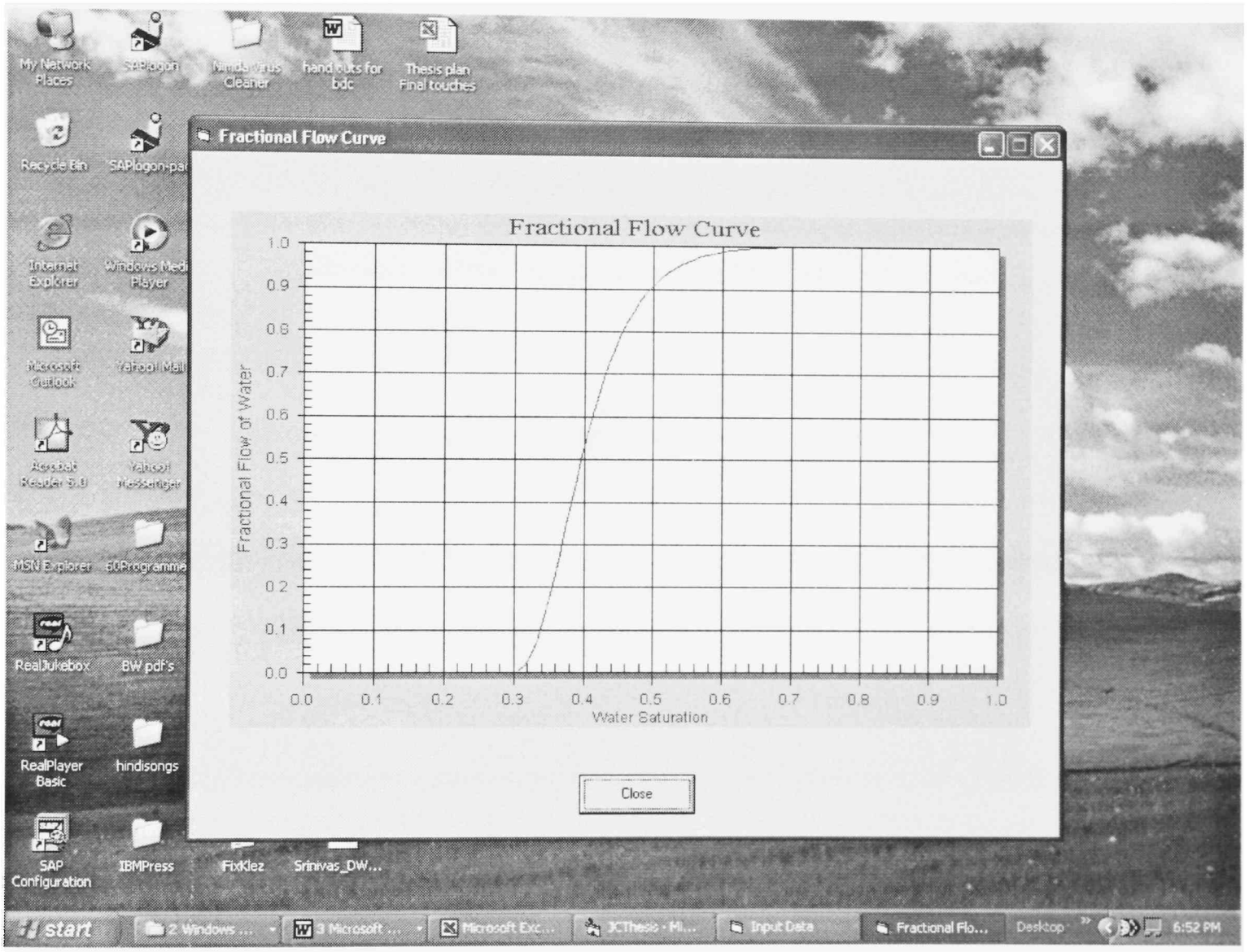

Figure 4.7. Fractional Flow curve after linking Excel and Access

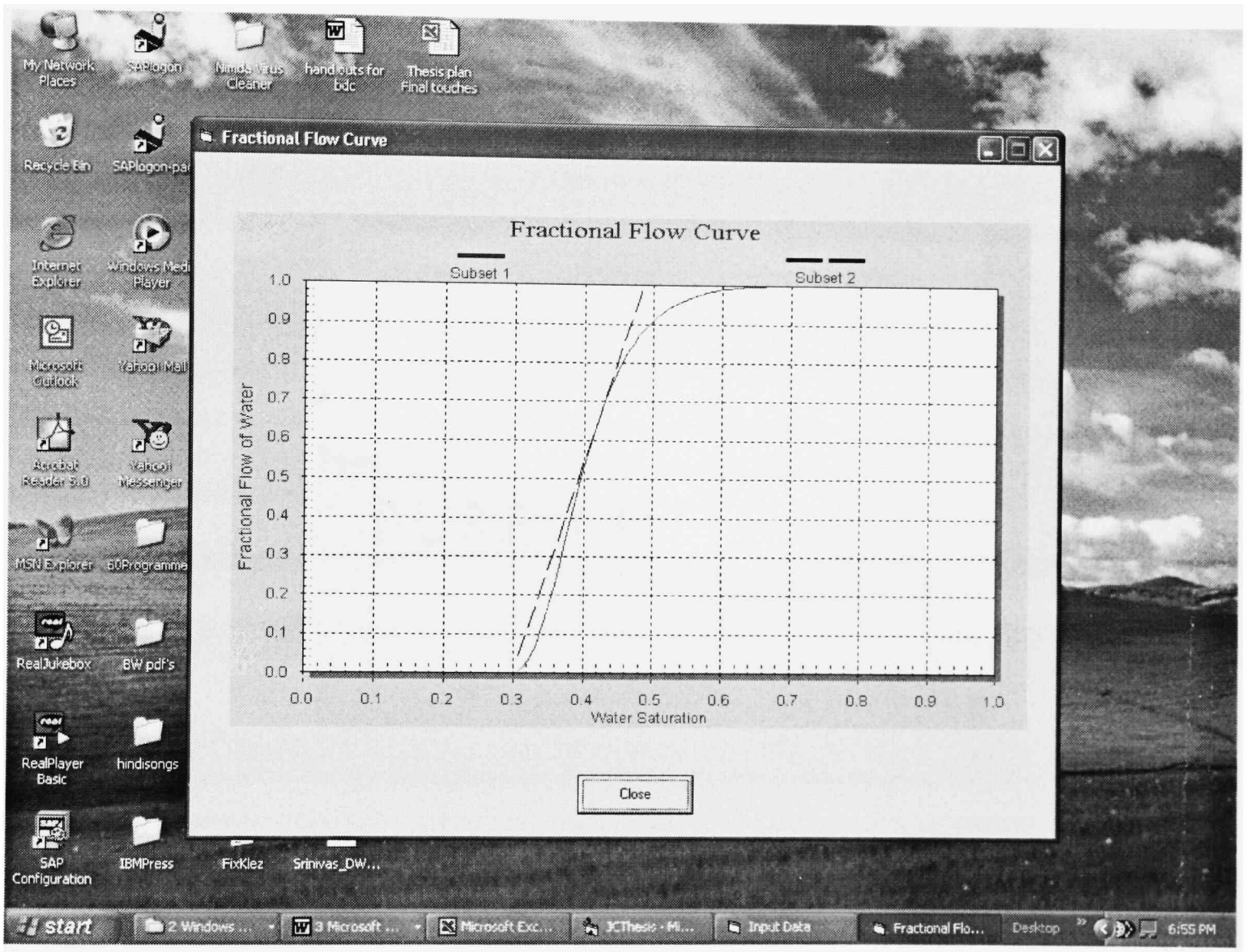

Figure 4.8. Fractional Flow Curve with Tangent after linking Excel and Access

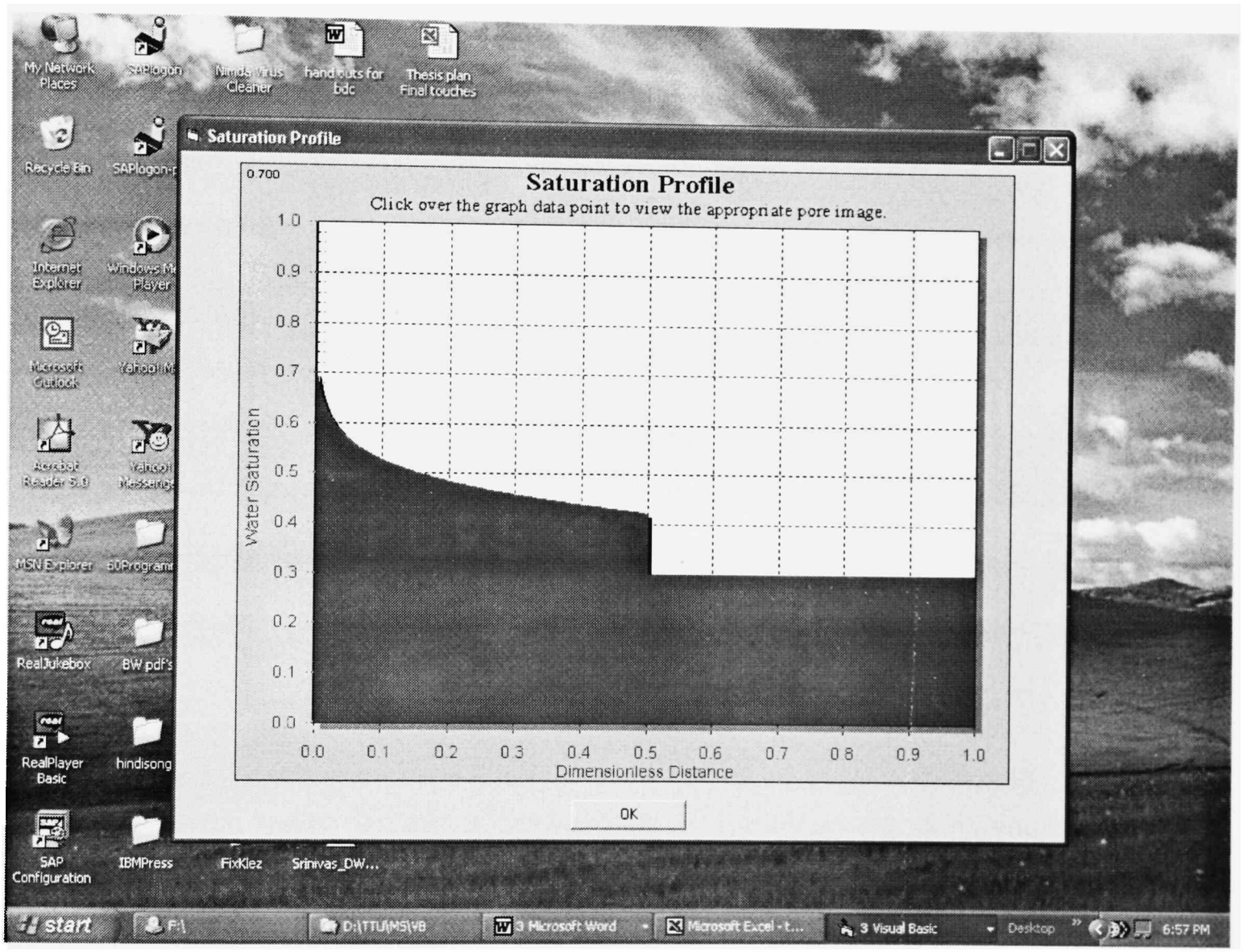

Figure 4.9. Saturation Profile when xD = 0.5, after linking Excel and Access

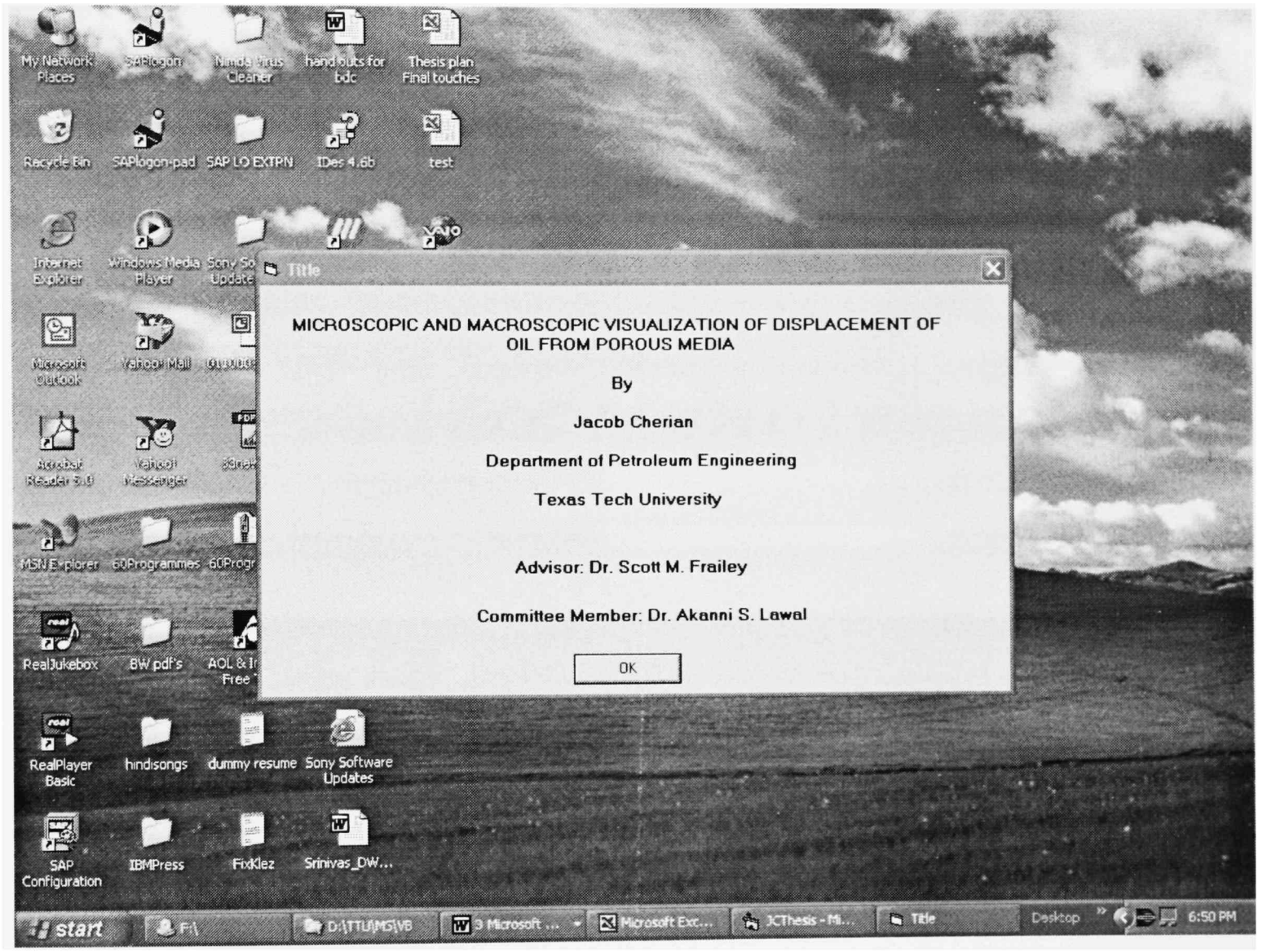

Figure 4.10. Initial screen

Figure 4.11. Browse screen prior to linking Excel and Access

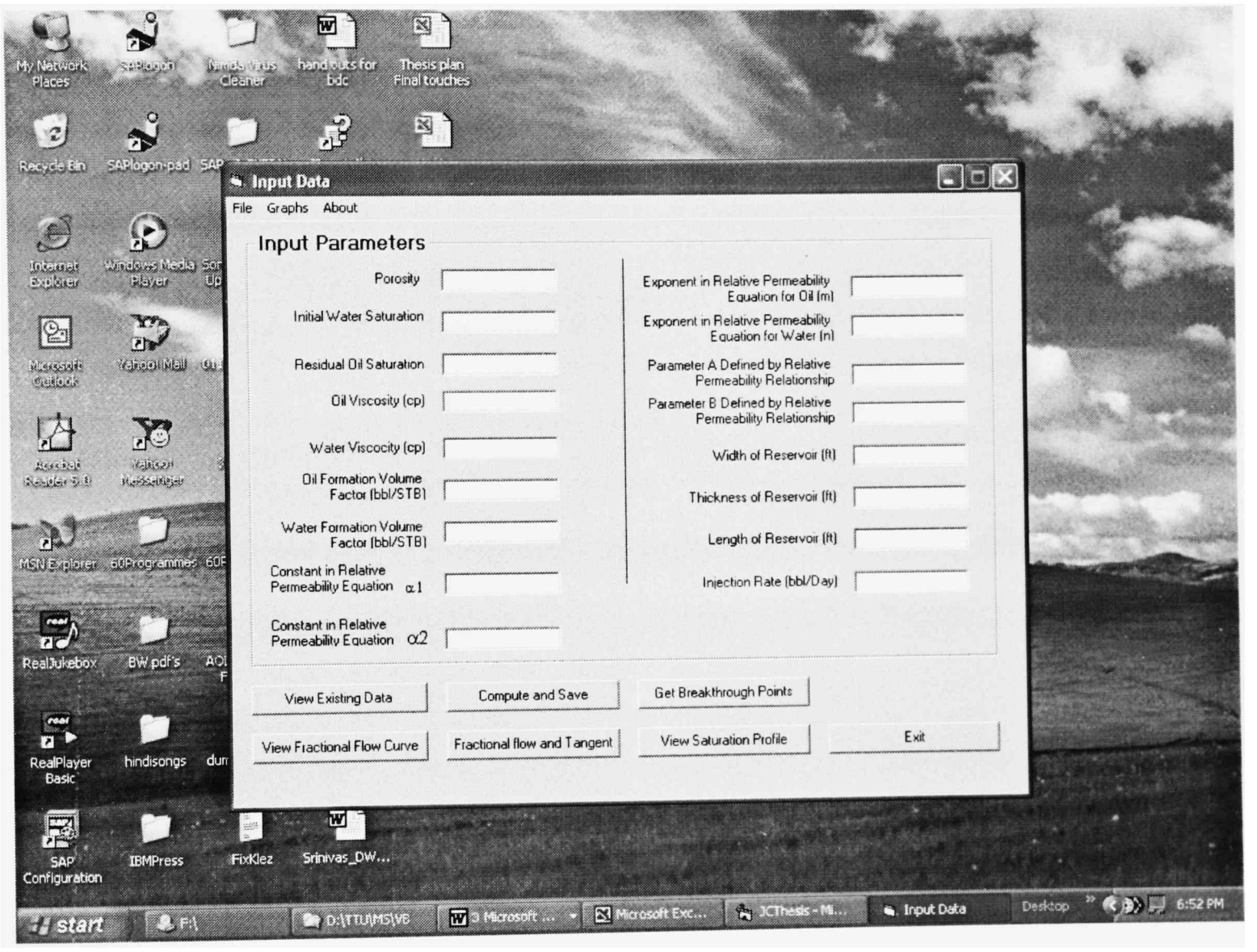

Figure 4.12. Main Screen

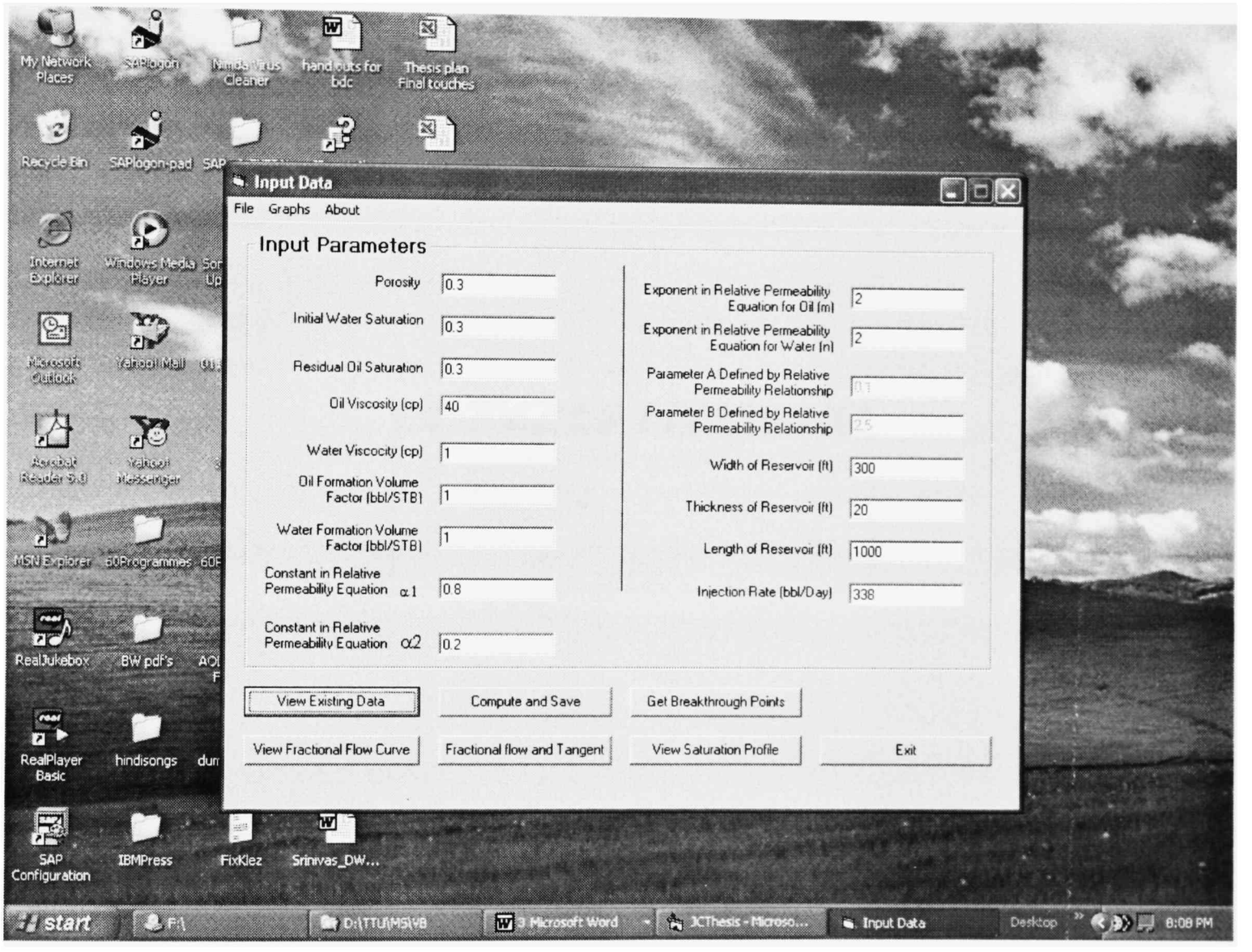

Figure 4.13. View Existing Data from the Excel Spreadsheet.

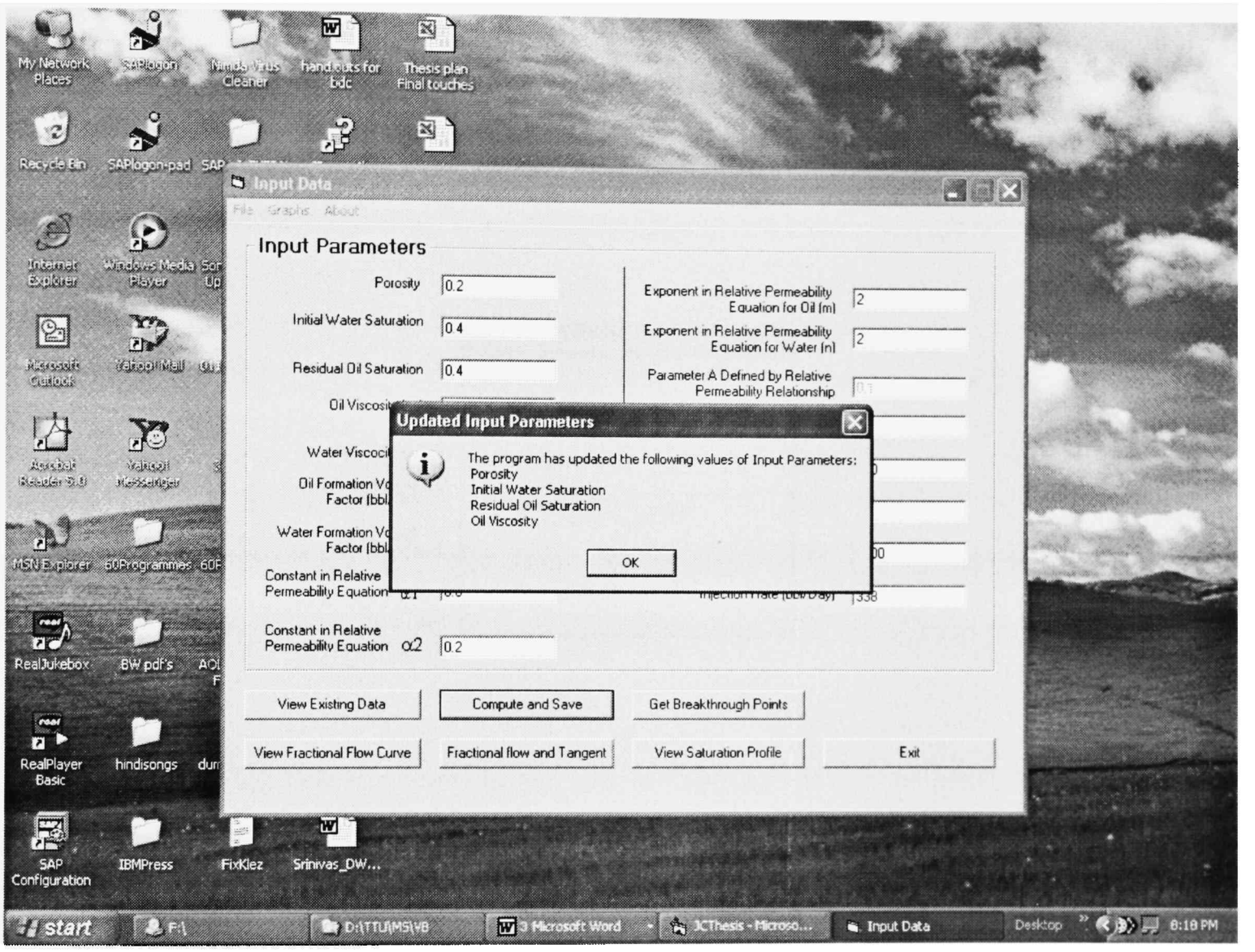

Figure 4.14. Updated parameters displayed by the program.

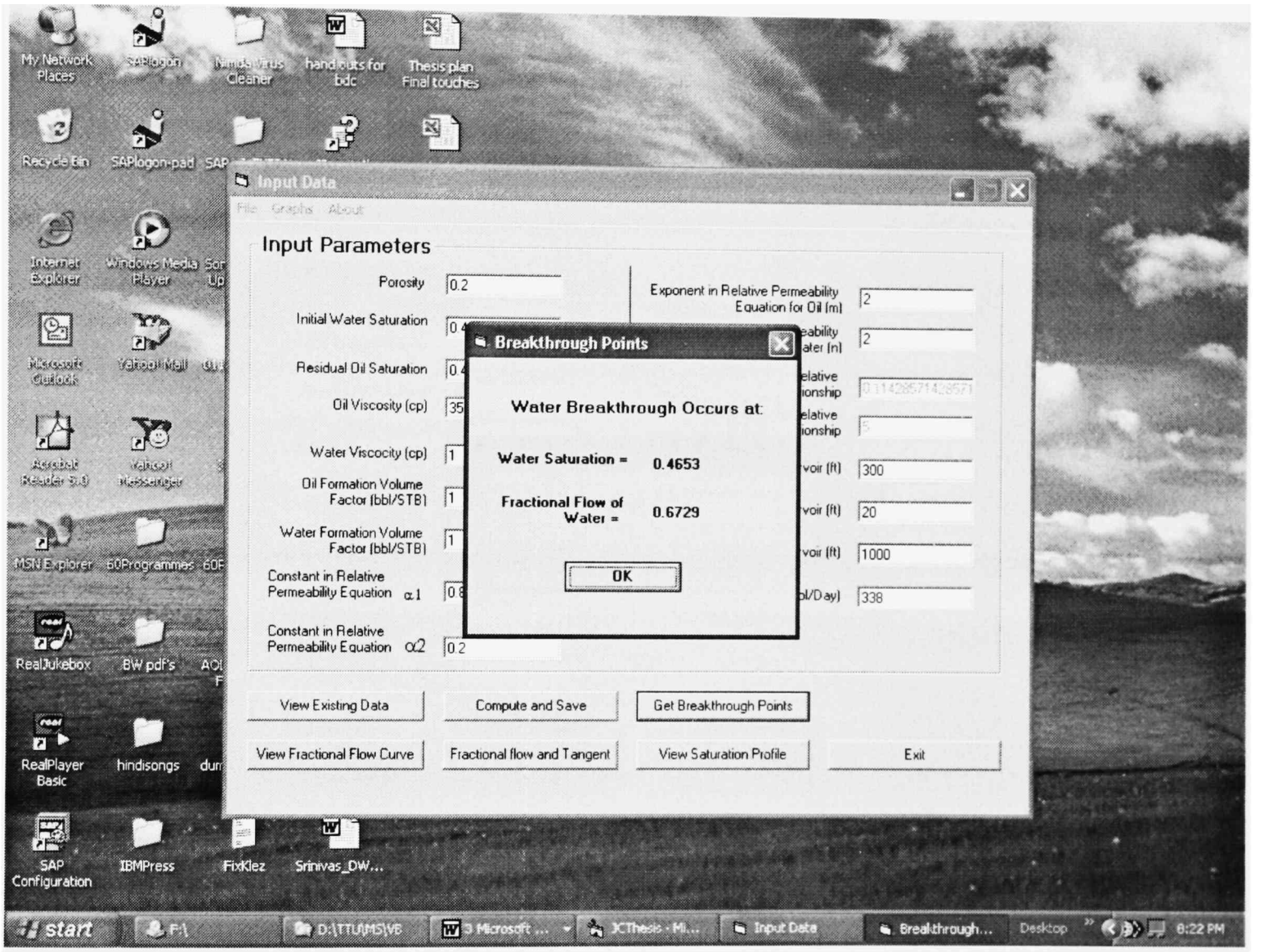

Figure 4.15. Breakthrough points displayed by the program.

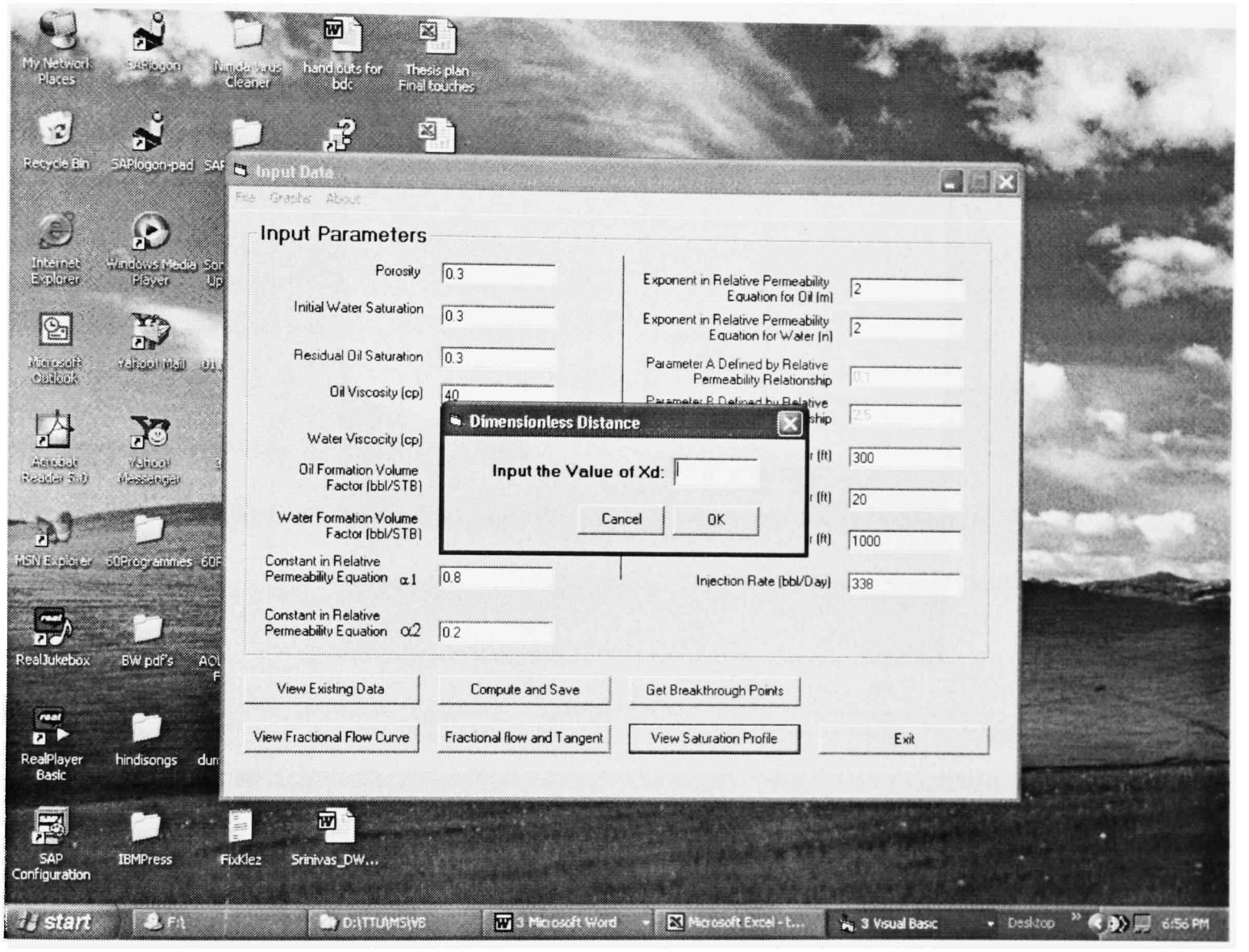

Figure 4.16. Screen for x_D input.

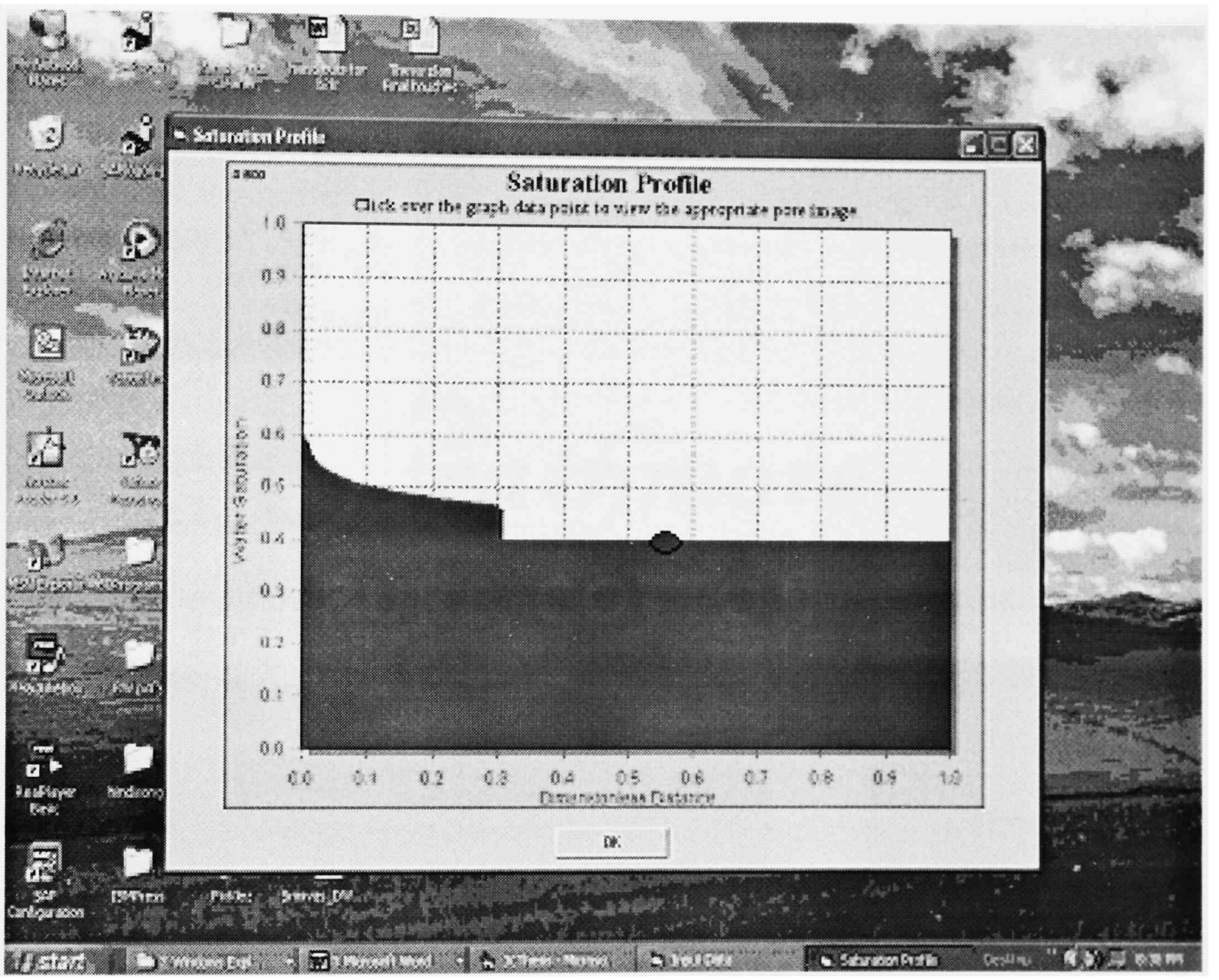

Figure 4.17. Hot spot where to click on, to display microscopic view.

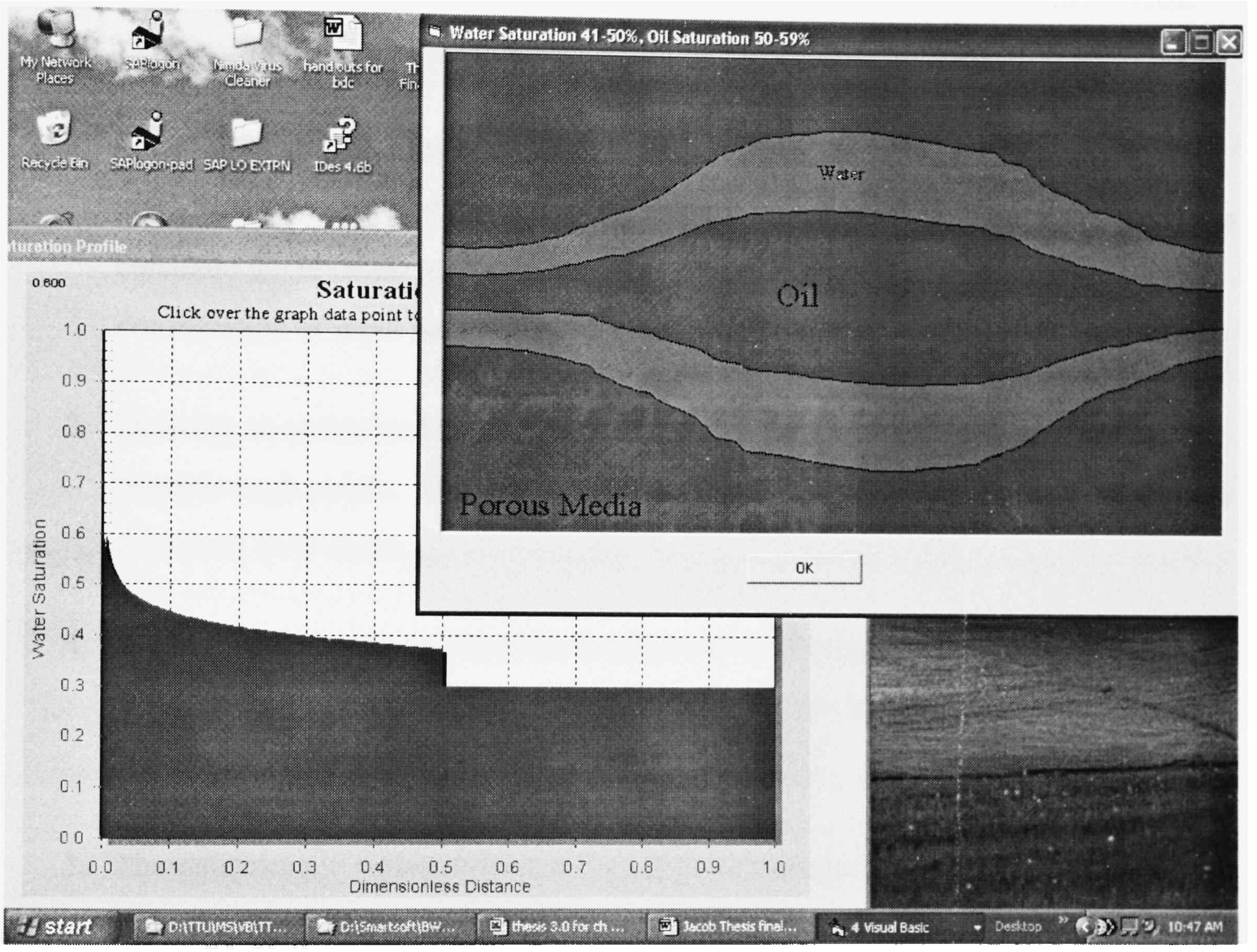

Figure 4.18. Display of microscopic view along with the macroscopic view when xD = 0.5 and water saturation = 45%.

CHAPTER 5

CONCLUSIONS

The following conclusions were drawn, based on the study:

1. Movement of oil through porous media during a waterflood process was studied extensively using various models developed by previous authors.

2. Creation of an automated fractional flow curve was identified to be useful in visualizing the shape of the curve. By using the automated method, it is possible to calculate the breakthrough saturations and fractional flow of water, for any combination of input parameters.

3. Drawing an automated tangent to the fractional flow curve helped to visualize the breakthrough points. This was helpful in determining the breakthrough points on a fractional flow curve.

4. A computer program to visualize the flow of oil through porous media was developed. The program was interactive and helped change the input parameters and see the effects immediately.

5. The microscopic views enabled to visualize distribution of oil and water inside a pore at various water saturations. It was possible to visualize via "snapshots" of the movement of oil and water through a single pore.

6. The macroscopic visualization method was interactive and displayed the saturations at various dimensionless distances. Different scenarios of saturation distribution could be viewed by changing the input parameters.

CHAPTER 6

RECOMMENDATIONS

The following recommendations are made, based on the present study:

1. This waterflooding study was conducted for a case of linear displacement model. Future studies should be conducted using two and three dimensional displacement methods.

2. The present study evaluated only the case of waterflooding. Future studies could concentrate on enhanced oil recovery.

3. It was assumed that the waterflooding process included no viscous fingering and the formation was homogeneous. Future studies could include viscous fingering and heterogeneity.

4. The present study considered only microscopic and macroscopic visualization. While considering actual reservoir, megascopic visualization methods also should be considered.

5. The present study has been limited to waterflooding up to water breakthrough. It is recommended to study the effects after breakthrough also.

REFERENCES

1. Craig, Forrest. F. Jr. *The Reservoir Engineering Aspect of Waterflooding* (fourth edition), SPE Monograph series, New York, 1993.

2. Craft. B. C. and Hawkins, M. F. *Applied Petroleum Reservoir Engineering*, Second Edition, Prentice Hall, Englewood Cliffs, New Jersey, 1991.

3. Smith, Charles R. *Mechanics of Secondary Oil Recovery*. Krieger Publishing Company, Malabar, Florida.1996.

4. Latil, M.: *Improved Oil Recovery*, Gulf Publishing Company, Houston, Texas, 1980.

5. Frick, T. C. and Taylor, R. W. *Petroleum Production Handbook*, Volume II, Reservoir Engineering, second edition, SPE series, Dallas, 1962.

6. Sahimi, Muhammad. *Flow and Transport in Porous Media and Fractured Rock*, VCH Verlagsgesellschaft mbH, Weinheim, 1995.

7. Willhite, G. P. *Waterflooding*. SPE Textbook Series, Richardson, Texas, 1986.

8. Green, D. W. and Willhite, G. P. *Enhanced Oil Recovery*, SPE Textbook Series, Richardson, Texas, Vol 6, 1998.

9. Amyx, J. M., Bass, D. M. Jr., and Whiting, R. L. *Petroleum Reservoir Engineering Physical Properties*, McGraw-Hill Book Company, New York, 1960.

10. Dyke, K. V. *Fundamentals of Petroleum*, Fourth Edition, Petroleum Extension Service, Austin, Texas, 1997.

11. Morris, Earl. E. and Wieland, Denton. R.: "A microscopic study of the effects of variable wettability conditions in immiscible fluid displacement," SPE paper 704, 1963.

12. Jones, S. C. and Roszelle, W. O.: "Graphical Techniques for Determining Relative Permeability from Displacement Experiments," SPE Paper 6045, 1978.

13. Dyes, A. B., Caudle, B. H., and Erickson, R. A.,: "Oil Production After Breakthrough –As Influenced by Mobility Ratio," *Trans.*, AIME (1954) **201**. 81-86.

14. Allen, F. R. and Puckett, D. A.: "Theoretical and experimental studies of rate dependent two phase immiscible flow," SPE paper 10972, 1986.

15. Yortsos, Yanis. C. and Fokas, Athanassios. F.: "An Analytical Solution for linear waterflood including the effects of Capillary Pressure," SPE paper 9407. 1980.

16. Buckley, S. E. and Leverett, M. C.: "Mechanism of Fluid Displacements in Sands," *Trans.*, AIME (1942) **146**, 107-116.

17. Cardwell, W.T. Jr.: "The meaning of the Triple Value in Noncapillary Buckley Leverett Theory," *Trans.*, AIME (1957) **216**, 271-276.

18. Welge, Henry J.: "A Simplified Method for Computing Oil Recovery by Gas or Water Drive," *Trans.*, AIME (1952) **195**, 39 – 46.

19. Dake, L. P,: "*Developments in Petroleum Science*, 36 -The Practice of Reservoir Engineering," Elsevier, Amsterdam, The Netherlands, 1994.

20. Snyder, R. W., Ramey, H. J.: "Application of Buckley Leverett Displacement Theory to Noncommunicating layered System," SPE Paper, 1645, 1967.

21. Higgins, R. V. and Leighton, A. J.: "Waterflood Performance in Stratified Reservoirs," RI5618, USBM (1960).

22. Hiatt, W. N.: "Injection-Fluid Coverage of Multi-Well Reservoirs with Permeability Stratification," *Drill. and Prod. Prac.*, API (1958) **165**.

23. Sethian, J. A., Chorin, A. J. and Concus, Paul.: "Numerical Solution of the Buckley Leverett Equations," SPE Paper, 12254, 1983.

24. Gelfand, I. M.: "Some problems in the theory of quasi linear equations," 1959, (in Russian), Uspekfri Mat. NaulG 24, No.2 (86), 87-158 (*Amer. Math. Soc.* Transl Ser.2, 1963, 295-381).

25. Yortsos, Yannis C. and Xu, Baomin,: " Phase diagram of the Fully Developed Drainage: A study of the Validity of the Buckley Leverett Equation," SPE Paper 49318, 1998.

26. Wilkinson, D. and Willemsen, J. F.: "Invasion percolation: a new form of percolation theory," *J. Phys.* A,: 3365-3376, 1983.

27. Langnes, G. L, Robertson, J. O., Jr., and Chilingar, G. V. *Secondary Recovery and Carbonate Reservoirs,* Elsevier, Amsterdam, The Netherlands, 1972.

28. Roberts, T. G.: "A permeability Block Method of Calculating a Water Drive Recovery Factor," *Pet Eng.* (1959) **31**, B-45

29. Johnson, C. E., Jr.: "Prediction of Oil Recovery by Waterflood – A Simplified Graphical Treatment of the Dykstra-Parsons Method," *Trans.*, AIME (1956) **207**, 354-346

30. Leverett, M. C.: "Capillary Behavior in Porous Solids," *Trans.*, AIME (1941) **142,** 152 - 169

31. Maranon, Julio,: "Some Results About Frontal Advance Theory," SPE Paper 5326. (Year Unknown)

32. Mohsen, M. F. N,: "Modification of Welge's Method of Shock Front Location in Buckley Leverett Problem for Nonzero Initial Condition," *Soc. Pet. Eng. J.* (Aug, 1985) 521-23.

33. El-Khatib, Noaman,: "Discussion of Modification of Welge's Method of Shock Front Location in Buckley Leverett Problem for Nonzero Initial Condition", SPE Paper 15193, 1985.

34. Mohsen, M. F. N.,: "Author's Reply to Discussion of Modification of Welge's Method of Shock Front Location in Buckley Leverett Problem for Nonzero Initial Condition," SPE Paper 15282, 1985.

35. Welge, Henry J.: "Discussion of Modification of Welge's Method of Shock Front Location in Buckley Leverett Problem for Nonzero Initial Condition," SPE Paper 1986.

36. Mohsen, M. F. N.: "Author's Reply to Discussion of Modification of Welge's Method of Shock Front Location in Buckley Leverett Problem for Nonzero Initial Condition," SPE Paper 15915, 1986.

37. Chen, Z. and Whitson, C. H.: "Further Discussion of Modification of Welge's Method of Shock Front Location in Buckley Leverett Problem for Nonzero Initial Condition," SPE Paper 16458, 1987.

38. Muskat, M.: *Flow of Homogenous Fluids*, McGraw-Hill Book Co., New York City, NY, 1946.

39. Deppe, J. C.: "Injection Rates-The Effects of Mobility Ratio, Areal Swept, and Pattern," *Soc. Pet. Eng. J.*, June 1961, 81-91.

40. Sandrea, R. J. and Farouq Ali, S. M.: "The Effects of Isolated Permeability Interfaces on the Sweep Efficiency and Conductivity of a Five Spot Network," *Soc. Pet. Eng. J.* March 1967, 20-30.

41. Landrum, B. L. and Crawford, P. B.: "Effect of Directional Permeability on Sweep Efficiency and Production Capacity," *Trans.*, AIME, 1960, **219**, 407-411.

42. Prats, M., Strickler, W. R. and Matthews, C.S.: "Single-Fluid Five Spots in Dipping Reservoirs," *Trans.*, AIME 1955, **204**, 160-167.

43. Matthews, C. S., and Fischer, M. J.: "Effect of Dip on Five Spot Sweep Patterns," *Trans.*, AIME, 1956 **207**, 111-117.

44. Craig, F. F., Jr., Geffen , T. M. and Morse, R. A.: "Oil Recovery Performance of Pattern Gas or Water Injection Operations from Model Tests," *Trans.*, AIME (1955) **204**, 7-15.

45. Habermann, B.: "The Efficiency of Miscible Displacement as a Function of Mobility Ratio," *Trans.*, AIME, (1960) **219**, 264-272.

46. Clark, J. B.: "A Hydraulic Process for Increasing the Productivity of Wells," *Trans.*, AIME, 1949, **186**, 1-6.

47. Dyes, A. B., Kemp, C. E. and Caudle, B. H.: "Effect Of Fractures on Sweep-Out Patterns," *Trans.*, AIME, 1958, **213**, 245-249.

48. Simmons, J., Landrum, B., Pinson, J. and Crawford, P.: "Swept Areas After Breakthrough in Vertically Fractured Five-Spot Patterns," *Trans.* AIME, **216**, 1959.

49. Frailey, S.M., Adisoemarta, P.S., Giussani, A. P. and Brown, T. J.: "A Method for Determining the Orientation of a Water Injection Induced Fracture," Southwestern Petroleum Short Course, Lubbock, 2000.

50. Spivak, A.: "Gravity Segregation in Two Phase Displacement Processes," *Soc. Pet. Eng. J.* Dec 1974, 619-32.

51. Wyckoff, R. D., Botest, H. G. and Muskat, M.: "The Mechanics of Porous Flow Applied to Water-flooding Problems," *Trans.*, AIME (1933) **103**, 219-242.

52. Craig, F. F., Jr., Sanderlin, J. L. and Moore, D W.: "A Laboratory Study of Gravity Segregation in Frontal Drives," *Trans.*, AIME (1957) **210**, 275-282.

53. Craig, F. F., Jr.: "Effect of Reservoir Description on Performance Predictions," *J. Pet Tech.* (Oct., 1970) 1239-1245.

54. Gaucher, D. H. and Lindley, D. C.: "Waterflood Performance in a Stratified Five-Spot Reservoir – A Scaled Model Study," *Trans.*, AIME (1960) **219**, 208-215.

55. Scheidegger, A. E.: *The Physics of Flow Through Porous Media*, The Macmillan Company, New York, 1956.

56. Bear, J.: *Dynamics of Fluids in Porous Media*, Dover Publications, Inc., New York, 1988.

57. Ryder, H. M.: "Effect of Production of Fluid Distribution and Relative Permeability in Sand," *World Oil*, June 1948, 142-50.

58. Arriola, A., Willhite, G. P. and Green, D. W.: "Trapping of Oil Drops in a Non-Circular Pore Throat," SPE Paper 9404, 1980.

59. Mohanty, K. K., Davis, H. T. and Scriven, L. E.: "Physics of Oil Entrapment in Water-Wet Rock," SPE Paper 9406, 1980.

60. Mohanty, K. K.: "Fluids in Porous Media: Two Phase Distribution and Flow," PhD dissertation, University of Minnesota, Twin Cities, MN (1980).

61. Castor, T. P. and Somerton, W. H.: "Interfacial Instabilities in Porous Media," SPE Paper 6516, 1977.

62. Haines, W. B.: "Studies in the Physical Properties of Soil: V. The Hysteresis Effect in Capillary Properties and the Modes of Moisture Distribution Associated Therewith," *J. Agri Sci.* (1930) Vol. 20, 97-116.

63. Oh, S. G. and Slattery, J. C.: "Interfacial Tension Required for Significant Displacement of Residual Oil," SPE Paper # 5992, 1979.

64. Pickell, J. J., Swanson, B. F. and Hickman, W. B.: "Application of Air-Mercury and Oil-Air Capillary Pressure Data in the Study of Pore Structure and Fluid Distributions," *Soc, Pet. Eng. J.* (March 1966) 55-61.

65. Roof, J. G.: "Snap-Off of Oil Droplets in Water-Wet Pores," *Soc. Pet. Eng. J.* (March, 1970) 85-90.

66. Egbogah, E. O., Wright R. J. and Dawe, R. A.: "A Model of Oil Ganglion Movement in Porous Media," SPE Paper 10115, 1981.

67. Egbogah, E. O.: "The Concept of Relative Ganglion Velocity and Generalization to Oil Bank Movements in Porous Media," SPE Paper 14876, 1985.

68. Halvorson, Michael. *Learn Microsoft Visual Basic 6.0 Now*, Microsoft Press, Buffalo, NY, 1999.

69. Holzner, Steven. *Visual Basic 6 Black Book*, Coriolis Technology Press, Scottsdale, AZ, 1998.

70. http://www.whatis.com

APPENDIX A

PERCOLATION THEORY

The percolation threshold is the main concept of percolation theory and can be explained as follows:

Let p be a parameter, which defines the average degree of connectivity between various sub-units of a certain arbitrary system. When p = 0, all sub units of the arbitrary system are totally isolated from every other sub-unit. When p = 1, all the sub-systems are connected to some maximum number of neighboring sub-units. Also, when p = 1, the system is connected from one side to the other, linking one sub-unit to the next one. When the connections are randomly broken at p = 1, the average connectivity decreases thus, reducing the value of p. The percolation threshold is the value of p at which there is no longer an unbroken path from one side of the system to the other. If the connections are randomly created at p = 0, the percolation threshold is the value of p when the first continuous connection appears from one end of the system to the other end

Invasion percolation is a new form of percolation theory that takes into account the fluid transport process. More details about the invasion percolation can be found at Reference 26.

APPENDIX B

GAUSSIAN CURVATURE

At any point on a curve in the plane, the line best approximating the curve that passes through this point is the tangent line. The reciprocal of the radius of this circle is the curvature of the curve at this point. The best approximating circle may lie either to the left of the curve, or to the right of the curve. By establishing a convention, the curvature could be assigned a positive sign if the circle lies to the left and negative sign if the circle lies to the right of the curve. This is known as signed curvature. The principal curvatures of a surface at a point are the minimum and maximum of the normal curvatures at that point. The Gaussian curvature of a surface at a point is the product of the principal curvatures at that point.

APPENDIX C

EXCEL MACRO TO POPULATE ACCESS DATABASE

```
Option Explicit

'Insert values into the access table - TA.
Public Function UpdateTA(StartRange As String, AccessPath As String)

Dim strSql As String
Dim WS As Worksheet
Dim i As Integer
Dim adoconnect As ADODB.Connection
Dim Rng As Range
Dim GetConnectionString As String

Set WS = Me.Application.ActiveWorkbook.ActiveSheet
Set Rng = WS.Range(StartRange)

'old path =  "C:\Documents and Settings\JCHERIAN\Desktop\db3.mdb

GetConnectionString = "Provider=Microsoft.Jet.OLEDB.4.0;Data Source=" & _
      AccessPath & ";Mode=ReadWrite;Persist Security Info=False"

Set adoconnect = New ADODB.Connection
adoconnect.Open GetConnectionString
strPK = Rng.Value
adoconnect.Execute ("delete from TA") 'delete the contents from the sheet
i = 0
Do While Rng.Offset(i, 0).Value <> ""

   'Insert into the appropriate table
   strSql = "INSERT INTO TA(Sw2.fw2,f'w2" & ") values(" & Rng.Offset(i.
0).Value & "," & Rng.Offset(i, 1).Value & "," & Rng.Offset(i. 2).Value & ")"
      adoconnect.Execute strSql
      i = i + 1
Loop

Set WS = Nothing
Set Rng = Nothing
Set adoconnect = Nothing

End Function
```

PERMISSION TO COPY

In presenting this thesis in partial fulfillment of the requirements for a master's degree at Texas Tech University or Texas Tech University Health Sciences Center, I agree that the Library and my major department shall make it freely available for research purposes. Permission to copy this thesis for scholarly purposes may be granted by the Director of the Library or my major professor. It is understood that any copying or publication of this thesis for financial gain shall not be allowed without my further written permission and that any user may be liable for copyright infringement.

Agree (Permission is granted.)

_____ _____

Student Signature Date

Disagree (Permission is not granted.)